**Priscilla Brandão Silva**

# Dynamic analysis of periodic structures via wave-based numerical approaches and substructuring techniques

## *Análise dinâmica de estruturas periódicas utilizando uma abordagem de propagação de ondas e técnicas de sub-estruturação*

97/2015

CAMPINAS
2015

i

**UNIVERSIDADE ESTADUAL DE CAMPINAS**

**FACULDADE DE ENGENHARIA MECÂNICA**

Priscilla Brandão Silva

# Dynamic analysis of periodic structures via wave-based numerical approaches and substructuring techniques

## *Análise dinâmica de estruturas periódicas utilizando uma abordagem de propagação de ondas e técnicas de sub-estruturação*

Doctoral Thesis presented to the School of Mechanical Engineering of the University of Campinas in partial fulfillment of the requirements for the degree of Doctor in Mechanical Engineering, in the Area of Solid Mechanics and Mechanical Design.

*Tese de Doutorado apresentada à Faculdade de Engenharia Mecânica da Universidade Estadual de Campinas como parte dos requisitos exigidos para obtenção do título de Doutora em Engenharia Mecânica, na Área de Mecânica dos Sólidos e Projeto Mecânico.*

Orientador: Prof. Dr. José Roberto de França Arruda
Co-orientador: Prof. Dr. Jean-Mathieu Mencik

ESTE EXEMPLAR CORRESPONDE À VERSÃO FINAL DA TESE DEFENDIDA PELA ALUNA PRISCILLA BRANDÃO SILVA, E ORIENTADA PELO PROF. DR. JOSÉ ROBERTO DE FRANÇA ARRUDA.

.....................................................
ASSINATURA DO ORIENTADOR

CAMPINAS
2015

iii

Informações para Biblioteca Digital

**Título em outro idioma:** Análise dinâmica de estruturas periódicas utilizando uma abordagem de propagação de ondas e técnicas de sub-estruturação
**Palavras-chave em inglês:**
Periodic structures
Wave propagation
Finite element method
Decomposition methods
Structural dynamics
**Área de concentração:** Mecânica dos Sólidos e Projeto Mecânico
**Titulação:** Doutora em Engenharia Mecânica
**Banca examinadora:**
José Roberto de França Arruda [Orientador]
Renato Pavanello
Marco Lúcio Bittencourt
Arcanjo Lenzi
Domingos Alves Rade
**Data de defesa:** 31-08-2015
**Programa de Pós-Graduação:** Engenharia Mecânica

# Dynamic analysis of periodic structures via wave-based numerical approaches and substructuring techniques

# Análise dinâmica de estruturas periódicas utilizando uma abordagem de propagação de ondas e técnicas de sub-estruturação

Autor: Priscilla Brandão Silva
Orientador: José Roberto de França Arruda
Co-Orientador: Jean-Mathieu Mencik

A Banca Examinadora composta pelos membros abaixo aprovou esta Tese:

_____
Prof. Dr. José Roberto de França Arruda, Presidente
DMC - Faculdade de Engenharia Mecânica - UNICAMP

_____
Prof. Dr. Renato Pavanello
DMC - Faculdade de Engenharia Mecânica - UNICAMP

_____
Prof. Dr. Marco Lúcio Bittencourt
DSI - Faculdade de Engenharia Mecânica - UNICAMP

_____
Prof. Dr. Arcanjo Lenzi
LVA - Departamento de Engenharia Mecânica - UFSC

_____
Prof. Dr. Domingos Alves Rade
IEM-P - Divisão de Engenharia Mecânica - ITA

Campinas, 31 de agosto de 2015.

# Dedication

*I dedicate this thesis to my dear grandmother Maria Eunízia and my parents.*

*Dedico esta tese à minha querida avó Maria Eunízia e aos meus pais.*

# Acknowledgements

I would like to thank all who in one way or another contributed to the completion of this thesis. First and foremost, I thank God for my life. I am grateful for the good health, wellbeing, and protection that were necessary to complete this thesis.

I wish to express my sincere thanks to my supervisor Prof. Dr. José Roberto de França Arruda for his continuous support, pleasant discussions, and his patience during this research. I have learned a lot from his experience in science and life. His continuous motivation with science have inspired me and motivates my future career. I also wish to express my gratitude to my co-supervisor Prof. Dr. Jean-Mathieu Mencik who has provided a great support for this thesis in the last two years. I would like to thank for his interest, for the continuous discussions, insightful comments and encouragement extended to me. I am also so grateful for his efforts to provide me a pleasant stay in France.

I would like also to thank Prof. Dr. Brian R. Mace who has supervised me during the research internship at the University of Auckland, in New Zealand. I am grateful for receiving me there, for the continuous meetings which have contributed to widen my understanding in the topic of this thesis.

I would like to thank the external members of the jury for coming to my defense and contribute with their experienced advices to improve this thesis. I am also thankful to Prof. Dr. Renato Pavanello and Prof. Dr. Marco Lúcio Bittencourt from the Faculty of Mechanical Engineering, and also members of the jury, for valuable discussions during this thesis and for their suggestions.

I am also grateful to the Faculty of Mechanical Engineering at UNICAMP, in special, the Department of Computational Mechanics, for providing me the facilities necessary to the development of this thesis. I am thankful to the secretary Beth Viana for her support in administrative tasks. I thank also the staff of SIFEM for their support during my thesis.

I wish to express my sincere gratitude to my friends and fellow labmates, in special, Danilo Beli, Daniela Damasceno, Belisário Hualpa, Lucas Cóser, Marcela Machado, Edílson Dantas, Flávio Bannwart, Josh Labaki, Nilson Inocente, and Diego Sivieiro. Our pleasant discussions, long hours of hard work, and all the fun we have had in the last four years have certainly contributed to make the difficult moments less hard. I would like also to thank my friend Rafael Cordeiro for his support and sincere encouragement extended to me during this thesis.

I am also thankful to the Laboratoire de Mécanique et Rhéologie at INSA Centre Val de Loire, all professors and fellow labmates for providing me the facilities and also the good environment for the development of my research during the stay in France.

I would like also to thank the Department of Mechanical Engineering at the University of Auckland and my fellow labmates for the support during the stay in New Zealand.

My sincere thanks to all the friends I made in New Zealand and in France, they made me feel like home even far away from Brazil.

Last but not the least, I would like to thank my family: my parents José Wilson and Ilca Helena, my brother Fernando José, and sister Fernanda, for their unconditional support throughout this thesis. I am really thankful for their encouragement and effort to help whenever I need since I was born. They were my strength in the writing of this thesis. I am also so thankful to my grandmother Maria Eunízia for being my major example of faith and determination. I thank my uncle Marcos Antônio who has been always my example of researcher. I would like to thank my aunts Terezinha and Liana for their encouragement throughout this thesis.

# Agradecimentos

ambiente para o desenvolvimento da minha pesquisa durante a estada na França.

Gostaria também de agradecer ao Departamento de Engenharia Mecânica da Universidade de Auckland e aos meus colegas de laboratório pelo apoio durante a minha estada na Nova Zelândia.

Meu sincero agradecimento a todos os amigos que fiz na Nova Zelândia e na França. Eles me fizeram me sentir em casa ainda que eu estivesse muito distante do Brasil.

Eu também sou grata à Fapesp que através dos processos 2010/17317-9, 2012/11809-2 e 2013/23542-3 me proporcionou o apoio financeiro necessário ao desenvolvimento desta tese e também por ter me dado a oportunidade de realizar dois estágios de pesquisa no exterior durante esta tese.

Por último, mas não menos importante, eu gostaria de agradecer à minha família: aos meus pais José Wilson e Ilca Helena, ao meu irmão Fernando José e à minha irmã Fernanda pelo apoio incondicional durante todo o decorrer desta tese. Eu sou muito agradecida a eles por me incentivarem e por todo o esforço em me ajudar sempre que eu preciso desde o momento que nasci. Eles foram a minha força para escrever esta tese. Eu sou muito grata também à minha avó Maria Eunízia por ser para mim o maior exemplo de fé e determinação. Eu agradeço ao meu tio Marcos Antônio que sempre foi meu exemplo de pesquisador. Gostaria de agradecer também às minhas tias Terezinha e Liana pelo incentivo que me deram durante todo o desenvolvimento desta tese.

*I discovered how good is to arrive when there is patience. And in order to arrive, wherever you want, I learned that it is not necessary to master the force, but the reason. It is necessary, first of all, to desire.*

Amyr Klink

*Descobri como é bom chegar quando se tem paciência. E para se chegar, onde quer que seja, aprendi que não é preciso dominar a força, mas a razão. É preciso, antes de mais nada, querer.*

Amyr Klink

# Resumo

SILVA, Priscilla Brandão. Análise dinâmica de estruturas periódicas utilizando uma abordagem de propagação de ondas e técnicas de sub-estruturação. 2015. 232p. Tese (Doutorado). Faculdade de Engenharia Mecânica, Universidade Estadual de Campinas, Campinas.

Nesta tese de doutorado, o método dos elementos finitos ondulatórios é utilizado para cálculo da resposta harmônica de sistemas mecânicos envolvendo estruturas com periodicidade unidimensional, *i.e.*, estruturas compostas por subestruturas idênticas arranjadas ao longo de uma direção. Tais sistemas mecânicos podem ser complexos e são comumente encontrados em aplicações de engenharia como, por exemplo, nas fuselagens de aviões. A primeira parte da tese é dedicada ao cálculo das ondas que se propagam ao longo dessas estruturas. Uma breve revisão da literatura sobre as formulações disponíveis para o problema de autovalor associado ao método dos elementos finitos ondulatórios é apresentada, assim como um estudo dos erros numéricos induzidos por estes problemas de autovalor no caso de um guia de ondas sólido. Na segunda parte desta tese, modelagens de superelementos para estruturas periódicas são propostas. Neste contexto, matrizes de rigidez dinâmica e de receptância ou flexibilidade de estruturas periódicas são expressas a partir dos modos de onda. Comparadas às matrizes de rigidez dinâmica e receptância obtidas pelo método dos elementos finitos convencional, as matrizes baseadas no método dos elementos finitos ondulatórios são calculadas de forma bastante rápida e sem perda de acuracidade. Ademais, uma estratégia eficiente de redução de ordem de modelo é apresentada. Comparada às formulações que utilizam a base completa de ondas, esta estratégia proporciona redução do tempo computacional requerido para cálculo da resposta forçada de estruturas periódicas. De fato, é mostrado que elementos espectrais numéricos de alta ordem podem ser construídos a partir do método dos elementos finitos ondulatórios. Isto constitui uma alternativa ao método dos elementos espectrais convencional, cuja utilização está limitada a estruturas simples para as quais soluções analíticas por ondas existam. A motivação por trás das formulações de matrizes de superelementos a partir do método dos elementos finitos ondulatórios está na utilização do conceito de ondas numéricas para calcular a resposta harmônica de sistemas mecânicos acoplados que envolvam estruturas com periodicidade unidimensional e junções elásticas a partir de procedimentos de montagem clássicos de elementos finitos ou técnicas de decomposição de domínio. Este assunto é tratado na terceira parte desta tese. Nesse caso, o método de Craig-Bampton é usado para expressar as matrizes de superelementos de junções por meio de modos estáticos e de interface fixa. Um critério baseado no método dos elementos finitos ondulatórios é considerado para a seleção dos modos da junção que mais contribuem para a resposta forçada do sistema. Isto também contribui para o aumento da eficiência da simulação numérica de sistemas acoplados. Finalmente, na quarta parte desta tese, o método dos elementos finitos ondulatórios é utilizado para mostrar que é possível projetar estruturas periódicas com potencial para funcionar como filtros de vibração em bandas de frequência específicas. Com o intuito de destacar a relevância dos desenvolvimentos propostos nessa tese, ensaios numéricos envolvendo guias de onda sólidos, pórticos planos e estruturas

tridimensionais do tipo fuselagem aeronáutica são realizados.

# Abstract

SILVA, Priscilla Brandão. Dynamic analysis of periodic structures via wave-based numerical approaches and substructuring techniques. 2015. 232p. Tese (Doutorado). Faculdade de Engenharia Mecânica, Universidade Estadual de Campinas, Campinas.

In this thesis, the wave finite element (WFE) method is used for assessing the harmonic forced response of mechanical systems that involve structures with one-dimensional periodicity, *i.e.*, structures which are made up of several identical substructures along one direction. Such mechanical systems can be quite complex and are commonly encountered in engineering applications, *e.g.*, aircraft fuselages. The first part of the thesis is concerned with the computation of wave modes traveling along these structures. A brief literature review is presented regarding the available formulations for the WFE eigenproblem, which need to be solved for expressing the wave modes, as well as a study of the numerical errors induced by these eigenproblems in the case of a solid waveguide. In the second part of the thesis, the WFE-based superelement modeling of periodic structures is proposed. In this context, the dynamic stiffness matrices and receptance matrices of periodic structures are expressed in terms of wave modes. Compared to the conventional FE-based dynamic stiffness and receptance matrices, the WFE-based matrices can be computed in a very fast way without loss of accuracy. In addition, an accurate strategy for WFE-based model order reduction is presented. It provides significant computational time savings for the forced response analysis of periodic structures compared to WFE-based superelement modeling, which makes use of the full wave basis. Indeed, it is shown that higher-order numerical spectral elements can be built by means of the WFE method. This is an alternative to the conventional spectral element method, which is limited to simple structures for which closed-form wave solutions exist. The motivation behind the formulation of WFE-based superelement matrices is the use of the concept of numerical wave modes to assess the forced response of coupled mechanical systems that involve structures with one-dimensional periodicity and coupling elastic junctions through classic finite element assembly procedures or domain decomposition techniques. This issue is addressed in the third part of this thesis. In this case, the Craig-Bampton method is used to express superelement matrices of coupling junctions by means of static and fixed-interface modes. A WFE-based criterion is considered to select among junction modes those that contribute most to the system forced response. This also contributes to enhancing the efficiency of the numerical simulation of coupled systems. Finally, in the fourth part of this thesis, the WFE method is used to show the potential of designing periodic structures which work as vibration filters within specific frequency bands. In order to highlight the relevance of the developments proposed in this thesis, numerical experiments which involve solid waveguides, two-dimensional frame structures, and three-dimensional aircraft fuselage-like structures are carried out.

*Keywords*: Periodic structures, Wave propagation, Finite element method, Decomposition methods,

Structural dynamics.

# List of Figures

# List of Tables

# List of Abbreviations and Acronyms

*Matrices and Vectors*

| | | |
|---|---|---|
| $\mathbf{A}, \mathbf{B}$ | - | Generic matrices |
| $\mathbf{A}_j$ | - | Matrix of size $2n \times 2n$ |
| $\mathcal{B}$ | - | Boolean matrix |
| $\mathbf{C}$ | - | Damping matrix |
| $\mathbf{C_q}$ | - | Matrix of size $n \times n$ |
| $\mathbb{C}$ | - | Matrix of reflection/transmission in terms of the full basis of wave modes |
| $\tilde{\mathbb{C}}$ | - | Matrix of reflection/transmission in terms of a reduced set of wave modes |
| $\mathbf{D}$ | - | Dynamic stiffness matrix |
| $\mathbf{E}$ | - | Perturbation matrix |
| $\mathbf{J}$ | - | Unit symplectic matrix |
| $\mathbf{I}$ | - | Identity matrix |
| $\mathbf{K}$ | - | Stiffness matrix |
| $\bar{\mathbf{K}}, \bar{\mathbf{M}}$ | - | Matrices of size $2n \times 2n$ |
| $\mathbf{L}, \mathbf{N}$ | - | Matrices of size $2n \times 2n$ used to express $(\mathbf{N}, \mathbf{L})$ eigenproblem |
| $\bar{\mathbf{L}}, \bar{\mathbf{N}}$ | - | Matrix of size $2n \times 2n$ used to express $(\bar{\mathbf{N}}, \bar{\mathbf{L}})$ eigenproblem |
| $\mathcal{L}$ | - | Incidence mesh matrix |
| $\mathbf{M}$ | - | Mass matrix |
| $\mathcal{N}$ | - | Direction cosine matrix |
| $\tilde{\mathbf{P}}$ | - | Projection matrix (between physical and generalized coordinates) |
| $\mathbf{R}$ | - | Receptance matrix |
| $\tilde{\mathbf{R}}$ | - | Receptance matrix in terms of generalized coordinates |
| $\mathcal{R}$ | - | Diagonal symmetry transformation matrix of size $n \times n$ |
| $\mathbf{S}$ | - | Symplectic transfer matrix |
| $\tilde{\mathbf{S}}$ | - | Reduced transfer matrix |
| $\tilde{\mathbf{T}}_{\mathrm{L}}, \tilde{\mathbf{T}}_{\mathrm{R}}$ | - | Transformation matrices |
| $\mathcal{T}$ | - | Diagonal symmetry transformation matrix of size $2n \times 2n$ |
| $\mathbf{U}_{\mathbf{A}_j}$ | - | Matrix of size $2n \times 2n$ |
| $\mathbf{V}_{\mathbf{A}_j}$ | - | Matrix of size $2 \times 2$ |
| $\mathbf{X}_{\mathrm{el}}$ | - | Matrix of fixed-interface modes |
| $\mathbf{X}_{\mathrm{st}}$ | - | Matrix of static modes |
| $\mathbf{Z}_1, \mathbf{Z}_2$ | - | Matrices of size $2n \times 2n$ used to express $(\mathbf{Z}_1, \mathbf{Z}_2)$ eigenproblem |

| | | |
|---|---|---|
| $\boldsymbol{\alpha}$ | - | Projection matrix (between the full basis and a reduced set of wave modes) |
| $\boldsymbol{\Phi}$ | - | Matrix of right-going wave mode shapes |
| $\boldsymbol{\Phi}^{\star}$ | - | Matrix of left-going wave mode shapes |
| $\boldsymbol{\Phi_u}$ | - | Matrix of right eigenvectors of $\mathbf{S}$ |
| $\boldsymbol{\Sigma}_{\mathbf{A}_j}$ | - | Diagonal matrix of size $2n \times 2$ |
| $\boldsymbol{\varphi}$ | - | Matrix of size $2n \times 1$ |
| | | |
| $\mathbf{a}$ | - | Vector of size $2 \times 1$ |
| $\mathbf{F}$ | - | Vector of external loads (forces/moments) |
| $\mathbf{f}$ | - | Vector of internal loads (forces/moments) |
| $\bar{\mathbf{p}}$ | - | Vector of component generalized coordinates |
| $\mathbf{q}$ | - | Vector of displacements/rotations |
| $\tilde{\mathbf{q}}, \tilde{\mathbf{F}}$ | - | Vectors of displacements/rotations and forces/moments in terms of generalized coordinates |
| $\mathbf{q}_0$ | - | Vector of prescribed displacements/rotations |
| $\mathbf{Q}$ | - | Vector of wave amplitudes |
| $\mathbf{r}$ | - | Vector of positions w.r.t. the reference frame |
| $\mathbf{u}$ | - | State vector |
| $\mathbf{x}, \mathbf{z}$ | - | Generic vectors |
| $\mathbf{w}$ | - | Right eigenvector of matrix pencils $(\mathbf{N},\mathbf{L})$, $(\bar{\mathbf{N}},\bar{\mathbf{L}})$, and $(\mathbf{Z}_1,\mathbf{Z}_2)$ |
| $\boldsymbol{\beta}$ | - | Vector of wavenumbers |
| $\boldsymbol{\lambda}_{\mathrm{LM}}$ | - | Vector of Lagrange multipliers |
| $\boldsymbol{\mu}$ | - | Diagonal matrix of right-going propagation constants (or eigenvalues of $\mathbf{S}$) |
| $\phi$ | - | Vector of wave mode shapes or right eigenvectors of $\mathbf{S}$ |
| $\tilde{\boldsymbol{\Phi}}$ | - | Vector of kept wave modes expressed in physical coordinates |
| $\psi$ | - | Left eigenvector of $\mathbf{S}$ |
| $\tilde{\boldsymbol{\Psi}}$ | - | Left eigenvectors relative to kept wave modes |
| $\tilde{\boldsymbol{\varphi}}$ | - | Vector of kept wave modes expressed in generalized coordinates |
| $\bar{\boldsymbol{\chi}}$ | - | Vector of generalized DOFs |

### *Superscripts*

| | | |
|---|---|---|
| $*$ | - | denotes condensed matrix |
| $\star$ | - | related to left-going waves |
| $b$ | - | relative to bending wave mode |
| $(c)$ | - | coupling elastic junction index |
| $H$ | - | vector/matrix conjugate transpose |
| $(k)$ | - | substructure index |
| $(p)$ | - | periodic structure index |
| $s$ | - | relative to shear wave mode |
| $(s)$ | - | relative to structure |
| $T$ | - | vector/matrix transpose |
| gl | - | relative to the global system |
| ref | - | reference value |

### *Subscripts*

| | | |
|---|---|---|
| $b$ | - | relative to a bending wave mode |
| B | - | relative to boundary degrees of freedom |
| $c$ | - | coupling elastic junction index |
| c | - | clamped boundary |
| d | - | dynamic part |
| f | - | free boundary |
| I | - | relative to internal degrees of freedom |
| L | - | relative to left degrees of freedom |
| R | - | relative to right degrees of freedom |
| $i$ | - | wave mode index |
| $j$ | - | wave mode index |
| $k$ | - | relative to kept wave modes |
| $lr$ | - | relative to resonant device |
| $m$ | - | index |
| $n$ | - | index |
| $p$ | - | periodic structure index |
| $Q$ | - | relative to the wave modes in $\mathcal{M}_Q$ |
| $r$ | - | relative to the wave modes in $\mathcal{M}_r$ |
| $R$ | - | relative to the wave modes in $\mathcal{M}_R$ |

| | | |
|---|---|---|
| $s$ | - | relative to shear wave mode |
| $w$ | - | relative to the wave modes in $\mathcal{M}_w$ |
| T | - | relative to a Timoshenko beam |
| el | - | relative to fixed-interface mode |
| gl | - | relative to the global system |
| st | - | relative to static mode |
| nom | - | nominal value |
| ref | - | reference value |
| RMS | - | root mean square value |
| w.r.t. | - | with respect to |

### *Latin Letters*

| | | |
|---|---|---|
| $A$ | - | cross-section area |
| $\bar{A}$ | - | averaged nodal cross-section area |
| $C$ | - | coefficient of ordinary differential equation |
| $c_g$ | - | group velocity |
| $d$ | - | first-order differentiation w.r.t. spatial variable |
| $d^2$ | - | second-order differentiation w.r.t. spatial variable |
| $e$ | - | finite element size |
| $E$ | - | Young's modulus |
| $f_{\max}$ | - | maximum frequency |
| $G$ | - | shear modulus |
| $h_y$ | - | height |
| $h_z$ | - | width |
| i | - | imaginary unit $\sqrt{-1}$ |
| $I$ | - | second moment of area |
| $\bar{I}$ | - | averaged nodal second moment of area |
| $l_\lambda$ | - | wavelength |
| $L$ | - | structure length |
| $\mathfrak{L}$ | - | general derivative function |
| $m$ | - | mass |
| $m_{CB}$ | - | multiplication factor |
| $m_\Delta$ | - | number of finite elements across the substructure length |
| $M, m$ | - | external/internal bending moment |
| $\mathbb{M}_Q, \mathbb{M}_R, \mathbb{M}_w, \mathbb{M}_r, \mathbb{M}_k$ | - | sets of wave modes |
| $n$ | - | number of degrees of freedom which discretizes the left (or the right) cross-section of a substructure |
| $N$ | - | number of substructures within a periodic system |
| $N_{DOF}$ | - | number of degrees of freedom defined over a boundary |
| $nr$ | - | number of truncated digits |

| | | |
|---|---|---|
| $\mathcal{O}$ | - | set of integers used to number periodic structures and coupling junctions |
| $P$ | - | component part |
| $r_{Q_j}, r_{Q_j^\star}$ | - | wave amplitude ratios |
| $R_p$ | - | number of periodic structures connected to a coupling junction |
| $t$ | - | time variable |
| $u$ | - | axial displacement along the $x$-direction |
| $v$ | - | transverse displacement |
| $V, f$ | - | external/internal transverse force |
| $\bar{x}$ | - | mean |
| $x$ | - | cartesian axis and direction of wave propagation in one-dimensional periodic systems |
| $y, z$ | - | cartesian axes |

### *Greek Letters*

| | | |
|---|---|---|
| $\sigma$ | - | standard deviation |
| $\omega$ | - | angular frequency |
| $\beta$ | - | wavenumber |
| $\Delta$ | - | substructure length |
| $\eta$ | - | structural damping loss factor |
| $\mu$ | - | propagation constant or eigenvalue of $\mathbf{S}$ |
| $\lambda$ | - | eigenvalue of the matrix pencil $(\mathbf{Z}_1, \mathbf{Z}_2)$ |
| $\sigma_{\mathbf{A}_j}^{(1)}, \sigma_{\mathbf{A}_j}^{(2)}$ | - | singular values of $\mathbf{A}_j$ |
| $\bar{\beta}$ | - | eigenvalue of $\mathbf{H}$ |
| $\rho$ | - | mass density |
| $\nu$ | - | Poisson's ratio |
| $\beta_f$ | - | frequency range of analysis |
| $\rho_s$ | - | spectral radius |
| $\epsilon$ | - | tolerance |
| $\epsilon_Q$ | - | threshold value |
| $\epsilon_{\mu_j}, \epsilon_{\boldsymbol{\mu}}$ | - | errors in eigenvalues |
| $\epsilon_{\phi_j}, \epsilon_{\boldsymbol{\Phi}}$ | - | errors in eigenvectors |
| $\varphi$ | - | rotation |
| $\kappa$ | - | shear correction factor |
| $\Gamma$ | - | boundary interface |
| $\gamma_j$ | - | modal mass |
| $\omega_j$ | - | eigenpulsation |

*Acronyms*

| | | |
|---|---|---|
| **AMLS** | - | Automated MultiLevel Substructuring |
| **BC** | - | Boundary Conditions |
| **BE** | - | Boundary Element |
| **BEM** | - | Boundary Element Method |
| **CB** | - | Craig-Bampton |
| **CMS** | - | Component-Mode Synthesis |
| **DOF** | - | Degree of Freedom |
| **DSM** | - | Dynamic Stiffness Matrix |
| | | or Dynamic Stiffness Method |
| **EFEM** | - | Energy Finite Element Method |
| **FDTD** | - | Finite Discrete Time Difference |
| **FE** | - | Finite Element |
| **FEM** | - | Finite Element Method |
| **FFT** | - | Fast Fourier Transform |
| **FRF** | - | Frequency Response Function |
| **IEM** | - | Infinite Element Method |
| **HF** | - | High-Frequency |
| **LF** | - | Low-Frequency |
| **LR** | - | Locally Resonant |
| **MAC** | - | Modal Assurance Criterion |
| **MC** | - | Monte Carlo |
| **MF** | - | Mid-Frequency |
| **PC** | - | Phononic Crystal |
| **PWE** | - | Plane Wave Expansion |
| **RM** | - | Receptance Matrix |
| | | or Receptance Method |
| **RMS** | - | Root Mean Square |
| **RO** | - | Reduced-Order |
| **SAFE** | - | Semi-Analytical Finite Element |
| **SAM** | - | Spectral Analysis Method |
| **SEA** | - | Statistical Energy Analysis |
| **SEM** | - | Spectral Element Method |
| **SFE** | - | Spectral Finite Element |
| **SmEdA** | - | Statistical modal Energy distribution Analysis |
| **SVD** | - | Singular Value Decomposition |
| **WB** | - | Wave Based |
| **WBM** | - | Wave Based Method |
| **WFE** | - | Wave Finite Element |
| **WSFEM** | - | Wave Spectral Finite Element Method |

## *Other Notations*

| | | |
|---|---|---|
| 0D | - | zero-dimensional |
| 1D | - | one-dimensional |
| 2D | - | two-dimensional |
| 3D | - | three-dimensional |
| $\Re(\ )$ | - | real part of a number |
| $\Im(\ )$ | - | imaginary part of a number |
| $\kappa(\ )$ | - | condition number of a matrix |
| $\mathrm{sgn}(\ )$ | - | sign function |
| $\|\ \|$ | - | absolute value of a number |
| $\{\ \}_j$ | - | Indexed family of vectors, where the index $j \in I$ and $I$ is an index set |
| $\|\ \|_p$ | - | $p$-Norm of a vector |
| $\|\ \|_F$ | - | Frobenius-Norm of a vector |
| $\dot{\ }$ | - | First-order differentiation w.r.t. time variable |
| $\tilde{\ }$ | - | expressed in terms of a reduced set of wave modes |
| $\bar{\ }$ | - | expressed in terms of a reduced set of fixed-interface modes |
| $\hat{\ }$ | - | expressed in terms of the global reference frame |
| bold font-weight | - | vectors and matrices |
| normal font-weight | - | scalars |

# TABLE OF CONTENTS

# 1 Introduction

## 1.1 Motivation

Since the early days of aeronautics, there has always been an interest in assessing the dynamic response of structural systems. The interest may be either at the design stage or during operation. In the former case, understanding the dynamic response of the system is important for the purpose of modeling. On the other hand, during operation, it allows structural health monitoring and control. Regarding the kind of analysis, analytical, numerical, or experimental studies can be performed. Although experimental tests may provide the best reproduction of the system behavior, they are usually expensive and may take a long time to be performed. At the design stage of the development of complex real engineering systems, a fast and cheap numerical analysis is sought for predicting their dynamic responses. This is because, at this stage, one of the main concerns is the difficulty in meeting the design criteria, which usually require structural optimization involving dynamic responses. Moreover, variability is often present in manufacturing processes and it causes a deviation from the nominal design specification which affects the structural response. Due to the growing demands for robust optimum design prediction, the development of numerical tools for uncertainty quantification in industrial applications is of importance for design engineers. However, either in optimization or uncertainty analyses, the use of conventional prediction tools for structural dynamics, such as the finite element method (FEM) (Petyt, 2010), may not be convenient due to excessive computational cost. This is because, in both cases, the dynamic problem under concern must be solved several times. The issue becomes critical when a very large number of degrees of freedom is involved. This motivates the development of reliable and efficient predictive numerical tools.

In this thesis, the interest lies in developing efficient numerical approaches for the forced response computation of periodic structures. Indeed, we are interested in mechanical systems which are composed of periodic structures or structures that can be approximately modeled as one. Engineering systems like those are common in real applications; we can mention, for instance, train rails (Figure 1.1(a)[1]), pipeline systems (Figure 1.1(b)[2]) in the oil and gas industry, some nanostructures

---

[1]available on www.blacknaija.com/new-update/lagos-calabar-rail-line-underway-jonathan on July 29th, 2015.

[2]available on www.pennenergy.com/articles/pennenergy/2013/02/magellan-acquires-800-miles-of-pipeline on July 29th, 2015.

like the nanorods, nanobeams and nanotubes (Figure 1.1(c)[3]), aircraft fuselages (Figure 1.1(d)[4]) or the fuselage of a space shuttle (which can be roughly regarded as stiffened cylindrical shells) in the aerospace industry, tires and chassis frames (Figure 1.1(e)[5]) in the automotive industry and the hull of a submarine (Figure 1.1(f)[6] ) in the naval industry. Since periodic structures are formed by a regular repetition of a periodic unit in space, by applying periodic boundary conditions, only one periodic unit needs to be modeled in order to describe the dynamics of the whole structure. This yields a reduction of the problem size to be solved and it allows for the use of less complicated numerical techniques. One of the aims of this thesis is, thus, to propose numerical approaches that can describe low-to-mid frequency dynamics of periodic structures and that can compete in accuracy and computational time with conventional numerical methods, such as FEM associated with substructuring techniques such as the Craig-Bampton (CB) method (Craig and Bampton, 1968a).



|     (a)     |     (b)     |     (c)     |



|     (d)     |     (e)     |     (f)     |
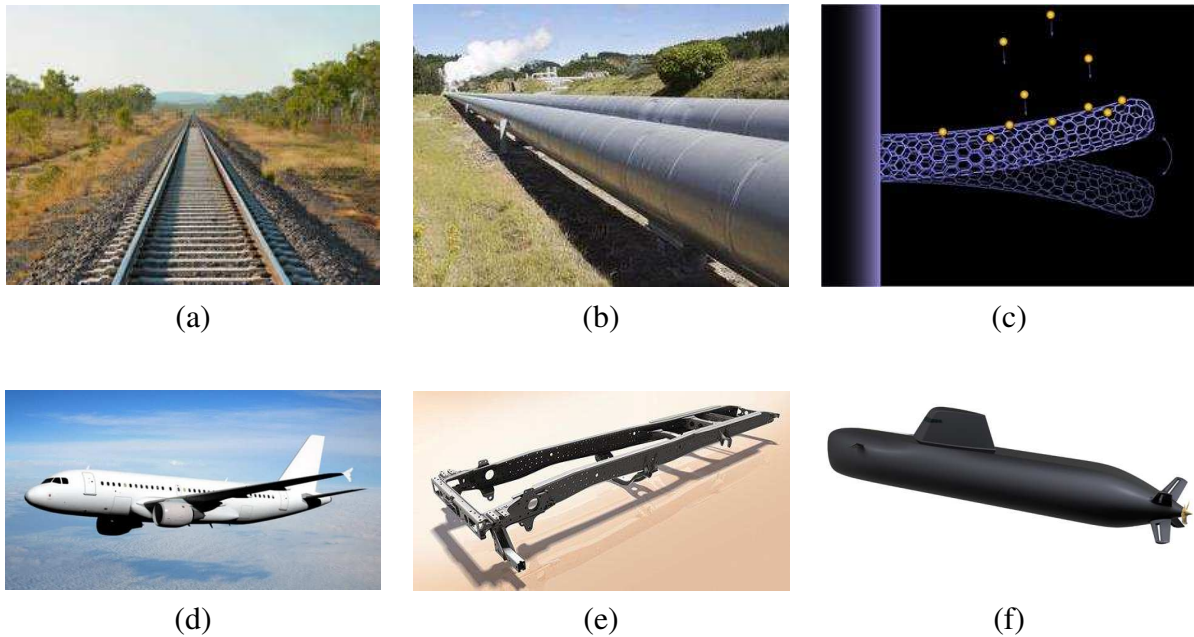
Figure 1.1: Examples of real engineering structures which can be regarded as waveguides (a, b, c) or which are composed of periodic parts (d, e, f): (a) train rail, (b) pipeline system, (c) nano sensor, (d) aircraft structure, (e) chassis frame, (f) submarine.

Besides, from the physical point of view, periodic structures have attracted a lot of attention due to the striking possibility of controlling mechanical and electromagnetic waves. Within the

---

[3]available on www2.lbl.gov/publicinfo/newscenter/features/2008/MSD-golden-scales on July 29th, 2015.

[4]available on business.citifmonline.com/2014/11/06/41227/ on July 29th, 2015.

[5]available on www.mercedes-benz.com.au/content/australia/mpc/mpc_australia__website/en/home_mpc/truck_home/home/trucks/actros/chassis on July 29th, 2015.

[6]available on www.naval-technology.com/projects/andrasta-submarine/andrasta-submarine2 on July 29th, 2015.

framework of this thesis, we are only concerned with the mechanical properties of these structures. The regular arrangement of such structures may give rise to frequency zones in which waves do not propagate or are highly attenuated — *i.e.*, the so-called band gaps or stop bands. The design of periodic structures with a view to optimize the positioning of band gaps within a specific frequency band and their characteristics make them good candidates to work as passive vibroacoustic filters.

In the context of structural dynamic analysis of weakly dissipative complex structures, three different frequency bands can be defined within the audio-frequency range, which is the frequency range of interest for automotive and aerospace structures (Ohayon and Soize, 1998; Desmet *et al.*, 2012). In practice, numerical methods for frequency response analysis are usually developed for a limited frequency range (see Figure 1.2). The limitations are either due to the practical limits of computing power or to the constraints imposed by the hypotheses underlying the employed theory. At low frequencies, *i.e.*, the domain of analysis characterized by low modal density, the FEM is one of the most powerful and popular computational methods. It allows to easily model complex structures and it is available in many commercial softwares. However, as it makes use of frequency independent shape functions to approximate structural responses, the mesh size should be sufficiently small compared to the smallest wavelength within the frequency range of analysis in order to guarantee an accurate solution. Thus, as the frequency rises, finite element (FE) models become extremely large and the computational cost sets a practical high frequency limit for the low-frequency (LF) range. Other deterministic methods can be used to perform LF analyses, such as the boundary element method (BEM) (Lachat and Watson, 1976), the infinite element method (IEM) (Bettess, 1977; Bettess and Zienkiewcz, 1977) and the spectral element method (SEM) (Doyle, 1997; Lee, 2009). The common feature of these methods is that in all of them the continuum domains or their boundary surfaces are discretized into elements within which the field variables — *i.e.*, kinematic (displacements/rotations) and kinetic (forces/moments) quantities — are described.

On the other hand, at high frequencies, vibroacoustic systems exhibit a high modal density and their responses are very sensitive to uncertainties in the model parameters, such as: geometrical component dimensions, material properties, and boundary conditions. Thus, differently from the LF range, where the structural response is deterministic and numerical methods such as FEM, BEM and SEM are computationally efficient, in the high-frequency (HF) range it is more appropriate to consider the averaged dynamic response and the associated confidence levels for a population of nominally identical systems. This has led to the development of probabilistic techniques, of which

3
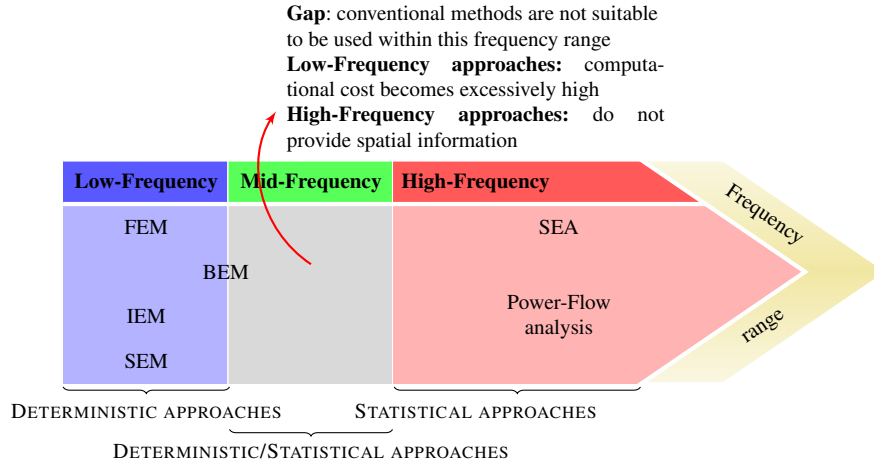
Figure 1.2: Scheme relating conventional numerical methods with distinct ranges of the frequency domain.

the most popular one is the statistical energy analysis (SEA) (Lyon, 1975; Maidanik, 1981). In developing this numerical method, a diffuse field is assumed — *i.e.*, the time-averaged energy is considered the same within a subsystem—, subsystems are assumed weakly coupled and the excitation forces uncorrelated. The methodology of HF numerical approaches is based on expressing the energy balance for various subsystems.

In recent years, researchers have been concerned about a mid-frequency (MF) gap in modeling capabilities (Desmet and Vandepitte, 2002; Mencik and Ichchou, 2008; Desmet *et al.*, 2012), *i.e.*, the available prediction techniques were not suitable to model structural acoustic systems at mid frequencies. In this intermediate frequency range, the modal density exhibits large variations, hence the dynamic behavior of coupled systems is expected to involve global as well as local resonances (Ohayon and Soize, 1998; Mencik and Ichchou, 2008). Thus, it is expected that the structure response might be affected by variability at mid frequencies. The lower and upper limits of this frequency range are qualitatively defined as the frequencies in which the computational cost of FE simulations becomes too high and the minimum frequency for which SEA solution is appropriate, respectively. Consider the case of a free-free rod subjected to uniform axial force applied to its left end as shown in Figure 1.3(a). In Figure 1.3(b), velocity responses obtained through Monte Carlo (MC) simulations (Metropolis and Ulam, 1949) with $197$ trials , $\bar{x}(E) = E_{\mathrm{nom}}$ and $\sigma(E) = 0.05\, E_{\mathrm{nom}}$ — where $E$ denotes the Young's modulus, and $\bar{x}$ and $\sigma$ stand for the mean and standard deviation of the sample, respectively — are plotted against the nominal response of the structure. The results confirm that at low frequencies — *i.e.*, below $300$ kHz in the present case — the structural response is deterministic. However, for frequencies higher than $300$ kHz, the

structure response becomes really sensitive to perturbations, which is a feature of the MF range. In order to bridge the gap in dynamic analysis, wave-based methods have been employed. A scheme is presented in Figure 1.2 to shed light on this frequency issue.



(a)　　　　　　　　　　　　　　　　　　　(b)
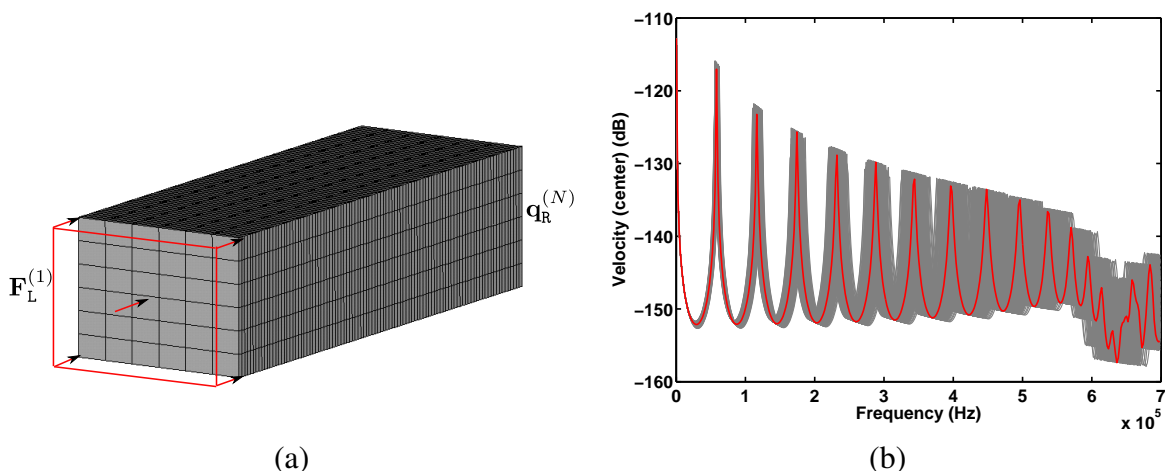
Figure 1.3: Dynamic analysis of a free-free rod subjected to axial force at its left end: (a) sketch of the problem case, velocity solution in the $x$-direction at the center of the right cross-section computed by means of WFE-based DSM (Section 3.2.2):(—) for $E = E_{\mathrm{nom}}$, (—) for MC simulations with 197 trials, $\bar{x}(E) = E_{\mathrm{nom}}$ and $\sigma(E) = 0.05\, E_{\mathrm{nom}}$.

According to Desmet and Vandepitte (2002), three major methodologies can be adopted to solve the mid-frequency issue. One of them consists in developing efficient deterministic-based methods for the MF range. A second one proposes probabilistic-based approaches which attempt to relax some stringent assumptions of SEA and provide spatial information. Among them, one can cite the energy finite element method (EFEM) (Nefske and Sung, 1989; Shorter and Langley, 2004; Shorter and Langley, 2005), the statistical modal energy distribution analysis (SmEdA) (Maxit and Guyader, 2001a; Maxit and Guyader, 2001b) and the wave intensity analysis (Langley, 1992). Finally, the third possible methodology combines deterministic and probabilistic techniques. In this case, the strongly coupled and stiff structures are modeled deterministically, while weakly coupled and flexible parts are modeled statistically using SEA (Soize, 1993; Ohayon and Soize, 1998; Langley and Bremner, 1999). The development of numerical methods for mid-frequency range analysis is also a motivation for this work. The numerical approaches considered here follow the first methodology. Hence, the computational performance of the novel techniques compared to the conventional finite element method is one of the major issues addressed in this thesis.

Here, wave-based numerical approaches have been developed. Although the use of such tech-

niques in structural dynamics analysis has a long history, the abundance of computing power has contributed to the dominance of modal approaches (Arruda and Silva, 2015). This might be explained by the widespread use of FEM in structural linear dynamic analysis. It was only recently, with the development of symbolic computation, that analytical and numerical wave-based methods have attracted some renewed interest. It is worth recalling here the main features of the wave and modal approaches.

The modal approach consists in approximating the response of finite structures as a superposition of mode shapes, which satisfy the same boundary conditions that the displacement field does. In other words, the mode shapes describe vibration patterns of the finite dynamic system at specific angular frequencies, *i.e.*, the natural frequencies, which depend on the boundary conditions. On the other hand, wave approaches involve the solution of the problem for an infinitely extended dynamic system by means of a superposition of waves. The response of a finite structure can also be addressed by considering wave reflections and transmissions within its boundaries. The modal and wave descriptions of finite systems are fully equivalent to each other. However, depending on the frequency range of interest or the aspect of structural vibration under concern, one description can be preferred in detriment of the other. For instance, the number of vibration modes required to describe the response of a dynamic system appears to be more influenced by the frequency rise than the number of wave modes. Indeed, the wave modes are not dependent on the structure length and boundary conditions. Vibration modes are due to the interference of waves and also their interaction with the system boundaries. Therefore, the number of waves to be considered is likely to be smaller than the corresponding number of vibration modes. For instance, let's consider the free-free rod problem previously stated (see Figure 1.3(a)). Table 1.1 provides a comparison between the number of wave modes and that of vibration modes to be considered in order to get accurate responses at the opposite end with respect to the WFE-based DSM solution (see Section 3.2.2). The velocity responses computed by means of a wave-based and a modal-based approach are shown in Figure 1.4. The results highlight the relevance of a wave-based approach — here, the reduced-order WFE-based approach was employed (see Section 3.3) — in terms of computational savings compared to a modal-based one — here, the CB method was employed (see Annexe A).

The development of wave-based approaches in this thesis is also motivated by the possibility of assessing the dynamic behavior of periodic structures by means of dispersion relations. This feature of wave-based approaches is interesting as it avoids the need of computing the forced response. As a matter of fact, the dispersion relations provide information about the characteristics of waves traveling along an infinite medium. Thus, far from the excitation source and boundaries,

6

Table 1.1: Comparison between wave and modal approaches in the simulation of a free-free rod structure subjected to uniform axial force.

| Maximum Frequency | $\lambda$ | Modal approach | | Wave approach | |
|---|---|---|---|---|---|
| | | nb of modes | error | nb of waves | error |
| 700 kHz | 0.0050 m | 650 | < 20 % | 6 | < 20 % |
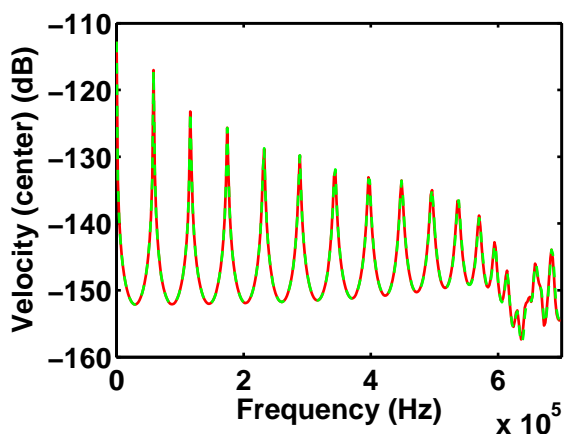


Figure 1.4: Velocity solution in the $x$-direction at the center of the right cross-section of a free-free rod subjected to axial force at its left end, computed by means of: (—) a wave-based approach, (- -) a modal-based approach.

the response of a finite structure is approximately known. Then, if one is interested in the far-field dynamic behavior of a structure, optimization and uncertainty quantification analyses can be performed based on the information provided by dispersion relations. Moreover, dispersion relations are important tools in the design of periodic structures exhibiting band gaps, as it will be discussed in Chapter 5.

In recent years, a lot of research has been conducted on the development of the wave finite element (WFE) method (Mace *et al.*, 2005; Mencik and Ichchou, 2005; Mencik, 2014; Silva *et al.*, 2014b). This is a numerical wave-based method for describing the dynamics of periodic structures. As it involves the modeling of only one periodic unit by means of conventional FEs, the

model size is considerably reduced compared to the full FE model. For this reason, the WFE method is often presented as a suitable method for describing MF dynamics (Desmet *et al.*, 2012; Mencik, 2010). As a wave-based method, the dynamic behavior of periodic structures can be assessed through the computation of dispersion relations and forced responses. Inspired on SEM, which uses a basis of analytical waves to build spectral superelements, this thesis is concerned about the formulation of WFE-based superelements of periodic structures composed of an arbitrary number of periodic units. The key point here is the possibility of using conventional assembly techniques to handle coupled systems. Moreover, the use of FEs to model the periodic unit makes it possible to describe complex structures, which, in the wave domain, are characterized by higher-order waves. Hence, another motivation for this work is the possibility of building numerical spectral elements of arbitrary order. The origin of this work was set by Nascimento (2009), who proposed a hybrid approach — *i.e.*, the wave spectral finite element method (WFSEM) — and used it to formulate numerical spectral elements of rod and Euler-Bernoulli beam. The scheme in Figure 1.5 summarizes the motivations for the developments in WFE-based superlement matrices.
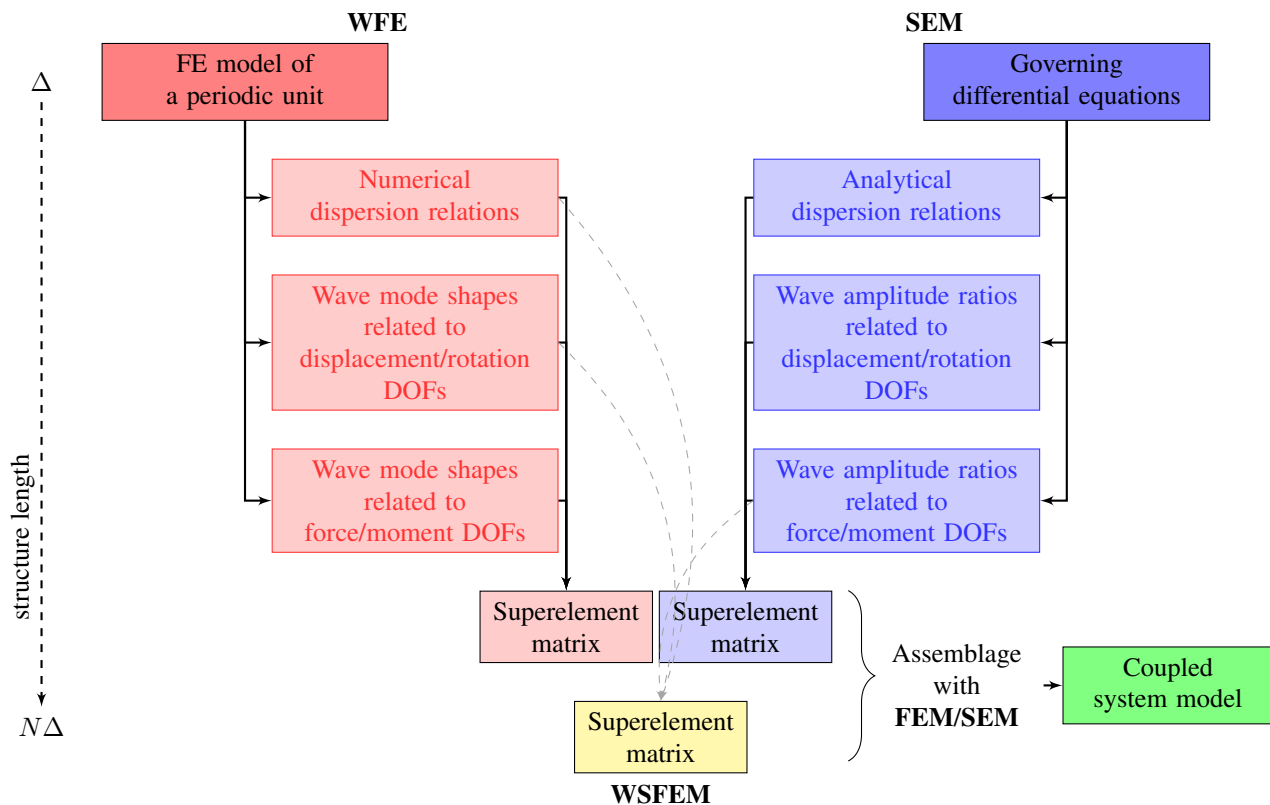


Figure 1.5: Graphical representation of the general scheme for the formulation of wave-based numerical superelement matrices in this thesis.

## 1.2 Literature review

### 1.2.1 Periodic structures

A periodic structure consists of a regular arrangement of identical elements along one or more directions. Within the framework of this thesis, only one-dimensional (1D) periodic structures have been considered. The study of wave propagation through periodic media has attracted the interest in various application fields as, for instance, solid state crystals, optics, acoustics and vibrations. The common feature among them is that, in all those fields, the wave propagation is governed by partial differential equations with periodic coefficients, which stand for material parameters related to the physics being described.
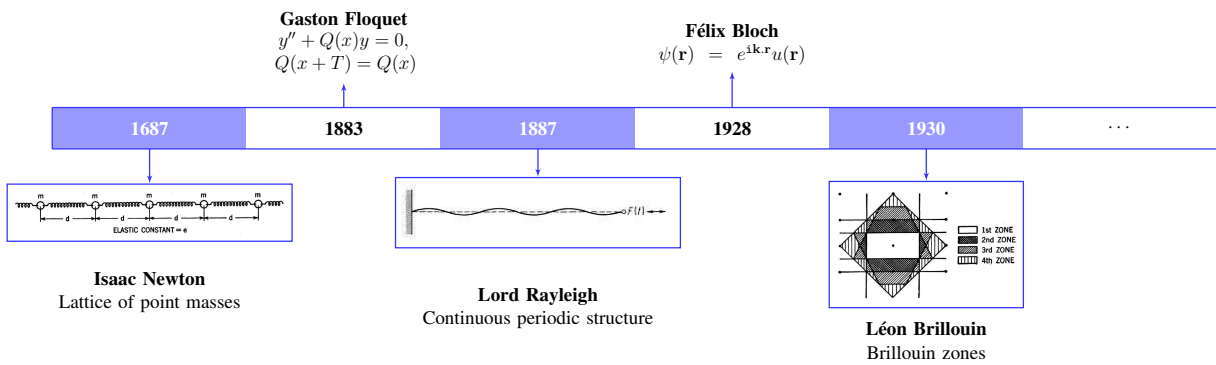


Figure 1.6: Historical timeline presenting remarkable contributions on the study of periodic structures.

The wave motion in periodic systems has been studied for centuries. It dates back to the seventeenth century when Newton attempted to determine the sound velocity in air by considering the elastic wave propagation through an one-dimensional lattice of point masses connected to springs (Newton, 1687 apud Brillouin, 1946). From a mathematical point of view, the basis for the study of periodic structures was pioneered by Floquet (1883), which proposed analytical solutions to ordinary differential equations with periodic coefficients. Until 1887, only discrete models of periodic structures composed of regular lattices of springs connected to point masses had been considered. In 1887, the first continuum model of a periodic structure was studied by Rayleigh (1887 apud Mead, 1996), which consisted in an stretched string with continuous and periodic variation of density along its length. Later, Bloch (1928) extended the results presented by Floquet (1883) for the

1D spatial periodicity to the three-dimensional (3D) case. He showed that the solutions for general periodic structures are such that

$$\mathbf{q}(\mathbf{r}) = \mathbf{q}_\beta(\mathbf{r})e^{\mathrm{i}\boldsymbol{\beta}\cdot\mathbf{r}}. \qquad (1.1)$$

The geometric interpretation concerning the wave behavior in periodic structures was proposed by Brillouin (1946). He showed that there are irreducible zones in the wavenumber 3D space in which the wave behavior in periodic structures is completely described — the so-called Brillouin zones. These first important milestones on the study of periodic structures are shown in Figure 1.6.

Since then, important developments on state-solid physics, optics and electrical transmission lines have been observed due to a broader understanding of the physical wave phenomena in periodic systems. Later, elastic wave propagation has been considered. Cremer and Leilich (1953) studied the flexural wave motion in periodic beam structures. By means of reflection and transmission coefficients, Heckl (1964) has studied the wave propagation in grillages. The interest in understanding the structural vibrations caused by the noise of jet engines has motivated a series of works concerning the wave propagation in periodic beams, rib-skin structures, plates and cylindrical shells developed at the University of Southampton since 1964 (Mead, 1996). At the beginning, receptance methods such as the direct method and the transfer matrix method have been used to study the free and forced responses of periodic structures. Later, much effort has been placed in developing numerical approaches which take advantage of the structure periodicity. Indeed, these methods in general make use of Bloch's theorem, which states that, regardless the nature of the propagating wave, only a special type of waveform may propagate in periodic media (Gazelet *et al.*, 2013). Among these approaches, the most popular ones are the plane wave expansion (PWE) method, the finite discrete time difference (FDTD) method and the WFE method. PWE or method of space-harmonics is a Fourier domain method for calculating the dispersion curves (or band structures) of infinite periodic structures (Economou and Sigalas, 1993; Miyashita, 2005; Xiao *et al.*, 2012; Gazelet *et al.*, 2013). The analysis of finite size periodic structures can be addressed by means of the FDTD method, which involves the discretization of both time and spatial domains. It has the advantage of enabling the simulation of the propagation in more complex periodic structures than analytical methods and it is of simple implementation. However, in order to guarantee stability and avoid numerical dispersion, very fine discretizations are necessary, which require the use of formidable computational resources (Busch *et al.*, 2007).

The wave behavior of periodic structures presents interesting features, which are due to the unusual dispersion relations that are characteristic of Bloch waves. Indeed, periodic media exhibit

band structure, *i.e.*, there may be frequency intervals in which the propagation of certain waves are not allowed. These frequency bands are usually known as band gaps or stop bands, as opposed to pass bands, *i.e.*, intervals of frequency in which waves are allowed to propagate.

Although the dispersive characteristics of general periodic media have been known for a long time, only recently the potential of these structures for enabling new technological devices and applications has been recognized. The papers of Yablonovitch (1987) and John (1987) are in general considered the responsible for opening this research in the electromagnetic field with photonic crystals. The success of this research in optics has motivated similar researches in the acoustic and vibration fields. Periodic systems designed for elastoacoustic wave propagation have the potential to be used as passive frequency filtering devices, beam splitters, sound or vibration protection devices, acoustic lasers and superlenses, acoustic cloaking devices, and waveguides, among other applications (Sigmund and Jensen, 2003; Deymier, 2013).

The development of passive vibration control strategies for periodic structures that use band gaps is a current research topic, which aims at proposing efficient lightweight solutions for global reduction of the vibration levels. There exist two band gap mechanisms which are Bragg scattering (Sigalas and Economou, 1992; Kushwaha *et al.*, 1993; Kushwaha *et al.*, 1994) and local resonance (Liu *et al.*, 2000; Goffaux *et al.*, 2002). Regarding Bragg scattering, band gaps represent zones of destructive interference between incident and reflected waves which occur when the wavelengths are of the same order as the dimension of the periodic units. This means that band gaps in the low-frequency range are usually possible only in large structures. In elastodynamics, this mechanism has been investigated in numerous engineering systems, which are usually named phononic crystals (PCs), such as rods, plates and cylindrical shells (Bennett and Accorsi, 1994; Lee *et al.*, 2010; Sorokin and Ershova, 2004; Goldstein *et al.*, 2011). More recently, researchers in the field have moved their attention to locally resonant (LR) structures motivated by the possibility of designing band gaps at low frequencies, up to two orders of magnitude smaller than those created via Bragg scattering (Liu *et al.*, 2000). For instance, one can mention locally resonant phononic crystals, also known as metamaterials, which exhibit effective negative elastic constants in certain frequency bands. The key idea here is to consider periodic arrays of locally resonant devices which are attached to periodic structures. Although the concept has been applied to academic structures such as strings, rods, beams, and plates (Xiao *et al.*, 2011; Xiao *et al.*, 2012; Xiao *et al.*, 2013; Wang *et al.*, 2013), its application to complex structures with periodic heterogeneities seems to constitute an open research topic.

### 1.2.2 Wave-based methods

The analytical wave propagation solution of a dynamic problem is possible through consideration of the governing differential equations for the structural model under consideration. The field variables — *i.e.*, kinematic (displacements/rotations) and kinetic (forces/moments) variables—, in this case, are functions of space and time. By making use of the Fourier transform, the displacements/rotations at a particular point can be expressed in spectral form as

$$\mathbf{q}(x,y,z,t) = \sum_n \hat{\mathbf{q}}_n(x,y,z,\omega_n)e^{\mathbf{i}\omega_n t}, \tag{1.2}$$

where the coefficients $\hat{\mathbf{q}}_n$ are functions of the space $(x, y, z)$ and angular frequency $\omega$. Substituting this expression in the equations of motion yields a frequency domain formulation, which can provide fast steady state solutions, as well as transient solutions in the case some damping is present, if the Fourier transform is applied.

Consider the following general, linear, and one-dimensional homogeneous equation of motion in the frequency domain:

$$C_0(x,\omega) + C_1(x,\omega)\frac{d\hat{\mathbf{q}}}{dx} + C_2(x,\omega)\frac{d^2\hat{\mathbf{q}}}{dx^2} + \cdots = 0, \tag{1.3}$$

where $C_0, C_1, \cdots$ are coefficients which may depend on the space and frequency. The subscript $n$ is dropped for the purpose of brevity. In the special case where these coefficients are periodic with respect to the space variable $x$ or constant — *i.e.*, is a particular case of the periodicity assumption —, a second Fourier transformation can be considered. Then, the harmonic solutions may expressed as

$$\hat{\mathbf{q}}(x,y,z,\omega) = \sum_m \bar{\mathbf{q}}_m(y,z,\omega,\beta_m)e^{-\mathbf{i}\beta_m(\omega)x}, \tag{1.4}$$

where $\beta_m$ are complex wavenumbers and the coefficients $\bar{\mathbf{q}}_m$ have the meaning of wave amplitudes.

Transforming the wave representation — which involves the computation of wave amplitudes — into a dynamic stiffness representation facilitates the use of wave-based methods by users familiar with dynamic analyses via the finite element method. This has been the motivation behind the development of the spectral element method (SEM) (Silva *et al.*, 2014a; Beli *et al.*, 2015), which was introduced by Narayanan and Beskos (1978) and, organized, later, by Doyle (1989).

A comprehensive reference concerning the method is the book published by Lee (2009). Like the dynamic stiffness method (DSM) (Kolousek, 1941 apud Lee, 2009; Leung, 1993), the exact dynamic stiffness matrix of a structural element is formulated. Then, because it is an element-based method, discretization is also possible and it might be required when externally applied loads or discontinuities of material or geometric type exist within the spatial domain of concern. As the conventional FEM, SEM is stiffness formulated, thus spectral element matrices of subsystems of a coupled problem can be assembled in an analogous way as in FEM in order to form a global system matrix. Moreover, as any other analytical approach, it gives accurate solutions, which are considered exact provided all assumptions made are within the scope of the theory adopted to model the problem. Thus, only one spectral element is sufficient to model a regular structure without discontinuities. It is also worth mentioning that the field variables are represented as a superposition of a finite number of wave modes at discrete frequencies, which results from the application of the fast Fourier transform (FFT) in the time and space domains as the spectral analysis method (SAM) does.
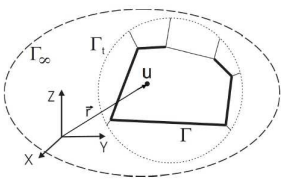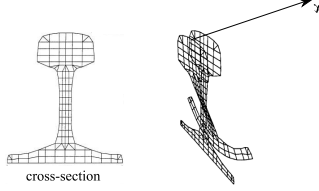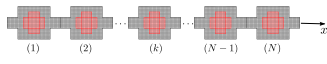
Many mechanical structures are made of thin panels and beams. Waves that propagate in waveguides formed by two parallel free surfaces are referred to as Lamb waves (Graff, 1975; Doyle, 1997). These include flexural, torsional, longitudinal and other types of elastic waves. Low order flexural waves can be modeled, at low frequencies, using theories such as Euler-Bernoulli's and Timoshenko's for beams and Kirchhoff's and Mindlin-Reissner's for plates. At higher frequencies, higher order theories such as Flügge's and Donnell-Mushtari's for cylindrical shells and Mindlin-Herrmann's for rods can be used to predict analytically the wave solution for simple geometries. In the case of more complex geometries, modeling can only be achieved practically using numerical methods such as finite and boundary element methods.

Wave-based methods can take advantage of the particular characteristics and symmetry of waveguides and allow in many cases a more accurate prediction of the dynamic behavior with less computational effort. Wave-based solutions either do not require mesh refinement (wave propagation solution, SEM) or the solutions are approximated by frequency dependent shape functions, which allow faster convergence than the ordinary ones used by the conventional FEM. Thus, they might be, in many applications, efficient numerical approaches for MF analysis.

As pointed out earlier, the ability of handling MF analysis has also motivated the development of such techniques. Among them, we may cite the wave based method (WBM), which makes use of an indirect Trefftz approach (Desmet and Vandepitte, 2002; Desmet *et al.*, 2012), the semi-

analytical finite element (SAFE) method (Gavrić, 1994; Gavrić, 1995), which has the spectral finite element (SFE) method (Finnveden, 1997; Birgersson *et al.*, 2005) as one of its variants, and the wave finite element (WFE) method (Mace *et al.*, 2005; Mencik and Ichchou, 2005). The main features of those wave-based methods are summarized in Table 1.2.

Table 1.2: Main features of wave-based methods for MF dynamic analysis.

| WBM | SAFE | WFE |
|---|---|---|
| (B. Pluymers, W. Desmet, D. Van-depitte) | (L. Gavrić, S. Finnveden, F. Birg-ersson, C. M. Nilsson, P. Loveday, A. Marzani) | (D. J. Mead, B. R. Mace, D. Duhamel, J.-M. Mencik, M. N. Ichchou, J. R. F. Arruda) |
|  |  |  |
| general bounded / unbounded domains | waveguides | waveguides / periodic struc-tures |
| indirect approach | FE model of the cross-section | FE model of a periodic unit |

The WBM has been developed for nearly a decade now and it is used to solve bounded and unbounded steady-state dynamic problems. The field variables are expressed as an expansion of wave functions. The wave functions are chosen such that the homogeneous form of the governing equations as well as certain global boundary conditions are satisfied. The degrees of freedom are not the dynamic field variables, but the weighting factors of the wave functions in the expansion. For this reason, it is considered an indirect approach. Using a weighted residual formulation in or-der to enforce boundary and continuity conditions, it yields a linear system of equations in terms of the wave weighting factors. Compared to element based methods (FEM or BEM), the wave based (WB) model does not require the discretization of the domain into small elements, only a partition-ing into convex subdomains, which can be large and their sizes are independent of frequency since exact wave functions are used to describe the dynamic response. On the other hand, the WB system matrices are dense and ill-conditioned, which makes the construction of WB matrices computation-ally more demanding than FE or boundary element (BE) matrices. However, as the problem size is usually much smaller and the convergence rate higher, it is still suitable for MF analysis.

While the WBM is a wave-based technique able to model structures that are not necessarily periodic, but which can be partitioned into convex subdomains (Genechten *et al.*, 2008), many researchers have been working in wave-based methods which make use of the symmetry and/or

periodicity of structural waveguides and periodic structures in order to efficiently describe MF dynamics.

The work published by Nelson *et al.* (1971) has led the way for the development of numerical wave-based methods for waveguides. The approach proposed in that work is, in fact, a semi-analytical technique, where the displacement field for a waveguide undergoing steady state harmonic motion with angular frequency $\omega$ is written as

$$\mathbf{q}(x,y,z,t) = \hat{\mathbf{q}}(y,z)e^{\mathbf{i}(-\beta x + \omega t)}. \tag{1.5}$$

Here, $\hat{\mathbf{q}}(y,z)$ is a spatial vector function which describes the displacements of the waveguide cross-section, $t$ is time variable, $x$ is the main axis of the waveguide and $\beta$ is the wavenumber relative to elastic waves traveling in the $x$-direction. The equations of motion in this case are obtained from Hamilton's principle by considering the expression for the waveguide displacements (Equation (1.5)). The displacement field of the waveguide cross-section $\hat{\mathbf{q}}(y,z)$ is described by means of a two-dimensional (2D) finite element formulation in the case of a 3D model — or 1D and zero-dimensional (0D) FE formulations for 2D and 1D models, respectively. The numerical problem here consists in solving matrix equations of motion of the discretized waveguide for complex valued-scalars $\beta$, *i.e.* the wavenumbers, and complex vectors $\breve{\mathbf{q}}$, which has the meaning of cross-section wave mode shapes, for a given frequency $\omega$.

Such a numerical method was used by Nelson *et al.* (1971) for the analysis of laminated orthotropic cylinders. Then, the study was also applied to laminated orthotropic plates (Dong and Nelson, 1972). One year later, Aalami (Aalami, 1973) analyzed 3D prismatic guides using a two-dimensional interpolation function to describe the displacement field in a bar with arbitrary cross section. Then, more recently, Gavrić (Gavrić, 1994; Gavrić, 1995) used a similar approach to obtain dispersion properties of thin-walled beams and a free rail. The strategy used by Gavrić in his works has been applied by many researchers to compute frequency and time transient responses of elastic and viscoelastic waveguides (Loveday, 2008; Marzani, 2008), or associated with classical finite element method to study the interaction of guided waves with non-axisymmetric damage (Benmeddour *et al.*, 2011). This method is usually known as the semi-analytical finite element (SAFE) method. Variants of this method have been applied by researchers to model, among other applications, rail tracks (Gry and Gontier, 1997), fluid-filled pipes (Finnveden, 1997), plates (Birgersson *et al.*, 2005)), beams and shells (Mazuch, 1996; Volovoi *et al.*, 1998), and thin-walled structures (Nilsson, 2002).

### 1.2.3 The wave finite element method

The study of the propagation of waves in periodic systems within the framework of Rayleigh's method and of the Rayleigh-Ritz technique was proposed independently by Mead (1973) and Abrahamson (1973). These studies revealed the possibility of applying approximate methods such as the finite element method to wave propagation in periodic structures. The paper published by Mead (1973) is regarded as the starting point for the development of a wave-based numerical method for general periodic structures: the WFE method. In this work, Mead presented the general theory of wave propagation for periodic structures. Initially, a simplified version of this theory was applied to rib-skin structures and beams with periodic supports, which were analyzed by means of analytical methods, such as the receptance method (Sen-Gupta, 1971), the direct solution (Mead, 1970), and the transfer matrix method (Lin and McDaniel, 1969). Then, the work published by Mead (1973) extended the wave propagation theory to general multi-coupled periodic structures — *i.e.*, structures which are coupled to other structural components through many degrees of freedom. The use of this theory for periodic structures in conjunction with the h-version of FEM was first performed by Orris and Petyt (1974). In the 1980's, the p-version of FEM was used to study the wave propagation in stiffened plates and cylindrical shells (Mead and Bardell, 1986; Mead and Bardell, 1987; Mead *et al.*, 1988; Bardell and Mead, 1989a; Bardell and Mead, 1989b). In association with FEM, the periodic structure theory was also used to investigate the vibrations in a periodic truss (Signorelli and von Flotow, 1988) and supported rails (Thompson, 1993). Using the symplectic property of the eigenvalue problem formulated by means of the WFE method for symmetric substructures, alternative procedures for computing the propagation constants and wave mode shapes related to waves propagating in periodic structures were proposed by Zhong and Williams (1995).

With the advent of powerful computers, recent works have been done with the aim of taking advantage of the structural periodicity and make finite element computations more efficient (Mace *et al.*, 2005; Mencik and Ichchou, 2005; Duhamel *et al.*, 2006; Mencik and Ichchou, 2008). These works have also been motivated by the necessity of developing numerical techniques capable of describing the dynamics of engineering systems in the MF range. Thus, closed-form formulations for the method which are based on the periodic structure theory (Mead, 1973) and use conventional finite elements to model a substructure were presented, independently, by Mace *et al.* (2005), and by Mencik and Ichchou (2005). Since then, the acronym WFE has been used to refer to this numerical method, which has received various names, such as waveguide finite element (Mace *et al.*, 2005;

Duhamel *et al.*, 2006), wave and finite element (Mace and Manconi, 2008; Renno and Mace, 2012) and wave finite element (Mencik and Ichchou, 2008). For the sake of clarity, in this thesis, WFE is always used as the acronym for wave finite element. Some important milestones on the development of the WFE method are presented in Figure 1.7.
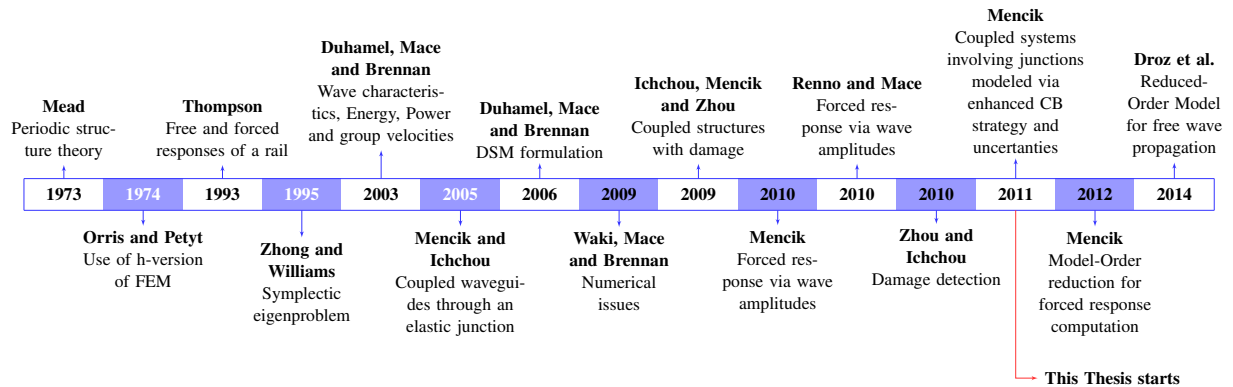


Figure 1.7: Historical timeline of the WFE method development.

The WFE method has been applied to address the dynamic analysis of various engineering systems, such as beams (Mace *et al.*, 2005; Waki *et al.*, 2009b; Nascimento, 2009; Silva *et al.*, 2013b), truss beams (Signorelli and von Flotow, 1988), simply-supported plates (Mace *et al.*, 2005; Silva and Arruda, 2012), multi-layered systems (Mencik and Ichchou, 2008), fluid-filled pipes (Manconi *et al.*, 2009), curved structures (Zhou and Ichchou, 2010; Silva *et al.*, 2013a), composite panels (Chronopoulos *et al.*, 2013), flat shells (Mencik, 2013), cylinders (Renno and Mace, 2014), stiffened and non-stiffened cylindrical shells (Renno and Mace, 2014; Silva *et al.*, 2014b). Also, using the WFE method, the problem of multiple periodic waveguides coupled through a common elastic coupling element has been addressed (Mencik and Ichchou, 2005). Later, by coupling the FE model of a damaged part and the WFE model of healthy structures, damage detection has been studied (Ichchou *et al.*, 2009; Zhou and Ichchou, 2010; Bouchoucha *et al.*, 2012). The method was also extended to 2D periodic structures (Mace and Manconi, 2008) and cylindrical structures (Manconi *et al.*, 2009).

The numerical issues involved in the computation of wave modes via the WFE method has been investigated for simple waveguides (Waki *et al.*, 2009b). The consistency of the wave solutions obtained via the WFE method was demonstrated through comparison with those obtained analytically via SEM (Arruda *et al.*, 2007). Later, the numerical wave modes of an one-dimensional waveguide predicted by means of the WFE method was compared to those computed via the SAFE method (Zhou *et al.*, 2011). The analysis showed that WFE solutions approach the SAFE solutions

when the element aspect ratio — *i.e.*, the ratio between the element size along the axial direction and the cross section dimension — is considerable small.

Besides, the forced response of periodic structures has also been addressed via the WFE method (Duhamel *et al.*, 2006; Mead, 2009; Waki *et al.*, 2009a; Waki *et al.*, 2009b; Mencik, 2010; Renno and Mace, 2010; Renno and Mace, 2011; Mencik, 2013; Mencik, 2014). In some works (Waki *et al.*, 2009a; Waki *et al.*, 2009b; Mencik, 2010; Mencik, 2013; Mencik, 2014), the strategy involved the explicit computation of the wave mode amplitudes. Although efficient, the WFE approach that uses the concept of wave mode amplitudes is, however, difficult to handle as it is based on complex matrix formulations that need to be expressed on a case-by-case basis. On the other hand, expressions for the condensed dynamic stiffness matrices of straight periodic structures by means of the WFE method were also proposed (Duhamel *et al.*, 2006; Mead, 2009). This approach appears to be an efficient alternative to the spectral element method (Doyle, 1997; Lee, 2009; Silva *et al.*, 2013b) that make use of analytical waves for expressing the condensed dynamic stiffness matrices of waveguides. This is so because the WFE method works well in the MF range, as opposed to the analytical methods, which are limited by LF assumptions.

Arruda and Nascimento (2008) showed that a spectral element, as defined by Doyle (1997), can be derived from the dynamic stiffness matrix of a waveguide slice modeled with conventional finite elements using the elastodynamic equations for the given structure. This method, called wave spectral finite element method (WSFEM), was applied to homogeneous rod problems (Goldstein *et al.*, 2010), and, also, to the investigation of phononic band gaps in periodic waveguide problems (Goldstein *et al.*, 2011). It is important to note here that the acronym, WSFEM, is also used in the literature to refer to the wavelet-based spectral finite element method, which, differently from the approach considered in this thesis consists in using Daubechies scaling functions for approximation in time and exact interpolating functions, from SEM, for spatial discretization (Mitra and Gopalakrishnan, 2006).

It is worth pointing out that, although the development of WFE method dates back to the 1970's, it has not yet been made available in commercial softwares. This might be explained by the fact that most of the developments have proposed formulations in terms of wave parameters which do not allow a direct link to FE codes — in general, based on dynamic stiffness or modal-based formulations. This explains the popular use of cyclic symmetry analysis, proposed by Thomas (1974) based on the work of Orris and Petyt (1974). He showed that, for rotationally periodic structures, the consideration of free wave propagation allows determining the normal modes of vibration of

the complete structure through the analysis of a single substructure. This is because the boundary condition which results from the fact that the chain of identical substructures is closed has always to be considered. As this technique, results in a modal-based solution, it has experimented widespread use, being available in most of commercial FE softwares. This thesis is motivated by the possibility of using wave-based approaches in commercial FE codes for general periodic structures. For this reason, WFE-based superelement models of structures with one-dimensional periodicity are proposed.

### 1.2.4 Dynamic analysis of coupled problems

In the last decades, the fast growth in computing power has motivated scientists and engineers to analyze ever larger and more complex systems. However, the resources are still limited. Thus, depending on the number of degrees of freedom and the number of steps involved, simulations can take very long time. This has led to the development of methods which optimize the efficiency of calculations. Within the framework of coupled problems, the concept of domain decomposition, which consists in decomposing the problem into subdomains that are described independently and solving the interface coupling problem, has often been used to solve complex engineering problems (Klerk *et al.*, 2008).

With the motivation of providing a further increase in efficiency, the so-called dynamic substructuring methods have been proposed. In this case, the dynamic behavior of individual subdomains is described by means of a reduced number of degrees of freedom for which approximate local solutions are obtained and then coupled. Among the reduction techniques proposed within the framework of dynamic substructuring, we may consider those in which the reduction process results of the application of a transformation matrix composed of Ritz vectors. Those usually combine the static response of the structure at the interfaces with internal displacement modes (Rixen, 2009). Two kinds of internal displacement modes are considered: the fixed-interface modes, as in the Craig-Bampton method (Craig and Bampton, 1968b), or the free-interface modes, as it is the case in the MacNeal (MacNeal, 1971) and the Rubin (Rubin, 1975) methods, or in the Craig-Chang (Craig and Chang, 1977) and the Dual Craig-Bampton (Rixen, 2004) methods. These methods are known as component-mode synthesis (CMS).

As discussed earlier (see Section 1.1), modal-based approaches are efficient for describing LF

dynamics. However, as frequency rises, a very high number of modes must be taken into account and wave-based approaches are preferred. It is worth pointing out that the potential of wave-based methods for modeling waveguides and uncoupled structures has been extensively investigated. Nevertheless, the use of wave-based approaches for solving coupled problems has rarely been proposed.

The formulation of superelement matrices by means of the WFE method appears to be of simple use in the framework of substructuring techniques, *i.e.*, when dealing with several superelements connected to each other. Wave-based matrix formulations which use the concept of wave mode amplitudes have been developed in (Mencik, 2013) to compute the frequency response functions (FRFs) of assemblies involving flat shells and coupling junctions at a very low computational cost compared to the conventional FE method. Within that framework, the coupling junctions are modeled by means of the CB method (Craig and Bampton, 1968a), i.e, in terms of static modes and a reduced number of fixed-interface modes, which are selected via a wave-based procedure (Mencik, 2011). By combining low and high-order wave modes for modeling periodic structures and fixed-interface modes for modeling coupling junctions, the WFE method constitutes an efficient numerical tool for assessing the MF dynamics of coupled systems. A qualitative comparison between the WFE method and other wave-based MF techniques such as analytical Trefftz techniques (Vanmaele *et al.*, 2007; Ladevèze and Riou, 2005) and enrichment techniques (Farhat *et al.*, 2001) has been proposed in (Mencik, 2013). One of the main features of the WFE method when compared to those MF techniques concerns the use of matrix equations which are likely to be well-conditioned. Also, a quantitative comparison between the WFE method and the conventional CB method — *i.e.*, when all the periodic structures are modeled in terms of fixed-interface modes instead of wave modes — has been performed in (Mencik, 2013) . It should be emphasized that, unlike the CB method or CB-like techniques such as the automated multilevel substructuring (AMLS) method (Kaplan, 2001), the WFE method does not require either the truncation of (wave) mode bases or the reduction of interface degrees of freedom (DOFs) for assessing the FRFs of periodic structures at a low computational cost. This can be explained by the fact that the WFE method usually deals with full sets of wave modes whose number appears to be much smaller than the total number of DOFs involved for modeling periodic structures. Thus, the WFE method appears to be more accurate than the CB and AMLS methods, while considering matrix equations of similar sizes. It should be noticed, however, that the WFE method remains applicable only to the study of periodic systems, even though those periodic systems can be connected by means of junctions of arbitrary shapes, which makes it a less general method than the conventional CB method and other wave-based MF techniques.

So far, the WFE method has never been applied to the study of truly periodic structures — *i.e.*, structures involving heterogeneous substructures which contain many internal DOFs — that may be coupled to complex elastic junctions. Thus, the motivation of the present thesis may be viewed as to propose efficient and ease-to-use superelement-based approaches based on the aforementioned WFE and CB procedures, and that can compete with other conventional model reduction techniques for predicting the harmonic response of complex structural systems. This research objective is addressed in this thesis in Chapter 4.

## 1.3  Objectives

The objectives of this thesis are listed in the following.

- Analyze the numerical errors associated to the WFE-based eigenproblem formulation for a 3D solid waveguide.

- Analyze the numerical errors associated to the FE mesh for a 3D solid waveguide.

- Present a general formulation for the WSFEM.

- Formulate the numerical spectral element of a Timoshenko beam by means of WSFEM.

- Formulate WFE-based superelement matrices of periodic structures.

- Propose a WFE-based model-order reduction strategy which yields a reduced eigenproblem to be solved and provides efficient computation of forced responses by means of superelement matrices.

- Propose WFE-based dynamic substructuring techniques for simulating nonacademic coupled systems like those encountered in real engineering applications, which can involve several truly periodic structures and arbitrarily-shaped elastic junctions.

- Use the WFE-based numerical approaches proposed in the thesis to design local resonant devices to be attached to a stiffened cylindrical shell and provide vibration attenuation at specific frequencies.

## 1.4  Outline of the thesis

This thesis is organized as follows.

In Chapter 2, a general form of the WFE method for the the analysis of free wave propagation in 1D periodic structures with symmetric substructures is presented. A comprehensive view of the method which includes the assumptions involved and alternative formulations for the WFE-based eigenproblem is provided. The numerical errors associated to the computation of the WFE-based eigenproblem are evaluated and discussed. Formulations of the WFE-based eigenproblem are compared in terms of the accuracy of numerical wave modes, which is checked through comparison with analytical wave modes. The relationship between left and right-going wave modes due to the substructure symmetry is also investigated. The errors in the computation of the WFE-based eigenproblem are analyzed with respect to the discretization level of the substructure. Finally, details regarding the implementation are presented.

Chapter 3 is mainly dedicated to the forced response computation of 1D periodic structures. The numerical wave mode basis computed by means of the WFE method in Chapter 2 is used to formulate superelement matrices of finite periodic structures: either the dynamic stiffness matrix (DSM) or the receptance matrix (RM). A WFE-based model-order reduction strategy is presented. It involves a selection criterion of wave modes, the formulation of reduced eigenvalue problems, and receptance matrices for the computation of free and forced wave propagation solutions. At the end, a general form of WSFEM is presented and a spectral element of a Timoshenko beam is formulated.

In Chapter 4, the objective is to deal with the dynamic analysis of coupled systems composed of periodic structures and elastic junctions by means of a WFE-based approach. The dynamic description of periodic parts is made by the superelement formulations presented in Chapter 3. A WFE-based strategy for modeling coupling elastic junctions is recalled. Dynamic substructuring techniques, such as the dynamic stiffness method and the receptance matrix method which makes use of Lagrange multipliers, are addressed. Numerical test cases are carried out in order to show that

the proposed WFE-based approaches may outperform conventional methods in terms of accuracy and computational time.

In Chapter 5, the interest in periodic structures from the point of view of engineering application is concerned. In particular, the possibility of designing vibration filters by attaching periodic resonators to the structure is highlighted. This feature of periodic structures is shown by means of dynamic analyses. Hence, the objective of this chapter is also to show that the WFE-based approaches proposed in this thesis can be used in the design of periodic structures with relevant applications.

Finally, in Chapter 6, the general conclusions regarding the work developed in this thesis are drawn. Then, the original contributions of this work are highlighted. At the end, a list of the publications that resulted from this thesis is presented.

# 2 The wave finite element method: free wave propagation analysis

## 2.1 Overview

In this chapter, the objective is to present the wave finite element (WFE) method for free wave propagation analysis. This method provides a numerical wave description for structures that are periodic in the sense that they are constituted by identical substructures coupled together along one or more directions(Mead, 1973; Mencik and Ichchou, 2005; Mace *et al.*, 2005). In this work, only structures with one-dimensional periodicity are considered. One of the advantages of this method is that conventional finite elements can be used to model a substructure, which thus may involve several materials or complex geometries, as depicted in Figure 2.1. Moreover, the wave propagation of the whole structure, which may be either infinite or finite, can be assessed from the analysis of a single substructure. This reduces the size of the numerical problem to be solved — which is directly related to the number of degrees of freedom to be analysed —, thus producing computational time savings and making possible to extend the analysis to the mid-frequency range, where sufficiently fine mesh discretizations are required. Compared to analytical wave-based methods, such as the spectral element method (SEM) (Doyle, 1997; Lee, 2009), the WFE method is clearly advantageous since complex dynamics produced either by geometric complexities or higher-order kinematics behaviors, which are difficult to be handled analytically (Arpaci *et al.*, 2003; Rafezy and Howson, 2006; Kim and Kim, 2004), can be described in a straightforward way. This is because conventional finite elements are used to model the substructure.
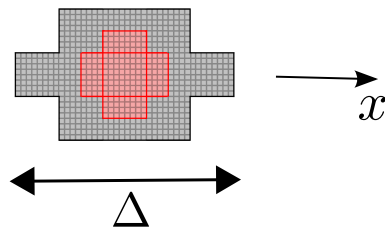


Figure 2.1: Substructure with complex heterogeneities — involving multiple materials and complex geometry — of a structure periodic along the $x$-direction with spatial period $\Delta$.

This chapter is organized as follows. In Section 2.2, the mathematical formulation of the WFE method is reviewed. The dynamic equilibrium of a substructure is considered in Section 2.2.1 and, equivalently, formulated in terms of state variables in Section 2.2.2. The eigenvalue problem related

to a periodic structure is formulated in Section 2.2.3. Then, the mathematical properties associated to the eigenproblem into consideration and the basics of the numerical waves computed by means of the WFE method are discussed in Section 2.2.4. Alternative eigenvalue formulations, which have the aim of preventing numerical errors, are presented in Section 2.2.5. Section 2.2.6 is concerned about strategies for following a given wave mode in frequency. A numerical analysis of errors involved in the WFE method is presented in Section 2.3. Next, in Section 2.4, the implementation of the method is discussed. Finally, the conclusions of this chapter are drawn (Section 2.5).

## 2.2 Mathematical formulation

### 2.2.1 Dynamic equilibrium formulation of a substructure

Consider an elastic system composed of $N$ identical substructures arranged along a certain straight direction — say, axis $x$ —, as shown in Figure 2.2. Each substructure has a length $\Delta$, which corresponds to the periodic unit length in case of periodic systems or an arbitrary small length in case of waveguides. The system is supposed to be linear elastic and the substructure is assumed symmetric with respect to a plane perpendicular to the $x$-axis[1].
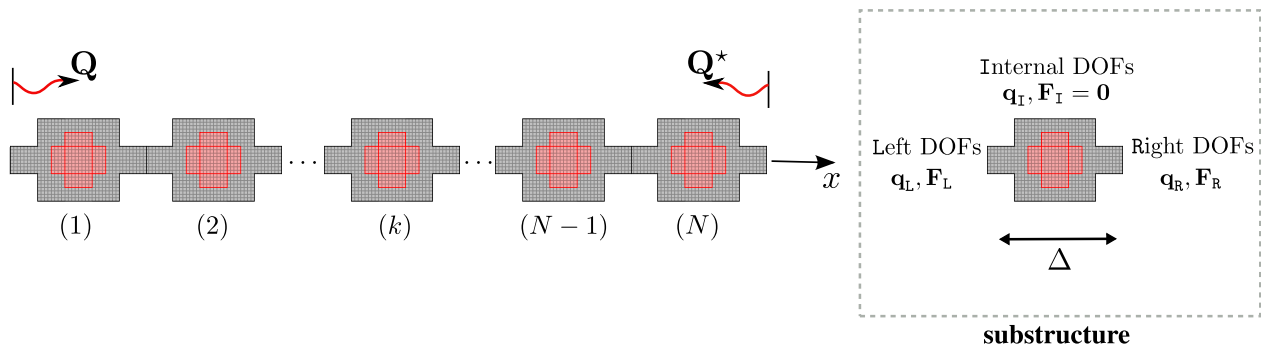


Figure 2.2: FE model of a one-dimensional periodic structure composed of $N$ substructures; in detail, the FE model of a substructure.

Within the framework of the WFE method, only one substructure is modeled by means of conventional finite elements (see Figure 2.2). Here, the left and right boundaries of the substructure are meshed in the same way, *i.e.*, by means of the same number $n$ of degrees of freedom

---

[1]It is worth mentioning that the symmetric assumption is not a requirement for the use of the WFE method. Recently, Mencik and Duhamel (2015) has addressed the issue of describing the dynamic behavior of a 1D periodic structures involving arbitrarily-shaped substructures by means of a WFE-based approach.

(DOFs). The stiffness and mass matrices ($\mathbf{K}$ and $\mathbf{M}$, respectively) of the substructure follow from this FE model, which yields, in the frequency domain, the so-called dynamic stiffness matrix $\mathbf{D} = -\omega^2 \mathbf{M} + (1 + \mathrm{i}\eta)\mathbf{K}$, where $\omega$ is the angular frequency and $\eta$ is the constant structural damping loss factor[2]. As a result, the dynamic equilibrium equation of the substructure is expressed in the frequency domain as

$$\mathbf{Dq} = \mathbf{F}, \tag{2.1}$$

where $\mathbf{q}$ and $\mathbf{F}$ are vectors of nodal displacements/rotations and forces/moments, respectively. By partitioning the DOFs into those on the left boundary L, right boundary R, and internal I DOFs (as depicted in Figure 2.2), this yields

$$\begin{bmatrix} \mathbf{D_{LL}} & \mathbf{D_{LI}} & \mathbf{D_{LR}} \\ \mathbf{D_{IL}} & \mathbf{D_{II}} & \mathbf{D_{IR}} \\ \mathbf{D_{RL}} & \mathbf{D_{RI}} & \mathbf{D_{RR}} \end{bmatrix} \begin{bmatrix} \mathbf{q_L} \\ \mathbf{q_I} \\ \mathbf{q_R} \end{bmatrix} = \begin{bmatrix} \mathbf{F_L} \\ \mathbf{0} \\ \mathbf{F_R} \end{bmatrix}. \tag{2.2}$$

Notice that the coupling actions (*i.e.*, external loads) are supposed to be confined to its left and right boundaries only (Mead, 1973). Therefore, the internal DOFs are not subject to external loads, which means that $\mathbf{F_I} = \mathbf{0}$. By condensing the matrix $\mathbf{D}$ on the left and right substructure boundaries, the dynamic equilibrium system of equations can be readily expressed as

$$\begin{bmatrix} \mathbf{D^*_{LL}} & \mathbf{D^*_{LR}} \\ \mathbf{D^*_{RL}} & \mathbf{D^*_{RR}} \end{bmatrix} \begin{bmatrix} \mathbf{q_L} \\ \mathbf{q_R} \end{bmatrix} = \begin{bmatrix} \mathbf{F_L} \\ \mathbf{F_R} \end{bmatrix}, \tag{2.3}$$

where $\mathbf{D^*}$ denotes the condensed dynamic stiffness matrix, which is expressed as $\mathbf{D^*} = \mathbf{D_{BB}} - \mathbf{D_{BI}} \mathbf{D_{II}^{-1}} \mathbf{D_{IB}}$, with the subscript B denoting the DOFs on the left and right boundaries of the substructure. This matrix relates external nodal forces/moments to nodal displacements/rotations defined at the left/right cross-sections of the substructure.

---

### 2.2.2 State space formulation
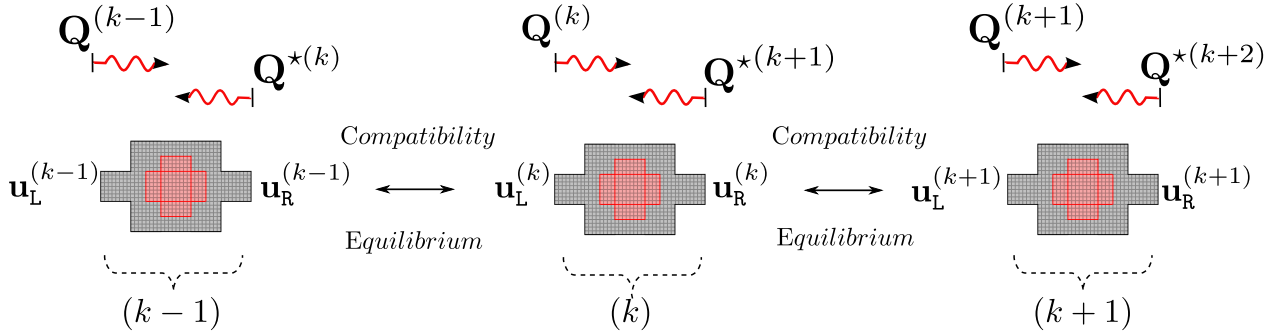


Figure 2.3: Schematics of three consecutive substructures with representation of state vectors.

In the state space formulation[3] nodal forces/moments and nodal displacements/rotations of adjacent substructures (or adjacent substructure boundaries) are linked. The formulation follows from the dynamic equilibrium equations. Using Equation (2.3), it is possible to express the vectors of nodal displacements/rotations and that of nodal forces/moments within the right cross-section of a substructure $k$ in terms of the corresponding vectors related to the left substructure boundary, as follows (Mencik and Ichchou, 2005)

$$\mathbf{u}_{\mathrm{R}}^{(k)} = \mathbf{S}\mathbf{u}_{\mathrm{L}}^{(k)}, \tag{2.4}$$

where $\mathbf{u}_{\mathrm{L}}^{(k)}$ and $\mathbf{u}_{\mathrm{R}}^{(k)}$ are $2n \times 1$ state vectors (shown in Figure 2.3), expressed as

$$\mathbf{u}_{\mathrm{L}}^{(k)} = \begin{bmatrix} \mathbf{q}_{\mathrm{L}}^{(k)} \\ \mathbf{f}_{\mathrm{L}}^{(k)} \end{bmatrix} = \begin{bmatrix} \mathbf{q}_{\mathrm{L}}^{(k)} \\ -\mathbf{F}_{\mathrm{L}}^{(k)} \end{bmatrix}, \quad \mathbf{u}_{\mathrm{R}}^{(k)} = \begin{bmatrix} \mathbf{q}_{\mathrm{R}}^{(k)} \\ \mathbf{f}_{\mathrm{R}}^{(k)} \end{bmatrix} = \begin{bmatrix} \mathbf{q}_{\mathrm{R}}^{(k)} \\ \mathbf{F}_{\mathrm{R}}^{(k)} \end{bmatrix}. \tag{2.5}$$

Notice that the vectors of internal elastic forces/moments $(\mathbf{f}_{\mathrm{L}}, \mathbf{f}_{\mathrm{R}})$ are related to the vectors of external forces/moments $(\mathbf{F}_{\mathrm{L}}, \mathbf{F}_{\mathrm{R}})$ by means of a sign convention. In Equation (2.5), $\mathbf{S}$ is a $2n \times 2n$ symplectic transfer matrix expressed as

$$\mathbf{S} = \begin{bmatrix} -\mathbf{D}_{\mathrm{LR}}^{*-1}\mathbf{D}_{\mathrm{LL}}^{*} & -\mathbf{D}_{\mathrm{LR}}^{*-1} \\ \mathbf{D}_{\mathrm{RL}}^{*} - \mathbf{D}_{\mathrm{RR}}^{*}\mathbf{D}_{\mathrm{LR}}^{*-1}\mathbf{D}_{\mathrm{LL}}^{*} & -\mathbf{D}_{\mathrm{RR}}^{*}\mathbf{D}_{\mathrm{LR}}^{*-1} \end{bmatrix}. \tag{2.6}$$

The consequences of the symplectic feature of matrix $\mathbf{S}$ are addressed in Section 2.2.4.

By considering two consecutive substructures $k-1$ and $k$, as shown in Figure 2.3, the cou-

---

[3]In general associated to state vectors in the form of $\left[\mathbf{q}^T \dot{\mathbf{q}}^T\right]^T$, where $\mathbf{q}$ is the displacement vector and $\dot{\mathbf{q}}$, the velocity vector (derivative of $\mathbf{q}$ with respect to time), in control engineering. Within the framework of this thesis, the state vector is of the form $\left[\mathbf{q}^T \mathbf{f}^T\right]^T$, where $\mathbf{f}$ is the vector of internal elastic forces/moments.

pling conditions — *i.e.*, compatibility of displacements/rotations and equilibrium of forces/moments — must be satisfied in the interface between them, which means that

$$\mathbf{q}_{\mathrm{R}}^{(k-1)} = \mathbf{q}_{\mathrm{L}}^{(k)}, \tag{2.7a}$$

$$\mathbf{F}_{\mathrm{R}}^{(k-1)} + \mathbf{F}_{\mathrm{L}}^{(k)} = 0, \tag{2.7b}$$

where the superscripts $(k-1)$ and $(k)$ are used to label the substructure which the vector is referred to. The application of those relations to Equation (2.4) allows one to establish a link between kinematic/kinetic (or mechanical) quantities on the left boundaries of substructures $k-1$ and $k$, as follows

$$\mathbf{u}_{\mathrm{L}}^{(k)} = \mathbf{S}\mathbf{u}_{\mathrm{L}}^{(k-1)}. \tag{2.8}$$

### 2.2.3 Bloch's theorem and the symplectic eigenvalue problem

As $\mathbf{u}^{(k)}$ is a state vector of size $2n \times 1$, it can be expanded in terms of a complete basis — *i.e.*, a set of $2n$ linearly independent vectors—, as

$$\mathbf{u}^{(k)} = \sum_{j=1}^{2n} \boldsymbol{\phi}_j Q_j^{(k)}, \tag{2.9}$$

where $\{\boldsymbol{\phi}_j\}_{j=1,\cdots,2n}$ and $\{Q_j\}_{j=1,\cdots,2n}$ are indexed families of vectors of wave shapes and wave amplitudes, respectively. As a result of Bloch's theorem for periodic systems (Mencik, 2010; Gazelet *et al.*, 2013), the wave amplitudes between two consecutive substructures $k$ and $k-1$ are linked as

$$Q_j^{(k)} = \mu_j Q_j^{(k-1)} \quad \text{with} \quad \mu_j = e^{-\mathrm{i}\beta_j\Delta}, \tag{2.10}$$

where $\{\beta_j\}_j$ have the meaning of wavenumbers. Using this relation in Equation (2.9), the state vector related to the left boundary of a substructures $k$ can be expressed as

$$\mathbf{u}_{\mathrm{L}}^{(k)} = \sum_{j=1}^{2n} \boldsymbol{\phi}_j e^{-\mathrm{i}\beta_j\Delta} Q_j^{(k-1)}. \tag{2.11}$$

Then, substituting Equation (2.11) into Equation (2.8), it yields the following eigenproblem

$$\mathbf{S}\boldsymbol{\phi}_j = \mu_j \boldsymbol{\phi}_j. \tag{2.12}$$

In this framework, the set of parameters $\{\mu_j\}_{j=1,\cdots,2n}$ are referred to as a family of the eigenvalues of the matrix $\mathbf{S}$ and $\{\phi_j\}_{j=1,\cdots,2n}$ appear to be a family of the right eigenvectors of $\mathbf{S}$, which can be partitioned into $n \times 1$ vectors of displacement/rotation and force/moment components, $\{\phi_{\mathrm{q}j}\}_{j=1,\cdots,2n}$ and $\{\phi_{\mathrm{F}j}\}_{j=1,\cdots,2n}$, respectively. The solutions $\{(\mu_j,\phi_j)\}_{j=1,\cdots,2n}$ of the symplectic eigenvalue problem (Equation (2.12)) are referred to as the waves modes of the periodic structure. The eigenvalues $\{\mu_j\}_{j=1,\cdots,2n}$ are propagation constants, which are related to the wavenumbers $\{\beta_j\}_{j=1,\cdots,2n}$ by means of Equation (2.10). Besides, the right eigenvectors provide a spatial description for the wave motion over the substructure boundaries. There are twice as many wave modes as the number of DOFs used to discretize each substructure boundary: $n$ of them being related to right-going waves $\{(\mu_j,\phi_j)\}_{j=1,\cdots,n}$, while the other $n$, to left-going waves $\{(\mu_j^\star,\phi_j^\star)\}_{j=1,\cdots,n}$ (see Figure 2.4).
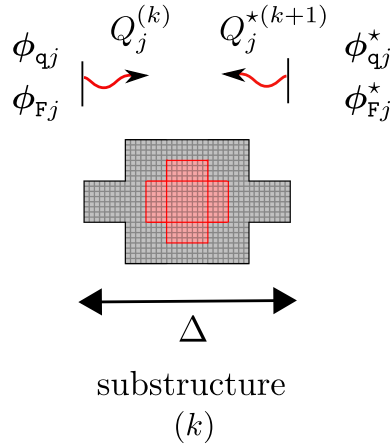


Figure 2.4: Illustration of a substructure, associated vectors of wave mode shapes, and wave amplitudes related to left- and right-going waves.

## 2.2.4 Properties of the eigensolutions

Due to the symmetric feature of the substructure model, the transfer matrix $\mathbf{S}$, Equation (2.6), is symplectic, *i.e.*, $\mathbf{S}^T \mathbf{J} \mathbf{S} = \mathbf{J}$ (Zhong and Williams, 1995), where $\mathbf{J}$ is the unit symplectic matrix, defined as

$$\mathbf{J} = \begin{bmatrix} \mathbf{0} & \mathbf{I}_n \\ -\mathbf{I}_n & \mathbf{0} \end{bmatrix}, \tag{2.13}$$

with $\mathbf{I}_n$ being a $n$-dimensional identity matrix. Matrix $\mathbf{J}$ has the following properties

$$\mathbf{J}^2 = -\mathbf{I}_{2n}, \ \mathbf{J}^T = \mathbf{J}^{-1} = -\mathbf{J}. \tag{2.14}$$

Due to the symplectic properties of matrix $\mathbf{S}$, if $\mu_j$ is an eigenvalue, it can be shown that $1/\mu_j$ is also an eigenvalue (Zhong and Williams, 1995). Indeed, left multiplying Equation (2.12) by $\mathbf{S}^T\mathbf{J}$, it yields

$$\mathbf{S}^T\mathbf{J}\mathbf{S}\boldsymbol{\phi}_j = \mu_j\mathbf{S}^T\mathbf{J}\boldsymbol{\phi}_j. \tag{2.15}$$

Then, using the symplectic relation — *i.e.*, $\mathbf{S}^T\mathbf{J}\mathbf{S} = \mathbf{J}$ — in Equation (2.15) and taking the transpose of the resultant equation, the following eigenproblem is formulated

$$\left(\boldsymbol{\phi}_j\mathbf{J}\right)^T \mathbf{S} = \mu_j^{-1}\left(\boldsymbol{\phi}_j\mathbf{J}\right)^T. \tag{2.16}$$

Notice that $\{\boldsymbol{\psi}_j\}_{j=1,\cdots,2n} = \{\left(\boldsymbol{\phi}_j\mathbf{J}\right)^T\}_{j=1,\cdots,2n}$ is a family of left eigenvectors of $\mathbf{S}$, so that $\mu_j^{-1}$ is also an eigenvalue. This confirms that $\mu_j$ and $\mu_j^{-1}$ are eigenvalues of the same problem. Therefore, the $2n$ eigenvalues can be divided into two groups

$$
\begin{aligned}
&\mu_j \text{ with } |\mu_j| \le 1, & j = 1, 2, \cdots, n, \\
&\mu_j^\star = \frac{1}{\mu_j} \text{ with } |\mu_j^\star| \ge 1, & j = 1, 2, \cdots, n.
\end{aligned}
\tag{2.17}
$$

From the physical point of view, this property of eigenvalue pairs means that a pair of waves travel to the left and right directions with equal phase speed, which is an expected consequence of the symmetric nature of the substructure model. Besides, the eigenvectors of Equation (2.12) are orthogonal in the symplectic sense[4]. Thus, given two right eigenvectors $\boldsymbol{\phi}_j$ and $\boldsymbol{\phi}_i$, or a left eigenvector $\boldsymbol{\psi}_j$ and a right eigenvector $\boldsymbol{\phi}_i$, the following conditions hold (Yao *et al.*, 2009)

$$\boldsymbol{\psi}_j\boldsymbol{\phi}_i = -\boldsymbol{\phi}_j^T\mathbf{J}\boldsymbol{\phi}_i = 0 \qquad , \quad \text{if } \mu_i - \frac{1}{\mu_j} \ne 0, \tag{2.18a}$$

$$\boldsymbol{\psi}_j\boldsymbol{\phi}_i = -\boldsymbol{\phi}_j^T\mathbf{J}\boldsymbol{\phi}_i = c \ne 0 \qquad , \quad \text{if } \mu_i - \frac{1}{\mu_j} = 0. \tag{2.18b}$$

From these relations, it follows that an eigenvector $\boldsymbol{\phi}_i$ associated to an eigenvalue $\mu_i$ is symplectic orthogonal to all other eigenvectors including itself but excluding its adjoint (Zhong and Williams, 1995)— *i.e.*, the one which is associated to an eigenvalue $1/\mu_i$.

---

[4]Notice that the relationship between these eigenvectors is different from the one among normal mode shapes — *i.e.*, those obtained by solving $\left(\mathbf{K} - \omega^2\mathbf{M}\right)\mathbf{q} = \mathbf{0}$ —, which are orthogonal with respect to the mass matrix $\mathbf{M}$.

Due to the non-symmetric nature of the symplectic matrix $\mathbf{S}$, the eigenvalues may be complex. Thus, a wavenumber $\beta_j$ can be expressed as

$$\beta_j = \Re\left(\beta_j\right) + \mathtt{i}\Im\left(\beta_j\right), \tag{2.19}$$

where the real and the imaginary parts of $\beta_j$ are referred to the phase and the attenuation constants per unit length, respectively. Regarding the representation of the wavenumbers $\{\beta_j\}_{j=1,\cdots,2n}$ in the complex plane, the wave modes can be classified as: purely propagating, *i.e.*, the imaginary part of the wavenumber is close to zero $(\Im\left(\beta_j\right) \approx 0)^5$; purely evanescent, *i.e.*, the real part of the wavenumber is close to zero $(\Re\left(\beta_j\right) \approx 0)$; or complex (decaying, but propagating), *i.e.*, the real and the imaginary part of the wavenumber are of the same order of magnitude $(\mathcal{O}\left(\Re\left(\beta_j\right)\right) \sim \mathcal{O}\left(\Im\left(\beta_j\right)\right))$.

As discussed earlier, the eigenvalues come in pairs as $(\mu_j, 1/\mu_j)$, which correspond to $n$ right-going wave shapes $\{\phi_j\}_{j=1,\cdots,n}$ and $n$ left-going wave shapes $\{\phi_j^\star\}_{j=1,\cdots,n}$. The right-going (respectively, left-going) waves are those whose energy travels in the direction of increasing (respectively, decreasing) spatial coordinate $x$. Langley (1994) has shown that the energy velocity is always equal to the group velocity $(c_g)$ for an undamped system. Therefore, in the absence of damping, the direction of purely propagating waves is determined by the sign of the energy flow, which corresponds to that of the group velocity (Equation (2.20)). The sign is positive if the wave propagates to the right, and negative, if it propagates to the left.

$$\mathrm{sgn}(c_{gj}) = \mathrm{sgn}\left(-\frac{1}{2}\Re\left(\phi_{\mathsf{F}j}^H \dot{\phi}_{\mathsf{q}j}\right)\right) = \mathrm{sgn}\left(-\frac{1}{2}\Re\left(\mathtt{i}\omega\phi_{\mathsf{F}j}^H \phi_{\mathsf{q}j}\right)\right) \tag{2.20}$$

On the other hand, near-field waves (*i.e.*, purely evanescent or complex waves) are classified as right-going (respectively, left-going) waves if their amplitudes decay in the direction of increasing (respectively, decreasing) spatial coordinate $x$ with respect to the member local coordinate system. Thus, for these waves, right-going and left-going wave shapes are associated to eigenvalues whose magnitudes are, respectively, less and greater than one. For damped systems, which is usually the case in real engineering structures, the classification of wave shapes as right-going or left-going follows the criterion used for evanescent and complex waves of undamped systems, as the magnitude of $\mu_j$ is always different from the unity when damping is present. Table 2.1 summarizes

---

[5]The imaginary part of the wavenumber of a purely propagating wave is not exactly zero, either because some damping is present or due to round-off errors, which may be avoided by improving the precision of the routines for solving the corresponding eigenvalue problem. Those errors are also avoided if the symplectic structure of the eigenvalue problem is preserved.

Table 2.1: Wave classification

| Type of wave | $\Re(\beta_j)$ | $\Im(\beta_j)$ | Direction |
|:---:|:---:|:---:|:---:|
| Purely Propagating | $\neq 0$ | $\approx 0$ | $\mathrm{sgn}(c_{gj}) > 0 \rightarrow$ right-going<br>$\mathrm{sgn}(c_{gj}) < 0 \rightarrow$ left-going |
| Purely Evanescent | $\approx 0$ | $\neq 0$ | $\lvert\mu_j\rvert < 1\ (\Im(\beta_j) < 0) \rightarrow$ right-going<br>$\lvert\mu_j\rvert > 1\ (\Im(\beta_j) > 0) \rightarrow$ left-going |
| Complex | $\neq 0$ | $\neq 0$ | $\lvert\mu_j\rvert < 1\ (\Im(\beta_j) < 0) \rightarrow$ right-going<br>$\lvert\mu_j\rvert > 1\ (\Im(\beta_j) > 0) \rightarrow$ left-going |

the classification of waves according to their type and direction.

For periodic systems that exhibit symmetric substructures — *i.e.*, the left and right parts of each substructure are symmetric with respect to a plane perpendicular to the main axis $x$ —, the right- and left-going wave shapes — *i.e.*, $\boldsymbol{\Phi} = \begin{bmatrix} \boldsymbol{\Phi}_\mathrm{q}^T & \boldsymbol{\Phi}_\mathrm{F}^T \end{bmatrix}^T$ and $\boldsymbol{\Phi}^\star = \begin{bmatrix} \boldsymbol{\Phi}_\mathrm{q}^{\star T} & \boldsymbol{\Phi}_\mathrm{F}^{\star T} \end{bmatrix}^T$, respectively — are linked as (Thompson, 1993; Mace *et al.*, 2005; Mencik, 2010)

$$\boldsymbol{\Phi} = \mathcal{T}\boldsymbol{\Phi}^\star, \tag{2.21}$$

or, alternatively, as

$$\boldsymbol{\Phi}_\mathrm{q}^\star = \mathcal{R}\boldsymbol{\Phi}_\mathrm{q} \quad , \quad \boldsymbol{\Phi}_\mathrm{F}^\star = -\mathcal{R}\boldsymbol{\Phi}_\mathrm{F}, \tag{2.22}$$

with

$$\mathcal{T} = \begin{bmatrix} \mathcal{R} & \mathbf{0} \\ \mathbf{0} & -\mathcal{R} \end{bmatrix}. \tag{2.23}$$

and $\mathcal{R}$ being a diagonal symmetry transformation matrix — *i.e.*, whose elements are $\pm 1$ and such that $\mathcal{R}^2 = \mathbf{I}_n$. Equations (2.21)-(2.22) provide an analytical means to strictly enforce the coherence between the right- and left-going wave shapes. It is used to circumvent the issue of numerical dispersion which results from the computation of the eigensolutions of the matrix $\mathbf{S}$, and which can be detrimental for the computation of the forced response of periodic structures.

Expressing the symplectic orthogonality between left and right eigenvectors (Equations

(2.18)) and using the relations in Equation (2.22), it is possible to verify that

$$\phi_j^{\star T} \mathbf{J} \phi_j = \phi_{\mathsf{F}j}^T \mathcal{R} \phi_{\mathsf{q}j} + \phi_{\mathsf{q}j}^T \mathcal{R} \phi_{\mathsf{F}j}, \tag{2.24a}$$

$$\phi_j^T \mathbf{J} \phi_j^{\star} = - \left( \phi_{\mathsf{F}j}^T \mathcal{R} \phi_{\mathsf{q}j} + \phi_{\mathsf{q}j}^T \mathcal{R} \phi_{\mathsf{F}j} \right), \tag{2.24b}$$

which means that

$$\phi_j^{\star T} \mathbf{J} \phi_j = -\phi_j^T \mathbf{J} \phi_j^{\star} \quad \text{or} \quad -\psi_j \phi_j = \psi_j^{\star} \phi_j^{\star} \tag{2.25}$$

A normalization procedure can be introduced between adjoint eigenvectors, which would make

$$\psi_j \phi_j = \psi_j^{\star} \phi_j^{\star} = 1. \tag{2.26}$$

It suffices to express the normalized left and right eigenvectors as

$$\psi_j\big|_{new} = -\frac{\phi_j^{\star T} \mathbf{J}}{\sqrt{\phi_j^{\star T} \mathbf{J} \phi_j}}, \quad \psi_j^{\star}\big|_{new} = \frac{\phi_j^T \mathbf{J}}{\sqrt{\phi_j^{\star T} \mathbf{J} \phi_j}}, \quad \forall j = 1, \dots, n, \tag{2.27a}$$

$$\phi_j\big|_{new} = \frac{\phi_j}{\sqrt{\phi_j^{\star T} \mathbf{J} \phi_j}}, \quad \phi_j\big|_{new} = \frac{\phi_j^{\star}}{\sqrt{\phi_j^{\star T} \mathbf{J} \phi_j}}, \quad \forall j = 1, \dots, n. \tag{2.27b}$$

### 2.2.5 Alternative eigenvalue problems

The eigenvalue problem as stated in Equation (2.12), is usually subject to numerical ill-conditioning. One of the possible sources of numerical errors is the inversion of the matrix $\mathbf{D}_{\mathsf{LR}}^*$ in Equation (2.6) (Zhong and Williams, 1995). Moreover, the matrix of right eigenvectors, *i.e.*,

$$\mathbf{\Phi_u} = \begin{bmatrix} \mathbf{\Phi_q} & \mathbf{\Phi_q^{\star}} \\ \mathbf{\Phi_F} & \mathbf{\Phi_F^{\star}} \end{bmatrix}, \tag{2.28}$$

has largely disparate components as it involves displacement/rotation and force/moment components, which contributes to increase its condition number and, thereafter, according to the Bauer-Fike theorem (Golub and Loan, 1998; Mencik, 2010) recalled below, the eigenvalue sensitivity.

**Theorem 2.1.** (Bauer-Fike) If $\tilde{\mu}_j$ is an eigenvalue of $\mathbf{S} + \mathbf{E} \in \mathbb{C}^{2n \times 2n}$, where $\mathbf{E}$ is a perturbation matrix with small norm —*i.e.*, $\|\mathbf{E}\|_p \ll \|\mathbf{S}\|_p$ —, and $\mathbf{\Phi_u^{-1}} \mathbf{S} \mathbf{\Phi_u} = \boldsymbol{\mu} = \mathtt{diag}(\mu_1, \mu_2, \cdots, \mu_{2n})$,

then

$$\min_{\mu \in \mu(\mathbf{S})} |\mu - \tilde{\mu}_j| \leq \kappa(\mathbf{\Phi_u}) \|\mathbf{E}\|_p,$$

where $\|\cdot\|_p$ denotes any of the $p$-norms[6] and $\kappa$ denotes the condition number[7] of a given matrix.

Signorelli and von Flotow (1988) showed numerical errors in their study of periodic truss beams, and attributed them to computational inaccuracy (*i.e.*, round-off errors). However, these errors might be the evidence of the numerical ill-conditioning of the eigenvalue problem. Later on, Zhong and Williams (1995) addressed the issue and proposed alternative formulations for the eigenvalue problem by making use of the symplectic property. The main idea behind the alternative formulations is to write the eigenvalue problem as a function of the vectors of displacements/rotations only, in order to avoid the conditioning problems related to the consideration of force/moment components. In the following, alternative formulations for the eigenproblem stated in Equation (2.12) are presented. Afterwards, their final expressions are summarized in Table 2.2.

### ($\mathbf{N}, \mathbf{L}$) **eigenvalue problem**

To begin with, the state vectors related to the left (right) cross-section of adjacent substructures are written as a function of the vectors of displacements/rotations, as follows

$$\mathbf{u}_{\mathrm{L}}^{(k)} = \mathbf{L}\mathbf{w}^{(k)}, \quad \mathbf{u}_{\mathrm{R}}^{(k)} = \mathbf{N}\mathbf{w}^{(k)}, \tag{2.29}$$

where

$$\mathbf{w}^{(k)} = \begin{bmatrix} \mathbf{q}_{\mathrm{L}}^{(k)T} & \mathbf{q}_{\mathrm{R}}^{(k)T} \end{bmatrix}^T, \tag{2.30}$$

$$\mathbf{L} = \begin{bmatrix} \mathbf{I} & \mathbf{0} \\ -\mathbf{D}_{\mathrm{LL}}^* & -\mathbf{D}_{\mathrm{LR}}^* \end{bmatrix} \quad \text{and} \quad \mathbf{N} = \begin{bmatrix} \mathbf{0} & \mathbf{I} \\ \mathbf{D}_{\mathrm{RL}}^* & \mathbf{D}_{\mathrm{RR}}^* \end{bmatrix}. \tag{2.31}$$

Using the relation in Equation (2.11), which results from Bloch's theorem, in Equations (2.29), an alternative eigenvalue problem is formulated

$$\mathbf{N}\mathbf{w}_j = \mu_j \mathbf{L}\mathbf{w}_j. \tag{2.32}$$

---

[6] The $p$-norms are defined by $\|\mathbf{x}\|_p = (|x_1|^p + |x_2|^p + \cdots + |x_n|^p)^{1/p}$.

[7] The condition number provides a measure of the sensitivity of the linear system $\mathbf{A}\mathbf{x} = \mathbf{b}$ (Golub and Loan, 1998). Here, the condition number is defined in terms of the 2-norm of $\mathbf{A}$ as $\kappa_2(\mathbf{A}) = \|\mathbf{A}\|_2 \|\mathbf{A}\|_2^{-1}$.

Notice that the relation between the matrix $\mathbf{S}$ and matrices $\mathbf{L}$ and $\mathbf{N}$ is given by $\mathbf{S} = \mathbf{N}\mathbf{L}^{-1}$. In Equation (2.32), $\{\mathbf{w}_j\}_j$ refer to right eigenvectors which involve displacement/rotation components, only. They can be partitioned into $n \times 1$ vectors of displacement/rotation defined at the left cross-section of the substructure $\{\boldsymbol{\phi}_{\mathsf{q}j}\}_j$ and $n \times 1$ vectors of displacement/rotation defined at the right cross-section of the substructure $\{\mu_j\boldsymbol{\phi}_{\mathsf{q}j}\}_j$. Thus, once these eigenvectors are computed by means of the eigenproblem in Equation (2.32), the wave shapes $\{\boldsymbol{\phi}_j\}_j$ can be easily retrieved as $\boldsymbol{\phi}_j = \mathbf{L}\mathbf{w}_j$ (Mencik, 2014).

## Zhong's eigenvalue problem

A second companion eigenvalue problem has been proposed by Zhong and Williams (1995). It takes advantage of the fact that the eigenvalues come in pairs as $\mu_j$ and $1/\mu_j$. Here, Equation (2.32) is left multiplied, independently, by $\mathbf{L}^T\mathbf{J}$ and by $\mathbf{N}^T\mathbf{J}$, which gives

$$\mathbf{L}^T\mathbf{J}\mathbf{N}\mathbf{w}_j = \mu_j\mathbf{L}^T\mathbf{J}\mathbf{L}\mathbf{w}_j, \tag{2.33a}$$

$$\mathbf{N}^T\mathbf{J}\mathbf{N}\mathbf{w}_j = \mu_j\mathbf{N}^T\mathbf{J}\mathbf{L}\mathbf{w}_j. \tag{2.33b}$$

Then, using the fact that

$$\mathbf{L}^T\mathbf{J}\mathbf{L} = \mathbf{N}^T\mathbf{J}\mathbf{N} = \begin{bmatrix} \mathbf{0} & -\mathbf{D}^*_{\mathsf{LR}} \\ \mathbf{D}^*_{\mathsf{RL}} & \mathbf{0} \end{bmatrix} \tag{2.34}$$

in the second equation, one can write

$$\mathbf{N}^T\mathbf{J}\mathbf{L}\mathbf{w}_j = 1/\mu_j\mathbf{L}^T\mathbf{J}\mathbf{L}\mathbf{w}_j. \tag{2.35}$$

Finally, adding Equations (2.33a) and (2.35), yields

$$\mathbf{Z}_1\boldsymbol{\varphi}_j = \lambda_j\mathbf{Z}_2\boldsymbol{\varphi}_j, \tag{2.36}$$

where

$$\mathbf{Z}_1 = (\mathbf{L}^T\mathbf{J}\mathbf{N} + \mathbf{N}^T\mathbf{J}\mathbf{L}) = \begin{bmatrix} (\mathbf{D}^*_{\mathsf{RL}} - \mathbf{D}^*_{\mathsf{LR}}) & (\mathbf{D}^*_{\mathsf{LL}} + \mathbf{D}^*_{\mathsf{RR}}) \\ -(\mathbf{D}^*_{\mathsf{LL}} + \mathbf{D}^*_{\mathsf{RR}}) & (\mathbf{D}^*_{\mathsf{RL}} - \mathbf{D}^*_{\mathsf{LR}}) \end{bmatrix} \tag{2.37}$$

and

$$\mathbf{Z}_2 = \mathbf{L}^T\mathbf{J}\mathbf{L} = \begin{bmatrix} \mathbf{0} & -\mathbf{D}^*_{\mathsf{LR}} \\ \mathbf{D}^*_{\mathsf{RL}} & \mathbf{0} \end{bmatrix}. \tag{2.38}$$

36

This alternative eigenvalue problem has double eigenvalues in the form $\lambda_j = (\mu_j + 1/\mu_j)$. Thus, assuming that $\mu_j \neq 0$, the original eigenvalues are the solutions of the quadratic polynomial equation $\mu_j^2 - \lambda_j \mu_j + 1 = 0$, *i.e.*,

$$\mu_j = \frac{1}{2}\left(\lambda_j \pm \sqrt{\lambda_j^2 - 4}\right). \tag{2.39}$$

Moreover, each double eigenvalue $\lambda_j$ has two corresponding linearly independent eigenvectors $\boldsymbol{\varphi}_j^{(1)}$ and $\boldsymbol{\varphi}_j^{(2)}$ of size $n \times 1$ each. The original right eigenvectors of Equation (2.12) can be viewed as a linear combination of the eigenvectors related to double eigenvalues of Equation (2.36) (Zhong and Williams, 1995). Thus, for an eigenvalue $\mu_j$, the corresponding eigenvector can be expressed as

$$\mathbf{w}_j = \boldsymbol{\varphi}_j \mathbf{a}_j = a_j^{(1)} \boldsymbol{\varphi}_j^{(1)} + a_j^{(2)} \boldsymbol{\varphi}_j^{(2)}, \tag{2.40}$$

where $\boldsymbol{\varphi}_j = \begin{bmatrix} \boldsymbol{\varphi}_j^{(1)} & \boldsymbol{\varphi}_j^{(2)} \end{bmatrix}$ is a $2n \times 2$ matrix, $\mathbf{a}_j = \begin{bmatrix} a_j^{(1)} & a_j^{(2)} \end{bmatrix}^T$ is a $2 \times 1$ vector composed of scalar coefficients $a_j^{(1)}$ and $a_j^{(2)}$. Substituting this equation into Equation (2.32), yields

$$(\mathbf{N} - \mu_j \mathbf{L})\boldsymbol{\varphi}_j \mathbf{a}_j = \mathbf{0}, \tag{2.41}$$

A natural way of obtaining the relationship between coefficients $a_j^{(1)}$ and $a_j^{(2)}$ consists in left multiplying Equation (2.41) by $\boldsymbol{\varphi}_j^{(1)H}$ (or, alternatively, by $\boldsymbol{\varphi}_j^{(2)H}$), which allows one to write

$$\frac{a_j^{(1)}}{a_j^{(2)}} = -\frac{\boldsymbol{\varphi}_j^{(1)H}(\mathbf{N} - \mu_j \mathbf{L})\boldsymbol{\varphi}_j^{(2)}}{\boldsymbol{\varphi}_j^{(1)H}(\mathbf{N} - \mu_j \mathbf{L})\boldsymbol{\varphi}_j^{(1)}}. \tag{2.42}$$

Although algebraically correct, this expression may suffer from numerical difficulties when $\boldsymbol{\varphi}_j^{(1)}$ is almost parallel to $\mathbf{w}_j$. An alternative way of determining $\mathbf{w}_j$ involves the use of singular value decomposition (SVD), as proposed by Waki *et al.* (2009b). For the sake of clarity and precision, the procedure is presented hereafter.

Let $\mathbf{A}_j = (\mathbf{N} - \mu_j \mathbf{L})\boldsymbol{\varphi}_j$. Using SVD, this matrix may be written as $\mathbf{A}_j = \mathbf{U}_{\mathbf{A}_j} \boldsymbol{\Sigma}_{\mathbf{A}_j} \mathbf{V}_{\mathbf{A}_j}^H$, where $\mathbf{U}_{\mathbf{A}_j}$ is a square $2n \times 2n$ matrix, $\boldsymbol{\Sigma}_{\mathbf{A}_j}$ is a $2n \times 2$ diagonal matrix of singular values and $\mathbf{V}_{\mathbf{A}_j}$ is a square $2 \times 2$ matrix, expressed as

$$\begin{bmatrix} \left(V_{\mathbf{A}_j}\right)_{11} & \left(V_{\mathbf{A}_j}\right)_{12} \\ \left(V_{\mathbf{A}_j}\right)_{21} & \left(V_{\mathbf{A}_j}\right)_{22} \end{bmatrix}.$$

Then, Equation (2.41) can be re-written as

$$\mathbf{U}_{\mathsf{A}_j} \begin{bmatrix} \sigma_{\mathsf{A}_j}^{(1)} \left( \left( \bar{V}_{\mathsf{A}_j} \right)_{11} a_j^{(1)} + \left( \bar{V}_{\mathsf{A}_j} \right)_{21} a_j^{(2)} \right) \\ \sigma_{\mathsf{A}_j}^{(2)} \left( \left( \bar{V}_{\mathsf{A}_j} \right)_{12} a_j^{(1)} + \left( \bar{V}_{\mathsf{A}_j} \right)_{22} a_j^{(2)} \right) \end{bmatrix} = \mathbf{0}_{(2n \times 1)}, \tag{2.43}$$

where $\bar{V}_{pq}$ indicates the complex conjugate of the matrix entry $V_{pq}$. As $\mathbf{w}_j$ is a linear combination of the eigenvectors related to double eigenvalues $\lambda_j$, $\mathbf{A}_j$ is rank-deficient, which makes $\sigma_{\mathsf{A}_j}^{(1)} \gg \sigma_{\mathsf{A}_j}^{(2)} \approx 0$, then the equality in Equation (2.43) is guaranteed by making $\left( \left( \bar{V}_{\mathsf{A}_j} \right)_{11} a_j^{(1)} + \left( \bar{V}_{\mathsf{A}_j} \right)_{21} a_j^{(2)} \right) = 0$, which requires

$$\frac{a_j^{(2)}}{a_j^{(1)}} = -\frac{\left( \bar{V}_{\mathsf{A}_j} \right)_{11}}{\left( \bar{V}_{\mathsf{A}_j} \right)_{21}}. \tag{2.44}$$

### Quadratic eigenvalue problem

It is also possible to solve a companion quadratic eigenvalue problem. This is possible through consideration of Bloch's theorem, *i.e.*, $\mathbf{u}_j^{(k)} = \mu_j \mathbf{u}_j^{(k-1)}$, which allows one to write $\mathbf{q}_{\mathsf{R}j} = \mu_j \mathbf{q}_{\mathsf{L}j}$ and $\mathbf{f}_{\mathsf{R}j} = -\mu_j \mathbf{f}_{\mathsf{L}j}$. Using these relations in Equation (2.3), yields

$$\mathbf{F}_{\mathsf{L}j} = \mathbf{D}_{\mathsf{LL}}^* \mathbf{q}_{\mathsf{L}j} + \mu_j \mathbf{D}_{\mathsf{LR}}^* \mathbf{q}_{\mathsf{L}j} \tag{2.45a}$$

$$-\mu_j \mathbf{F}_{\mathsf{L}j} = \mathbf{D}_{\mathsf{RL}}^* \mathbf{q}_{\mathsf{L}j} + \mu_j \mathbf{D}_{\mathsf{RR}}^* \mathbf{q}_{\mathsf{L}j} \tag{2.45b}$$

Substituting Equation (2.45a) into Equation (2.45b), a quadratic eigenvalue problem of the form

$$\mathbf{C_q} \phi_{\mathsf{q}j} = \mathbf{0}_{(n \times 1)} \tag{2.46}$$

is formulated, where $\mathbf{C_q} = \left( \mu_j^2 \mathbf{D}_{\mathsf{LR}}^* + \mu_j \left( \mathbf{D}_{\mathsf{LL}}^* + \mathbf{D}_{\mathsf{RR}}^* \right) + \mathbf{D}_{\mathsf{RL}}^* \right)$.

### Eigenvalue problem with symmetric matrices

From Equation (2.46), an eigenvalue problem with symmetric matrices can be formulated (Arruda *et al.*, 2007), which enhances the performance of the eigenvalue problem computation. The key idea here is to associate to Equation (2.46) additional equations which would make the matrices $\mathbf{A}$ and $\mathbf{B}$ of a generalized eigenvalue problem $\mathbf{Az} = \lambda \mathbf{Bz}$ symmetric. To begin with,

Equation (2.46) is re-written in terms of $\mathbf{w}_j$, which yields

$$\begin{bmatrix} -\mathbf{D}^*_{\mathrm{RL}} & \mathbf{0} \end{bmatrix} \mathbf{w}_j = \mu_j \begin{bmatrix} (\mathbf{D}^*_{\mathrm{RR}} + \mathbf{D}^*_{\mathrm{LL}}) & \mathbf{D}^*_{\mathrm{LR}} \end{bmatrix} \mathbf{w}_j. \tag{2.47}$$

To this equation the following equation is associated

$$\begin{bmatrix} \mathbf{0} & \mathbf{D}^{*T}_{\mathrm{LR}} \end{bmatrix} \mathbf{w}_j = \mu_j \begin{bmatrix} \mathbf{D}^{*T}_{\mathrm{LR}} & \mathbf{0} \end{bmatrix} \mathbf{w}_j, \tag{2.48}$$

which allows one to express the following eigenvalue problem

$$\bar{\mathbf{N}}\mathbf{w}_j = \mu_j \bar{\mathbf{L}}\mathbf{w}_j, \tag{2.49}$$

where $\bar{\mathbf{N}} = \begin{bmatrix} -\mathbf{D}^*_{\mathrm{RL}} & \mathbf{0} \\ \mathbf{0} & \mathbf{D}^{*T}_{\mathrm{LR}} \end{bmatrix}$ and $\bar{\mathbf{L}} = \begin{bmatrix} (\mathbf{D}^*_{\mathrm{RR}} + \mathbf{D}^*_{\mathrm{LL}}) & \mathbf{D}^*_{\mathrm{LR}} \\ \mathbf{D}^{*T}_{\mathrm{LR}} & \mathbf{0} \end{bmatrix}$.

Table 2.2: Overview of the eigenproblems used to compute the wave modes of a periodic structure.

| Eigenvalue Problem | Associated Eigenvector | Reference Equation |
|---|---|---|
| $\mathbf{S}\boldsymbol{\phi}_j = \mu_j \boldsymbol{\phi}_j$ | $\boldsymbol{\phi}_j \begin{bmatrix} \boldsymbol{\phi}^T_{\mathrm{q}j} & \boldsymbol{\phi}^T_{\mathrm{F}j} \end{bmatrix}^T$ | (2.12) |
| $(\mathbf{J}\boldsymbol{\phi}_j)^T \mathbf{S} = \mu_j^{-1} (\mathbf{J}\boldsymbol{\phi}_j)^T$ | $\boldsymbol{\psi}_j = (\mathbf{J}\boldsymbol{\phi}_j)^T$ | (2.16) |
| $\mathbf{N}\mathbf{w}_j = \mu_j \mathbf{L}\mathbf{w}_j$ | $\mathbf{w}_j = \begin{bmatrix} \boldsymbol{\phi}^T_{\mathrm{q}j} & \mu_j \boldsymbol{\phi}^T_{\mathrm{q}j} \end{bmatrix}^T$ | (2.32) |
| $\bar{\mathbf{N}}\mathbf{w}_j = \mu_j \bar{\mathbf{L}}\mathbf{w}_j$ | $\mathbf{w}_j = \begin{bmatrix} \boldsymbol{\phi}^T_{\mathrm{q}j} & \mu_j \boldsymbol{\phi}^T_{\mathrm{q}j} \end{bmatrix}^T$ | (2.49) |
| $\mathbf{Z}_1\boldsymbol{\varphi}_j = \lambda_j \mathbf{Z}_2\boldsymbol{\varphi}_j$ | $\boldsymbol{\varphi}_j$ <br> $\mathbf{w}_j = a_j^{(1)}\boldsymbol{\varphi}_j^{(1)} + a_j^{(2)}\boldsymbol{\varphi}_j^{(2)}$ | (2.36) |
| $\mathbf{C}\boldsymbol{\phi}_{\mathrm{q}j} = \mathbf{0}_{(n\times 1)}$ | $\boldsymbol{\phi}_{\mathrm{q}j}$ | (2.46) |

## Additional comments regarding the eigenvalue problem formulation for periodic structures

The mathematical formulation presented in this chapter is stated in the frequency domain. The displacements/rotations and force/moments vectors ($\mathbf{q}$ and $\mathbf{F}$, respectively) are harmonic solutions of the dynamic problem under concern — *i.e.*, the free wave propagation through a 1D periodic system —, with the harmonic term $e^{\mathrm{i}\omega t}$ being omitted for the sake of conciseness. Thus, the associated eigenvalue problems are functions of the angular frequency $\omega$ and the wavenumber $\beta$. There are two ways of solving these eigenvalue problems: the direct and the inverse methods. The inverse method is considered to solve the numerical problems that will be presented in this thesis. It consists in solving the eigenvalue problem with respect to the wavenumber $\beta_j$, for specified angular frequencies within the range of analysis. One of the advantage of this approach is that complex wavenumbers are possible.

On the other hand, the direct method consists in solving an eigenproblem, for prescribed values of the wavenumber $\beta$, with respect to the angular frequency $\omega$. This approach is typically used to evaluate the dispersion relation of undamped periodic systems. Here, phase constant surfaces ($\omega = f(\beta)$ in the 1D case, $\omega = f(\beta_x, \beta_y)$ in the 2D case, $\omega = f(\beta_x, \beta_y, \beta_z)$ in the 3D case) are obtained, which are convenient to the identification of attenuation zones (or band gaps), typical in periodic structures. The eigenproblem into consideration here is formulated without condensing internal degrees of freedom as it must be linear with respect to $\omega^2$. This yields a problem of large size, compared to those solved via inverse method (where the condensation of internal DOFs is possible). From Bloch's theorem (stated in Section 2.2.3), $\mathbf{q}_{\mathrm{R}j} = \mu_j \mathbf{q}_{\mathrm{L}j}$ and $\mathbf{F}_{\mathrm{R}j} = -\mu_j \mathbf{F}_{\mathrm{L}j}$. Using these relations in Equation (2.3) and by assuming that damping is not present, it yields

$$\left(\tilde{\mathbf{K}}(\mu) - \omega^2 \tilde{\mathbf{M}}(\mu)\right) \boldsymbol{\phi}_{\mathbf{q}} = \mathbf{0}, \tag{2.50}$$

where

$$\tilde{\mathbf{K}}(\mu) = \begin{bmatrix} (\mu^2 \mathbf{K}_{\mathrm{LR}} + \mu\left(\mathbf{K}_{\mathrm{LL}} + \mathbf{K}_{\mathrm{RR}}\right) + \mathbf{K}_{\mathrm{RL}}) & \mathbf{K}_{\mathrm{RI}} + \mu \mathbf{K}_{\mathrm{LI}} \\ \mathbf{K}_{\mathrm{IL}} + \mu \mathbf{K}_{\mathrm{IR}} & \mathbf{K}_{\mathrm{II}} \end{bmatrix}$$

and

$$\tilde{\mathbf{M}}(\mu) = \begin{bmatrix} (\mu^2 \mathbf{M}_{\mathrm{LR}} + \mu\left(\mathbf{M}_{\mathrm{LL}} + \mathbf{M}_{\mathrm{RR}}\right) + \mathbf{M}_{\mathrm{RL}}) & \mathbf{M}_{\mathrm{RI}} + \mu \mathbf{M}_{\mathrm{LI}} \\ \mathbf{M}_{\mathrm{IL}} + \mu \mathbf{M}_{\mathrm{IR}} & \mathbf{M}_{\mathrm{II}} \end{bmatrix},$$

both of them are symmetric matrices.

## 2.2.6 Frequency tracking of wave modes

Within the WFE framework, the dispersion curve of each wave mode is obtained by analyzing the frequency evolution of the wavenumbers $\beta_j$ which are defined so that $\mu_j = e^{-i\beta_j\Delta}$ (Equation (2.10)). Tracking each wave mode over the frequency domain appears to be a crucial task aiming at providing a deep physical insight of the dynamic behavior of periodic structures. Indeed, the dispersion curves can be used to predict the far-field dynamic behavior of periodic structures composed of a sufficient number of substructures. The issue when assessing the frequency evolution of $\beta_j$ (or $\mu_j$) consists in tracking each wave mode over the frequency domain, it being understood that many wave modes are to be computed at several discrete frequencies and there exists a priori no direct connection to link these modes between two consecutive frequencies. In other words, a given mode $r$ defined at a frequency $\omega_i$ may not match with the mode $r$ defined at the previous frequency $\omega_{i-1}$. By comparing the dispersion curves relative to tracked and non-tracked wave modes in frequency (see Figure 2.5), the importance of tracking the wave modes in frequency is highlighted.

Two approaches are usually used for that purpose, they are: the modal assurance criterion (MAC), which provides information about eigenvectors correlation and originally applied to normal vibration modes (Allemang, 2003), and another one which makes use of the symplectic orthogonality of wave mode shapes.

The MAC consists in evaluating the consistency (degree of linearity) between two wave modes evaluated at consecutive angular frequencies, $\omega_{i-1}$ and $\omega_i = \omega_{i-1} + \Delta\omega$, where $\Delta\omega$ is sufficiently small. It is important to notice that the wave modes are not orthogonal in the Euclidean space due to the symplectic property of matrix $\mathbf{S}$. Thus, within the framework of the WFE method, MAC only provides information about the correlation between two wave modes, it cannot be used for orthogonality check. It is stated, as follows. Given a wave mode $j$ at the frequency $\omega_{i-1}$, the same wave mode $j$ at the consecutive frequency $\omega_i$ is chosen so that

$$\frac{\left|\phi_j^H(\omega_{i-1})\phi_j(\omega_i)\right|^2}{\|\phi_j(\omega_i)\|\|\phi_j(\omega_i)\|} = \max_{k}\left\{\frac{\left|\phi_j^H(\omega_{i-1})\phi_k(\omega_i)\right|^2}{\|\phi_j(\omega_{i-1})\|\|\phi_k(\omega_i)\|}\right\}. \tag{2.51}$$

An alternative procedure makes use of the symplectic orthogonality properties of the wave

modes (Zhong and Williams, 1995) between two consecutive discrete frequencies $\omega_{i-1}$ and $\omega_i$ spaced by a small step $\Delta\omega$. The procedure can be stated as follows (Mencik, 2010). Given two wave modes $j$ and $l$ verifying $\mu_l = 1/\mu_j$ at the frequency $\omega_{i-1}$, the wave mode $m$ at the frequency $\omega_i$ is chosen so that

$$\left| \frac{\phi_j(\omega_{i-1})^T}{\|\phi_j(\omega_{i-1})\|} \mathbf{J} \frac{\phi_l(\omega_i)}{\|\phi_l(\omega_i)\|} \right| = \max_k \left\{ \left| \frac{\phi_j(\omega_{i-1})^T}{\|\phi_j(\omega_{i-1})\|} \mathbf{J} \frac{\phi_k(\omega_i)}{\|\phi_k(\omega_i)\|} \right| \right\}. \tag{2.52}$$
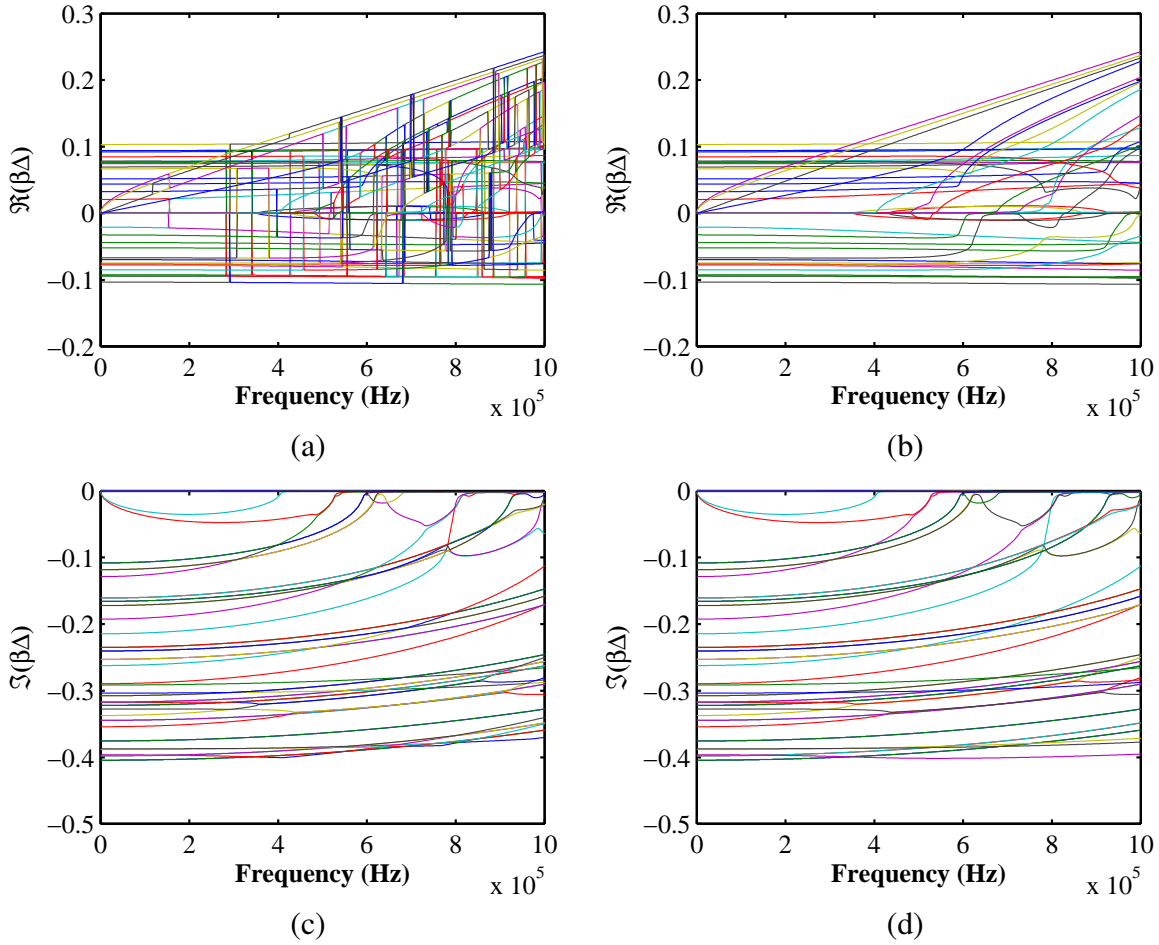


Figure 2.5: Dispersion curves of a solid waveguide plotted (a,c) before tracking wave modes, (b,d) after applying a wave mode tracking procedure: (a,b) magnitude of the real part of normalized wavenumbers $|\Re\left(\beta_j\Delta\right)|$, (c,d) imaginary part of the normalized wavenumbers $\Im\left(\beta_j\Delta\right)$.

## 2.3 Error analysis

The WFE method, as other numerical methods, is prone to errors, which arise at different steps of the method. They may be of different types, for instance, round-off errors, discretization errors, truncation errors, among others. It is important to be aware of the possible sources of errors in order to seek for alternatives, if they exist, and know the maximum accuracy level that can be reached with the method. In Figure 2.6, a schematics of the different steps involved in the WFE method as long as the numerical errors that can be associated to them is presented.

The first step of the WFE method is to construct the FE model of the substructure. To this step, a discretization error is associated. This occurs because, in FEM, the interpolation shape functions are polynomials independent of the frequency. Thus, as a consequence of Shannon's sampling theorem (Jerry, 1977), a minimum number of elements per wavelength is required to obtain accurate solutions via FEM. The common applied rule of thumb consists in using FE meshes with six to ten nodes per wavelength (Marburg, 2008), *i.e.*,

$$e \leq \frac{l_\lambda}{8}, \tag{2.53}$$

where $e$ is the element size and $l_\lambda$ is the wavelength. In this thesis, we will be dealing with multi-coupled periodic structures, which means that multiple wave modes are involved. In this case, the minimum element size is related to the wave mode of minimum wavelength, which corresponds to a wave mode whose real part of the corresponding wavenumber is maximum, as stated below:

$$l_{\lambda min} = \frac{2\pi}{\max_j \left( \Re \left( \beta_j \right) \right)}. \tag{2.54}$$

Let's consider that $m_\Delta$ elements are used to discretize the substructure along the $x$-axis. Recalling that the substructure has a length of $\Delta$, the element size along the $x$-direction is $e = \Delta/m_\Delta$. Using this expression and Equation (2.54) in Equation (2.53), it yields

$$\frac{\Delta}{m_\Delta} \leq \frac{\pi}{4} \left( \max_j \left( \Re \left( \beta_j \right) \right) \right)^{-1}, \quad \max_j \left( \Re \left( \beta_j \right) \right) \Delta \leq \frac{m_\Delta \pi}{4}. \tag{2.55}$$

As $|\Re \left( \beta_j \right)|$ is typically a monotonically increasing function with respect to $\omega$, Equation (2.55) provides the upper endpoint of the interval of discrete frequencies in which $\beta_j$ is evaluated for a given discretization. Moreover, notice that a bound for $|\Re \left( \beta_j \Delta \right)|$ is completely determined by the

number of finite elements across the substructure length $m_\Delta$.
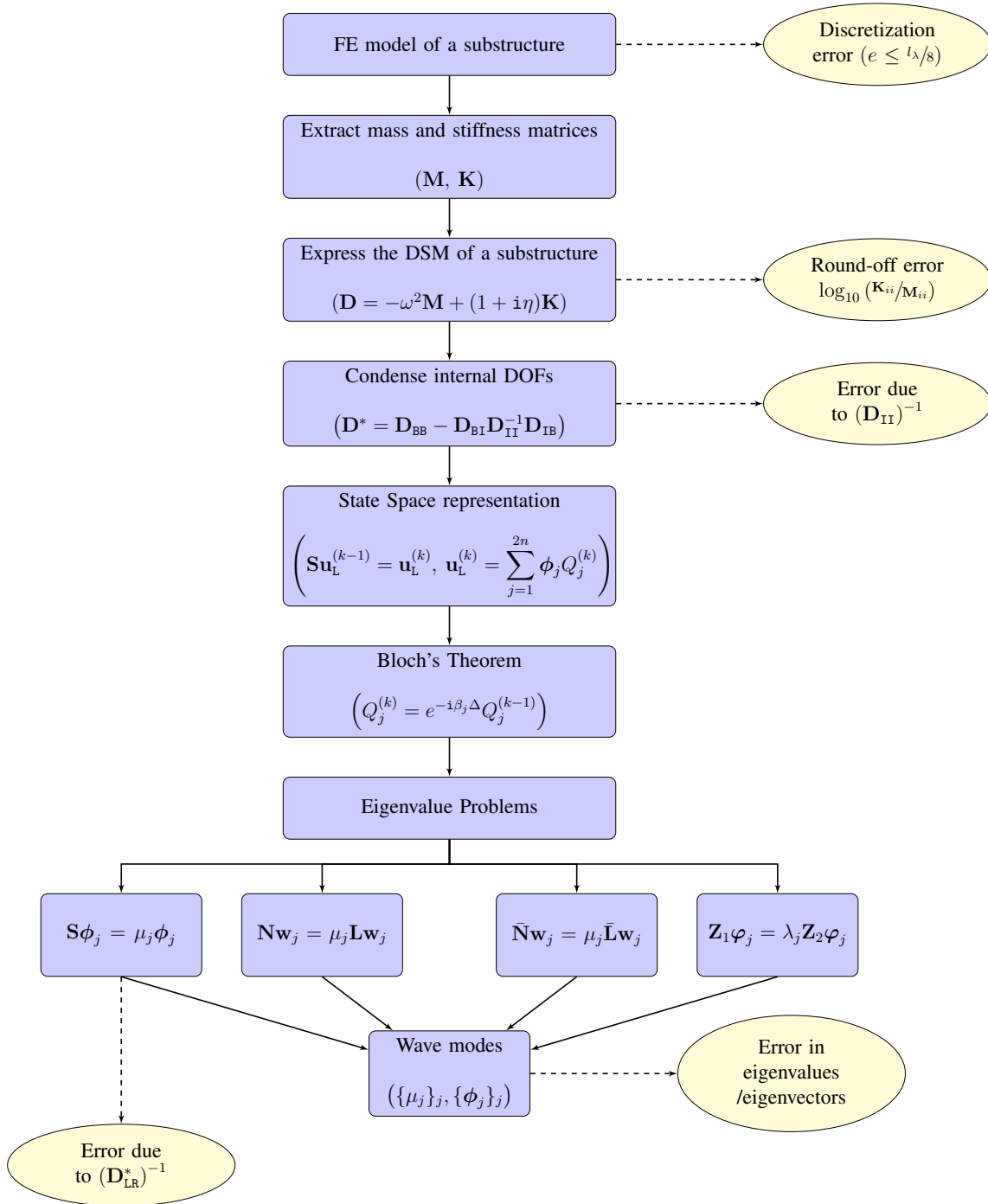


Figure 2.6: Flowchart of the different steps and associated numerical errors within the WFE method.

Round-off errors are those associated to finite precision with which computers represent floating-point numbers. This kind of error may occur in every arithmetic operation. However, within the WFE method, it is crucial when the dynamic stiffness matrix of the substructure is formulated. In this step, the round-off error occurs if any of the elements of the stiffness matrix, for instance, $\mathbf{K}_{ij}$), is very large compared to the corresponding mass proportional value $\omega^2 \mathbf{M}_{ij}$ leading to the truncation of inertia terms after the subtraction. As explained by Waki *et al.* (2009b), the number of truncated digits may be approximate by $nr_{ij} = \log_{10}\left(|\mathbf{K}_{ij}/\omega^2\mathbf{M}_{ij}|\right)$, which allows one to conclude that the numerical errors associated to the round-off of inertia terms affect mainly at very low frequency. Besides, if the number of digits lost is greater than 16, for double arithmetic precision, all information regarding the mass matrix is lost. This constitutes a frequency limit below which the numerical solution is not acceptable. Such errors can be prevented without need of remeshing. Indeed, the initial mesh size is retained, but the number of elements within a substructure $(m_\Delta)$ is increased, which means an increase of the substructure length (thus, large $\mathbf{M}_{ij}$).

The WFE method is also subject to numerical errors due to the inversion of matrices with high condition numbers. This is the case in the process of condensing the internal DOFs, which involves the inversion of $\mathbf{D}_{\mathrm{II}}$. This kind of error may also cause numerical difficulties when the eigenvalue problem is formulated by means of the symplectic transfer matrix $\mathbf{S}$. As discussed in Section 2.2.2, matrix $\mathbf{S}$ involves the inversion of $\mathbf{D}_{\mathrm{LR}}^*$.

### 2.3.1 Numerical errors related to the eigenvalue problem formulation
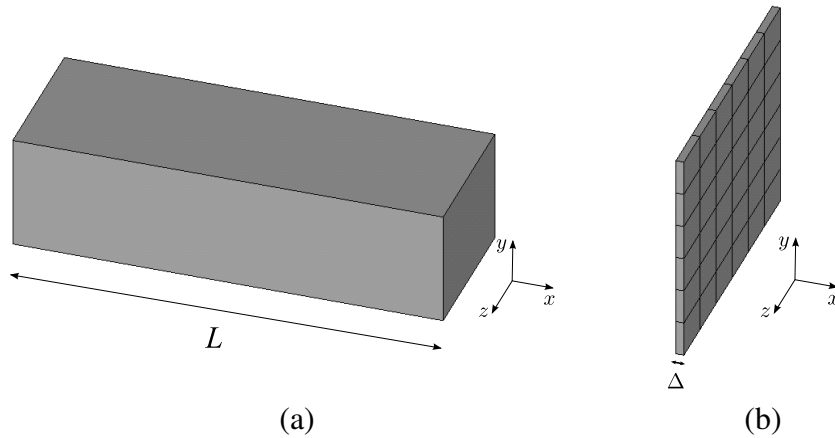


Figure 2.7: Schematics of the solid waveguide used to analyze numerical errors related to the WFE method: (a) full waveguide, (b) FE model of the substructure.

Consider a linear elastic and damped waveguide as shown in Figure 2.7(a). A substructure of length $\Delta = 0.004/36$ m is modeled by means of 3D solid hexahedral elements with eight nodes and three DOFs per node — *i.e.*, translations along the $x$, $y$ and $z$ axes —, the SOLID45 elements from ANSYS® (see Figure 2.7(b)). The structure is made of steel (Young's modulus $E = 2.1 \times 10^{11}$ Pa, density $\rho = 7800$ kg.m$^{-3}$, Poisson's ratio $\nu = 0.3$, and internal loss factor $\eta = 0.01$) and it has a rectangular cross-section (height $h_y = 0.003$ m and width $h_z = 0.004$ m). The numerical errors involved in the computation of the numerical wave modes of this waveguide by means of the WFE method are analyzed. The frequency range of interest here is $\beta_f = [200\ \text{Hz} - 2\ \text{MHz}]$, evaluated at every 2000 Hz. It is important to point out here that substructure model was built using a fine enough FE mesh for the maximum frequency within the range under concern.

Here, the different eigenproblems presented in Section 2.2.5 are compared in terms of the accuracy of the computed numerical wave modes. To begin with, low-order numerical wave modes are compared to the analytical ones computed by means of the elementary theory of rods and Timoshenko's beam theory. The comparison is restricted to the frequency range for the validity of these theories, which according to Doyle (1997), would be below

$$f_{\max} \approx \frac{3}{4} \frac{c_s}{h}, \tag{2.56}$$

where $c_s$ is the speed of shear S-waves given by $\sqrt{G/\rho}$, with $G$ being the shear modulus, and $h$, the cross-section length. This frequency is chosen to be close to the first cut-on frequencies of the Lamb symmetric and antisymmetric modes. For the structural model into consideration here, $f_{\max} \approx 0.4$ MHz. In Figure 2.8, the dispersion curves — $|\Re(\beta_j \Delta)|$ in the positive $y$-axis, $\Im(\beta_j \Delta)$ in the negative $y$-axis — for some low-order wave modes computed by means of the various numerical formulations and analytical relations are plotted as well as the relative errors associated to the computation of the propagation constants $\mu_j$ and the wave mode shapes $\phi_j$. These errors are expressed as

$$\epsilon_{\mu_j}(\omega_i) = \frac{|\mu_j(\omega_i) - \mu_{j\,\texttt{ref}}(\omega_i)|}{|\mu_{j\,\texttt{ref}}(\omega_i)|}, \quad \epsilon_{\phi_j}(\omega_i) = \frac{\|\phi_j(\omega_i) - \phi_{j\,\texttt{ref}}(\omega_i)\|_2}{\|\phi_{j\,\texttt{ref}}(\omega_i)\|_2}, \tag{2.57}$$

respectively, where the subscript `ref` is used to denote reference, which, in this case, is the analytical value. From this analysis, one may notice that all eigenproblem formulations provide almost the same accuracy, with exception of the (**N**,**L**) eigenproblem (Equation (2.32)), which seems to be more sensitive to errors at very low frequencies. Moreover, a good agreement is observed until the first cut-on frequency of the shear mode w.r.t. the $y$-axis.
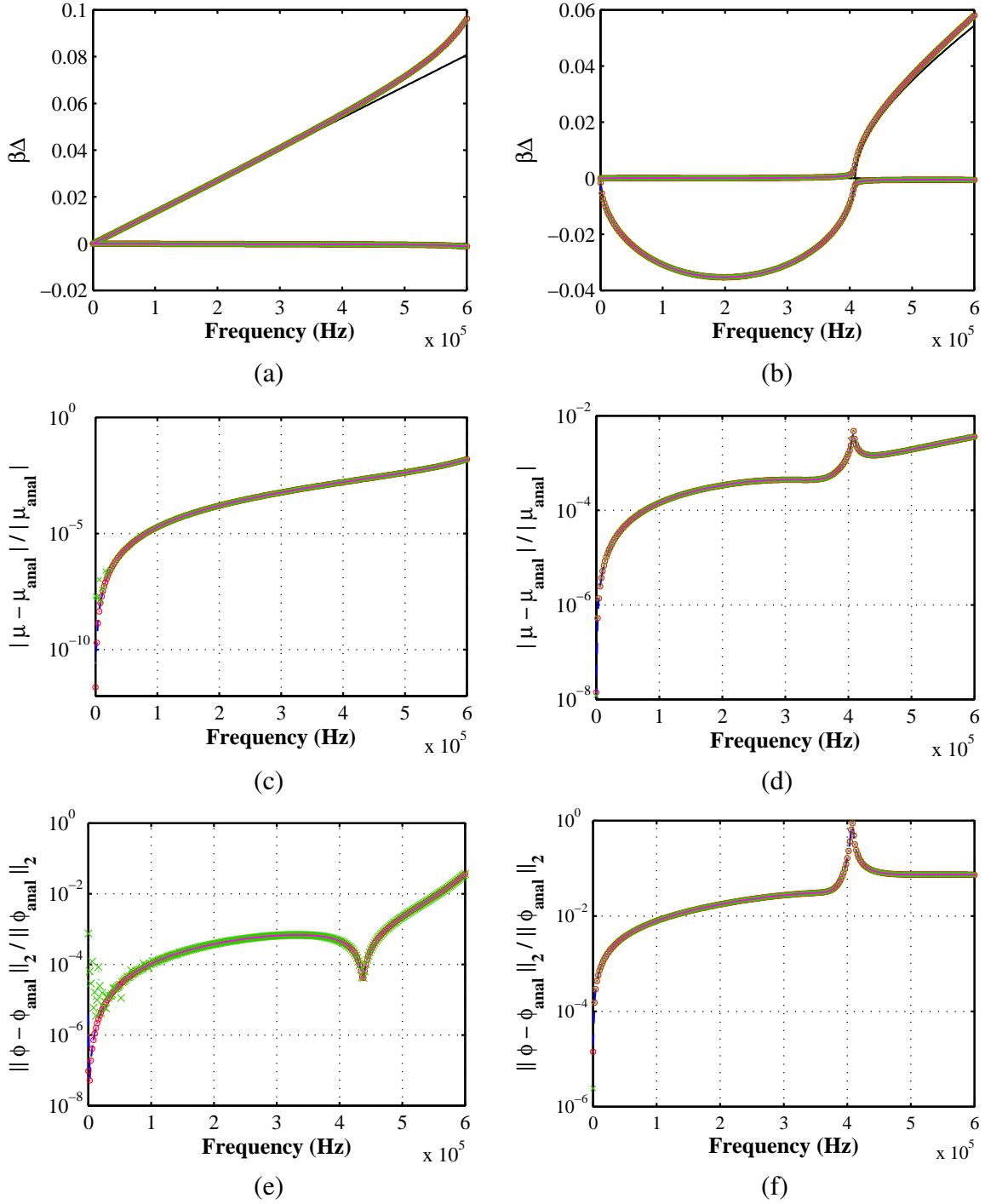
Figure 2.8: Comparison of numerical wave modes, related to the longitudinal wave (a,c,e) and the shear wave w.r.t. the $y$-axis (b,d,f), computed by means of WFE method with the corresponding analytical values. (a,b) Dispersion curves, (c,d) $\epsilon_{\mu_j}$, (e,f) $\epsilon_{\phi_j}$ (Equation (2.57)). The following approaches are compared: (—) analytical solution, (- - -) Equation (2.36), ( $\circ$ ) Equation (2.12), ( $\bullet$ ) Equation (2.32), ( x ) Equation (2.49).

The various formulations for the WFE-based eigenproblem are also compared with respect to the symplectic and symmetry conditions between left- and right-going wave modes. As discussed in Section 2.2.4, due to the symplectic property of the eigenvalue problems the eigenvalues might be in pairs $\mu_j$ and $1/\mu_j$, which means that if a wave travels to the right direction with a propagating constant $\mu_j$, the corresponding left-going wave would travel with a propagating constant $\mu_j^\star = 1/\mu_j$. With exception to the generalized eigenproblem with antisymmetric matrices which provides pairs of repetitive eigenvalues (Equation (2.36)), we expect that all other formulations provide pairs ($\mu_j$, $1/\mu_j$) as eigenvalues. The error associated to the guarantee of obtaining as eigenvalues $\mu_j$ and $1/\mu_j$, or double eigenvalues in the case of Equation (2.36), is presented in Figure 2.9(a). The expressions for the error in the eigenvalue computation are given by

$$
\epsilon_{\boldsymbol{\mu}}(\omega_i) = \sqrt{\sum_{j=1}^{n} \left( \frac{|\mu_{n+j}(\omega_i) - \mu_j(\omega_i)|}{|\mu_j(\omega_i)|} \right)^2}, \quad \text{for the eigenproblem stated in Equation (2.36),}
$$

$$(2.58a)$$

$$
\epsilon_{\boldsymbol{\mu}}(\omega_i) = \sqrt{\sum_{j=1}^{n} \left( \frac{|\mu_j^\star(\omega_i) - 1/\mu_j(\omega_i)|}{|1/\mu_j(\omega_i)|} \right)^2}, \quad \text{for all other eigenproblems.} \quad (2.58b)
$$

Notice that the errors are really small for almost all formulations, with exception to the (**N**,**L**) eigenproblem (Equation (2.32)). For this eigenproblem, the error regarding the eigenvalues is investigated with respect to the wave mode rank in Figure 2.10. The magnitude of the corresponding right-going propagating constants is also plotted as a function of the wave mode rank and frequency. From the results shown in Figure 2.10, one may conclude that the eigenvalues which are prone to more errors are neither purely evanescent or propagating. The propagation of those errors can be avoided by enforcing the property of the eigenvalues related to left- and right-going waves.

Regarding the wave mode shapes, the symmetry condition stated in Equation (2.22) is evaluated by means of the following error expression

$$
\epsilon_{\boldsymbol{\Phi}}(\omega_i) = \sqrt{\sum_{j=1}^{n} \left( \frac{\left\| \boldsymbol{\phi}_{n+j}(\omega_i) - \mathcal{T}\boldsymbol{\phi}_j(\omega_i) \right\|_2}{\left\| \mathcal{T}\boldsymbol{\phi}_j(\omega_i) \right\|_2} \right)^2}. \quad (2.59)
$$

This error analysis is performed for all eigenproblem formulations with exception of the Zhong's eigenproblem (Equation (2.36)), as in this case the symmetry condition is always enforced. The results are presented in Figure 2.9(b). As in the previous analysis, the eigenproblem of Equa-

tion (2.32) provides the worst results, thus requiring the enforcement of the symmetry condition at each frequency step.



(a)

(b)
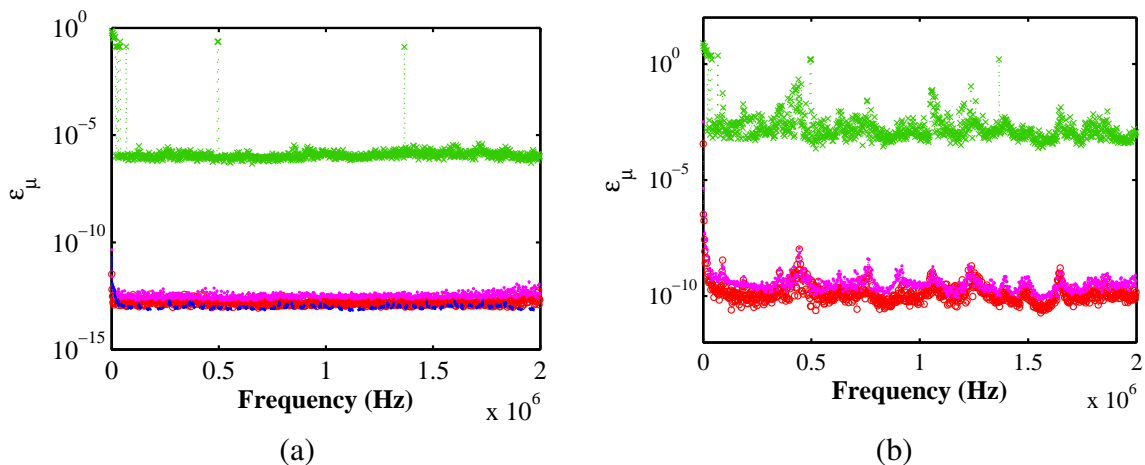
Figure 2.9: Verification of the symmetry relation, by means of : (a) $\epsilon_\mu$ (Equation (2.58)), (b) $\epsilon_\Phi$ (Equation (2.59)), for the following approaches: (- - -) Zhong's $(\mathbf{Z}_1,\mathbf{Z}_2)$ eigenproblem (Equation (2.36)), ( $\circ$ ) $\mathbf{S}$ eigenproblem (Equation (2.12)), ( $\bullet$ ) $(\mathbf{N},\mathbf{L})$ eigenproblem (Equation (2.32)), ( x )$(\bar{\mathbf{N}},\bar{\mathbf{L}})$ eigenproblem (Equation (2.49)).



(a)

(b)
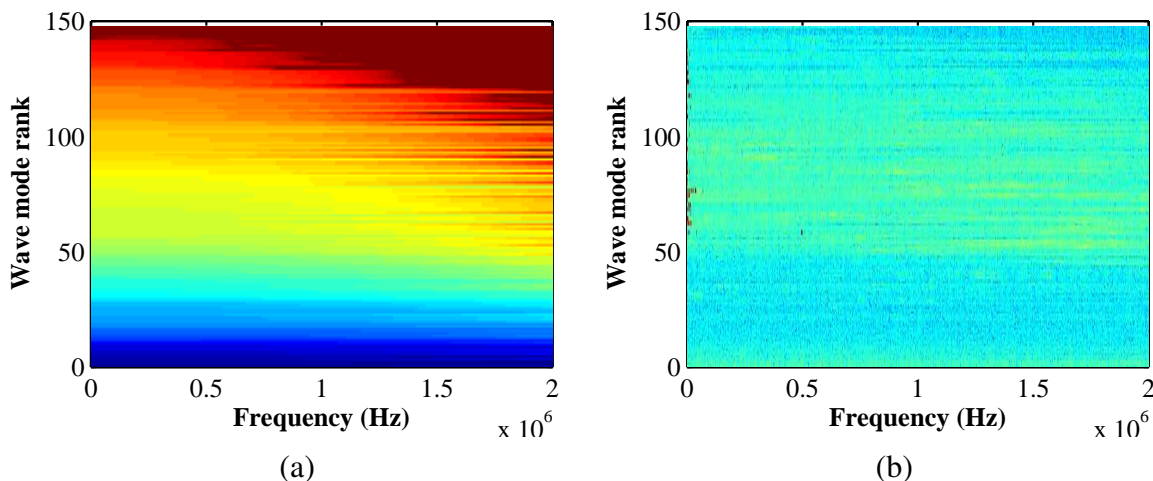
Figure 2.10: (a)Magnitude of right-going propagation constants $(|\mu_j|_{j,=1,\cdots,n})$, (b) error $\epsilon_\mu$ computed via the $(\mathbf{N},\mathbf{L})$ eigenproblem stated in Equation (2.32) as a function of the wave mode rank and frequency.

The WFE eigenproblems have also been compared in terms of the sensitivity of their corresponding eigenvalues to numerical errors. The Bauer-Fike theorem (Section 2.2.5) demonstrates

that the sensitivity of the eigenvalues can be measured by evaluating the condition number of the eigenvector matrix, which is plotted in Figure 2.11(a). As expected, for small perturbations, the eigenvalues computed by means of Equation (2.12) seem to be the highly prone to errors. The alternative formulations are related to small condition numbers of almost the same order of magnitude.

Moreover, WFE-based eigenproblems are compared in terms of computational time in Figure 2.11(b). The results show that the eigenproblem stated in Equation (2.12) is the fastest one, it saves 72.6 % of the time used for solving Zhong's eigenproblem (Equation (2.36)). However, as just discussed, it may be prone to numerical errors. The same justification holds for avoiding the L/N eigenproblem in Equation (2.32) although it saves 12.6 % of computational time. In order to meet a good compromise in terms of performance and accuracy, the eigenproblems in Equations (2.36) and (2.49) are preferred.



(a)                              (b)
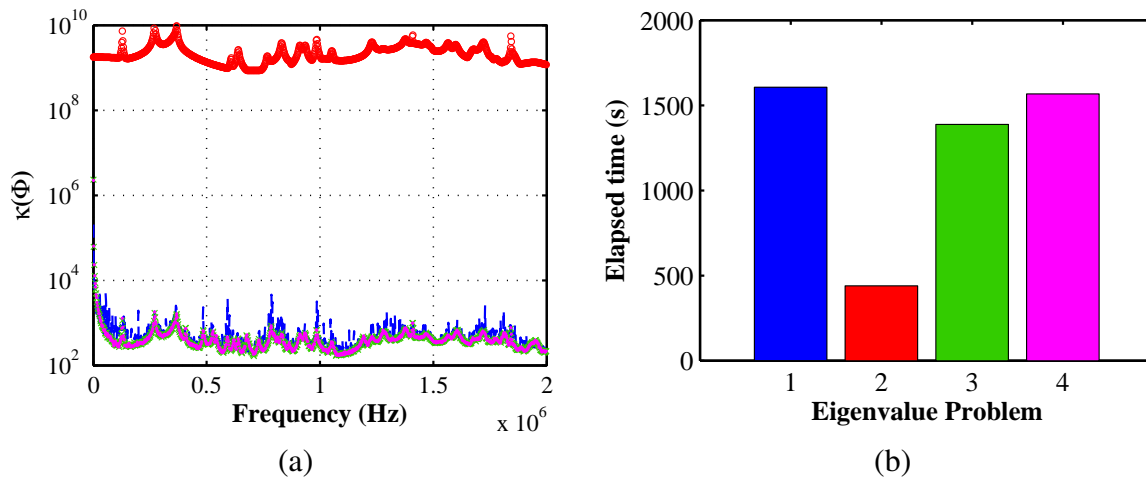
Figure 2.11: (a) Condition number of the matrix of eigenvectors and (b) elapsed times are compared for the following eigenproblems: (- - -) or $1$ Equation (2.36) , ( $\circ$ ) or $2$ Equation (2.12), ( $\bullet$ ) or $3$ Equation (2.32), ( x ) or $4$ Equation (2.49).

## 2.3.2 Numerical errors related to the FE mesh

In this section, the effect of the finite element mesh size in the computation of the numerical wave modes is investigated. Here, the eigenproblem stated in Equation (2.36) is used to compute the numerical wave modes. The accuracy of the wave modes for three different models (see Figure

50
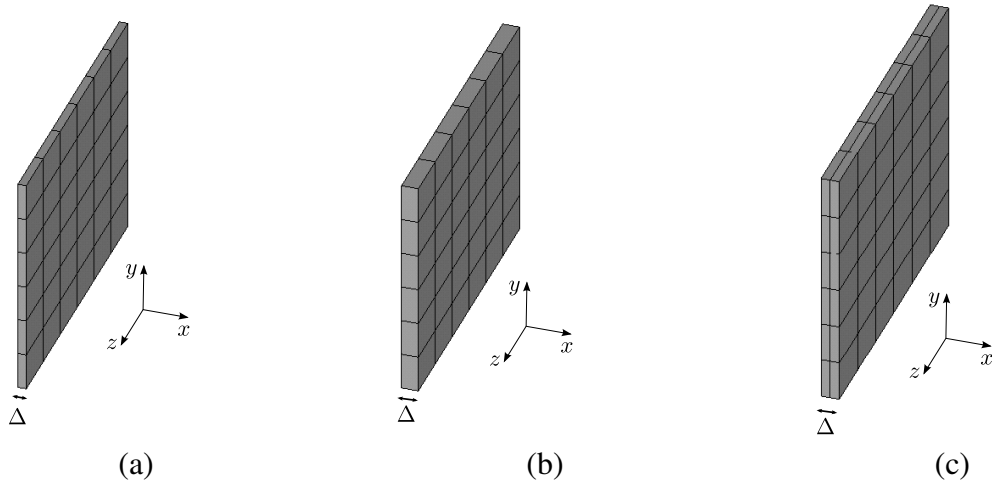
Figure 2.12: FE models of the substructures used to investigate the numerical errors related to the FE mesh size along the main $x$-axis (the element sizes along the orthogonal $y$ and $z$-axes remained unchanged): (a) substructure with length $\Delta = \Delta_{\mathrm{ref}} = 0.004/36$ m, (b) substructure with length $\Delta = 2\Delta_{\mathrm{ref}}$, (c) substructure with length $\Delta = 2\Delta_{\mathrm{ref}}$ and internal DOFs.

2.12) — (a) same model used in the previous section with length $\Delta = \Delta_{\mathrm{ref}}$ of $0.004/36$ m and without internal DOFs, (b) substructure with length $\Delta = 2\Delta_{\mathrm{ref}}$ and without internal DOFs, (c) substructure with length $\Delta = 2\Delta_{\mathrm{ref}}$ and with internal DOFs — are compared.

The accuracy provided by each substructure model is assessed by comparing the numerical wave modes to the low-order analytical modes (the longitudinal mode, Timoshenko's bending and shear modes w.r.t. $y$-axis). The dispersion curves for the three substructure models and errors relative to the propagating constants and the wave mode shapes are shown in Figure 2.13. Notice that, as expected, the substructure model with the smallest thickness (Figure 2.12(a)) provides the most accurate values for the propagating constants. On the other hand, the wave mode shapes seem to be less affected by the mesh size. However, it is important to notice that although some improvement in the accuracy of the wave modes computed for the model in (Figure 2.12(c)) is obtained compared to that of model in Figure 2.12(b), the inclusion of internal DOFs may add some perturbation to the wave mode shapes.

51
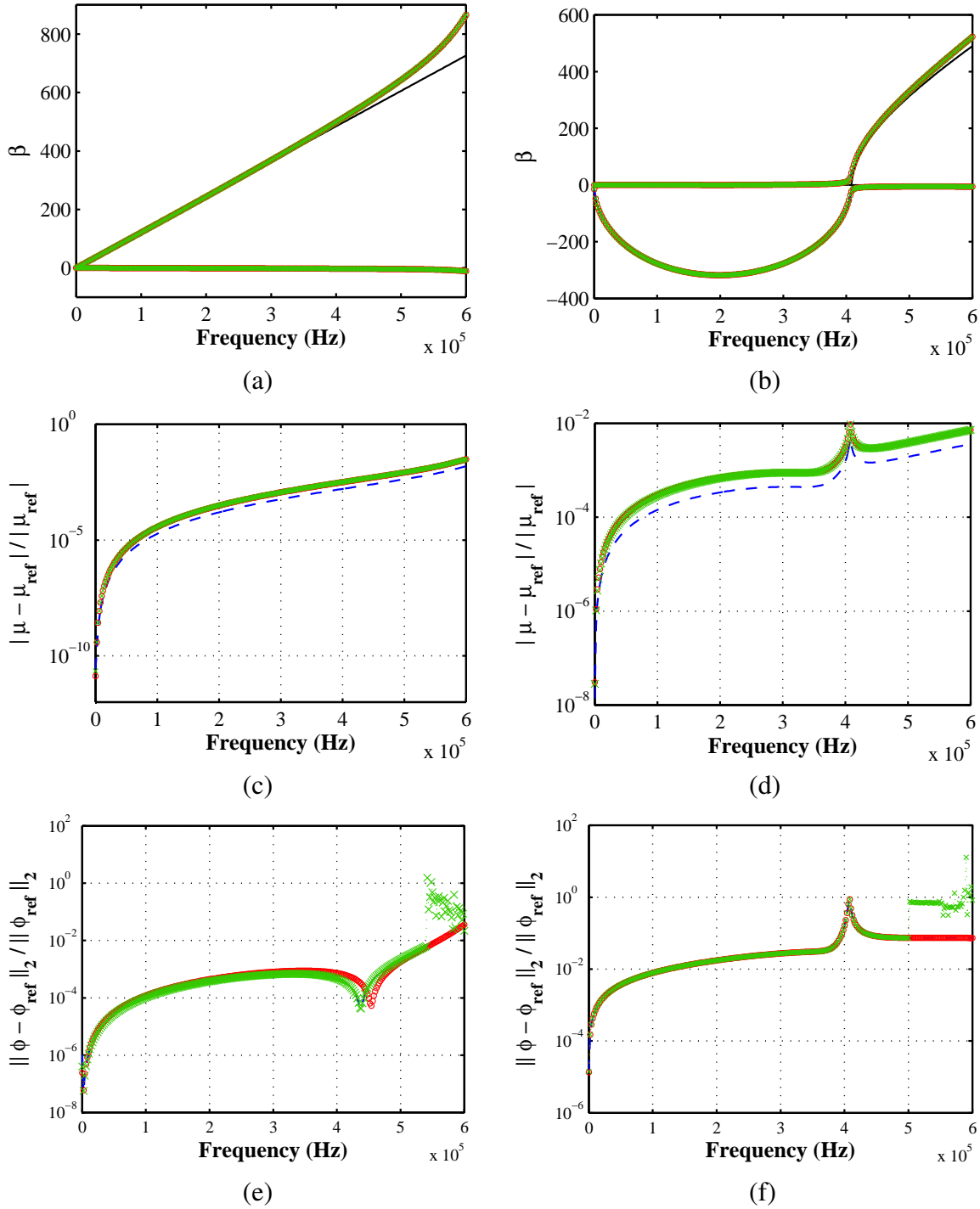
Figure 2.13: Comparison of numerical wave modes, related to the longitudinal wave (a,c,e) and the shear wave w.r.t. the $y$-axis (b,d,f), computed by means of WFE method with the corresponding analytical values. (a,b) Dispersion curves, (c,d) $\epsilon_{\mu_j}$, (e,f) $\epsilon_{\phi_j}$. The following substructure models are compared: (——) analytical model, (- - -) $\Delta = \Delta_{\mathrm{ref}} = 0.004/36$ m without internal DOFs, ( ○ ) $\Delta = 2\Delta_{\mathrm{ref}} = 0.004/18$ m without internal DOFs, ( ● ) $\Delta = 2\Delta_{\mathrm{ref}} = 0.004/18$ m with internal DOFs.

## 2.4 Implementation

For the sake of clarity, the numerical tasks and platform environments involved in the WFE method are shown in Figure 2.14. ANSYS® is used as a means to assess the mass and stiffness matrices of substructures. Post-treatment of those matrices is achieved using MATLAB® with a view to compute the numerical wave basis which describe the dynamic behavior of a periodic structure of arbitrary length. All the numerical simulations are performed in double precision.

A procedure for extracting FE matrices ($\mathbf{M}$, $\mathbf{C}$, $\mathbf{K}$) and the information regarding nodal coordinates and DOFs obtained with the aid of ANSYS® and making them available to be handled in MATLAB® has been implemented. Notice that this task is a crucial step within the WFE method, the reasons are twofold: there is no automatic link between the two softwares (as occurs, for instance, with COMSOL® and MATLAB®), and there is not a unique way of performing matrix extraction in ANSYS®, depending on which one is chosen to be implemented, the extraction of matrices relative to substructures having a large number of DOFs may be become prohibitive. The procedure implemented in this thesis provides an efficient way for accessing the FE data. The codes are available in Appendix A.

Regarding the numerical steps involved in the WFE method, the choice of the eigenproblem formulation to be solved in order to get information from the numerical wave modes is among the most critical steps. It is known that the eigenproblem of Equation (2.36) performs better, but it requires additional manipulations to get the original propagation constants and wave modes. In a practical sense, we usually avoid the use of ($\mathbf{N}$,$\mathbf{L}$) eigenproblem stated in Equation (2.32), and choose one among the alternative ones. Moreover, in order to avoid numerical issues in the use of the WFE method for forced response analysis, which is the topic addressed in Chapter 3, some analytical relations might be enforced. For instance, although the eigenproblem is inherently symplectic, one must ensure that the eigenvalues are in pairs ($\mu$ and $1/\mu$) as the numerical computation of the eigenvalue problem is subject to numerical errors. Additionally, the symmetric relation between left- and right-going wave modes may not be well stated when obtaining them from the eigenvectors. For this reason, we include a numerical task which enforces the symmetric feature.

FE model of substructure

Extract mass and stiffness matrices
$(\mathbf{M}, \mathbf{K})$

Express the DSM of a substructure
$(\mathbf{D} = -\omega^2\mathbf{M} + (1 + \mathrm{i}\eta)\mathbf{K})$

Condense internal DOFs
$\left(\mathbf{D}^* = \mathbf{D_{BB}} - \mathbf{D_{BI}}\mathbf{D_{II}^{-1}}\mathbf{D_{IB}}\right)$

State Space representation
$\left(\mathbf{S}\mathbf{u}_{\mathrm{L}}^{(k-1)} = \mathbf{u}_{\mathrm{L}}^{(k)}, \; \mathbf{u}_{\mathrm{L}}^{(k)} = \sum_{j=1}^{2n} \boldsymbol{\phi}_j Q_j^{(k)}\right)$

Bloch's Theorem
$\left(Q_j^{(k)} = e^{-\mathrm{i}\beta_j \Delta} Q_j^{(k-1)}\right)$

Eigenvalue Problem

$\mathbf{S}\boldsymbol{\phi}_j = \mu_j \boldsymbol{\phi}_j$

$\mathbf{N}\mathbf{w}_j = \mu_j \mathbf{L}\mathbf{w}_j$

$\bar{\mathbf{N}}\mathbf{w}_j = \mu_j \bar{\mathbf{L}}\mathbf{w}_j$

$\mathbf{Z}_1\boldsymbol{\varphi}_j = \lambda_j \mathbf{Z}_2\boldsymbol{\varphi}_j$

$(\{\mu_j\}_j, \{\boldsymbol{\phi}_j\}_j)$

Classifying according to the direction
$(\mu_j, \boldsymbol{\Phi}_j), \quad j = 1, 2, \cdots, n$
$(\mu_j^\star, \boldsymbol{\Phi}_j^\star), \quad j = 1, 2, \cdots, n$

Eigenvalues in pairs
$(\{\mu_j\}_j, \{^1\!/\!_{\mu_j}\}_j), \quad j = 1, 2, \cdots, n$

Symmetry between wave modes
$\boldsymbol{\Phi}_{\mathsf{q}}^\star = \mathcal{R}\boldsymbol{\Phi}_{\mathsf{q}} \quad , \quad \boldsymbol{\Phi}_{\mathsf{F}}^\star = -\mathcal{R}\boldsymbol{\Phi}_{\mathsf{F}}$

Figure 2.14: Flowchart illustrating the different numerical steps involved in the WFE method.

## 2.5 Conclusions

This chapter has presented the general formulation of the WFE method for the free wave propagation analysis of one-dimensional periodic structures. Several formulations of the WFE-based eigenvalue problem were presented and discussed. The main sources of numerical errors in the use of the WFE method for the computation of the wave modes traveling along a periodic structure were discussed. Considering a 3D beam-like structure modeled with solid finite elements, the numerical errors in the computation of the associated wavenumbers and wave mode shapes via the WFE method were analyzed. The numerical wave modes were compared to analytical ones predicted by the elementary theory of rods and Timoshenko's beam theory. As expected, they are in agreement at low frequencies within the limits of the corresponding theory. The effect of the eigenvalue problem formulation on the computation of wave modes were also analyzed. They were compared in terms of: (i) accuracy of wavenumbers and wave mode shapes, (ii) analytical relation between right- and left-going wave modes, (iii) conditioning of the eigenvalue problem and (iv) computational time. In addition, the accuracy of the wave modes were analyzed with respect to the FE mesh. Finally, some considerations were made with respect to the implementation of the WFE method in this thesis.

# 3 WFE-based superelement modeling for the forced response analysis of periodic structures

## 3.1 Overview

In this chapter, the WFE method is used to compute the forced response of one-dimensional periodic structures (see Figure 3.1). The main objective here is to use the concept of numerical wave modes to express the dynamic stiffness matrix (DSM) or the receptance matrix (RM) of a periodic structure. The issue may be viewed as circumventing the computational cost of the conventional finite element method or the Craig-Bampton (CB) method when large-sized numerical models are to be solved at many discrete frequencies, while keeping a high level of accuracy.
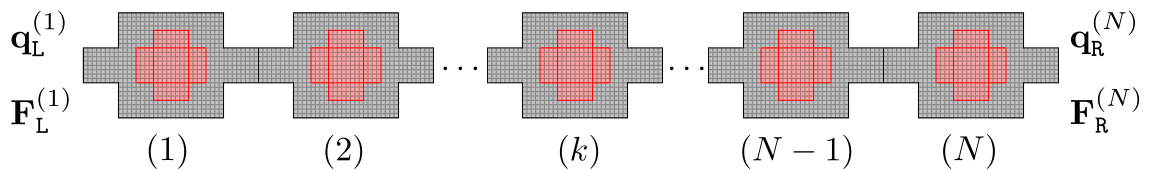


Figure 3.1: Illustration of a superelement model of a periodic structure.

Although WFE-based DSM formulations have been proposed earlier by Duhamel *et al.* (2006) and Mead (2009), the formulations proposed in this thesis provide new contributions which are listed in the following.

- In this thesis, not only a DSM formulation is proposed, but it is also shown that by making use of wave modes the RM of a periodic structure is built without explicitly inverting the DSM and, then, avoiding numerical issues.

- The WFE-based DSM formulated in this chapter involve better conditioned matrices than the previous formulations.

- The formulation of WFE-based DSM and RM are motivated by the possibility of analyzing low-to-mid frequency dynamics of complex engineering systems which involve periodic structures in a very efficient way by using the concepts of superelement modeling and dynamic substructuring — this issue is addressed in Chapter 4.

Besides, the superelement modelings treated in this chapter were also motivated by the concept of spectral element. Originally, SEM involves the construction of dynamic stiffness matrices of periodic structures through consideration of analytical waves. However, exact wave descriptions are not always available, for instance, in the case of structures involving complex heterogeneities. Thus, the possibility of obtaining a numerical description for the waves traveling in a periodic structure by means of the WFE method has brought new perspectives for building high-order spectral elements — *i.e.*, which consider not only elementary wave motions, but also highly oscillating waves which are typical of MF dynamics. A first attempt in this sense,the so-called WSFEM, was proposed by Arruda and Nascimento (2008). The general idea of the WSFEM is to use the numerical wavenumbers and the displacement components of the wave mode shapes obtained by means of the WFE method in the governing differential equations of motion, which allows one to find approximate expressions for the related forces and moments and, then, derive the spectral element matrix. The inconvenient here is that analytical expressions for the forces/moments acting on the structure are still required, thus limiting the application of the method to simple periodic structures. Alternatively, numerical spectral elements of arbitrary order can be built by means of a WFE-based model order reduction strategy. From the author's knowledge, such kind of strategy within the framework of the WFE method has been addressed for the first time in this thesis.

The chapter starts with the formulation of WFE-based dynamic stiffness and receptance matrices expressed by means of the full wave basis. The second part of the chapter is dedicated to formulation of reduced-order WFE-based superelement matrices. The WSFEM is proposed in the third part of the chapter. Finally, numerical results which validate the proposed approaches with reference solutions are presented for various one-dimensional periodic structures.

## 3.2 WFE-based superelement modeling for periodic structures

### 3.2.1 Wave expansion

In Chapter 2, the WFE method has been used to compute numerical wave modes $\{\mu_j, \ \phi_j\}_j$ of a given periodic structure. Now, if one considers the family $\{\phi_j\}_j \cup \{\phi_j^\star\}_j$ as a wave basis, where $\{\phi_j\}_j$ and $\{\phi_j^\star\}_j$ are subsets of wave mode shapes related to right- and left-going waves, respectively, it becomes possible by considering Equation (2.11) to express the state vector $\mathbf{u}^{(k)}$ at the left and right boundaries of a substructure within a periodic structure composed of $N$ substructures, as
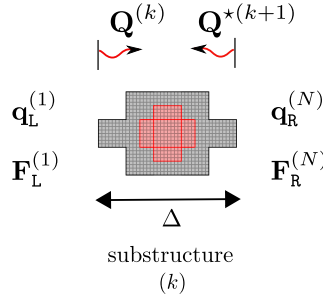
Figure 3.2: Illustration of the waves propagating along a periodic structure and the vectors of displacement/rotation and force/moment for a substructure $(k)$. The reference positions for the wave amplitudes related to right- and left-going waves are shown.

follows

$$\mathbf{u}_{\text{L}}^{(k)} = \boldsymbol{\Phi}\mathbf{Q}^{(k)} + \boldsymbol{\Phi}^{\star}\boldsymbol{\mu}\mathbf{Q}^{\star(k)} \quad , \quad \mathbf{u}_{\text{R}}^{(k)} = \boldsymbol{\Phi}\boldsymbol{\mu}\mathbf{Q}^{(k)} + \boldsymbol{\Phi}^{\star}\mathbf{Q}^{\star(k)} \quad k = 1,\ldots,N, \qquad (3.1)$$

where

$$\boldsymbol{\Phi} = \begin{bmatrix} \boldsymbol{\Phi}_{\text{q}} \\ \boldsymbol{\Phi}_{\text{F}} \end{bmatrix}, \qquad \boldsymbol{\Phi}^{\star} = \begin{bmatrix} \boldsymbol{\Phi}_{\text{q}}^{\star} \\ \boldsymbol{\Phi}_{\text{F}}^{\star} \end{bmatrix}, \qquad (3.2)$$

*i.e.*, $2n \times n$ matrices of wave mode shapes composed of $n \times n$ sub-matrices $\boldsymbol{\Phi}_{\text{q}}$, $\boldsymbol{\Phi}_{\text{q}}^{\star}$, $\boldsymbol{\Phi}_{\text{F}}$ and $\boldsymbol{\Phi}_{\text{F}}^{\star}$ expressed as $\boldsymbol{\Phi}_{\text{q}} = [\boldsymbol{\phi}_{\text{q}1} \cdots \boldsymbol{\phi}_{\text{q}n}]$, $\boldsymbol{\Phi}_{\text{q}}^{\star} = [\boldsymbol{\phi}_{\text{q}1}^{\star} \cdots \boldsymbol{\phi}_{\text{q}n}^{\star}]$, $\boldsymbol{\Phi}_{\text{F}} = [\boldsymbol{\phi}_{\text{F}1} \cdots \boldsymbol{\phi}_{\text{F}n}]$ and $\boldsymbol{\Phi}_{\text{F}}^{\star} = [\boldsymbol{\phi}_{\text{F}1}^{\star} \cdots \boldsymbol{\phi}_{\text{F}n}^{\star}]$. Also, $\mathbf{Q}^{(k)} = \left[Q_1^{(k)} \cdots Q_n^{(k)}\right]^T$ and $\mathbf{Q}^{\star(k)} = \left[Q_1^{\star(k)} \cdots Q_n^{\star(k)}\right]^T$ are vectors of wave amplitudes defined at the left and right boundaries of a substructure $(k)$, as shown in Figure 3.2. Finally, $\boldsymbol{\mu}$ is the $n \times n$ diagonal matrix whose components are the eigenvalues $\{\mu_j\}_j$ related to right-going waves.
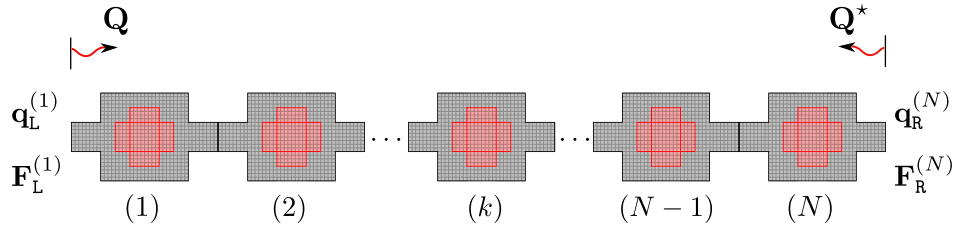


Figure 3.3: Illustration of the waves propagating along a periodic structure and the vectors of displacement/rotation and force/moment for the full periodic structure. The reference positions for the wave amplitudes related to right- and left-going waves are shown.

Consider now vectors of wave amplitudes $\mathbf{Q} = [Q_1 \cdots Q_n]^T$ and $\mathbf{Q}^{\star} = [Q_1^{\star} \cdots Q_n^{\star}]^T$ defined

at the left and right ends of the global periodic structure, respectively (see Figure 3.3). By making use of Bloch's Theorem (Equation (2.10)), the following relations can be expressed

$$\mathbf{Q}^{(k)} = \boldsymbol{\mu}^{k-1}\mathbf{Q}, \qquad \mathbf{Q}^{\star(k)} = \boldsymbol{\mu}^{N-k}\mathbf{Q}^{\star}. \tag{3.3}$$

Substituting these into Equation (3.1), it yields

$$\mathbf{u}_{\mathrm{L}}^{(k)} = \boldsymbol{\Phi}\boldsymbol{\mu}^{k-1}\mathbf{Q} + \boldsymbol{\Phi}^{\star}\boldsymbol{\mu}^{N+1-k}\mathbf{Q}^{\star} \quad , \quad \mathbf{u}_{\mathrm{R}}^{(k)} = \boldsymbol{\Phi}\boldsymbol{\mu}^{k}\mathbf{Q} + \boldsymbol{\Phi}^{\star}\boldsymbol{\mu}^{N-k}\mathbf{Q}^{\star} \quad k = 1,\dots,N. \tag{3.4}$$

It is important to point out here that the reference for the vector of wave amplitudes related to left-going waves is placed at the right end of the global periodic structure in order to avoid numerical errors. Otherwise, Equation (3.4) might invoke terms of extremely low and of extremely high amplitudes, related, respectively, to $\boldsymbol{\mu}$ and $\boldsymbol{\mu}^{-1}$.

As defined in Equation (2.5), the state vectors can be split into a vector of displacements/rotations and a vector of forces/moments, which allows one to re-write the equations in (3.4) as

$$\mathbf{q}_{\mathrm{L}}^{(k)} = \boldsymbol{\Phi}_{\mathrm{q}}\boldsymbol{\mu}^{k-1}\mathbf{Q} + \boldsymbol{\Phi}_{\mathrm{q}}^{\star}\boldsymbol{\mu}^{N+1-k}\mathbf{Q}^{\star} \quad , \qquad \mathbf{q}_{\mathrm{R}}^{(k)} = \boldsymbol{\Phi}_{\mathrm{q}}\boldsymbol{\mu}^{k}\mathbf{Q} + \boldsymbol{\Phi}_{\mathrm{q}}^{\star}\boldsymbol{\mu}^{N-k}\mathbf{Q}^{\star} \quad k = 1,\dots,N, \tag{3.5a}$$

$$-\mathbf{F}_{\mathrm{L}}^{(k)} = \boldsymbol{\Phi}_{\mathrm{F}}\boldsymbol{\mu}^{k-1}\mathbf{Q} + \boldsymbol{\Phi}_{\mathrm{F}}^{\star}\boldsymbol{\mu}^{N+1-k}\mathbf{Q}^{\star} \quad , \qquad \mathbf{F}_{\mathrm{R}}^{(k)} = \boldsymbol{\Phi}_{\mathrm{F}}\boldsymbol{\mu}^{k}\mathbf{Q} + \boldsymbol{\Phi}_{\mathrm{F}}^{\star}\boldsymbol{\mu}^{N-k}\mathbf{Q}^{\star} \quad k = 1,\dots,N. \tag{3.5b}$$

### 3.2.2 Dynamic stiffness matrix (DSM)

In this section, the condensed dynamic stiffness matrix $\mathbf{D}^{(p)}$ of a given periodic structure — namely $(P_p)$ — in terms of WFE wave modes $\{\mu_j,\ \phi_j\}_j$ (discussed in Chapter 2) is formulated. This dynamic stiffness matrix links the vector of nodal displacements/rotations to the vector of nodal forces/moments on the structure ends — $i.e.$, the left end of the substructure $1$ and the right end of the substructure $N$ (see Figure 3.3(b)) —, as follows

$$\mathbf{D}^{(p)}\mathbf{q}^{(p)} = \mathbf{F}^{(p)}, \tag{3.6}$$

where

$$\mathbf{q}^{(p)} = \begin{bmatrix} \mathbf{q}_{\mathrm{L}}^{(1)} \\ \mathbf{q}_{\mathrm{R}}^{(N)} \end{bmatrix} \quad , \quad \mathbf{F}^{(p)} = \begin{bmatrix} \mathbf{F}_{\mathrm{L}}^{(1)} \\ \mathbf{F}_{\mathrm{R}}^{(N)} \end{bmatrix}. \tag{3.7}$$

The motivation behind the use of WFE wave modes is to compute the matrix $\mathbf{D}^{(p)}$, as well as its inverse (see Section 3.2.3), at a low computational cost compared to the conventional approaches. Compared to the FE-based DSM, it is smaller in size, as it is written in terms of the DOFs on the left and the right ends of the periodic structure. Indeed, if the same level of discretization is considered in the FE model of whole periodic structure, $\mathbf{D}^{(p)}$ seems to be as accurate as the FE-based DSM after dynamic condensation of internal DOFs and, also, it is of fast computation. Moreover, as the full wave basis is considered — *i.e.*, there is no truncation — the WFE-based DSM is more accurate than the DSM issued from CB method, for which a truncated set of normal modes is considered (see Annexe A).

The WFE procedure is achieved in this way. Using Equations (3.5a) and (3.5b), the vectors of nodal displacements/rotations and forces/moments on the left and right ends of the periodic structure are expressed as

$$\mathbf{q}_{\mathrm{L}}^{(1)} = \mathbf{\Phi}_{\mathrm{q}} \mathbf{Q} + \mathbf{\Phi}_{\mathrm{q}}^{\star} \boldsymbol{\mu}^{N} \mathbf{Q}^{\star} \quad , \qquad\qquad \mathbf{q}_{\mathrm{R}}^{(N)} = \mathbf{\Phi}_{\mathrm{q}} \boldsymbol{\mu}^{N} \mathbf{Q} + \mathbf{\Phi}_{\mathrm{q}}^{\star} \mathbf{Q}^{\star}, \tag{3.8a}$$

$$-\mathbf{F}_{\mathrm{L}}^{(1)} = \mathbf{\Phi}_{\mathrm{F}} \mathbf{Q} + \mathbf{\Phi}_{\mathrm{F}}^{\star} \boldsymbol{\mu}^{N} \mathbf{Q}^{\star} \quad , \qquad\qquad \mathbf{F}_{\mathrm{R}}^{(N)} = \mathbf{\Phi}_{\mathrm{F}} \boldsymbol{\mu}^{N} \mathbf{Q} + \mathbf{\Phi}_{\mathrm{F}}^{\star} \mathbf{Q}^{\star}. \tag{3.8b}$$

In matrix form, this yields

$$\begin{bmatrix} \mathbf{q}_{\mathrm{L}}^{(1)} \\ \mathbf{q}_{\mathrm{R}}^{(N)} \end{bmatrix} = \begin{bmatrix} \mathbf{\Phi}_{\mathrm{q}} & \mathbf{\Phi}_{\mathrm{q}}^{\star} \boldsymbol{\mu}^{N} \\ \mathbf{\Phi}_{\mathrm{q}} \boldsymbol{\mu}^{N} & \mathbf{\Phi}_{\mathrm{q}}^{\star} \end{bmatrix} \begin{bmatrix} \mathbf{Q} \\ \mathbf{Q}^{\star} \end{bmatrix}, \tag{3.9}$$

and

$$\begin{bmatrix} \mathbf{F}_{\mathrm{L}}^{(1)} \\ \mathbf{F}_{\mathrm{R}}^{(N)} \end{bmatrix} = \begin{bmatrix} -\mathbf{\Phi}_{\mathrm{F}} & -\mathbf{\Phi}_{\mathrm{F}}^{\star} \boldsymbol{\mu}^{N} \\ \mathbf{\Phi}_{\mathrm{F}} \boldsymbol{\mu}^{N} & \mathbf{\Phi}_{\mathrm{F}}^{\star} \end{bmatrix} \begin{bmatrix} \mathbf{Q} \\ \mathbf{Q}^{\star} \end{bmatrix}. \tag{3.10}$$

To derive the condensed dynamic stiffness matrix $\mathbf{D}^{(p)}$ of the periodic structure, Equation (3.9) is left multiplied by the following matrix

$$\begin{bmatrix} \mathbf{\Phi}_{\mathrm{q}}^{-1} & \mathbf{0} \\ \mathbf{0} & \mathbf{\Phi}_{\mathrm{q}}^{\star-1} \end{bmatrix}, \tag{3.11}$$

which yields

$$\begin{bmatrix} \boldsymbol{\Phi}_{\mathsf{q}}^{-1} & \mathbf{0} \\ \mathbf{0} & \boldsymbol{\Phi}_{\mathsf{q}}^{\star-1} \end{bmatrix} \begin{bmatrix} \mathbf{q}_{\mathsf{L}}^{(1)} \\ \mathbf{q}_{\mathsf{R}}^{(N)} \end{bmatrix} = \begin{bmatrix} \mathbf{I} & \boldsymbol{\Phi}_{\mathsf{q}}^{-1}\boldsymbol{\Phi}_{\mathsf{q}}^{\star}\boldsymbol{\mu}^{N} \\ \boldsymbol{\Phi}_{\mathsf{q}}^{\star-1}\boldsymbol{\Phi}_{\mathsf{q}}\boldsymbol{\mu}^{N} & \mathbf{I} \end{bmatrix} \begin{bmatrix} \mathbf{Q} \\ \mathbf{Q}^{\star} \end{bmatrix}. \tag{3.12}$$

The motivation behind the use of the matrix (3.11) is to provide a matrix, on the right-hand side of Equation (3.12), which is of the form

$$\begin{bmatrix} \mathbf{I} & \boldsymbol{\Phi}_{\mathsf{q}}^{-1}\boldsymbol{\Phi}_{\mathsf{q}}^{\star}\boldsymbol{\mu}^{N} \\ \boldsymbol{\Phi}_{\mathsf{q}}^{\star-1}\boldsymbol{\Phi}_{\mathsf{q}}\boldsymbol{\mu}^{N} & \mathbf{I} \end{bmatrix}. \tag{3.13}$$

From Equation (2.22) and using the fact that $\mathcal{R} = \mathcal{R}^T = \mathcal{R}^{-1}$, it is possible to show that

$$\boldsymbol{\Phi}_{\mathsf{q}}^{-1}\boldsymbol{\Phi}_{\mathsf{q}}^{\star} = \boldsymbol{\Phi}_{\mathsf{q}}^{-1}\mathcal{R}\boldsymbol{\Phi}_{\mathsf{q}} = \left(\mathcal{R}\boldsymbol{\Phi}_{\mathsf{q}}\right)^{-1}\boldsymbol{\Phi}_{\mathsf{q}} = \boldsymbol{\Phi}_{\mathsf{q}}^{\star-1}\boldsymbol{\Phi}_{\mathsf{q}}. \tag{3.14}$$

Notice also that if one considers a periodic structure with a clamped boundary — *i.e.*, either $\mathbf{q}_{\mathsf{L}}^{(1)} = \mathbf{0}$ or $\mathbf{q}_{\mathsf{R}}^{(N)} = \mathbf{0}$ — it is possible to write

$$\mathbf{Q} = \mathbb{C}_{\mathsf{c}}\boldsymbol{\mu}^{N}\mathbf{Q}^{\star} \quad \text{or} \quad \mathbf{Q}^{\star} = \mathbb{C}_{\mathsf{c}}\boldsymbol{\mu}^{N}\mathbf{Q}, \tag{3.15}$$

where $\mathbb{C}_{\mathsf{c}} = -\boldsymbol{\Phi}_{\mathsf{q}}^{-1}\boldsymbol{\Phi}_{\mathsf{q}}^{\star} = -\boldsymbol{\Phi}_{\mathsf{q}}^{\star-1}\boldsymbol{\Phi}_{\mathsf{q}}$, as a result of Equation (3.14), and it corresponds, physically, to the reflection/transmission matrix in the case of a clamped boundary. Thus, matrix (3.13) can be re-written as

$$\begin{bmatrix} \mathbf{I} & -\mathbb{C}_{\mathsf{c}}\boldsymbol{\mu}^{N} \\ -\mathbb{C}_{\mathsf{c}}\boldsymbol{\mu}^{N} & \mathbf{I} \end{bmatrix}. \tag{3.16}$$

From Equation (3.12) and using the notation in (3.16), the vectors of wave amplitudes $\mathbf{Q}$ and $\mathbf{Q}^{\star}$ can be expressed as

$$\begin{bmatrix} \mathbf{Q} \\ \mathbf{Q}^{\star} \end{bmatrix} = \begin{bmatrix} \mathbf{I} & -\mathbb{C}_{\mathsf{c}}\boldsymbol{\mu}^{N} \\ -\mathbb{C}_{\mathsf{c}}\boldsymbol{\mu}^{N} & \mathbf{I} \end{bmatrix}^{-1} \begin{bmatrix} \boldsymbol{\Phi}_{\mathsf{q}}^{-1} & \mathbf{0} \\ \mathbf{0} & \boldsymbol{\Phi}_{\mathsf{q}}^{\star-1} \end{bmatrix} \begin{bmatrix} \mathbf{q}_{\mathsf{L}}^{(1)} \\ \mathbf{q}_{\mathsf{R}}^{(N)} \end{bmatrix}. \tag{3.17}$$

Now, substituting Equation (3.17) into Equation (3.10), the DSM of the periodic structure is readily derived, as follows

$$\mathbf{D}^{(p)} = \begin{bmatrix} -\boldsymbol{\Phi}_{\mathsf{F}} & -\boldsymbol{\Phi}_{\mathsf{F}}^{\star}\boldsymbol{\mu}^{N} \\ \boldsymbol{\Phi}_{\mathsf{F}}\boldsymbol{\mu}^{N} & \boldsymbol{\Phi}_{\mathsf{F}}^{\star} \end{bmatrix} \begin{bmatrix} \mathbf{I} & -\mathbb{C}_{\mathsf{c}}\boldsymbol{\mu}^{N} \\ -\mathbb{C}_{\mathsf{c}}\boldsymbol{\mu}^{N} & \mathbf{I} \end{bmatrix}^{-1} \begin{bmatrix} \boldsymbol{\Phi}_{\mathsf{q}}^{-1} & \mathbf{0} \\ \mathbf{0} & \boldsymbol{\Phi}_{\mathsf{q}}^{\star-1} \end{bmatrix}, \tag{3.18}$$

which is a dense complex matrix expressed in terms of the left and right DOFs of the periodic

structure.

The motivation behind the use of the premultiplication by (3.11) is to formulate a condensed dynamic stiffness matrix which involves the inversion of a matrix, (3.14) or (3.16), that is likely to be well-conditioned (Mencik, 2010). This is a $2n \times 2n$ matrix — *i.e.*, it is related to the number of DOFs on the left and right ends of the structure, only — which appears to be very small compared to the number of DOFs that would be used to model the whole periodic structure (which is $2(N + 1)n + Nn_i$ DOFs, where $n_i$ is the number of internal DOFs within a substructure). Also, it is sparse, as it has identity matrices as diagonal block terms. Finally, the inversion of matrix (3.16) can be performed in an efficient way, as depicted in the following. The analytic formula for blockwise inversion is expressed as (Banachiewicz, 1937 apud Puntanen and Styan, 2005)

$$\begin{bmatrix} \mathbf{A} & \mathbf{B} \\ \mathbf{C} & \mathbf{D} \end{bmatrix}^{-1} = \begin{bmatrix} (\mathbf{A} - \mathbf{B}\mathbf{D}^{-1}\mathbf{C})^{-1} & -\mathbf{A}^{-1}\mathbf{B}(\mathbf{D} - \mathbf{C}\mathbf{A}^{-1}\mathbf{B})^{-1} \\ -\mathbf{D}^{-1}\mathbf{C}(\mathbf{A} - \mathbf{B}\mathbf{D}^{-1}\mathbf{C})^{-1} & (\mathbf{D} - \mathbf{C}\mathbf{A}^{-1}\mathbf{B})^{-1} \end{bmatrix}. \tag{3.19}$$

Hence, the inverse of (3.16) is given by

$$\begin{bmatrix} \mathbf{I} & -\mathbb{C}_{\mathsf{c}}\boldsymbol{\mu}^N \\ -\mathbb{C}_{\mathsf{c}}\boldsymbol{\mu}^N & \mathbf{I} \end{bmatrix}^{-1} = \begin{bmatrix} \left(\mathbf{I} - (\mathbb{C}_{\mathsf{c}}\boldsymbol{\mu}^N)^2\right)^{-1} & \mathbb{C}_{\mathsf{c}}\boldsymbol{\mu}^N\left(\mathbf{I} - (\mathbb{C}_{\mathsf{c}}\boldsymbol{\mu}^N)^2\right)^{-1} \\ \mathbb{C}_{\mathsf{c}}\boldsymbol{\mu}^N\left(\mathbf{I} - (\mathbb{C}_{\mathsf{c}}\boldsymbol{\mu}^N)^2\right)^{-1} & \left(\mathbf{I} - (\mathbb{C}_{\mathsf{c}}\boldsymbol{\mu}^N)^2\right)^{-1} \end{bmatrix}, \tag{3.20}$$

which can be, alternatively, written as

$$\begin{bmatrix} \mathbf{I} & -\mathbb{C}_{\mathsf{c}}\boldsymbol{\mu}^N \\ -\mathbb{C}_{\mathsf{c}}\boldsymbol{\mu}^N & \mathbf{I} \end{bmatrix}^{-1} = \begin{bmatrix} \mathbf{I} & \mathbb{C}_{\mathsf{c}}\boldsymbol{\mu}^N \\ \mathbb{C}_{\mathsf{c}}\boldsymbol{\mu}^N & \mathbf{I} \end{bmatrix} \begin{bmatrix} \left(\mathbf{I} - (\mathbb{C}_{\mathsf{c}}\boldsymbol{\mu}^N)^2\right)^{-1} & \mathbf{0} \\ \mathbf{0} & \left(\mathbf{I} - (\mathbb{C}_{\mathsf{c}}\boldsymbol{\mu}^N)^2\right)^{-1} \end{bmatrix}. \tag{3.21}$$

Due to the nature of (3.16), its inversion requires only the inversion of $\left(\mathbf{I} - (\mathbb{C}_{\mathsf{c}}\boldsymbol{\mu}^N)^2\right)$, which is a $n \times n$ matrix — *i.e.*, a half of the size of the original matrix. Moreover, if the spectral radius of $(\mathbb{C}_{\mathsf{c}}\boldsymbol{\mu}^N)^2$ is inferior to one, the following identity is verified

$$\left(\mathbf{I} - (\mathbb{C}_{\mathsf{c}}\boldsymbol{\mu}^N)^2\right)^{-1} = \sum_{i=0}^{\infty} (\mathbb{C}_{\mathsf{c}}\boldsymbol{\mu}^N)^{2i}, \tag{3.22}$$

which corresponds to a convergent Neumann series. Assumption 1 is verified as follows. By definition, the spectral radius of a matrix $\mathbf{A}$ verifies $\rho_s(\mathbf{A}) < \|\mathbf{A}\|$, where $\rho_s$ stands for the spectral radius of a matrix. Thus, one may write $\rho_s\left((\mathbb{C}_{\mathsf{c}}\boldsymbol{\mu}^N)^2\right) < \|\mathbb{C}_{\mathsf{c}}^2\|\|\boldsymbol{\mu}^{2N}\|$. Since $\|\boldsymbol{\mu}\| \leq 1$ (see Equa-

tion (2.17)) and $\|\mathbb{C}_c\| \leq \|\boldsymbol{\Phi}_q^{-1}\|\|\mathcal{R}\|\|\boldsymbol{\Phi}_q^\star\| = 1$, Assumption 1 is satisfied provided that $\|\boldsymbol{\mu}\|$ is small enough compared to one (which depends on the structure damping). In this case, the series in Equation (3.22) can be truncated to the first $m$ terms, such that $\rho_s\left(\boldsymbol{\mu}^{2N(m+1)}\right) < \epsilon$ with $\epsilon$ being a small tolerance value (for instance, $10^{-16}$, which is about the limit of floating point representation). Then, the dynamic stiffness matrix of the periodic structure can be approximated to

$$\mathbf{D}^{(p)} \approx \begin{bmatrix} -\boldsymbol{\Phi}_F & -\boldsymbol{\Phi}_F^\star \boldsymbol{\mu}^N \\ \boldsymbol{\Phi}_F \boldsymbol{\mu}^N & \boldsymbol{\Phi}_F^\star \end{bmatrix} \begin{bmatrix} \mathbf{I} & \mathbb{C}_c \boldsymbol{\mu}^N \\ \mathbb{C}_c \boldsymbol{\mu}^N & \mathbf{I} \end{bmatrix} \begin{bmatrix} \sum_{i=0}^m \left(\mathbb{C}_c \boldsymbol{\mu}^N\right)^{2i} & \mathbf{0} \\ \mathbf{0} & \sum_{i=0}^m \left(\mathbb{C}_c \boldsymbol{\mu}^N\right)^{2i} \end{bmatrix} \begin{bmatrix} \boldsymbol{\Phi}_q^{-1} & \mathbf{0} \\ \mathbf{0} & \boldsymbol{\Phi}_q^{\star -1} \end{bmatrix}.$$

(3.23)

In this case, the computation of $\mathbf{D}^{(p)}$ involves only the inversion of $\boldsymbol{\Phi}_q$ (as $\boldsymbol{\Phi}_q^{\star -1} = \boldsymbol{\Phi}_q^{-1}\mathcal{R}$, see Equation (2.22)), a dense complex matrix of size $n \times n$, the evaluation of a power series of size $n \times n$ and matrix multiplications of size $2n \times 2n$.

### 3.2.3 Receptance matrix (RM)

One interesting feature behind the use of wave modes is to formulate the inverse of the dynamic stiffness matrix $\mathbf{D}^{(p)}$ without the need of explicitly inverting the matrix appearing on the right-hand side of Equation (3.6). Such an inverse is usually called receptance matrix $\left(\mathbf{R}^{(p)}\right)$. It links the vector of nodal forces/moments to the vector of nodal displacements/rotations, as follows

$$\mathbf{q}^{(p)} = \mathbf{R}^{(p)}\mathbf{F}^{(p)}.$$

(3.24)

The derivation of $\mathbf{R}^{(p)}$ is presented hereafter. To begin with, Equation (3.10) is left multiplied by the following matrix

$$\begin{bmatrix} -\boldsymbol{\Phi}_F^{-1} & \mathbf{0} \\ \mathbf{0} & \boldsymbol{\Phi}_F^{\star -1} \end{bmatrix},$$

(3.25)

which yields

$$\begin{bmatrix} -\boldsymbol{\Phi}_F^{-1} & \mathbf{0} \\ \mathbf{0} & \boldsymbol{\Phi}_F^{\star -1} \end{bmatrix} \begin{bmatrix} \mathbf{F}_L^{(1)} \\ \mathbf{F}_R^{(N)} \end{bmatrix} = \begin{bmatrix} \mathbf{I} & \boldsymbol{\Phi}_F^{-1}\boldsymbol{\Phi}_F^\star \boldsymbol{\mu}^N \\ \boldsymbol{\Phi}_F^{\star -1}\boldsymbol{\Phi}_F \boldsymbol{\mu}^N & \mathbf{I} \end{bmatrix} \begin{bmatrix} \mathbf{Q} \\ \mathbf{Q}^\star \end{bmatrix}.$$

(3.26)

In a similar way as in Equation (3.12), the matrix appearing on the right-hand side of Equation (3.26) is sparse with identity matrices as diagonal block terms, *i.e.*, it is likely to be invertible.

64

In addition, if one considers a periodic structure with one of its end free from external excitations, — *i.e.*, either $\mathbf{F}_{\mathrm{L}}^{(1)} = \mathbf{0}$ or $\mathbf{F}_{\mathrm{R}}^{(N)} = \mathbf{0}$ — using Equation (3.8b), one gets

$$\mathbf{Q} = \mathbb{C}_{\mathrm{f}} \boldsymbol{\mu}^N \mathbf{Q}^\star \quad \text{or} \quad \mathbf{Q}^\star = \mathbb{C}_{\mathrm{f}} \boldsymbol{\mu}^N \mathbf{Q}, \tag{3.27}$$

where $\mathbb{C}_{\mathrm{f}} = -\boldsymbol{\Phi}_{\mathrm{F}}^{-1} \boldsymbol{\Phi}_{\mathrm{F}}^\star = -\boldsymbol{\Phi}_{\mathrm{F}}^{\star-1} \boldsymbol{\Phi}_{\mathrm{F}}$ is the reflection/transmission matrix in the case of a free boundary. Thus, it turns out that the vectors of wave amplitudes $\mathbf{Q}$ and $\mathbf{Q}^\star$ can be expressed as

$$\begin{bmatrix} \mathbf{Q} \\ \mathbf{Q}^\star \end{bmatrix} = \begin{bmatrix} \mathbf{I} & -\mathbb{C}_{\mathrm{f}} \boldsymbol{\mu}^N \\ -\mathbb{C}_{\mathrm{f}} \boldsymbol{\mu}^N & \mathbf{I} \end{bmatrix}^{-1} \begin{bmatrix} -\boldsymbol{\Phi}_{\mathrm{F}}^{-1} & \mathbf{0} \\ \mathbf{0} & \boldsymbol{\Phi}_{\mathrm{F}}^{\star-1} \end{bmatrix} \begin{bmatrix} \mathbf{F}_{\mathrm{L}}^{(1)} \\ \mathbf{F}_{\mathrm{R}}^{(N)} \end{bmatrix}. \tag{3.28}$$

Then, from Equations (3.9) and (3.28), the receptance matrix of a periodic structure is expressed as

$$\mathbf{R}^{(p)} = \begin{bmatrix} \boldsymbol{\Phi}_{\mathrm{q}} & \boldsymbol{\Phi}_{\mathrm{q}}^\star \boldsymbol{\mu}^N \\ \boldsymbol{\Phi}_{\mathrm{q}} \boldsymbol{\mu}^N & \boldsymbol{\Phi}_{\mathrm{q}}^\star \end{bmatrix} \begin{bmatrix} \mathbf{I} & -\mathbb{C}_{\mathrm{f}} \boldsymbol{\mu}^N \\ -\mathbb{C}_{\mathrm{f}} \boldsymbol{\mu}^N & \mathbf{I} \end{bmatrix}^{-1} \begin{bmatrix} -\boldsymbol{\Phi}_{\mathrm{F}}^{-1} & \mathbf{0} \\ \mathbf{0} & \boldsymbol{\Phi}_{\mathrm{F}}^{\star-1} \end{bmatrix}, \tag{3.29}$$

which, as the DSM, is a dense complex matrix expressed in terms of the DOFs on the left and right ends.

Analogously to the case of the dynamic stiffness matrix, the inversion of the matrix in the right-hand side of Equation (3.26), *i.e.*,

$$\begin{bmatrix} \mathbf{I} & -\mathbb{C}_{\mathrm{f}} \boldsymbol{\mu}^N \\ -\mathbb{C}_{\mathrm{f}} \boldsymbol{\mu}^N & \mathbf{I} \end{bmatrix}, \tag{3.30}$$

can be computed as

$$\begin{bmatrix} \mathbf{I} & -\mathbb{C}_{\mathrm{f}} \boldsymbol{\mu}^N \\ -\mathbb{C}_{\mathrm{f}} \boldsymbol{\mu}^N & \mathbf{I} \end{bmatrix}^{-1} = \begin{bmatrix} \mathbf{I} & \mathbb{C}_{\mathrm{f}} \boldsymbol{\mu}^N \\ \mathbb{C}_{\mathrm{f}} \boldsymbol{\mu}^N & \mathbf{I} \end{bmatrix} \begin{bmatrix} \displaystyle\sum_{i=0}^{\infty} \left( \mathbb{C}_{\mathrm{f}} \boldsymbol{\mu}^N \right)^{2i} & \mathbf{0} \\ \mathbf{0} & \displaystyle\sum_{i=0}^{\infty} \left( \mathbb{C}_{\mathrm{f}} \boldsymbol{\mu}^N \right)^{2i} \end{bmatrix}. \tag{3.31}$$

This allows one to approximate the receptance matrix in an efficient way to

$$
\mathbf{R}^{(p)} \approx
\begin{bmatrix} -\boldsymbol{\Phi}_{\mathsf{q}} & -\boldsymbol{\Phi}_{\mathsf{q}}^{\star}\boldsymbol{\mu}^N \\ \boldsymbol{\Phi}_{\mathsf{q}}\boldsymbol{\mu}^N & \boldsymbol{\Phi}_{\mathsf{q}}^{\star} \end{bmatrix}
\begin{bmatrix} \mathbf{I} & \mathbb{C}_{\mathsf{f}}\boldsymbol{\mu}^N \\ \mathbb{C}_{\mathsf{f}}\boldsymbol{\mu}^N & \mathbf{I} \end{bmatrix}
\begin{bmatrix} \sum\limits_{i=0}^{m}\left(\mathbb{C}_{\mathsf{f}}\boldsymbol{\mu}^N\right)^{2i} & \mathbf{0} \\ \mathbf{0} & \sum\limits_{i=0}^{m}\left(\mathbb{C}_{\mathsf{f}}\boldsymbol{\mu}^N\right)^{2i} \end{bmatrix}
\begin{bmatrix} \boldsymbol{\Phi}_{\mathsf{F}}^{-1} & \mathbf{0} \\ \mathbf{0} & \boldsymbol{\Phi}_{\mathsf{F}}^{\star-1} \end{bmatrix},
$$

$$(3.32)$$

where $m$ is such that $\rho_s\left(\boldsymbol{\mu}^{2N(m+1)}\right) < \epsilon$ with $\epsilon$ being a small tolerance value (for instance, $10^{-16}$, which is about the limit of floating point representation). It is worth pointing out that the computation of matrix $\mathbf{R}^{(p)}$ involves the inversion of $\boldsymbol{\Phi}_{\mathsf{F}}$ (as $\boldsymbol{\Phi}_{\mathsf{F}}^{\star-1} = -\boldsymbol{\Phi}_{\mathsf{F}}^{-1}\mathcal{R}$, see Equation (2.22)), a dense complex matrix of size $n \times n$, the evaluation of a power series of size $n \times n$ and multiplications of matrices whose size is $2n \times 2n$.

## 3.3 Reduced-order WFE-based superelement modeling for periodic structures

In previous sections, the full wave mode basis has been used to express the dynamic stiffness matrix and the receptance matrix of a periodic structure $(P_p)$. Here, the objective is to describe superelement models based on a reduced set of wave modes obtained by means of the WFE method.

As discussed in Section 2.2.3, the number of wave modes that can be computed by means of the WFE method depends on the number of DOFs used to discretize the substructure boundaries. Moreover, it was shown in Section 2.3 that FE mesh size determines the accuracy of numerical wave modes. In other words, as the maximum frequency within the range of analysis increases, the element size must decrease in order to better approximate short wavelengths. Depending on the problem boundary conditions, not all wave modes effectively contribute to the structure response. Besides, some wave modes are highly evanescent. Thus, even if they are locally excited, they may not propagate or their amplitude decays rapidly, which avoids that they reach the opposite end where they would be reflected or transmitted to a coupled structure — *i.e.*, they may not have far-field effect. For the purpose of improving computational performance, it would be useful if we could select among all wave modes the most contributing ones and use them to obtain accurate forced responses of periodic structures. In the following, a strategy for building reduced-order WFE-based models is proposed. It involves three main steps: in the first step, a set of WFE wave modes is selected by means of a convenient criterion; then, the reduced set of wave modes is used to build reduced WFE-based eigenproblems; finally, by considering the reduced set of WFE wave

modes computed in the second step, the superelement model is constructed.

### 3.3.1 Selection criterion of WFE wave modes

The complexity of the dynamic response of a structure increases with frequency. Thus, it is expected that, at the highest frequency within the frequency range of analysis, the number of wave modes that contribute to the structure response is maximum. In order to accurately describe the dynamic behavior of periodic structures within the whole frequency range, the selection procedure must be repeated for some discrete frequencies within the frequency band $\beta_f$. This is because the wave mode shapes related to propagating waves may change their directions as they evolve in frequency. Variations in the wave shapes usually occur at cut-on frequencies — *i.e.*, when evanescent waves start propagating —, at high frequencies due to boundary effects, or as result of coupling effects (Droz *et al.*, 2014). Thus, considering $m$ sub-frequency bands $\tilde{\beta}_{fi} = \left[\omega_{i-1}^{\texttt{ref}} + \Delta\omega, \quad \omega_i^{\texttt{ref}}\right]$, the selection criterion is applied only to the maximum frequency within the sub-frequency band, *i.e.*, $\omega_i^{\texttt{ref}}$, where the structure response is evaluated by means of the DSM or the RM formulations presented in Section 3.2, which make use of full wave mode basis. At first, the wave modes are selected in terms of the magnitude of the corresponding wave amplitudes.

We recall from Section 2.2.4 that the left and right eigenvectors of the eigenproblem stated in Equation (2.12), by means of a normalization procedure, can be related as follows

$$\boldsymbol{\Psi_u}\boldsymbol{\Phi_u} = \mathbf{I}_{2n}, \tag{3.33}$$

where

$$\boldsymbol{\Psi_u} = \begin{bmatrix} \boldsymbol{\Psi}_{\text{F}} & \boldsymbol{\Psi}_{\text{q}} \\ \boldsymbol{\Psi}_{\text{F}}^{\star} & \boldsymbol{\Psi}_{\text{q}}^{\star} \end{bmatrix} \tag{3.34}$$

and

$$\boldsymbol{\Phi_u} = \begin{bmatrix} \boldsymbol{\Phi}_{\text{q}} & \boldsymbol{\Phi}_{\text{q}}^{\star} \\ \boldsymbol{\Phi}_{\text{F}} & \boldsymbol{\Phi}_{\text{F}}^{\star} \end{bmatrix}. \tag{3.35}$$

From Equation (3.4), the state vectors at the left and the right ends of periodic structure can be expressed as

$$\mathbf{u}_{\text{L}}^{(1)} = \boldsymbol{\Phi}\mathbf{Q} + \boldsymbol{\Phi}^{\star}\boldsymbol{\mu}^N\mathbf{Q}^{\star} \quad , \quad \mathbf{u}_{\text{R}}^{(N)} = \boldsymbol{\Phi}\boldsymbol{\mu}^N\mathbf{Q} + \boldsymbol{\Phi}^{\star}\mathbf{Q}^{\star}. \tag{3.36}$$

Left multiplying $\mathbf{u}_L^{(1)}$ by $\boldsymbol{\Psi}$ and $\mathbf{u}_R^{(N)}$ by $\boldsymbol{\Psi}^\star$, yields

$$\mathbf{Q} = \begin{bmatrix} \boldsymbol{\Psi}_F & \boldsymbol{\Psi}_q \end{bmatrix} \mathbf{u}_L^{(1)}, \quad \mathbf{Q}^\star = \begin{bmatrix} \boldsymbol{\Psi}_F^\star & \boldsymbol{\Psi}_q^\star \end{bmatrix} \mathbf{u}_R^{(N)}. \tag{3.37}$$

Thus, for a given wave mode $j$, the related wave amplitudes $Q_j$ and $Q_j^\star$ can be expressed as

$$\begin{bmatrix} Q_j \\ Q_j^\star \end{bmatrix} = \begin{bmatrix} \psi_{Fj} & \mathbf{0} \\ \mathbf{0} & \psi_{Fj}^\star \end{bmatrix} \begin{bmatrix} \mathbf{q}_L^{(1)} \\ \mathbf{q}_R^{(N)} \end{bmatrix} + \begin{bmatrix} -\psi_{qj} & \mathbf{0} \\ \mathbf{0} & \psi_{qj}^\star \end{bmatrix} \begin{bmatrix} \mathbf{F}_L^{(1)} \\ \mathbf{F}_R^{(N)} \end{bmatrix}, j = 1, \ldots, n. \tag{3.38}$$

If the solution for the boundary value problem is known, two amplitude ratios ($r_{Q_j}$ and $r_{Q_j^\star}$) can be defined

$$r_{Q_j} = \frac{|Q_j|}{\max\left(\{|Q_j|\}_j\right)}, \quad j = 1, \ldots, n, \tag{3.39a}$$

$$r_{Q_j^\star} = \frac{|Q_j^\star|}{\max\left(\{|Q_j^\star|\}_j\right)}, \quad j = 1, \ldots, n, \tag{3.39b}$$

which are used to measure the contribution of a given wave mode $j$ to the structure response. Then, a criterion for selecting the wave modes which effectively contribute to the structure response can be stated as

*S*election Criterion 1:

1. Let $\mathbb{M} = \{\mu_j, \boldsymbol{\phi}_j\}_{j=1,\cdots,n} \cup \{\mu_j^\star, \boldsymbol{\phi}_j^\star\}_{j=1,\cdots,n}$, with $\mu_j^\star = 1/\mu_j$ and $\boldsymbol{\phi}_j^\star = \mathcal{T}\boldsymbol{\phi}_j$.

2. If $r_{Q_j} > \epsilon_Q$ or $r_{Q_j^\star} > \epsilon_Q$, then $(\mu_j, \boldsymbol{\phi}_j) \in \mathbb{M}_Q$.

3. Otherwise, $(\mu_j, \boldsymbol{\phi}_j) \in \mathbb{M}_R$ in such a way that $\mathbb{M} = \mathbb{M}_Q \cup \mathbb{M}_R$.

Here, $\mathbb{M}_Q$ is the set of $2n_Q$ wave modes — as wave modes are considered in pairs of left- and right-going waves — which effectively contribute to the forced response of the periodic structure, and $\epsilon_Q$ is the threshold value — by experience, we usually choose $\epsilon_Q = 10^{-6}$ in order to guarantee accurate results (some investigation regarding the choice of $\epsilon_Q$ is carried out in Section 3.5). Thus, in the complement of this set, *i.e.*, $\mathbb{M}_R$, which is denoted as the set of rejected wave modes, there might be $2n_R = 2n - 2n_Q$ wave modes.

It is worth pointing out that the number of propagating wave modes tends to increase as the frequency rises (a numerical validation is proposed in Section 3.5.1, see Figure 3.13). This occurs because wave modes which are initially evanescent at low frequencies, may become purely propagating or complex at angular frequencies greater than $\omega_{cj} \neq 0$, which corresponds to the cut-on frequency for a given wave mode $(\mu_j, \phi_j)$. The construction of a spectral element of order $n_w$ involves the consideration of the $n_w$ most propagating right-going wave modes and corresponding left-going wave modes. Thus, in order to build higher-order superelement models, a second selection criterion of wave modes must be applied to the set of wave modes in $\mathbb{M}_Q$, as follows

*S*election Criterion 2:

1. Let $\{\mu_j, \phi_j\}_{j=1,\cdots,m_Q} \subset \mathbb{M}_Q$ such that $|\mu_j| < 1$, sort $\{\mu_j, \phi_j\}_{j=1,\cdots,m_Q}$ in ascending order of $|\mu_j|$.

2. Among them, select the first $n_w$ wave modes, *i.e.*,

$$\{\mu_j, \phi_j\}_{j=1,\cdots,n_w} \subset \mathbb{M}_w \subset \mathbb{M}_Q, \quad \text{with } |\mu_1| \leq |\mu_2| \leq \cdots \leq |\mu_{n_w}| \ .$$

3. Then, $\mathbb{M}_w = \{\mu_j, \phi_j\}_{j=1,\cdots,n_w} \cup \{\mu_j^\star, \phi_j^\star\}_{j=1,\cdots,n_w}$, with $\mu_j^\star = 1/\mu_j$ and $\phi_j^\star = \mathcal{T}\phi_j$.

4. Otherwise, $(\mu_j, \phi_j) \in \mathbb{M}_r$, where $\mathbb{M}_r \cup \mathbb{M}_w = \mathbb{M}_Q$.

## 3.3.2 Reduced-order WFE method

Using the reduced set of $2n_k$ wave modes selected by application of Criterion 1 , associated or not with Criterion 2 — in the former case, $n_k = n_Q$; otherwise, $n_k = n_w$ —, transformation matrices for model order reduction — *i.e.*, the left- and right-hand side transformation matrices $\tilde{\mathbf{T}}_\mathrm{L}$ and $\tilde{\mathbf{T}}_\mathrm{R}$ of sizes $2n_k \times 2n$ and $2n \times 2n_k$, respectively — can be constructed. For each sub-frequency band $\tilde{\beta}_{fi}$ defined before, in which a reduced set of wave modes $\{\mu_j, \phi_j\}_j \subset \mathbb{M}_k(\omega_i^{\texttt{ref}})$ has been selected, $\tilde{\mathbf{T}}_\mathrm{R}$ can be defined as

$$\tilde{\mathbf{T}}_\mathrm{R} = \begin{bmatrix} \mathbf{\Phi}_{\mathrm{q}k} & \mathbf{\Phi}_{\mathrm{q}k}^\star \\ \mathbf{\Phi}_{\mathrm{F}k} & \mathbf{\Phi}_{\mathrm{F}k}^\star \end{bmatrix} = \mathbf{\Phi}_{\mathbf{u}k}. \tag{3.40}$$

The right-hand side transformation matrix $\tilde{\mathbf{T}}_{\text{R}}$ is used to project the state vector expressed in terms of physical DOFs $\mathbf{u}^{(k)}$ into a vector of generalized coordinates $\tilde{\mathbf{u}}^{(k)}$, as follows

$$\mathbf{u}^{(k)} = \tilde{\mathbf{T}}_{\text{R}}\tilde{\mathbf{u}}^{(k)}, \tag{3.41}$$

which allows for the system linear projection

$$\tilde{\mathbf{S}} = \tilde{\mathbf{T}}_{\text{L}}\mathbf{S}\tilde{\mathbf{T}}_{\text{R}}, \tag{3.42}$$

where $\mathbf{S}$ is the original symplectic transfer matrix of size $2n \times 2n$, $\tilde{\mathbf{T}}_{\text{L}}$ is the left-hand side transformation matrix and $\tilde{\mathbf{S}}$ is the reduced system matrix of size $2n_k \times 2n_k$. In order to guarantee numerical stability in the reduction process, $\tilde{\mathbf{T}}_{\text{L}}$ and $\tilde{\mathbf{T}}_{\text{R}}$ must be orthogonal and satisfy

$$\tilde{\mathbf{T}}_{\text{L}}\tilde{\mathbf{T}}_{\text{R}} = \mathbf{I}_{2n_k}. \tag{3.43}$$

Using the relation between the left and right eigenvectors of $\mathbf{S}$, defined in Equation (3.33), $\tilde{\mathbf{T}}_{\text{L}}$ can be expressed as

$$\tilde{\mathbf{T}}_{\text{L}} = \boldsymbol{\Psi}_{\mathbf{u}k}. \tag{3.44}$$

By writing $\tilde{\mathbf{u}}_{\text{L}}^{(k)}$ as a series expansion and applying Bloch's Theorem, as stated in Section 2.2.3, the following reduced eigenproblem can be formulated:

$$\tilde{\mathbf{S}}\tilde{\boldsymbol{\varphi}}_j = \tilde{\mu}_j\tilde{\boldsymbol{\varphi}}_j. \tag{3.45}$$

The eigenvectors of the reduced eigenproblem are related to the ones defined in terms of the physical DOFs, as follows

$$\tilde{\boldsymbol{\phi}}_j(\omega) = \tilde{\mathbf{T}}_{\text{R}}\tilde{\boldsymbol{\varphi}}_j(\omega). \tag{3.46}$$

An alternative scheme is proposed in Appendix B to formulate the reduced WFE-based eigenproblem (Equation 3.45).

### Additional comments about the reduced system matrix

As $\mathbf{S}$ is diagonalizable, one may write $\mathbf{S}$ as

$$\mathbf{S} = \begin{bmatrix} \boldsymbol{\Phi}_{\mathbf{u}k} & \boldsymbol{\Phi}_{\mathbf{u}r} \end{bmatrix} \begin{bmatrix} \boldsymbol{\mu}_k & \mathbf{0}_{n_k n_r} \\ \mathbf{0}_{n_r n_k} & \boldsymbol{\mu}_r \end{bmatrix} \begin{bmatrix} \boldsymbol{\Phi}_{\mathbf{u}k} & \boldsymbol{\Phi}_{\mathbf{u}r} \end{bmatrix}^{-1} . \tag{3.47}$$

If this eigendecomposition is used at the same frequency used to express the reduced wave basis —$i.e.$, $\omega = \omega_i^{\mathtt{ref}}$—, one may re-write Equation (3.42) as

$$\tilde{\mathbf{S}}(\omega_i^{\mathtt{ref}}) = \begin{bmatrix} \mathbf{I}_{n_k} & \mathbf{0}_{n_k n_r} \end{bmatrix} \begin{bmatrix} \boldsymbol{\mu}_k(\omega_i^{\mathtt{ref}}) & \mathbf{0}_{n_k n_r} \\ \mathbf{0}_{n_r n_k} & \boldsymbol{\mu}_r(\omega_i^{\mathtt{ref}}) \end{bmatrix} \begin{bmatrix} \mathbf{I}_{n_k} \\ \mathbf{0}_{n_r n_k} \end{bmatrix} = \boldsymbol{\mu}_k(\omega_i^{\mathtt{ref}}). \tag{3.48}$$

Moreover, at this frequency, one may show that $\tilde{\mathbf{S}}(\omega_i^{\mathtt{ref}})$ is symplectic as

$$\begin{aligned} \tilde{\mathbf{S}}(\omega_i^{\mathtt{ref}})^T \mathbf{J}_{n_k} \tilde{\mathbf{S}}(\omega_i^{\mathtt{ref}}) &= \boldsymbol{\mu}_k(\omega_i^{\mathtt{ref}}) \mathbf{J}_{n_k} \boldsymbol{\mu}_k(\omega_i^{\mathtt{ref}}) \\ &= \boldsymbol{\mu}_k(\omega_i^{\mathtt{ref}}) \mathbf{J}_{n_k} \boldsymbol{\mu}_k(\omega_i^{\mathtt{ref}}) = \mathbf{J}_{n_k}. \end{aligned} \tag{3.49}$$

For an angular frequency $\omega_i \in \tilde{\beta}_{fi}$ distinct from that used to get the reduced basis $(\omega_i^{\mathtt{ref}})$ — usually, the maximum frequency within the range —, one can show that $\tilde{\mathbf{S}}(\omega_i)$ may not be symplectic, but close to it. Using the original eigenvalues/eigenvectors to decompose the symplectic transfer matrix at $\omega_i$, the reduced matrix at this frequency can be written as

$$\begin{aligned} \tilde{\mathbf{S}}(\omega_i) &= \boldsymbol{\Psi}_{\mathbf{u}k}(\omega_i^{\mathtt{ref}}) \boldsymbol{\Phi}_{\mathbf{u}}(\omega_i) \boldsymbol{\mu}(\omega_i) \boldsymbol{\Phi}_{\mathbf{u}}^{-1}(\omega_i) \boldsymbol{\Phi}_{\mathbf{u}k}(\omega_i^{\mathtt{ref}}) \\ &= \begin{bmatrix} \boldsymbol{\Psi}_{\mathbf{u}k}(\omega_i^{\mathtt{ref}}) \boldsymbol{\Phi}_{\mathbf{u}}(\omega_i) \end{bmatrix} \boldsymbol{\mu}(\omega_i) \begin{bmatrix} \boldsymbol{\Phi}_{\mathbf{u}}^{-1}(\omega_i) \boldsymbol{\Phi}_{\mathbf{u}k}(\omega_i^{\mathtt{ref}}) \end{bmatrix}. \end{aligned} \tag{3.50}$$

One can expand the wave mode shapes evaluated at $\omega_i$ in terms of the wave modes at the frequency the reduction basis is set $(\omega_i^{\mathtt{ref}})$, as follows

$$\begin{bmatrix} \boldsymbol{\Phi}_{\mathbf{u}k}(\omega_i) & \boldsymbol{\Phi}_{\mathbf{u}r}(\omega_i) \end{bmatrix} = \begin{bmatrix} \boldsymbol{\Phi}_{\mathbf{u}k}(\omega_i^{\mathtt{ref}}) & \boldsymbol{\Phi}_{\mathbf{u}r}(\omega_i^{\mathtt{ref}}) \end{bmatrix} \begin{bmatrix} \boldsymbol{\alpha}_{kk} & \boldsymbol{\alpha}_{kr} \\ \boldsymbol{\alpha}_{rk} & \boldsymbol{\alpha}_{rr} \end{bmatrix} . \tag{3.51}$$

Left multiplying Equation (3.51) by

$$\begin{bmatrix} \boldsymbol{\Psi}_{\mathbf{u}k}(\omega_i^{\mathtt{ref}}) \\ \boldsymbol{\Psi}_{\mathbf{u}r}(\omega_i^{\mathtt{ref}}) \end{bmatrix} \tag{3.52}$$

and making use of the symplectic orthogonality as stated in Equation (3.33), one may write

$$
\begin{bmatrix} \mathbf{\Psi}_{\mathbf{u}k}(\omega_i^{\texttt{ref}}) & \mathbf{\Phi}_{\mathbf{u}r}(\omega_i^{\texttt{ref}}) \end{bmatrix}
\begin{bmatrix} \mathbf{\Psi}_{\mathbf{u}k}(\omega_i^{\texttt{ref}})\mathbf{\Phi}_{\mathbf{u}k}(\omega_i) & \mathbf{\Phi}_{\mathbf{u}k}(\omega_i^{\texttt{ref}})\mathbf{\Phi}_{\mathbf{u}r}(\omega_i) \\ \mathbf{\Psi}_{\mathbf{u}r}(\omega_i^{\texttt{ref}})\mathbf{\Phi}_{\mathbf{u}k}(\omega_i) & \mathbf{\Psi}_{\mathbf{u}r}(\omega_i^{\texttt{ref}})\mathbf{\Phi}_{\mathbf{u}r}(\omega_i) \end{bmatrix}
=
\begin{bmatrix} \mathbf{I}_{n_k} & \mathbf{0}_{n_k n_r} \\ \mathbf{0}_{n_r n_k} & \mathbf{I}_{n_r} \end{bmatrix}
\begin{bmatrix} \boldsymbol{\alpha}_{kk} & \boldsymbol{\alpha}_{kr} \\ \boldsymbol{\alpha}_{rk} & \boldsymbol{\alpha}_{rr} \end{bmatrix},
$$
$$(3.53)$$

which yields

$$
\begin{bmatrix} \boldsymbol{\alpha}_{kk} & \boldsymbol{\alpha}_{kr} \\ \boldsymbol{\alpha}_{rk} & \boldsymbol{\alpha}_{rr} \end{bmatrix}
=
\begin{bmatrix} \mathbf{\Psi}_{\mathbf{u}k}(\omega_i^{\texttt{ref}})\mathbf{\Phi}_{\mathbf{u}k}(\omega_i) & \mathbf{\Psi}_{\mathbf{u}k}(\omega_i^{\texttt{ref}})\mathbf{\Phi}_{\mathbf{u}k}(\omega_i) \\ \mathbf{\Psi}_{\mathbf{u}r}(\omega_i^{\texttt{ref}})\mathbf{\Phi}_{\mathbf{u}k}(\omega_i) & \mathbf{\Psi}_{\mathbf{u}r}(\omega_i^{\texttt{ref}})\mathbf{\Phi}_{\mathbf{u}r}(\omega_i) \end{bmatrix}
\tag{3.54}
$$

Assuming that $\boldsymbol{\alpha}_{kr} = \boldsymbol{\alpha}_{rk} = \mathbf{0}$ and using Equation (3.51) in Equation (3.50), yields

$$
\tilde{\mathbf{S}}(\omega_i) = \boldsymbol{\alpha}_{kk}\boldsymbol{\mu}_k(\omega_i)\boldsymbol{\alpha}_{kk}^{-1}
\tag{3.55}
$$

Thus, the nature of $\tilde{\mathbf{S}}(\omega_i)$ is directly related to the form of $\boldsymbol{\alpha}_{kk}$. As a result of the symplectic orthogonality of wave mode shapes (Equation (3.33)), $\boldsymbol{\alpha}_{kk}$ tends to the identity matrix, which makes $\tilde{\mathbf{S}}(\omega_i)$ close to symplectic. It is worth to emphasize here that procedures which respect the structure are usually preferred with the interest of guaranteeing efficiency, stability and accuracy ((Watkins, 2007), (Hogben, 2013)). It is also important to point out that the unsymmetric Lanczos process, which is the algorithm used when the MATLAB® function eigs is called, is a structure-preserving method when applied to the skew-Hamiltonian matrix $\mathbf{S} + \mathbf{S}^{-1}$ (Watkins, 2004). The consideration of Lanczos method for the computation of the generalized eigenvalue problem based on the skew-Hamiltonian matrix $\mathbf{S} + \mathbf{S}^{-1}$ within the framework of the WFE method has been recently proposed by Mencik and Duhamel (2015). Moreover, if the symplectic nature is preserved, one might make use of algorithms which by exploiting the structure leads to reduced computational time as, for instance, the SR algorithm based on the butterfly form (Fassbender, 2002) or the condensed symplectic Lanczos process (Watkins, 2004). Regarding the proposed reduced eigenvalue problem, which is not strictly symplectic, one may not profit from the efficiency of symplectic-based algorithms and may not enforce that if $\tilde{\mu}_j$ is an eigenvalue of $\tilde{\mathbf{S}}$, then $1/\tilde{\mu}_j$ might be an eigenvalue as well either. However, the key idea behind the proposed eigenvalue problem is the possibility of computing only the desired wave modes, which are not necessarily the ones of highest or lowest magnitudes, and thus may not be efficiently performed by means of Lanczos method.

### 3.3.3 Reduced-order RM matrix

Associated to the proposed reduced-order (RO) WFE method, a reduced receptance matrix in terms of generalized DOFs can be built. The solution of the reduced eigenproblem stated in Equation (3.45) yields a reduced basis of wave modes expressed in generalized coordinates $(\tilde{\mu}_j, \tilde{\varphi}_j)_j$. In order to recover displacements/rotations and forces/moments components of the wave mode shapes, one may make use of the associated right-hand transformation matrix $\tilde{\mathbf{T}}_{\mathrm{R}}$, as follows

$$\tilde{\mathbf{\Phi}} = \begin{bmatrix} \tilde{\mathbf{\Phi}}_{\mathsf{q}} \\ \tilde{\mathbf{\Phi}}_{\mathsf{F}} \end{bmatrix} = \tilde{\mathbf{T}}_{\mathrm{R}}\tilde{\boldsymbol{\varphi}}. \tag{3.56}$$

Notice that the transformation matrix $\tilde{\mathbf{T}}_{\mathrm{R}}$ is applied to the wave modes related to right-going waves only. In order to express the reduced set of left-going wave mode shapes in terms of physical DOFs, one might make use the symmetry relation stated in Equation (2.22). Then, using the orthogonality relation between the left and right eigenvectors of $\mathbf{S}$ (Equation (2.18)) and the normalization procedure stated in Equation (3.33), the corresponding left eigenvectors $(\tilde{\mathbf{\Psi}}, \tilde{\mathbf{\Psi}}^\star)$ are obtained.

Given the reduced basis of wave modes expressed in the physical DOFs, the vector of displacements/rotations at the ends of a periodic structure composed of $N$ substructures can be expressed as

$$\begin{bmatrix} \mathbf{q}_{\mathrm{L}}^{(1)} \\ \mathbf{q}_{\mathrm{R}}^{(N)} \end{bmatrix} = \begin{bmatrix} \tilde{\mathbf{\Phi}}_{\mathsf{q}} & \tilde{\mathbf{\Phi}}_{\mathsf{q}}^\star\tilde{\boldsymbol{\mu}}^N \\ \tilde{\mathbf{\Phi}}_{\mathsf{q}}\tilde{\boldsymbol{\mu}}^N & \tilde{\mathbf{\Phi}}_{\mathsf{q}}^\star \end{bmatrix} \begin{bmatrix} \tilde{\mathbf{Q}} \\ \tilde{\mathbf{Q}}^\star \end{bmatrix}. \tag{3.57}$$

This system of equations is over-determined as it is composed of $2N$ equations, but it is expressed in terms of only $2n_w$ variables: the vectors of wave amplitudes $\mathbf{Q}$ and $\mathbf{Q}^\star$. In order to make it full-ranked some constraints are considered. It consists in writing the vectors of displacements/rotations in terms of independent vectors of generalized coordinates, as follows

$$\begin{bmatrix} \mathbf{q}_{\mathrm{L}}^{(1)} \\ \mathbf{q}_{\mathrm{R}}^{(N)} \end{bmatrix} = \tilde{\mathbf{P}}_{\mathsf{q}} \begin{bmatrix} \tilde{\mathbf{q}}_{\mathrm{L}}^{(1)} \\ \tilde{\mathbf{q}}_{\mathrm{R}}^{(N)} \end{bmatrix}, \tag{3.58}$$

where

$$\tilde{\mathbf{P}}_{\mathsf{q}} = \begin{bmatrix} \tilde{\mathbf{\Phi}}_{\mathsf{q}} & \mathbf{0} \\ \mathbf{0} & \tilde{\mathbf{\Phi}}_{\mathsf{q}}^\star \end{bmatrix}. \tag{3.59}$$

Thus, by substituting Equation (3.58) in 3.57, one gets

$$\begin{bmatrix} \tilde{\Phi}_q & 0 \\ 0 & \tilde{\Phi}_q^\star \end{bmatrix} \begin{bmatrix} \tilde{q}_L^{(1)} \\ \tilde{q}_R^{(N)} \end{bmatrix} = \begin{bmatrix} \tilde{\Phi}_q & \tilde{\Phi}_q^\star \tilde{\mu}^N \\ \tilde{\Phi}_q \tilde{\mu}^N & \tilde{\Phi}_q^\star \end{bmatrix} \begin{bmatrix} \tilde{Q} \\ \tilde{Q}^\star \end{bmatrix}. \tag{3.60}$$

Left multiplying Equation (3.60) by

$$\begin{bmatrix} \tilde{\Psi}_F & 0 \\ 0 & \tilde{\Psi}_F^\star \end{bmatrix}, \tag{3.61}$$

allows one to write

$$\begin{bmatrix} \tilde{q}_L^{(1)} \\ \tilde{q}_R^{(N)} \end{bmatrix} = \begin{bmatrix} \tilde{\Psi}_F \tilde{\Phi}_q & 0 \\ 0 & \tilde{\Psi}_F^\star \tilde{\Phi}_q^\star \end{bmatrix}^{-1} \begin{bmatrix} \tilde{\Psi}_F \tilde{\Phi}_q & \tilde{\Psi}_F \tilde{\Phi}_q^\star \tilde{\mu}^N \\ \tilde{\Psi}_F^\star \tilde{\Phi}_q \tilde{\mu}^N & \tilde{\Psi}_F^\star \tilde{\Phi}_q^\star \end{bmatrix} \begin{bmatrix} \tilde{Q} \\ \tilde{Q}^\star \end{bmatrix}. \tag{3.62}$$

The reduced wave mode basis can also be used to express the vectors of forces/moments at the ends of the periodic structure, as follows

$$\begin{bmatrix} F_L^{(1)} \\ F_R^{(N)} \end{bmatrix} = \begin{bmatrix} -\tilde{\Phi}_F & -\tilde{\Phi}_F^\star \tilde{\mu}^N \\ \tilde{\Phi}_F \tilde{\mu}^N & \tilde{\Phi}_F^\star \end{bmatrix} \begin{bmatrix} \tilde{Q} \\ \tilde{Q}^\star \end{bmatrix}. \tag{3.63}$$

Left multiplying this system of equations by

$$\begin{bmatrix} -\tilde{\Psi}_q & 0 \\ 0 & \tilde{\Psi}_q^\star \end{bmatrix}, \tag{3.64}$$

it yields

$$\begin{bmatrix} -\tilde{\Psi}_q & 0 \\ 0 & \tilde{\Psi}_q^\star \end{bmatrix} \begin{bmatrix} F_L^{(1)} \\ F_R^{(N)} \end{bmatrix} = \begin{bmatrix} \tilde{\Psi}_q \tilde{\Phi}_F & \tilde{\Psi}_q \tilde{\Phi}_F^\star \tilde{\mu}^N \\ \tilde{\Psi}_q^\star \tilde{\Phi}_F \tilde{\mu}^N & \tilde{\Psi}_q^\star \tilde{\Phi}_F^\star \end{bmatrix} \begin{bmatrix} \tilde{Q} \\ \tilde{Q}^\star \end{bmatrix}. \tag{3.65}$$

Then, considering the pre-multiplication of this system of equations by

$$\begin{bmatrix} \left( \tilde{\Psi}_q \tilde{\Phi}_F \right)^{-1} & 0 \\ 0 & \left( \tilde{\Psi}_q^\star \tilde{\Phi}_F^\star \right)^{-1} \end{bmatrix}, \tag{3.66}$$

one gets

$$\begin{bmatrix} -\left( \tilde{\Psi}_q \tilde{\Phi}_F \right)^{-1} \tilde{\Psi}_q & 0 \\ 0 & \left( \tilde{\Psi}_q^\star \tilde{\Phi}_F^\star \right)^{-1} \tilde{\Psi}_q^\star \end{bmatrix} \begin{bmatrix} F_L^{(1)} \\ F_R^{(N)} \end{bmatrix} = \begin{bmatrix} I_{n_k} & -\tilde{\mathbb{C}}_f \tilde{\mu}^N \\ -\tilde{\mathbb{C}}_f \tilde{\mu}^N & I_{n_k} \end{bmatrix} \begin{bmatrix} \tilde{Q} \\ \tilde{Q}^\star \end{bmatrix}, \tag{3.67}$$

74

where $\tilde{\mathbb{C}}_{\mathrm{f}} = -\left(\tilde{\boldsymbol{\Psi}}_{\mathrm{q}}\tilde{\boldsymbol{\Phi}}_{\mathrm{F}}\right)^{-1}\left(\tilde{\boldsymbol{\Psi}}_{\mathrm{q}}\tilde{\boldsymbol{\Phi}}_{\mathrm{F}}^{\star}\right)$, which can be shown to be equivalent to $-\left(\tilde{\boldsymbol{\Psi}}_{\mathrm{q}}^{\star}\tilde{\boldsymbol{\Phi}}_{\mathrm{F}}^{\star}\right)^{-1}\left(\tilde{\boldsymbol{\Psi}}_{\mathrm{q}}^{\star}\tilde{\boldsymbol{\Phi}}_{\mathrm{F}}\right)$. Here, the generalized vectors of forces/moments defined at the left and right ends of the periodic structure are defined as

$$\begin{bmatrix} \tilde{\mathbf{F}}_{\mathrm{L}}^{(1)} \\ \tilde{\mathbf{F}}_{\mathrm{R}}^{(N)} \end{bmatrix} = \tilde{\mathbf{P}}_{\mathrm{F}} \begin{bmatrix} \mathbf{F}_{\mathrm{L}}^{(1)} \\ \mathbf{F}_{\mathrm{R}}^{(N)} \end{bmatrix}, \tag{3.68}$$

where

$$\tilde{\mathbf{P}}_{\mathrm{F}} = \begin{bmatrix} -\left(\tilde{\boldsymbol{\Psi}}_{\mathrm{q}}\tilde{\boldsymbol{\Phi}}_{\mathrm{F}}\right)^{-1}\tilde{\boldsymbol{\Psi}}_{\mathrm{q}} & \mathbf{0} \\ \mathbf{0} & \left(\tilde{\boldsymbol{\Psi}}_{\mathrm{q}}^{\star}\tilde{\boldsymbol{\Phi}}_{\mathrm{F}}^{\star}\right)^{-1}\tilde{\boldsymbol{\Psi}}_{\mathrm{q}}^{\star} \end{bmatrix}. \tag{3.69}$$

Thus, the vector of wave amplitudes can be expressed in terms of these generalized vectors, as follows

$$\begin{bmatrix} \tilde{\mathbf{Q}} \\ \tilde{\mathbf{Q}}^{\star} \end{bmatrix} = \begin{bmatrix} \mathbf{I}_{n_k} & -\tilde{\mathbb{C}}_{\mathrm{f}}\tilde{\boldsymbol{\mu}}^N \\ -\tilde{\mathbb{C}}_{\mathrm{f}}\tilde{\boldsymbol{\mu}}^N & \mathbf{I}_{n_k} \end{bmatrix}^{-1} \begin{bmatrix} \tilde{\mathbf{F}}_{\mathrm{L}}^{(1)} \\ \tilde{\mathbf{F}}_{\mathrm{R}}^{(N)} \end{bmatrix} \tag{3.70}$$

Using Equations 3.62 and 3.70, a reduced-order receptance matrix can be formulated in terms of generalized DOFs and it is given by

$$\tilde{\mathbf{R}} = \begin{bmatrix} \tilde{\boldsymbol{\Psi}}_{\mathrm{F}}\tilde{\boldsymbol{\Phi}}_{\mathrm{q}} & \mathbf{0} \\ \mathbf{0} & \tilde{\boldsymbol{\Psi}}_{\mathrm{F}}^{\star}\tilde{\boldsymbol{\Phi}}_{\mathrm{q}}^{\star} \end{bmatrix}^{-1} \begin{bmatrix} \tilde{\boldsymbol{\Psi}}_{\mathrm{F}}\tilde{\boldsymbol{\Phi}}_{\mathrm{q}} & \tilde{\boldsymbol{\Psi}}_{\mathrm{F}}\tilde{\boldsymbol{\Phi}}_{\mathrm{q}}^{\star}\tilde{\boldsymbol{\mu}}^N \\ \tilde{\boldsymbol{\Psi}}_{\mathrm{F}}^{\star}\tilde{\boldsymbol{\Phi}}_{\mathrm{q}}\tilde{\boldsymbol{\mu}}^N & \tilde{\boldsymbol{\Psi}}_{\mathrm{F}}^{\star}\tilde{\boldsymbol{\Phi}}_{\mathrm{q}}^{\star} \end{bmatrix} \begin{bmatrix} \mathbf{I}_{n_k} & -\tilde{\mathbb{C}}_{\mathrm{f}}\tilde{\boldsymbol{\mu}}^N \\ -\tilde{\mathbb{C}}_{\mathrm{f}}\tilde{\boldsymbol{\mu}}^N & \mathbf{I}_{n_k} \end{bmatrix}^{-1}. \tag{3.71}$$

The structural response in terms of the physical DOFs are recovered by means of Equations 3.58 and 3.68. A schematics of the numerical steps involved in the formulation of reduced-order WFE-based superelement models is presented in Figure 3.4 .

## 3.4 The wave spectral finite element method

The (wave spectral finite element method) WSFEM provides a procedure for deriving numerical spectral matrices of periodic structures. The method proposed here can be considered a semi-analytical numerical method. This is because the displacement field is expressed by means of a numerical wave basis obtained via the WFE method and the elastodynamic equations are used to express the corresponding loads as a function of the displacement field as SEM does. The motivation behind the use of the WSFEM is the possibility of deriving spectral elements of periodic

For $\omega = \omega_i^{\text{ref}}$

**Selection Criteria**

Criterion 1: based on $r_{Q_j}, r_{Q_j}^\star$.

Criterion 2: based on $|\mu_j|$.

For $\omega \in \beta_{fi}$

**RO wave basis**

Transformation matrices
$\tilde{T}_L = \Psi_{uk}, \tilde{T}_R = \Phi_{uk}$

Reduced substructure
$\tilde{S}^{(k)} = \tilde{T}_L S^{(k)} \tilde{T}_R$

Reduced WFE Eigen-
problem $\tilde{S}\tilde{\Phi}_j = \tilde{\mu}_j \tilde{\Phi}_j$

For $\omega \in \beta_f$

**RO Forced Response Problem**

Reduced Receptance matrix $\tilde{R}^{(s)}$

Forced Problem $\tilde{R}^{(s)} F^{(s)} = q^{(s)}$
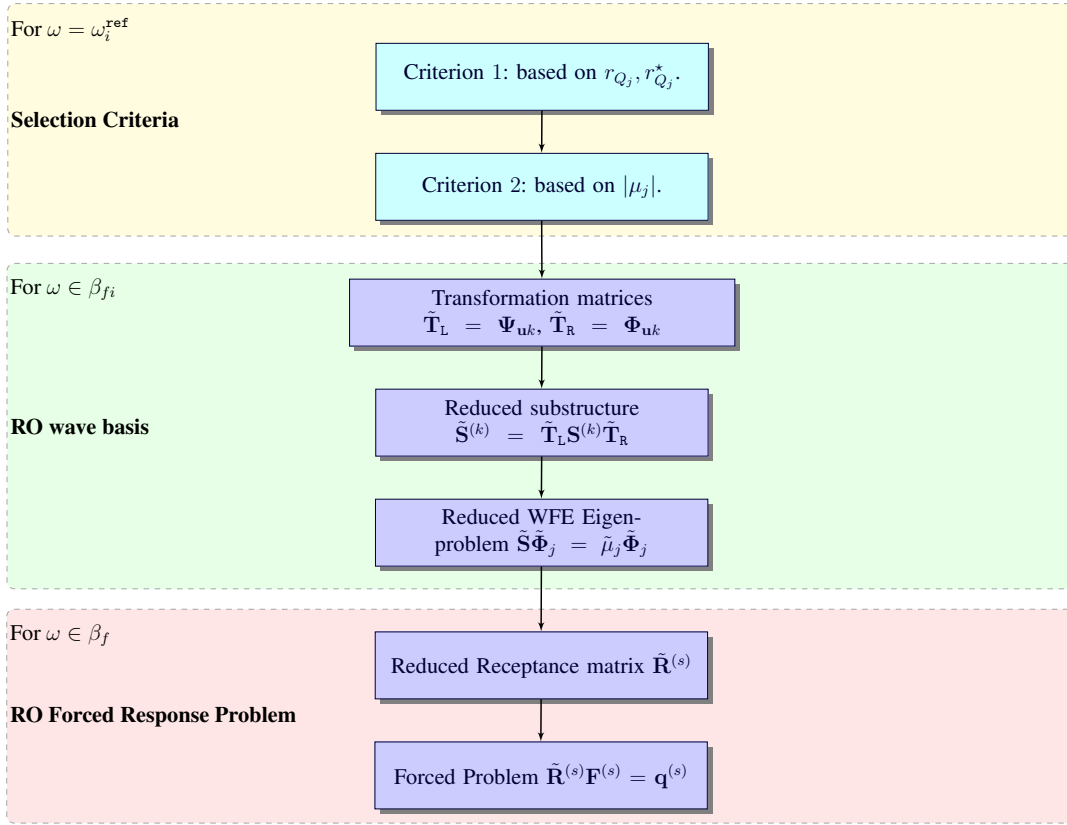
Figure 3.4: Flowchart illustrating the different numerical steps to build the ROM.

structures with geometric and material complexities in a straightforward way, as finite elements are used to model the substructure. On the other hand, the method remains limited as it requires analytical expressions for the applied loads. The method was pioneered by Arruda and Nascimento (2008), and it is clearly stated for an elementary rod and the Euler-Bernoulli beam in (Nascimento, 2009). Here, the method is described in a general form and, then, extended to the case of a Timoshenko beam.

For a given structure, a set of wave modes is selected among those obtained via the WFE method. The choice of the wave modes is determined by the dynamic behavior being described. For instance, if an elementary rod is modeled, only the longitudinal wave mode is kept. In contrast, if a frame is considered, not only the longitudinal mode, but also bending and shear wave modes should be kept. Considering the displacement/rotation component of the set of wave modes kept $\tilde{\Phi}_q = \{\phi_j\}_{j \in \mathbb{M}_k} \cup \tilde{\Phi}_q^\star = \{\phi_j^\star\}_{j \in \mathbb{M}_k}$ — $\mathbb{M}_k$ being the set of $n_k$ wave modes kept — as a wave basis, the vector of nodal displacements/rotations at the left and at the right ends of a substructure within

the full periodic structure may be expressed as in Equation (3.5a), which yields

$$\mathbf{q}_{\mathrm{L}}^{(k)} = \tilde{\mathbf{\Phi}}_{\mathsf{q}}\tilde{\boldsymbol{\mu}}^{k-1}\tilde{\mathbf{Q}} + \tilde{\mathbf{\Phi}}_{\mathsf{q}}^{\star}\tilde{\boldsymbol{\mu}}^{N+1-k}\tilde{\mathbf{Q}}^{\star} \quad , \quad \mathbf{q}_{\mathrm{R}}^{(k)} = \tilde{\mathbf{\Phi}}_{\mathsf{q}}\tilde{\boldsymbol{\mu}}^{k}\tilde{\mathbf{Q}} + \tilde{\mathbf{\Phi}}_{\mathsf{q}}^{\star}\tilde{\boldsymbol{\mu}}^{N-k}\tilde{\mathbf{Q}}^{\star} \quad k = 1,\dots,N. \quad (3.72)$$

Notice that the wave shapes $\tilde{\mathbf{\Phi}}_{\mathsf{q}}$ and $\tilde{\mathbf{\Phi}}_{\mathsf{q}}^{\star}$ may be discrete functions of the cross-section coordinates ($y$ in a 2D case, $y$ and $z$ in a 3D case). Besides, the diagonal matrices of propagation constants $\tilde{\boldsymbol{\mu}}$ and $\tilde{\boldsymbol{\mu}}^{\star}$ are discrete functions of $x$. Thus, the vector of displacements/rotations can be written, in general form, as

$$\begin{aligned}
\mathbf{q}(x,y,z) &= \tilde{\mathbf{\Phi}}_{\mathsf{q}}(y,z)\,\mathrm{diag}\left(e^{-\mathrm{i}\beta_j x}\right)_{j\in\mathbb{M}_k}\tilde{\mathbf{Q}} + \tilde{\mathbf{\Phi}}_{\mathsf{q}}^{\star}(y,z)\,\mathrm{diag}\left(e^{-\mathrm{i}\beta_j(N\Delta - x)}\right)_{j\in\mathbb{M}_k}\tilde{\mathbf{Q}}^{\star}, \\
x &\in [0, \Delta, 2\Delta, \dots, N\Delta], \\
y &\in [0, h, 2h, \dots, N_y h], \\
z &\in [0, w, 2w, \dots, N_z w],
\end{aligned} \quad (3.73)$$

where $h$ and $w$ are, respectively, the element sizes along the $y$- and the $z$-axis, and the number of finite elements used to the discretize the cross-section along these axes are $N_y$ and $N_z$, respectively.

Approximate structural theories are derived by means of variational methods, such as Hamilton's Principle. With the aid of these methods, natural boundary conditions (BC), which corresponds, in this case, to Neumann BC, *i.e.*, forces and moments expressions, are specified for classical and higher-order structural theories. Forces and moments are expressed in terms of derivatives of displacements and rotations. They can be, in general form, expressed as

$$\mathbf{F}(x,y,z) = \pm\mathfrak{L}(\mathbf{q}(x,y,z)) \quad (3.74)$$

where $\mathbf{F}(x,y,z)$ and $\mathbf{q}(x,y,z)$ are, respectively, the vectors of forces/moments and displacements/rotations evaluated at an arbitrary $(x,y,z)$ position along the structure, and $\mathfrak{L}$ is used to denote a general function which involves derivatives of $\mathbf{q}(x,y,z)$. In fact, the vectors of displacements/rotations and forces/moments ($\mathbf{q}$ and $\mathbf{F}$, respectively) consist of $N_{DOF}$ DOFs each, which may correspond to some of or all of the DOFs used to discretize the cross-section within a FE model. Equation (3.74) can be used with Equation (3.73) to express the vectors of forces/moments,

as follows

$$
\mathbf{F}(x,y,z) = \pm\mathfrak{L}\left(\tilde{\mathbf{\Phi}}_{\mathsf{q}}(y,z)\operatorname{diag}\left(e^{-\mathrm{i}\beta_j x}\right)_{j\in\mathbb{M}_k}\tilde{\mathbf{Q}} + \tilde{\mathbf{\Phi}}_{\mathsf{q}}^{\star}(y,z)\operatorname{diag}\left(e^{-\mathrm{i}\beta_j(N\Delta-x)}\right)_{j\in\mathbb{M}_k}\tilde{\mathbf{Q}}^{\star}\right),
$$
$$
x \in [0, \Delta, 2\Delta, \ldots, N\Delta],
$$
$$
y \in [0, h, 2h, \ldots, N_y h],
$$
$$
z \in [0, w, 2w, \ldots, N_z w],
$$

(3.75)

which can be re-written as

$$
\mathbf{F}(x,y,z) = \pm\tilde{\mathbf{\Phi}}_{\mathsf{F}}(y,z)\operatorname{diag}\left(e^{-\mathrm{i}\beta_j x}\right)_{j\in\mathbb{M}_k}\tilde{\mathbf{Q}} + \tilde{\mathbf{\Phi}}_{\mathsf{F}}^{\star}(y,z)\operatorname{diag}\left(e^{-\mathrm{i}\beta_j(N\Delta-x)}\right)_{j\in\mathbb{M}_k}\tilde{\mathbf{Q}}^{\star},
$$
$$
x \in [0, \Delta, 2\Delta, \ldots, N\Delta],
$$
$$
y \in [0, h, 2h, \ldots, N_y h],
$$
$$
z \in [0, w, 2w, \ldots, N_z w],
$$

(3.76)

where

$$
\tilde{\mathbf{\Phi}}_{\mathsf{F}} = \mathfrak{L}\left(\mathbf{\Phi}_{\mathsf{q}}(y,z)\operatorname{diag}\left(e^{-\mathrm{i}\beta_j x}\right)_{j\in\mathbb{M}_k}\right)\operatorname{diag}\left(e^{\mathrm{i}\beta_j x}\right)_{j\in\mathbb{M}_k}
$$

and

$$
\tilde{\mathbf{\Phi}}_{\mathsf{F}}^{\star} = \mathfrak{L}\left(\mathbf{\Phi}_{\mathsf{q}}^{\star}(y,z)\operatorname{diag}\left(e^{-\mathrm{i}\beta_j(N\Delta-x)}\right)_{j\in\mathbb{M}_k}\right)\operatorname{diag}\left(e^{\mathrm{i}\beta_j(N\Delta-x)}\right)_{j\in\mathbb{M}_k}.
$$

As we are dealing with discrete functions, their derivatives are calculated by means of the finite difference method. Using Equation (3.76), the vector of nodal forces/moments at the left and at the right ends of a substructure within the full periodic structure can be expressed as

$$
\mathbf{F}_{\mathsf{L}}^{(k)} = -\tilde{\mathbf{\Phi}}_{\mathsf{F}}\tilde{\boldsymbol{\mu}}^{k-1}\tilde{\mathbf{Q}} - \tilde{\mathbf{\Phi}}_{\mathsf{F}}^{\star}\tilde{\boldsymbol{\mu}}^{N+1-k}\tilde{\mathbf{Q}}^{\star} \quad , \quad \mathbf{F}_{\mathsf{R}}^{(k)} = \tilde{\mathbf{\Phi}}_{\mathsf{F}}\tilde{\boldsymbol{\mu}}^{k}\tilde{\mathbf{Q}} + \tilde{\mathbf{\Phi}}_{\mathsf{F}}^{\star}\tilde{\boldsymbol{\mu}}^{N-k}\tilde{\mathbf{Q}}^{\star} \quad k = 1,\ldots,N. \quad (3.77)
$$

Then, using Equations (3.72) and (3.77), respectively, to relate, in matrix form, the vector of displacements/rotations and the vector of forces/moments evaluated at the ends of the full periodic structure with the vector of wave amplitudes, one may write

$$
\begin{bmatrix} \mathbf{q}_{\mathsf{L}}^{(1)} \\ \mathbf{q}_{\mathsf{R}}^{(N)} \end{bmatrix}_{(2N_{DOF}\times 1)} = \begin{bmatrix} \tilde{\mathbf{\Phi}}_{\mathsf{q}} & \tilde{\mathbf{\Phi}}_{\mathsf{q}}^{\star}\tilde{\boldsymbol{\mu}} \\ \tilde{\mathbf{\Phi}}_{\mathsf{q}}\tilde{\boldsymbol{\mu}} & \tilde{\mathbf{\Phi}}_{\mathsf{q}}^{\star} \end{bmatrix}_{(2N_{DOF}\times 2n_k)} \begin{bmatrix} \tilde{\mathbf{Q}} \\ \tilde{\mathbf{Q}}^{\star} \end{bmatrix}_{(2n_k\times 1)},
$$

(3.78a)

$$
\begin{bmatrix} \mathbf{F}_{\mathsf{L}}^{(1)} \\ \mathbf{F}_{\mathsf{R}}^{(N)} \end{bmatrix}_{(2N_{DOF}\times 1)} = \begin{bmatrix} -\tilde{\mathbf{\Phi}}_{\mathsf{F}} & -\tilde{\mathbf{\Phi}}_{\mathsf{F}}^{\star}\tilde{\boldsymbol{\mu}} \\ \tilde{\mathbf{\Phi}}_{\mathsf{F}}\tilde{\boldsymbol{\mu}} & \tilde{\mathbf{\Phi}}_{\mathsf{F}}^{\star} \end{bmatrix}_{(2N_{DOF}\times 2n_k)} \begin{bmatrix} \tilde{\mathbf{Q}} \\ \tilde{\mathbf{Q}}^{\star} \end{bmatrix}_{(2n_k\times 1)}.
$$

(3.78b)

Unless the full wave mode basis is kept, the matrices in the above equations are not square. Thus,

they cannot be directly inverted. Let $\tilde{\mathbf{P}}_{(2N_{DOF}\times 2n_k)}$ be a matrix of the form

$$\tilde{\mathbf{P}}_{(2N_{DOF}\times 2n_k)} = \begin{bmatrix} \bar{\mathbf{P}}_{(N_{DOF}\times n_k)} & \mathbf{0}_{(N_{DOF}\times n_k)} \\ \mathbf{0}_{(N_{DOF}\times n_k)} & \bar{\mathbf{P}}_{(N_{DOF}\times n_k)} \end{bmatrix}, \tag{3.79}$$

which relates the simulated DOFs (*i.e.*, those that come from the FE model discretization) with the condensed ones (*i.e.*, those used within the WSFEM) on the left and the right cross-sections, as follows

$$\begin{bmatrix} \mathbf{q}_L^{(1)} \\ \mathbf{q}_R^{(N)} \end{bmatrix} = \tilde{\mathbf{P}} \begin{bmatrix} \tilde{\mathbf{q}}_L^{(1)} \\ \tilde{\mathbf{q}}_R^{(N)} \end{bmatrix}, \tag{3.80a}$$

$$\begin{bmatrix} \tilde{\mathbf{F}}_L^{(1)} \\ \tilde{\mathbf{F}}_R^{(N)} \end{bmatrix} = \tilde{\mathbf{P}}^H \begin{bmatrix} \mathbf{F}_L^{(1)} \\ \mathbf{F}_R^{(N)} \end{bmatrix}. \tag{3.80b}$$

By substituting Equation (3.80a) into Equation (3.78a), and left-multiplying the resultant equation by $\tilde{\mathbf{P}}^H$, one gets

$$\tilde{\mathbf{P}}^H \tilde{\mathbf{P}} \begin{bmatrix} \tilde{\mathbf{q}}_L^{(1)} \\ \tilde{\mathbf{q}}_R^{(N)} \end{bmatrix} = \tilde{\mathbf{P}}^H \begin{bmatrix} \tilde{\mathbf{\Phi}}_q & \tilde{\mathbf{\Phi}}_q^\star \tilde{\boldsymbol{\mu}} \\ \tilde{\mathbf{\Phi}}_q \tilde{\boldsymbol{\mu}} & \tilde{\mathbf{\Phi}}_q^\star \end{bmatrix} \begin{bmatrix} \tilde{\mathbf{Q}} \\ \tilde{\mathbf{Q}}^\star \end{bmatrix}. \tag{3.81}$$

Now, the matrices multiplying the wave amplitudes on the right-hand side yield a square matrix, which allows one to express the vector of wave amplitudes as

$$\begin{bmatrix} \tilde{\mathbf{Q}} \\ \tilde{\mathbf{Q}}^\star \end{bmatrix} = \left( \tilde{\mathbf{P}}^H \begin{bmatrix} \tilde{\mathbf{\Phi}}_q & \tilde{\mathbf{\Phi}}_q^\star \tilde{\boldsymbol{\mu}} \\ \tilde{\mathbf{\Phi}}_q \tilde{\boldsymbol{\mu}} & \tilde{\mathbf{\Phi}}_q^\star \end{bmatrix} \right)^{-1} \tilde{\mathbf{P}}^H \tilde{\mathbf{P}} \begin{bmatrix} \tilde{\mathbf{q}}_L^{(1)} \\ \tilde{\mathbf{q}}_R^{(N)} \end{bmatrix}. \tag{3.82}$$

Substituting this into Equation (3.78b) and using Equation (3.80b), the following condensed dynamic equilibrium system of equations is derived for the full periodic structure

$$\begin{bmatrix} \tilde{\mathbf{F}}_L^{(1)} \\ \tilde{\mathbf{F}}_R^{(N)} \end{bmatrix} = \tilde{\mathbf{P}}^H \begin{bmatrix} -\tilde{\mathbf{\Phi}}_F & -\tilde{\mathbf{\Phi}}_F^\star \tilde{\boldsymbol{\mu}} \\ \tilde{\mathbf{\Phi}}_F \tilde{\boldsymbol{\mu}} & \tilde{\mathbf{\Phi}}_F^\star \end{bmatrix} \left( \tilde{\mathbf{P}}^H \begin{bmatrix} \tilde{\mathbf{\Phi}}_q & \tilde{\mathbf{\Phi}}_q^\star \tilde{\boldsymbol{\mu}} \\ \tilde{\mathbf{\Phi}}_q \tilde{\boldsymbol{\mu}} & \tilde{\mathbf{\Phi}}_q^\star \end{bmatrix} \right)^{-1} \tilde{\mathbf{P}}^H \tilde{\mathbf{P}} \begin{bmatrix} \tilde{\mathbf{q}}_L^{(1)} \\ \tilde{\mathbf{q}}_R^{(N)} \end{bmatrix}. \tag{3.83}$$

Using a simplified notation, this system of equations can be re-written as

$$\begin{bmatrix} \tilde{\mathbf{F}}_L^{(1)} \\ \tilde{\mathbf{F}}_R^{(N)} \end{bmatrix} = \tilde{\mathbf{D}} \begin{bmatrix} \tilde{\mathbf{q}}_L^{(1)} \\ \tilde{\mathbf{q}}_R^{(N)} \end{bmatrix}, \tag{3.84}$$

where

$$\tilde{\mathbf{D}} = \tilde{\mathbf{P}}^H \begin{bmatrix} -\tilde{\mathbf{\Phi}}_\mathrm{F} & -\tilde{\mathbf{\Phi}}_\mathrm{F}^\star \tilde{\boldsymbol{\mu}} \\ \tilde{\mathbf{\Phi}}_\mathrm{F} \tilde{\boldsymbol{\mu}} & \tilde{\mathbf{\Phi}}_\mathrm{F}^\star \end{bmatrix} \left( \tilde{\mathbf{P}}^H \begin{bmatrix} \tilde{\mathbf{\Phi}}_\mathrm{q} & \tilde{\mathbf{\Phi}}_\mathrm{q}^\star \tilde{\boldsymbol{\mu}} \\ \tilde{\mathbf{\Phi}}_\mathrm{q} \tilde{\boldsymbol{\mu}} & \tilde{\mathbf{\Phi}}_\mathrm{q}^\star \end{bmatrix} \right)^{-1} \tilde{\mathbf{P}}^H \tilde{\mathbf{P}}, \tag{3.85}$$

*i.e.*, the condensed numerical spectral matrix of size $(2n_k \times 2n_k)$.

### 3.4.1  Case of a Timoshenko beam

In this subsection, the numerical spectral matrix of a Timoshenko beam is derived. The Timoshenko beam theory considers the effects of rotational inertia and shear deformation in beam bending, which are not taken into account by the classical beam theory (*i.e.*, the Euler-Bernoulli beam theory). For this reason, the limit of validity of the Timoshenko beam theory is extended in comparison to that of the Euler-Bernoulli beam theory, which means that it is suitable to model thicker beams and predict the behavior of a beam at higher frequencies.

The kinematics of a Timoshenko beam which experiences bending about the $z$-axis is described by two independent variables: $v(x)$ and $\varphi_z(x)$, respectively, the transverse displacement and the rotation about the $z$-axis. They are considered constant across the cross-section, varying only along the beam length. The rotation is expressed as

$$\varphi_z(x) = - \left. \frac{\partial u}{\partial y} \right|_{y=0}, \tag{3.86}$$

where $u$ is the axial displacement along the $x$-direction. Besides, the displacements of a Timoshenko beam can be written as

$$u(x,y) = -y\varphi_z(x), \quad v(x,y) = v(x). \tag{3.87}$$

Using Hamilton's Principle, it is possible to derive the equations of motion for a Timoshenko beam (Doyle, 1997), which in the frequency domain are given by

$$\kappa G A \frac{\partial}{\partial x} \left[ \frac{\partial v}{\partial x} - \varphi_z \right] = -\omega^2 \rho A v - q_y, \tag{3.88a}$$

$$E I_z \frac{\partial^2 \varphi_z}{\partial x^2} + \kappa G A \left[ \frac{\partial v}{\partial x} - \varphi_z \right] = -\omega^2 \rho I_z \varphi_z. \tag{3.88b}$$

where $\rho$ is the material density, $E$ is the Young's modulus, $G$ is the shear modulus, $\kappa$ is the shear correction factor ($\kappa = 0.89$ was adopted in this work for rectangular cross-sections), $A$ is the cross-section area, $I_z$ is the second moment of area with respect to (w.r.t.) the $z$-axis, $q_y$ is the distributed transverse load, and $\omega$ is the angular frequency. To these equations, the following natural boundary conditions are associated

$$f_y = V = \kappa G A \left( \frac{\partial v}{\partial x} - \varphi_z \right), \quad m_z = M = E I_z \frac{\partial \varphi_z}{\partial x}, \tag{3.89}$$

where $f_y$ is the transverse force and $m_z$ is the bending moment about the $z$-axis. In order to apply the WSFEM to the case of a Timoshenko beam, a substructure of arbitrary length $\Delta$ is modeled with finite elements — either beam or solid finite elements can be used. Then, the WFE method is used to obtain the wave mode basis associated to the substructure modeled. This allows one to select propagation constants and wave mode shapes associated to bending and shear wave modes with respect to the $z$-axis — thus, $n_k = 2$ in this case —, which are used to express the nodal displacement vector, as follows

$$\begin{bmatrix} \mathbf{u}(x,y,z) \\ \mathbf{v}(x,y,z) \end{bmatrix} = \begin{bmatrix} \phi_{\mathsf{q_x}}^b(y,z) & \phi_{\mathsf{q_x}}^s(y,z) \\ \phi_{\mathsf{q_y}}^b(y,z) & \phi_{\mathsf{q_y}}^s(y,z) \\ \phi_{\mathsf{q_x}}^{\star b}(y,z) & \phi_{\mathsf{q_x}}^{\star s}(y,z) \\ \phi_{\mathsf{q_y}}^{\star b}(y,z) & \phi_{\mathsf{q_y}}^{\star s}(y,z) \end{bmatrix} \begin{bmatrix} e^{-\mathrm{i}\beta_b x} & 0 \\ 0 & e^{-\mathrm{i}\beta_s x} \end{bmatrix} \tilde{\mathbf{Q}} + \\ \begin{bmatrix} e^{-\mathrm{i}\beta_b(N\Delta - x)} & 0 \\ 0 & e^{-\mathrm{i}\beta_s(N\Delta - x)} \end{bmatrix} \tilde{\mathbf{Q}}^{\star} ,$$
$$x \in [0, \Delta, 2\Delta, \ldots, N\Delta],$$
$$y \in [0, h, 2h, \ldots, N_y h],$$
$$z \in [0, w, 2w, \ldots, N_z w], \tag{3.90}$$

where the super/subscripts $b$ and $s$ are used to denote bending and shear wave modes, respectively. Using Equations (3.86) and (3.90), the rotation can also be expressed by means of the selected numerical wave modes, as follows

$$\boldsymbol{\varphi_z}(x,y,z) = \begin{bmatrix} \phi_{\varphi_z}^b & \phi_{\varphi_z}^s \end{bmatrix} \begin{bmatrix} e^{-\mathrm{i}\beta_b x} & 0 \\ 0 & e^{-\mathrm{i}\beta_s x} \end{bmatrix} \tilde{\mathbf{Q}} + \\ \begin{bmatrix} \phi_{\varphi_z}^{\star b} & \phi_{\varphi_z}^{\star s} \end{bmatrix} \begin{bmatrix} e^{-\mathrm{i}\beta_b(N\Delta - x)} & 0 \\ 0 & e^{-\mathrm{i}\beta_s(N\Delta - x)} \end{bmatrix} \tilde{\mathbf{Q}}^{\star} ,$$
$$x \in [0, \Delta, 2\Delta, \ldots, N\Delta],$$
$$y \in [0, h, 2h, \ldots, N_y h],$$
$$z \in [0, w, 2w, \ldots, N_z w], \tag{3.91}$$

81

where $\phi_{\varphi_{\rm z}}^b = -\frac{\partial \phi_{\rm q_x}^b}{\partial y}$, $\phi_{\varphi_{\rm z}}^s = -\frac{\partial \phi_{\rm q_x}^s}{\partial y}$, $\phi_{\varphi_{\rm z}}^{\star b} = -\frac{\partial \phi_{\rm q_x}^{\star b}}{\partial y}$ and $\phi_{\varphi_{\rm z}}^{\star s} = -\frac{\partial \phi_{\rm q_x}^{\star s}}{\partial y}$. The expression above requires the differentiation of the wave mode shapes with respect to $y$, which is accomplished by making use of a finite difference scheme.

Alternatively, assuming solutions of the form $v(x) = \hat{v}(\beta)e^{-\mathrm{i}\beta x}$ and $\varphi_z(x) = \hat{\varphi}_z(\beta)e^{-\mathrm{i}\beta x}$ for a Timoshenko beam problem and, if transverse distributed loads are not applied, Equation (3.88a) may be expressed as

$$\kappa GA \left(-\mathrm{i}\beta\right)^2 \hat{v}e^{-\mathrm{i}\beta x} - \left(-\mathrm{i}\beta\right) \hat{\varphi}_z e^{-\mathrm{i}\beta x} = -\omega^2 \rho A \hat{v}e^{-\mathrm{i}\beta x}, \tag{3.92}$$

which yields

$$\hat{\varphi}_z = \left[\kappa GA \left(-\mathrm{i}\beta\right) + \frac{\omega^2 \rho A}{-\mathrm{i}\beta}\right] \hat{v}, \tag{3.93}$$

or, in terms of wave modes,

$$\begin{aligned}
\phi_{\varphi_{\rm z}}^b &= \phi_{\rm q_y}^b \left(\kappa GA \left(-\mathrm{i}\beta_b\right) + \frac{\omega^2 \rho A}{-\mathrm{i}\beta_b}\right), \\
\phi_{\varphi_{\rm z}}^s &= \phi_{\rm q_y}^s \left(\kappa GA \left(-\mathrm{i}\beta_s\right) + \frac{\omega^2 \rho A}{-\mathrm{i}\beta_s}\right), \\
\phi_{\varphi_{\rm z}}^{\star b} &= \phi_{\rm q_y}^{\star b} \left(\kappa GA \left(\mathrm{i}\beta_b\right) + \frac{\omega^2 \rho A}{\mathrm{i}\beta_b}\right), \\
\phi_{\varphi_{\rm z}}^{\star s} &= \phi_{\rm q_y}^{\star s} \left(\kappa GA \left(\mathrm{i}\beta_s\right) + \frac{\omega^2 \rho A}{\mathrm{i}\beta_s}\right).
\end{aligned} \tag{3.94}$$

The advantage here is that discrete differentiation is not required.

Using the transverse displacement and the rotation about the $z$-axis to write the displacement field for a Timoshenko beam, yields

$$\begin{aligned}
\begin{bmatrix} \mathbf{v}(x,y,z) \\ \boldsymbol{\varphi}(x,y,z) \end{bmatrix} &= \begin{bmatrix} \phi_{\rm q_y}^b & \phi_{\rm q_y}^s \\ \phi_{\varphi_{\rm z}}^b & \phi_{\varphi_{\rm z}}^s \\ \phi_{\rm q_y}^{\star b} & \phi_{\rm q_y}^{\star s} \\ \phi_{\varphi_{\rm z}}^{\star b} & \phi_{\varphi_{\rm z}}^{\star s} \end{bmatrix} \begin{bmatrix} e^{-\mathrm{i}\beta_b x} & 0 \\ 0 & e^{-\mathrm{i}\beta_s x} \\ e^{-\mathrm{i}\beta_b(N\Delta-x)} & 0 \\ 0 & e^{-\mathrm{i}\beta_s(N\Delta-x)} \end{bmatrix} \begin{matrix} \tilde{\mathbf{Q}} + \\ \\ \tilde{\mathbf{Q}}^\star \end{matrix}, \\
&\quad x \in [0, \Delta, 2\Delta, \ldots, N\Delta], \\
&\quad y \in [0, h, 2h, \ldots, N_y h], \\
&\quad z \in [0, w, 2w, \ldots, N_z w].
\end{aligned} \tag{3.95}$$

The vectors of displacements/rotations evaluated at the left and at the right ends of the beam may

be expressed as

$$
\begin{bmatrix} \mathbf{q}_L^{(1)} \\ \mathbf{q}_R^{(N)} \end{bmatrix} = \begin{bmatrix} \mathbf{v}_L^{(1)} \\ \boldsymbol{\varphi}_L^{(1)} \\ \mathbf{v}_R^{(N)} \\ \boldsymbol{\varphi}_R^{(N)} \end{bmatrix} = \begin{bmatrix} \tilde{\boldsymbol{\Phi}}_{\mathrm{qT}} & \tilde{\boldsymbol{\Phi}}_{\mathrm{qT}}^{\star} \tilde{\boldsymbol{\mu}}_{\mathrm{T}} \\ \tilde{\boldsymbol{\Phi}}_{\mathrm{qT}} \tilde{\boldsymbol{\mu}}_{\mathrm{T}} & \tilde{\boldsymbol{\Phi}}_{\mathrm{qT}}^{\star} \end{bmatrix} \begin{bmatrix} \tilde{\mathbf{Q}} \\ \tilde{\mathbf{Q}}^{\star} \end{bmatrix}, \tag{3.96}
$$

where

$$
\tilde{\boldsymbol{\Phi}}_{\mathrm{qT}} = \begin{bmatrix} \phi_{\mathrm{q_y}}^{b} & \phi_{\mathrm{q_y}}^{s} \\ \phi_{\varphi_z}^{b} & \phi_{\varphi_z}^{s} \end{bmatrix}, \quad \tilde{\boldsymbol{\Phi}}_{\mathrm{qT}}^{\star} = \begin{bmatrix} \phi_{\mathrm{q_y}}^{\star b} & \phi_{\mathrm{q_y}}^{\star s} \\ \phi_{\varphi_z}^{\star b} & \phi_{\varphi_z}^{\star s} \end{bmatrix}
$$

and

$$
\tilde{\boldsymbol{\mu}}_{\mathrm{T}} = \begin{bmatrix} e^{-\mathrm{i}\beta_b N\Delta} & 0 \\ 0 & e^{-\mathrm{i}\beta_s N\Delta} \end{bmatrix}.
$$

As discussed before, in the case of a Timoshenko beam, the transverse displacement and the rotation are considered constant across the cross-section, thus the sub-matrix $\bar{\mathbf{P}}_{\mathrm{T}}$ of $\tilde{\mathbf{P}}_{\mathrm{T}}$ (Equation (3.79)) is expressed as

$$
\bar{\mathbf{P}}_{\mathrm{T}} = \begin{bmatrix} & \begin{bmatrix} 1 & 0 \\ \vdots & \vdots \\ 1 & 0 \end{bmatrix}_{(N_{DOF}/2 \times 2)} \\ & \begin{bmatrix} 0 & 1 \\ \vdots & \vdots \\ 0 & 1 \end{bmatrix}_{(N_{DOF}/2 \times 2)} \end{bmatrix}, \tag{3.97}
$$

where $N_{DOF}$ is the number of DOFs corresponding to transverse displacements and rotations about the $z$-axis across a cross-section of the FE model.

The expressions for the transverse force and bending moment applied to the beam can also be written as function of wave modes. Substituting Equation (3.95) in Equation (3.89), the vectors of nodal loads applied to the Timoshenko beam at the left and at the right cross-sections are expressed as

$$
\begin{bmatrix} \mathbf{F}_L^{(1)} \\ \mathbf{F}_R^{(N)} \end{bmatrix} = \begin{bmatrix} \mathbf{V}_{yL}^{(1)} \\ \mathbf{M}_{zL}^{(1)} \\ \mathbf{V}_{yR}^{(N)} \\ \mathbf{M}_{zR}^{(N)} \end{bmatrix} = \begin{bmatrix} -\tilde{\boldsymbol{\Phi}}_{\mathrm{FT}} & -\tilde{\boldsymbol{\Phi}}_{\mathrm{FT}}^{\star} \tilde{\boldsymbol{\mu}}_{\mathrm{T}} \\ \tilde{\boldsymbol{\Phi}}_{\mathrm{FT}} \tilde{\boldsymbol{\mu}}_{\mathrm{T}} & \tilde{\boldsymbol{\Phi}}_{\mathrm{FT}}^{\star} \end{bmatrix} \begin{bmatrix} \tilde{\mathbf{Q}} \\ \tilde{\mathbf{Q}}^{\star} \end{bmatrix}, \tag{3.98}
$$

where

$$
\tilde{\boldsymbol{\Phi}}_{\mathrm{FT}} = \begin{bmatrix} \kappa G\bar{A} \left[ -\mathrm{i}\beta_b \phi_{\mathrm{q_y}}^{b} - \phi_{\varphi_z}^{b} \right] & \kappa G\bar{A} \left[ -\mathrm{i}\beta_s \phi_{\mathrm{q_y}}^{s} - \phi_{\varphi_z}^{s} \right] \\ -\mathrm{i}\beta_b E\bar{I}_z \phi_{\varphi_z}^{b} & -\mathrm{i}\beta_s E\bar{I}_z \phi_{\varphi_z}^{s} \end{bmatrix},
$$

$$\tilde{\mathbf{\Phi}}_{\text{FT}}^{\star} = \begin{bmatrix} \kappa G \bar{A} \left[ \mathrm{i}\beta_b \phi_{\mathsf{q}_y}^{\star b} - \phi_{\varphi_z}^{\star b} \right] & \kappa G \bar{A} \left[ \mathrm{i}\beta_s \phi_{\mathsf{q}_y}^{\star s} - \phi_{\varphi_z}^{\star s} \right] \\ \mathrm{i}\beta_b E \bar{I}_z \phi_{\varphi_z}^{\star b} & \mathrm{i}\beta_s E \bar{I}_z \phi_{\varphi_z}^{\star s} \end{bmatrix},$$

$\bar{A} = 2A/N_{DOF}$ and $\bar{I}_z = 2I_z/N_{DOF}$ are, respectively, the cross-section area and the second moment of area corresponding to a node assuming a uniform average over the number of nodes. The condensed vectors of nodal loads at the left and at the right ends of the beam can be expressed in terms of the original DOFs by means of Equation (3.80b). Besides, using the procedure described in Equations (3.80)-(3.85), the condensed numerical spectral matrix for a Timoshenko beam is obtained.

An alternative procedure for deriving the condensed numerical spectral matrix of a Timoshenko beam consists in writing the vector of condensed displacements/rotations in terms of the original vector of displacements/rotations as

$$\begin{bmatrix} \tilde{\mathbf{q}}_{\text{L}}^{(1)} \\ \tilde{\mathbf{q}}_{\text{R}}^{(N)} \end{bmatrix} = \left( \tilde{\mathbf{P}}_{\text{T}}^{H} \tilde{\mathbf{P}}_{\text{T}} \right)^{-1} \tilde{\mathbf{P}}_{\text{T}}^{H} \begin{bmatrix} \mathbf{q}_{\text{L}}^{(1)} \\ \mathbf{q}_{\text{R}}^{(N)} \end{bmatrix}, \tag{3.99}$$

which yields

$$\begin{bmatrix} \tilde{\mathbf{q}}_{\text{L}}^{(1)} \\ \tilde{\mathbf{q}}_{\text{R}}^{(N)} \end{bmatrix} = \begin{bmatrix} v_{\text{L}}^{(1)} \\ \varphi_{\text{L}}^{(1)} \\ v_{\text{R}}^{(N)} \\ \varphi_{\text{R}}^{(N)} \end{bmatrix} = \begin{bmatrix} \tilde{\mathbf{\Phi}}_{\mathsf{qT}} & \tilde{\mathbf{\Phi}}_{\mathsf{qT}}^{\star} \tilde{\boldsymbol{\mu}}_{\text{T}} \\ \tilde{\mathbf{\Phi}}_{\mathsf{qT}} \tilde{\boldsymbol{\mu}}_{\text{T}} & \tilde{\mathbf{\Phi}}_{\mathsf{qT}}^{\star} \end{bmatrix} \begin{bmatrix} \tilde{\mathbf{Q}} \\ \tilde{\mathbf{Q}}^{\star} \end{bmatrix}, \tag{3.100}$$

where

$$\tilde{\mathbf{\Phi}}_{\mathsf{qT}} = \frac{2}{N_{DOF}} \begin{bmatrix} \sum_i \phi_{\mathsf{q}_y i}^{b} & \sum_i \phi_{\mathsf{q}_y i}^{s} \\ \sum_i \phi_{\varphi_z i}^{b} & \sum_i \phi_{\varphi_z i}^{s} \end{bmatrix}$$

and

$$\tilde{\mathbf{\Phi}}_{\mathsf{qT}}^{\star} = \frac{2}{N_{DOF}} \begin{bmatrix} \sum_i \phi_{\mathsf{q}_y i}^{\star b} & \sum_i \phi_{\mathsf{q}_y i}^{\star s} \\ \sum_i \phi_{\varphi_z i}^{\star b} & \sum_i \phi_{\varphi_z i}^{\star s} \end{bmatrix}.$$

Then, using Equation (3.89) with Equation (3.100) to write the condensed vector of applied loads evaluated at the ends of the beam, yields

$$\begin{bmatrix} \tilde{\mathbf{F}}_{\text{L}}^{(1)} \\ \tilde{\mathbf{F}}_{\text{R}}^{(N)} \end{bmatrix} = \begin{bmatrix} V_{y\text{L}}^{(1)} \\ M_{z\text{L}}^{(1)} \\ V_{y\text{R}}^{(N)} \\ M_{z\text{R}}^{(N)} \end{bmatrix} = \begin{bmatrix} -\tilde{\mathbf{\Phi}}_{\text{FT}} & -\tilde{\mathbf{\Phi}}_{\text{FT}}^{\star} \tilde{\boldsymbol{\mu}}_{\text{T}} \\ \tilde{\mathbf{\Phi}}_{\text{FT}} \tilde{\boldsymbol{\mu}}_{\text{T}} & \tilde{\mathbf{\Phi}}_{\text{FT}}^{\star} \end{bmatrix} \begin{bmatrix} \tilde{\mathbf{Q}} \\ \tilde{\mathbf{Q}}^{\star} \end{bmatrix}, \tag{3.101}$$

where

$$\tilde{\Phi}_{\text{FT}} = \frac{2}{N_{DOF}} \begin{bmatrix} \kappa GA \left[ -\mathtt{i}\beta_b \sum_i \phi^b_{\mathtt{q}_\mathtt{y}i} - \sum_i \phi^b_{\varphi_z i} \right] & \kappa GA \left[ -\mathtt{i}\beta_s \sum_i \phi^s_{\mathtt{q}_\mathtt{y}i} - \sum_i \phi^s_{\varphi_z i} \right] \\ -\mathtt{i}\beta_b EI_z \sum_i \phi^b_{\varphi_z i} & -\mathtt{i}\beta_s EI_z \sum_i \phi^s_{\varphi_z i} \end{bmatrix},$$

$$\tilde{\Phi}^\star_{\text{FT}} = \frac{2}{N_{DOF}} \begin{bmatrix} \kappa GA \left[ \mathtt{i}\beta_b \sum_i \phi^{\star b}_{\mathtt{q}_\mathtt{y}i} - \sum_i \phi^{\star b}_{\varphi_z i} \right] & \kappa GA \left[ \mathtt{i}\beta_s \sum_i \phi^{\star s}_{\mathtt{q}_\mathtt{y}i} - \sum_i \phi^{\star s}_{\varphi_z i} \right] \\ \mathtt{i}\beta_b EI_z \sum_i \phi^{\star b}_{\varphi_z i} & \mathtt{i}\beta_s EI_z \sum_i \phi^{\star s}_{\varphi_z i} \end{bmatrix}.$$

## 3.5  Numerical Results

In this section, the WFE-based superelement formulations presented in this chapter are used to compute the harmonic response of periodic structures. The following test cases are considered: (1) a 3D beam-like structure (Figure 3.5(a)) and (2) a 3D aircraft fuselage-like structure (Figure 3.5(b)).



(a)                                                                                              (b)
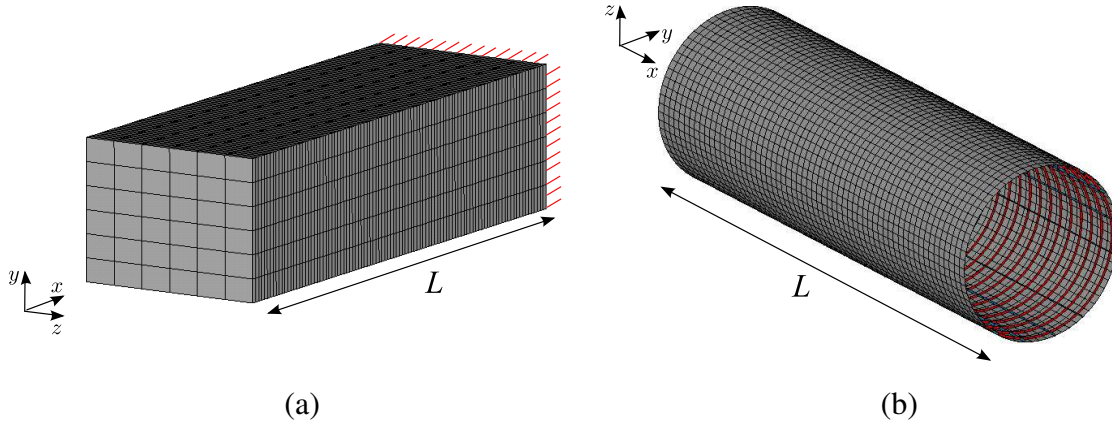
Figure 3.5: Test cases considered in this chapter: (a) 3D beam-like structure, and (b) 3D aircraft fuselage-like structure.

For each test case, the frequency response functions (FRFs) provided by the WFE-based superelement formulations are compared with a reference FE solution. Regarding the WFE modelings, ANSYS® is used as a means to assess the mass and stiffness matrices of substructures. Post-treatment of those matrices are achieved using MATLAB®. This software is used to compute the WFE wave modes and the forced responses of the structures into consideration. Moreover, the performances of the WFE-based formulations in terms of computational time savings are assessed

by means of the MATLAB®'s built-in *tic*/*toc* functions. The reference FE solutions are provided by ANSYS®, which builds the global dynamic stiffness matrices for the complete periodic structure and solves the harmonic problems using the direct method. All the numerical simulations are performed in double precision using a 64-bit CPU equipped with an Intel® Xeon® E5345 2.33 GHz processor and 32 GB of RAM memory.

### 3.5.1 Forced response analysis of a beam-like structure via WFE-based DSM and RM

In this section, the harmonic forced response of a straight clamped-free 3D beam-like structure is addressed (see Figure 3.5(a)). The free end is subjected to either axial or transverse loads, as shown in Figure 3.6. Here, the homogeneous beam-like structure has the following characteristics: length $L = 0.011$ m, density $\rho = 7800$ Kg/m$^3$, Young's modulus $E = 210$ GPa, loss factor $\eta = 0.01$, Poisson's ratio $\nu = 0.3$ and a rectangular cross-section of size $h_z = 0.004 \, \text{m} \times h_y = 0.003 \, \text{m}$. The full structure is composed of $100$ identical substructures along the $x$-axis. Besides, solid linear hexahedral finite elements, with eight nodes and three DOFs per node — *i.e.*, translations along the $x$, $y$ and $z$ axes —, the SOLID45 elements from ANSYS®, are used to model the substructures. Each substructure (Figure 2.7(b)) is of length $\Delta = 0.111$ mm and meshed by means of $6 \times 6$ brick finite elements, which yields $n = 147$ DOFs over its left/right boundary and no internal DOFs. As a result, the corresponding FE model (Figure 3.5(a)) of the global periodic structure contains $14{,}847$ DOFs.



(a)          (b)          (c)

Figure 3.6: Schematics of the clamped-free 3D beam-like structure subjected to: (a) uniformly distributed transverse forces over the left surf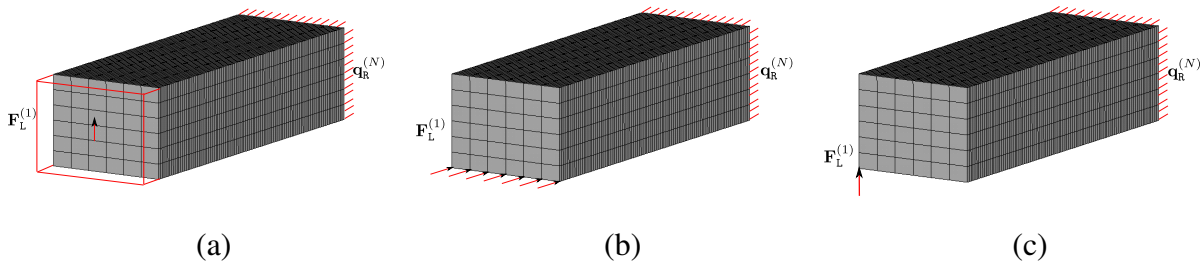ace boundary, (b) axial forces over a line on the left boundary, (c) a punctual transverse force applied at an edge node on the left boundary.

The forced responses of the global structure under either axial or transverse loads are ana-

lyzed over a frequency band $\beta_f = [200\text{ Hz}\text{---}2\text{ MHz}]$, which involves discrete frequencies equally spaced steps of 2000 Hz.

Within the WFE framework, 147 right-going and 147 left-going wave modes are obtained through the WFE eigenvalue problem stated in Equation (2.49). Thus, regarding the WFE-based superelement approaches which makes use of the full wave basis, the dimension of the problem is $2n$, $i.e.$, 294, which corresponds to the number of boundary DOFs of the periodic structure. Besides, one may use the CB method to model the periodic structure. In this case, if all fixed-interface modes whose eigenfrequencies are below $2 \times \omega_{max}$ are considered — $i.e.$, the rule of thumb —, 1,882 fixed-interface modes are kept, which means that the dimension of the model is 2,176, which corresponds to the sum of static and fixed-interface modes. On the other hand, the dimension of the reference FE model is 14,847. The WFE-based solutions are compared with the results issued from the conventional FE method in terms of accuracy. The relative error of the WFE-based solutions, averaged over several sub-frequency bands of same width $\{\beta_f^i\}_i$, is expressed as

$$\epsilon_{\beta_f^i} = \frac{< \|\mathbf{q}_{\text{RMS}}\|_2 - \|\mathbf{q}_{\text{RMS}}^{\texttt{ref}}\|_2 >_{\beta_f^i}}{< \|\mathbf{q}_{\text{RMS}}^{\texttt{ref}}\|_2 >_{\beta_f^i}}, \tag{3.102}$$

where $\mathbf{q}_{\text{RMS}}$ denote the the root mean square (RMS) value of the total velocity at the left excited boundary, $\texttt{ref}$ is used to denote the reference solution, while the notation $< \ . \ >_{\beta_i}$ denotes the quadratic mean over a sub-frequency band $\beta_f^i$. Here, twenty sub-frequency bands $\{\beta_f^i\}_i$ are considered which cover the whole frequency band $\beta_f$ ($i.e.$, $\beta_f = \cup_i \beta_f^i$). The performance of WFE-based approaches in terms of elapsed time is compared to that of CB method.

In the case the beam is subjected to uniformly distributed transverse forces (Figure 3.6(a)), the WFE solutions which make use of the full wave mode basis — $i.e.$, DSM and RM approaches (Sections 3.2.2 and 3.2.3, respectively) — are compared to solutions issued from the DSM approach proposed by Duhamel $et\ al.$ (2006) and the conventional FE method in Figure 3.7(a). The responses issued by the CB method, which makes use of 1,882 fixed-interface modes and 294 static modes — which correspond to the number of DOFs over the left and right ends of the structure —, and Guyan reduction (or static reduction), which reduces the size of the model to 9,898 DOFs — $i.e.$, it considers only the static modes related to axial ($x$) and the transverse ($y$) displacement DOFs of the whole periodic structure — are compared to the conventional FE solution in Figure 3.7(b).

The relative errors of the WFE-based, CB and Guyan solutions are displayed in Figure 3.7(c).

Figure 3.7: (a,b) RMS total velocity at the left boundary of the beam-like structure subjected to uniformly distributed transverse forces, (c) relative error, Equation (3.102), (d) zoom over forced-response solutions within $[1.5 — 1.9]$ MHz: (——) FE solution; ( x ) CB method which makes use of $1,882$ fixed-interface modes; ( + ) Guyan reduction which makes use of $9,898$ static modes; (- - -) WFE-based DSM approach; ( ○ ) WFE-based RM approach; ( ● ) WFE-based Duhamel's DSM approach.

As it can be seen, all WFE-based approaches are completely in agreement and show extremely low error with respect to the conventional FE solution — *i.e.*, of order $10^{-4}\%$—, which validates the proposed DSM and RM approaches and confirms that WFE-based solutions which make use of the full wave mode basis can be considered as accurate as the conventional FE solution for equivalent mesh density. The CB solution provides a good approximation to the reference solution, but it produce considerably higher errors than WFE-based approaches. The worst solution is the one provided by Guyan reduction, which is one of the most popular reduction techniques. This

approach fails in simulating the structure dynamics even if a large number of DOFs are retained —
$9,898$ over $14,847$ DOFs, *i.e.*, $67\%$, are considered — because it neglects the inertia effect of the
degrees of freedom that are neglected. The accuracy of the different approaches is highlighted by
making a zoom over a narrow band, as in Figure 3.7(d).
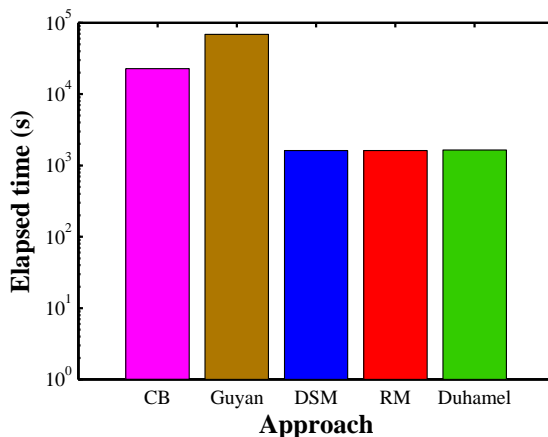


Figure 3.8: Elapsed times for the forced response computation of the beam-like structure subjected
to uniformly distributed transverse forces, by means of: (magenta color) CB method which makes
use of $1,882$ fixed-interface modes; (brown color) Guyan reduction which makes use of $9,898$ static
modes; (blue color) WFE-based DSM formulation; (red color) WFE-based RM formulation; and
(green color) WFE-based Duhamel's DSM formulation.

In terms of elapsed time, WFE-based superelement approaches (DSM, RM and Duhamel's
DSM) perform better than CB method and Guyan reduction, as shown in Figure 3.8. Table 3.1
summarizes the total number of DOFs and elapsed times involved in the various solutions.

Table 3.1: Total number of DOFs, maximum errors, and elapsed times involved by the proposed
approaches regarding the beam-like structure subjected to a uniformly distributed transverse load.

| Approach | Total number of DOFs | Maximum error | Elapsed time | Reduction |
|---|---|---|---|---|
| FE | 14,847 | ref | — | — |
| Guyan reduction | 9,898 | $5.1\ 10^4$ % | 68,814 s | ref |
| CB | 2,176 | 8.7 % | 22,772 s | 67 % |
| DSM | 294 | 0.0005 % | 1,619 s | 98 % |
| RM | 294 | 0.0005 % | 1,622 s | 98 % |
| Duhamel's DSM | 294 | 0.0005 % | 1,639 s | 98 % |

The WFE-based DSM and RM approaches have also been used to compute the forced re-
sponse in the case the beam is subjected to axial forces over a line (Figure 3.6(b)). The results are

shown in Figure 3.9. As in the first load case, all WFE-based approaches are in agreement and provide very low level of error.
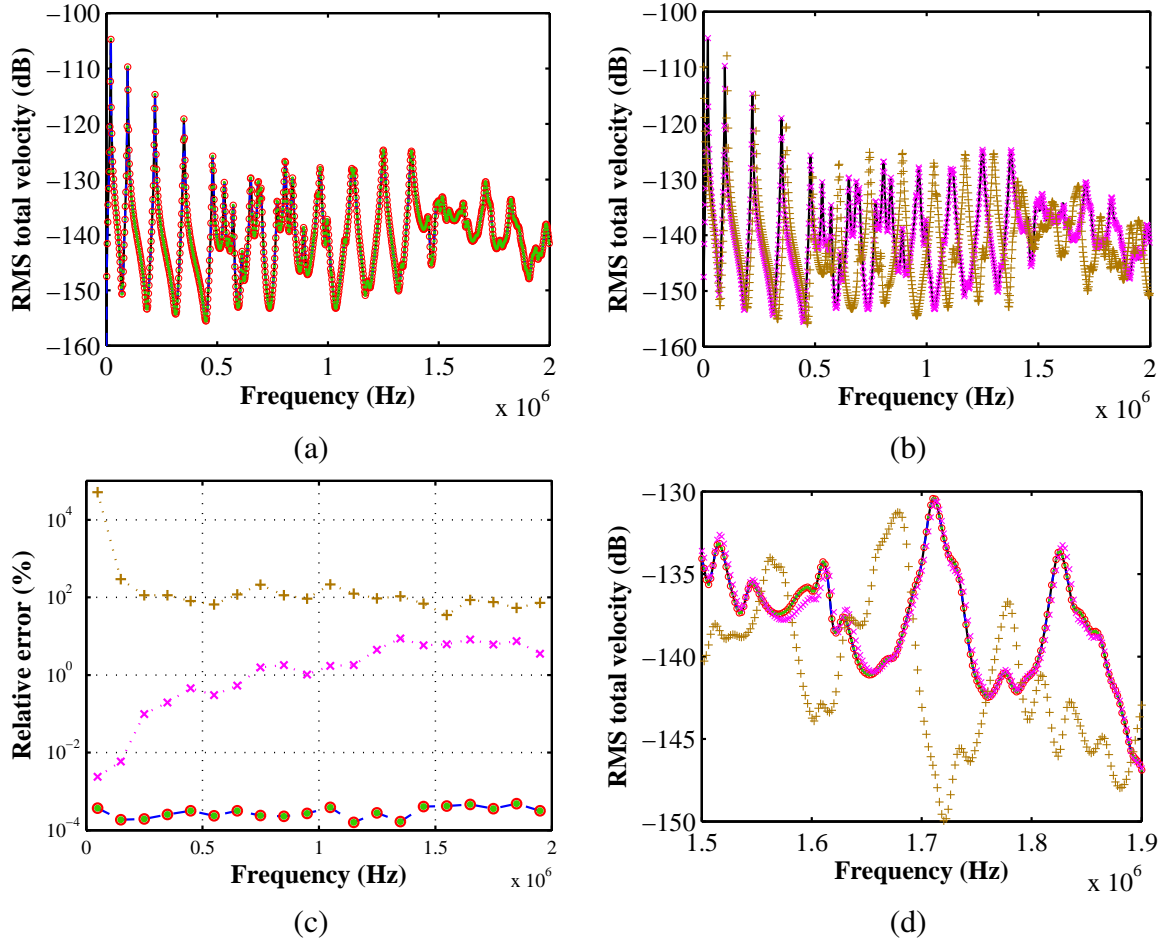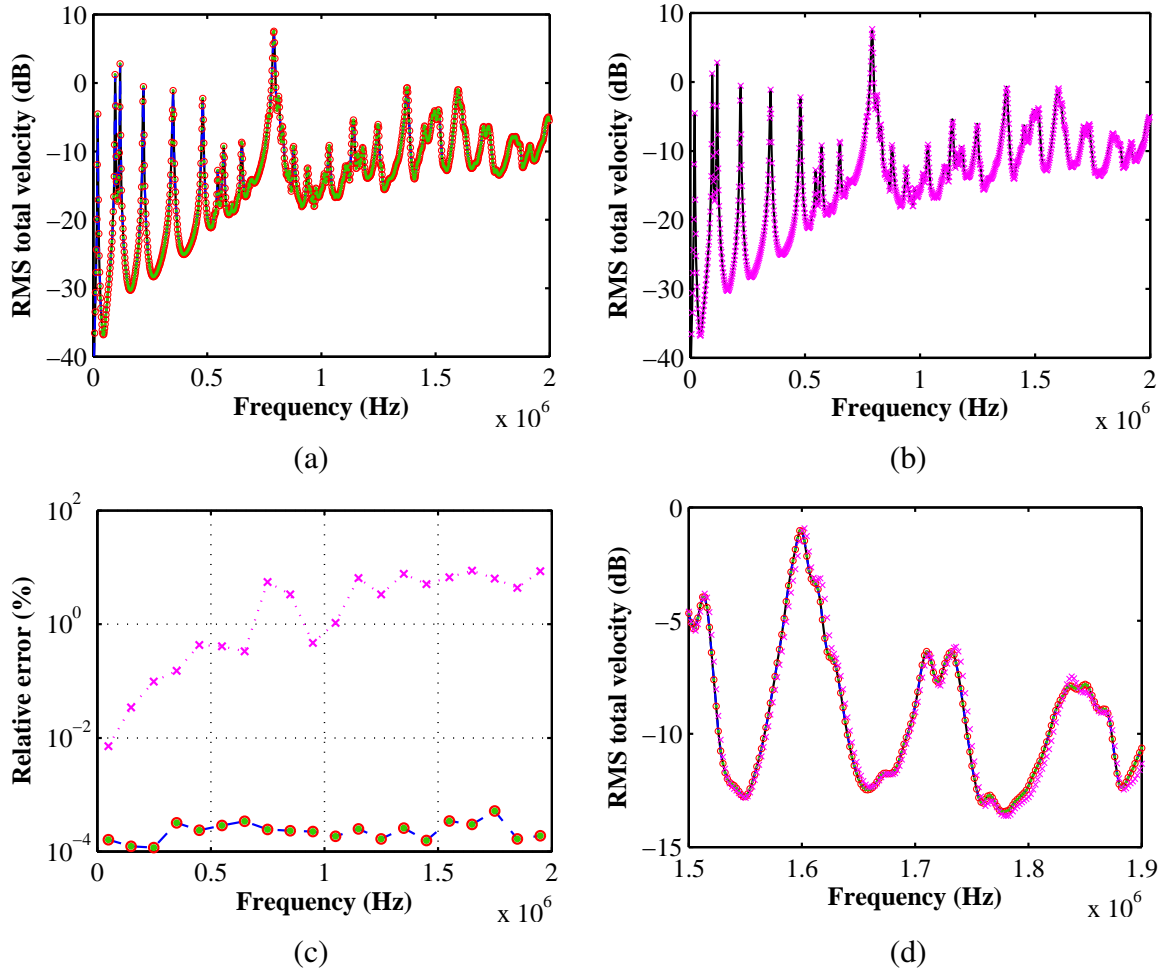


Figure 3.9: (a,b) RMS total velocity at the left boundary of the 3D beam-like structure subjected to uniformly distributed transverse forces, (c) relative error, Equation (3.102), (d) zoom of forced-response solutions over $[1.5 - 1.9]$ MHz: (——) FE solution; ( x ) CB method which makes use of $1,882$ fixed-interface modes; (- - -) WFE-based DSM approach; ( o ) WFE-based RM approach; ( • ) WFE-based Duhamel's DSM approach.

The last load condition considered is the beam subjected to a punctual vertical load (Figure 3.6(c)). Although the level of error relative to the conventional FE solution has increased compared to the WFE-based solutions for the previous load cases, the error is still negligible (the mean error value is inferior to $0.001\%$).
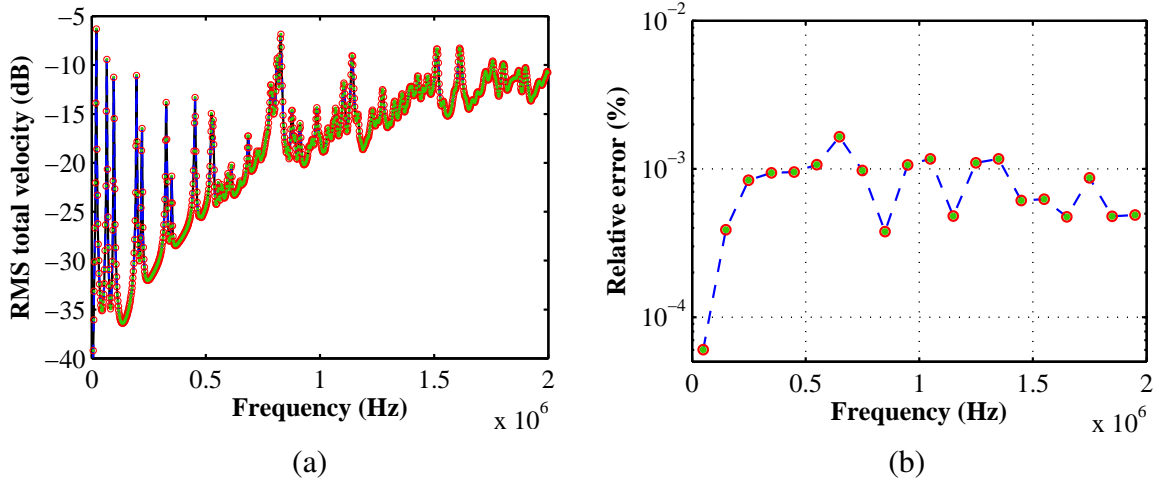
Figure 3.10: (a) RMS total velocity at the left boundary of the 3D beam-like structure subjected to axial forces over a line and (b) relative error, Equation (3.102): (——) FE solution; (- - -) WFE-based DSM approach; ( ○ ) WFE-based RM approach; ( ● ) WFE-based Duhamel's DSM approach.

The WFE-based approaches which makes use of the full wave basis are also investigated in terms of conditioning and elapsed time. The WFE-based DSM, RM and Duhamel's DSM approaches involve the inversion of the following sparse matrices

$$
\begin{bmatrix} \mathbf{I} & -\mathbb{C}_{\mathrm{c}}\boldsymbol{\mu}^N \\ -\mathbb{C}_{\mathrm{c}}\boldsymbol{\mu}^N & \mathbf{I} \end{bmatrix},
\tag{3.103}
$$

$$
\begin{bmatrix} \mathbf{I} & -\mathbb{C}_{\mathrm{f}}\boldsymbol{\mu}^N \\ -\mathbb{C}_{\mathrm{f}}\boldsymbol{\mu}^N & \mathbf{I} \end{bmatrix}
\tag{3.104}
$$

and

$$
\begin{bmatrix} \boldsymbol{\Phi}_{\mathrm{q}}^{\star-1}\boldsymbol{\mu}^N - \boldsymbol{\Phi}_{\mathrm{q}}^{\star} & \mathbf{I} \\ \mathbf{I} & \boldsymbol{\Phi}_{\mathrm{q}}^{-1}\boldsymbol{\mu}^N - \boldsymbol{\Phi}_{\mathrm{q}} \end{bmatrix},
\tag{3.105}
$$

respectively. For the beam-like structure, the condition numbers of these matrices within the frequency range $\beta_f$ are shown in Figure 3.11. Notice that all the three approaches are well-conditioned.

In Figure 3.12, the elapsed times required by each approach to compute the forced response of the beam-like structure subjected to either an axial line force or a punctual transverse force are compared.
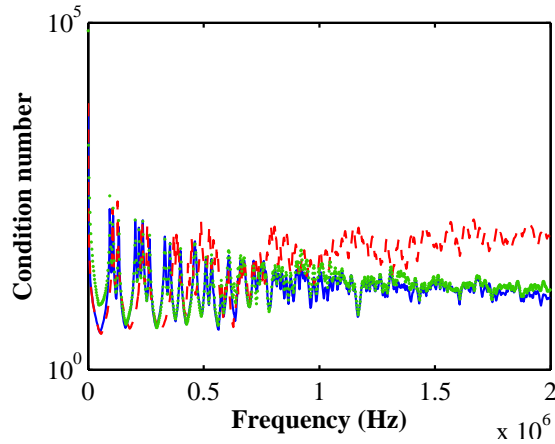
Figure 3.11: Condition number of the sparse matrix required to be inverted in WFE-based approaches: (——) WFE-based DSM formulation, (- - -) WFE-based RM formulation and ( • ) WFE-based Duhamel's DSM formulation.
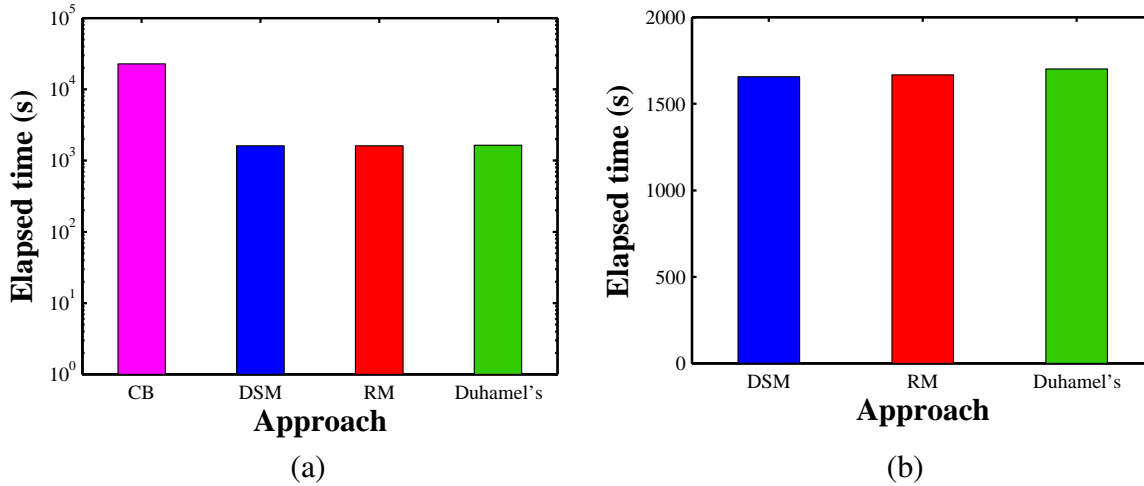


Figure 3.12: Elapsed times for the forced response computation of the beam-like structure subjected to: (a) axial forces over a line, (b) punctual transverse force , by means of WFE-based superelement formulations: (magenta color) CB method which makes use of $1,882$ fixed-interface modes, (blue color) WFE-based DSM formulation, (red color) WFE-based RM formulation and (green color) WFE-based Duhamel's DSM formulation.

In the following, reduced-order WFE-based superelement models of a clamped-free beam-like structure are investigated. In this section, the alternative scheme proposed in Appendix B is used to formulate the reduced WFE-based eigenproblem. To begin with, it is confirmed in Figure 3.13 that the number of propagating waves tends to increase as the frequency rises. In the case the

selection criterion 1 alone is used for the selection of WFE wave modes, it seems that the number of waves which effectively contribute to the structure forced response may not vary with frequency if a sufficient low threshold value ($\epsilon_Q$) is chosen. This is shown, for instance, for the case of uniformly distributed transverse forces (Figure 3.6(a)) in Figure 3.14 and it occurs because there is a minimum set of highly contributing wave modes to the structure forced response. This issue is highlighted in Figure 3.15(a), where the maximum value among the wave amplitude ratios $r_Q$ and $r_Q^\star$, evaluated at the maximum frequency, is plotted for each right-going wave mode (147 in total).
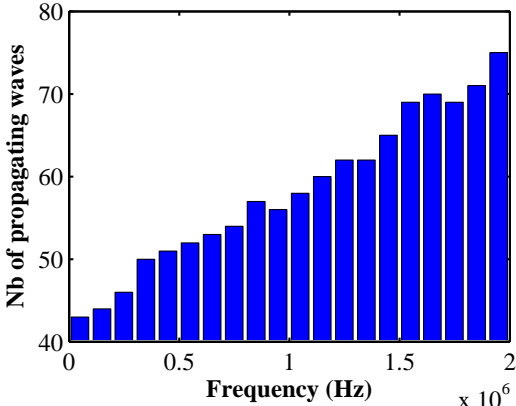


Figure 3.13: Average number of propagating wave modes for 20 sub-bands of frequencies within $\beta_f$.
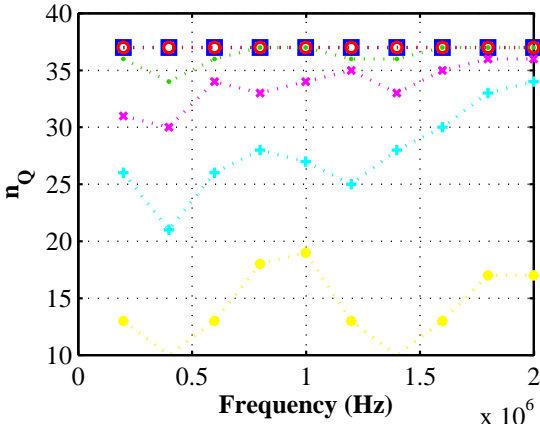


Figure 3.14: Number of kept wave modes ($n_Q$) using the selection criterion 1 (Section 3.3.1) for ten discrete frequencies within $\beta_f$ and six values for $\epsilon_Q$ for the 3D beam-like structure subjected to a uniformly distributed transverse load. Threshold values: ($\cdot\square\cdot$) $10^{-6}$, ($\cdot\circ\cdot$) $10^{-5}$, ($\cdot\bullet\cdot$) $10^{-4}$, ($\cdot\times\cdot$) $10^{-3}$, ($\cdot+\cdot$) $10^{-2}$ and ($\cdot *\cdot$) $10^{-1}$.

Besides, the forced response and the associated error for the beam-like structure subjected to
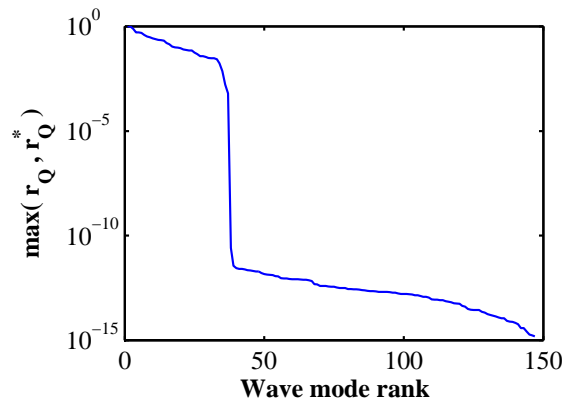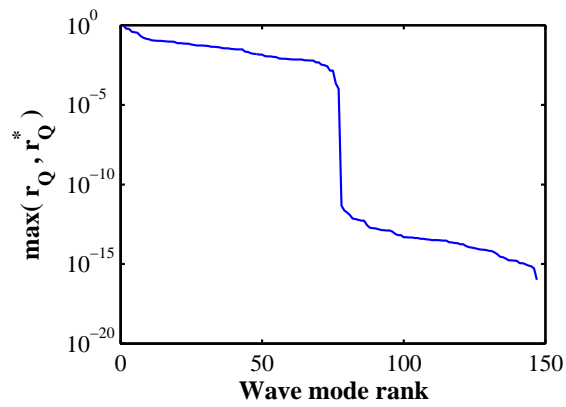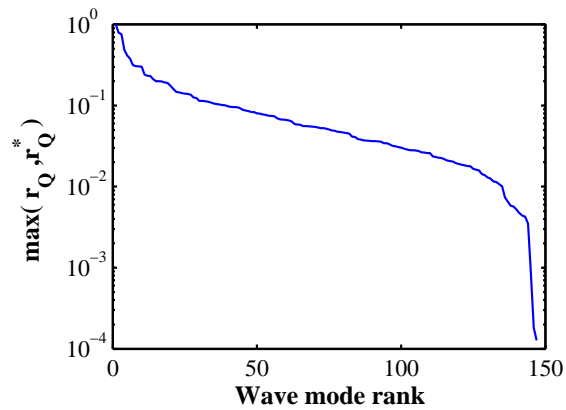
Figure 3.15: At the maximum frequency, value of $\max(r_Q, r_Q^\star)$ for each wave mode for three load cases: (a) uniformly distributed transverse force, (b) axial force over a line, and (c) punctual transverse force applied to an edge node.
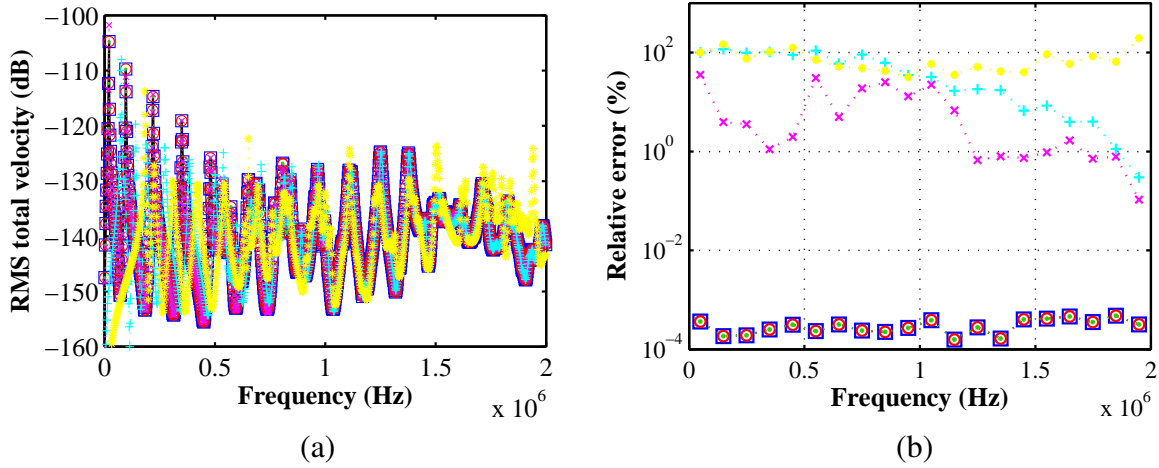
Figure 3.16: Clamped-free 3D beam-like structure subjected to uniformly distributed transverse forces: (a) RMS total velocity at the left boundary and (b) relative error (Equation (3.102)) computed by means of the reduced-order RM for six values for $\epsilon_Q$ ($\cdot\square\cdot$) $10^{-6}$, ($\cdot\circ\cdot$) $10^{-5}$, ($\cdot\bullet\cdot$) $10^{-4}$, ($\cdot\text{x}\cdot$) $10^{-3}$, ($\cdot+\cdot$) $10^{-2}$ and ($\cdot*\cdot$) $10^{-1}$, and wave modes selected at the maximum frequency within $\beta_f$.

a uniformly distributed transverse load are shown in Figure 3.16 for various reduced sets of wave modes — which were chosen by fixing different threshold values ($\epsilon_Q$) at the maximum frequency within $\beta_f$. Notice that if threshold values inferior to $10^{-4}$ are chosen — *i.e.*, 37 wave modes computed at the maximum frequency are used to build the reduced matrix —, very accurate responses are obtained, the errors being comparable to that obtained using WFE-based approaches which make use of the full wave basis. The RMS total velocity of the structure at the left boundary computed by means of the reduced-order RM formulation (Section 3.3.3), which makes use of 37 wave modes is compared to WFE-based RM formulation which considers the full wave basis in Figure 3.16(a). The associated relative error with respect to the conventional FE solution is presented in Figure 3.16(b). Notice that the proposed reduced-order model seems to be as accurate as the WFE-based RM approach which makes use of the full wave basis. The effect of considering a reduced-order model in elapsed time is shown in Figure 3.17(a). As expected, the time increases with the number of kept waves modes. However, if one compares the elapsed time expended by the ROM which makes use of 37 wave modes, *i.e.*, the most conservative solution among the ROMs, with the time expended by WFE-based approaches which makes use of the full wave basis, a reduction of 95.3 % is achieved. Compared to the CB approach, the time reduction achieved with the ROM is of 99.7%. The accuracy and computational speed of the ROM clearly highlight the importance of the proposed reduced order formulation; they are summarized and compared to conventional FE

method, WFE-based RM and CB method in Table 3.2.
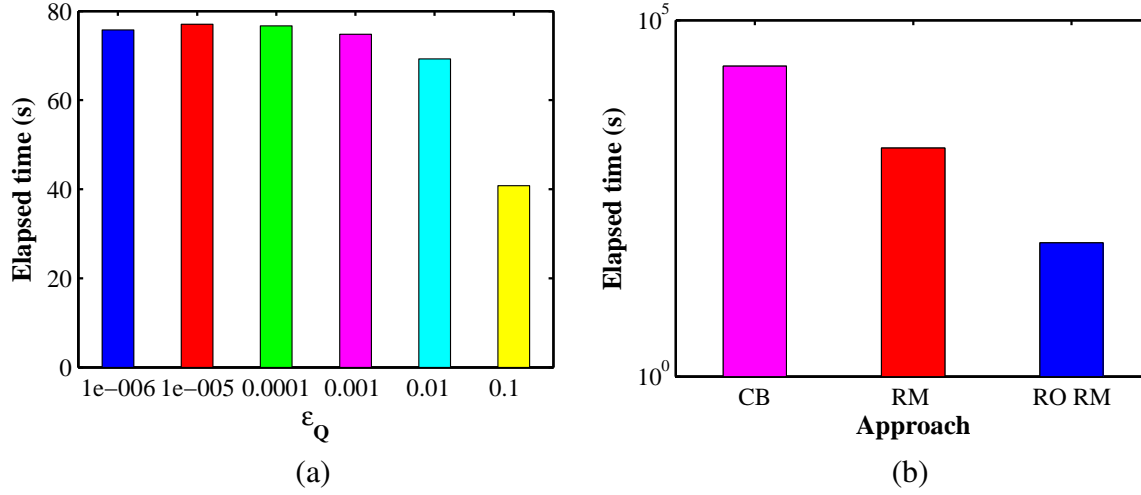


Figure 3.17: Elapsed times involved in reduced-order (RO) RM analysis of the 3D beam-like structure subjected to uniformly distributed transverse forces, (a) for various threshold values ($\epsilon_Q$): (blue color) $10^{-6}$, (red color) $10^{-5}$, (green color) $10^{-4}$, (magenta color) $10^{-3}$, (cyan color) $10^{-2}$ and (yellow color) $10^{-1}$; (b) for $\epsilon_Q = 10^{-6}$ (blue color) — *i.e.*, $n_Q = 37$ wave modes — compared to CB method (magenta color) and the WFE-based RM (red color) which makes use of the full wave basis.

Table 3.2: Total number of DOFs, maximum errors, and elapsed times involved by the proposed approaches regarding the beam-like structure subjected to a uniformly distributed transverse load.

| Approach | Total number of DOFs | Maximum error | Elapsed time | Time reduction |
|---|---|---|---|---|
| FE | 14,847 | ref | — | — |
| CB | 2,176 | 8.7 % | 22,772 s | ref |
| RM | 294 | 0.0005 % | 1,622 s | 92.9 % |
| RO RM | 74 | 0.0005 % | 76 s | 99.7 % |

A reduced-order model has also been built for the case axial forces are applied to a line over the left boundary (Figure 3.6(b)). The effect of the threshold value ($\epsilon_Q$) and the frequency on the number of selected wave modes is shown in Figure 3.18. Thus, considering $\epsilon_Q = 10^{-6}$, 77 over 147 wave modes are kept. The RMS value of the nodal total velocity over the left boundary and the associated error with respect to the conventional FE solution are shown in Figure 3.19. As in the previous load case, the accuracy of the proposed reduced-order model is comparable to that of the WFE-based approaches which make use of the full wave basis. Regarding elapsed time, the reduction in time achieved with the reduced model is of $82.4$ % with respect to WFE-based

approaches and 98.8 % with respect to the CB method. The accuracy, model size and computational time involved in the forced response computations for this load case are summarized in Table 3.3.



(a)　　　　　　　　　　　　　　　　　(b)
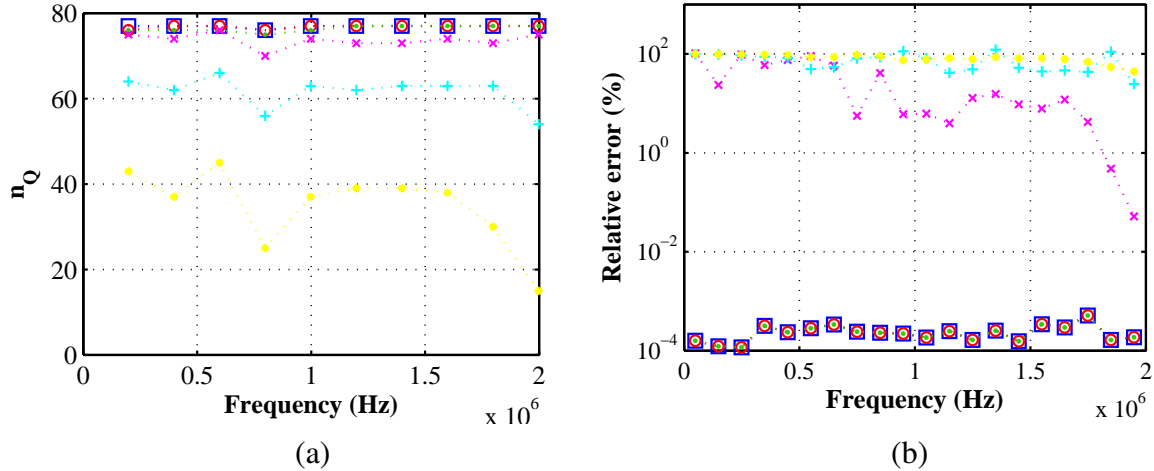
Figure 3.18: Clamped-free 3D beam-like structure subjected to axial forces over a line on the left boundary: (a) number of kept wave modes by means of Selection Criterion 1 (Section 3.3.1) for 10 sub-bands of frequencies within $\beta_f$ and six values for $\epsilon_Q$ , (b) relative error of reduced-order solutions for six values for $\epsilon_Q$ and wave modes selected at the maximum frequency, (c) value of $\max(r_Q, r_Q^\star)$ for each right-going wave mode at the maximum frequency. Threshold values: $(\cdot\square\cdot)$ $10^{-6}$, $(\cdot\circ\cdot)$ $10^{-5}$, $(\cdot\bullet\cdot)$ $10^{-4}$, $(\cdot\times\cdot)$ $10^{-3}$, $(\cdot+\cdot)$ $10^{-2}$ and $(\cdot\ast\cdot)$ $10^{-1}$.



(a)　　　　　　　　　　　　　　　　　(b)
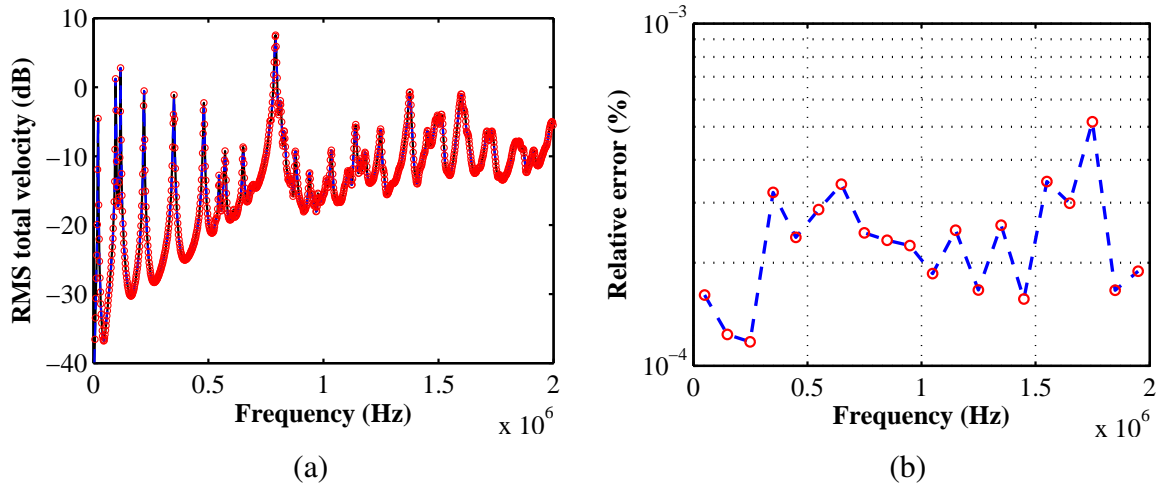
Figure 3.19: (a) FRF of the the clamped-free 3D beam-like structure subjected to axial forces over a line on the left boundary and (b) relative error, Equation (3.102): (——) conventional FE solution; ( $\circ$ ) WFE-based RM approach; (- - -) WFE-based reduced order RM approach which makes use of 77 over 147 wave modes.

97
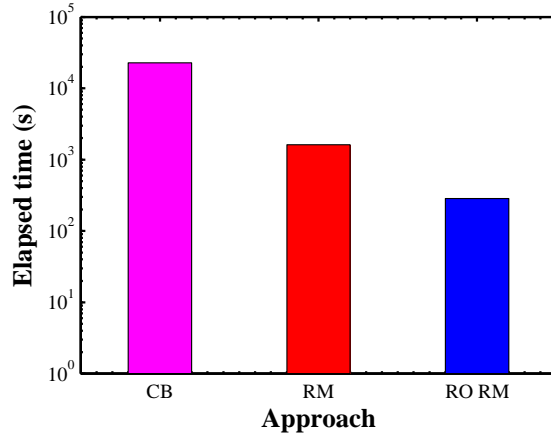
Figure 3.20: Elapsed times involved in the proposed approaches regarding the 3D beam-like structure subjected to axial forces over a line on the left boundary: (magenta) CB method that uses 1,882 fixed-interface modes; (red) WFE-based RM approach; (blue) WFE-based reduced-order (RO) model which considers 77 over 147 wave modes.

Table 3.3: Total number of DOFs, maximum errors, and elapsed times involved by the proposed approaches regarding the beam-like structure subjected to axial forces over a line.

| Approach | Total number of DOFs | Maximum error | Elapsed time | Time reduction |
|----------|---------------------|---------------|--------------|----------------|
| FE | 14,847 | `ref` | — | — |
| CB | 2,176 | 8.7 % | 22,852 s | `ref` |
| RM | 294 | 0.0005 % | 1,621 s | 92.9 % |
| RO RM | 74 | 0.0005 % | 285 s | 98.8 % |

It is worth pointing out that the number of wave modes that must be kept is related to the boundary condition. Indeed, Figure 3.15 shows that the number of kept wave modes increases as the degree of homogeneity of the load condition decreases — *i.e.*, a non-homogeneous surface load must require a higher number of wave modes than a homogeneous one, or, in other words, the smoother the surface load distribution, the smaller the number of wave modes needed to form a basis to approximate it. Further evidence of this behavior is provided by evaluating the number of wave modes required to model a beam-like structure under a punctual transverse force (Figure 3.6(c)). In Figure 3.21, the effect of the threshold value ($\epsilon_Q$) and the frequency on the dimension of the reduced basis used to model the clamped-free beam under punctual load is shown. Notice that for very accurate solutions, all the wave modes (*i.e.*, 147) should be kept.
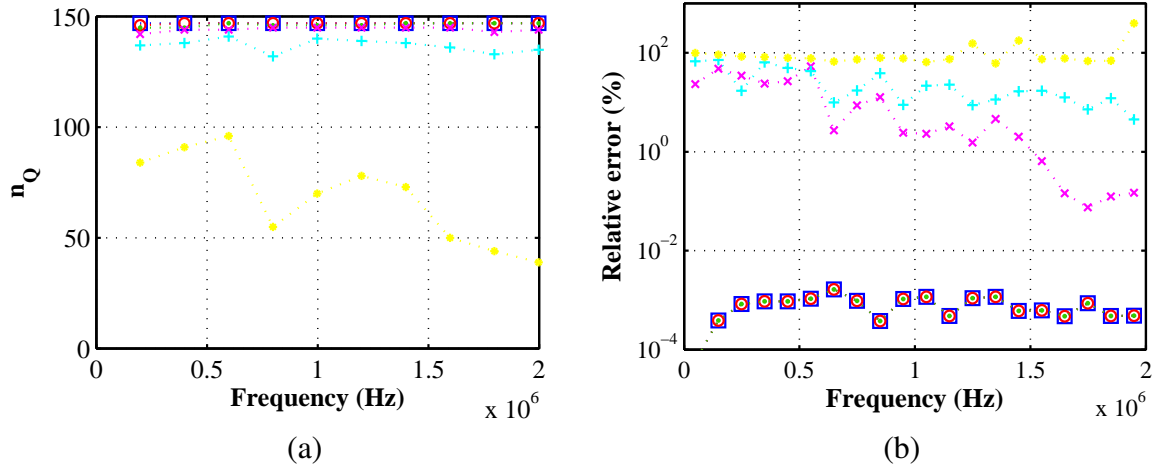
Figure 3.21: Clamped-free 3D beam-like structure subjected to a punctual transverse force at an edge node on the left boundary: (a) number of kept wave modes using the Selection Criterion 1 (Section 3.3.1) for 10 sub-bands of frequencies within $\beta_f$ and 6 values for $\epsilon_Q$ , (b) relative error of reduced-order solutions for six values for $\epsilon_Q$ and wave modes selected at the maximum frequency. Threshold values: $(\cdot\square\cdot)\ 10^{-6}$, $(\cdot\circ\cdot)\ 10^{-5}$, $(\cdot\bullet\cdot)\ 10^{-4}$, $(\cdot x\cdot)\ 10^{-3}$, $(\cdot+\cdot)\ 10^{-2}$ and $(\cdot*\cdot)\ 10^{-1}$.

### 3.5.2 Forced response analysis of a beam-like structure via WSFEM

In this section, the objective is to show that numerical spectral elements can be built either by means of WSFEM (Section 3.4.1) or by making use of the reduced-order WFE-based approach (Section 3.3). A clamped-free beam-like structure sufficiently long to behave as an one-dimensional structure is considered. It is composed of $400$ substructures ($L = 400\Delta$) and it is subjected at its free end to a uniform transverse harmonic force in the $z$-direction, as shown in Figure 3.22. The material and geometric properties of this solid beam are the same of the beam considered in Section 3.5.1. Thus, the same substructure FE model has been considered here (see Figure 2.7(b)). Here, the forced response of the global structure is analyzed over a frequency band $\beta_f = [200\,\text{Hz}\text{—}500\,\text{kHz}]$, which involves discrete frequencies equally spaced steps of $2000$ Hz.

As a transverse load in the $z$-direction is applied to the structure, bending and shear wave modes w.r.t. to the $y$-axis have been considered in order to build the spectral element matrices analytically via SEM and numerically by means of WSFEM. The response of the structure at the center point of its left end is shown in Figure 3.23. As expected, at very low frequencies, one can observe a good agreement between analytical (SEM) and numerical solutions (WFE-based DSM
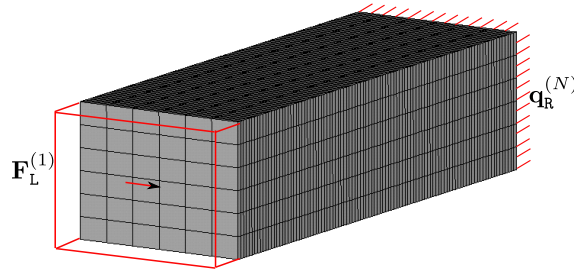
Figure 3.22: FE model of the 3D beam-like structure considered in this section.

approach and WSFEM). The results also highlights the potential of WSFEM, which by making use of only 2 waves modes instead of the full wave basis of 147 wave modes can be conveniently used to describe the dynamics of a 3D beam at low frequencies.



(a)

(b)

Figure 3.23: (a) FRF of the the clamped-free 3D beam-like structure subjected to uniformly distributed transverse forces over the left surface boundary, and (b) relative error w.r.t the analytical solution provided via SEM: (—) SEM; (- - -) FEM; ( ○ ) WSFEM for Timoshenko's beam.

The forced response of the beam-like structure has also been computed by means of the reduced-order (RO) WFE-based approach proposed in Section 3.3. Here, criteria 1 and 2 have been used to select the wave modes. Moreover, instead of solving the full eigenvalue problem of size $294 \times 294$ at each frequency, this is done for just 25 over 250 frequency steps. At the remaining frequencies, a WFE-based eigenvalue problem of reduced size is solved. Sets of wave modes of several sizes have been considered ($n_w = 2$, $n_w = 5$, $n_w = 10$ and $n_w = 15$). The responses

issued by means of the RO WFE-based approach are compared to the ones obtained via WSFEM and WFE-based DSM approach in Figure 3.24. The error is computed with respect to the WFE-based DSM approach, as it makes use of the full wave basis. Notice that the accuracy increases with the number of kept wave modes. This confirms that the accuracy of WFE-based solutions can be enhanced by increasing the number of kept wave modes. In other words, high-order spectral elements can be built by means of the WFE method. The main advantage of considering a reduced set of waves modes instead of the full wave basis is the possibility of saving computational time. This point is highlighted in Figure 3.25.



(a)                                                                                    (b)
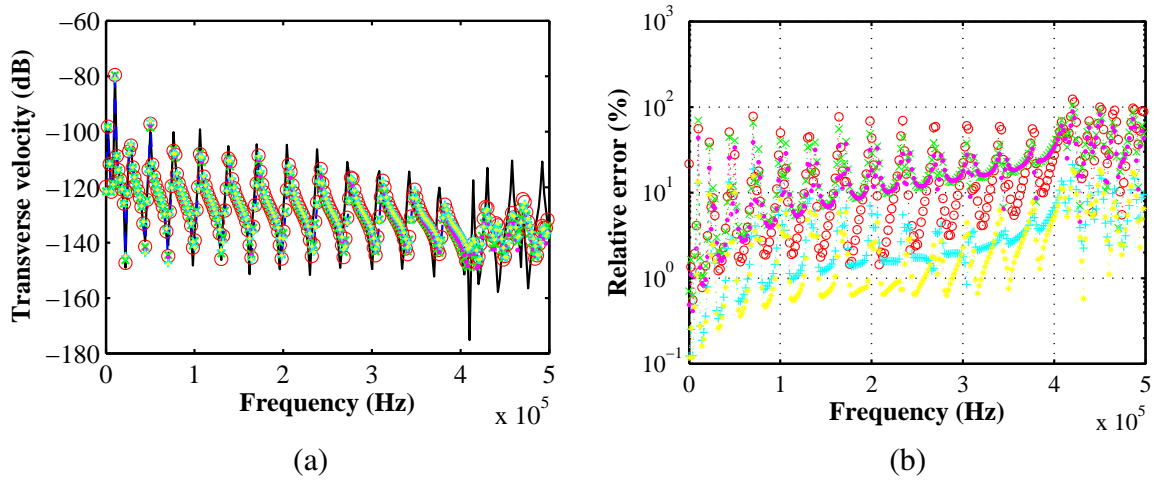
Figure 3.24: (a) FRF of the the clamped-free 3D beam-like structure subjected to uniformly distributed transverse forces over the left surface boundary and (b) relative error w.r.t solution issued by WFE-based DSM approach: (—) SEM; (- - -) FEM; ( ○ ) WSFEM for Timoshenko's beam;( • ) RO WFE-based approach with ($\epsilon_Q = 10^{-6}, n_w = 2$); ( x ) RO WFE-based approach with ($\epsilon_Q = 10^{-6}, n_w = 5$); ( + ) RO WFE-based approach with ($\epsilon_Q = 10^{-6}, n_w = 10$); ( * ) RO WFE-based approach with ($\epsilon_Q = 10^{-6}, n_w = 15$).

### 3.5.3 Forced response analysis of 3D fuselage-like structure via WFE-based DSM and RM

In this section, the harmonic forced response of a free-free 3D stiffened fuselage-like structure is addressed. The left end is subjected to the transient load shown in Figure 3.27, which is uniformly distributed in the radial direction (see Figure 3.26(a)). No kinematic constraints are applied. Due to the loading condition, only one-quarter of the cylindrical shell including axial (stringers) and circumferential (frames) stiffeners periodically distributed over the cylinder are modeled and
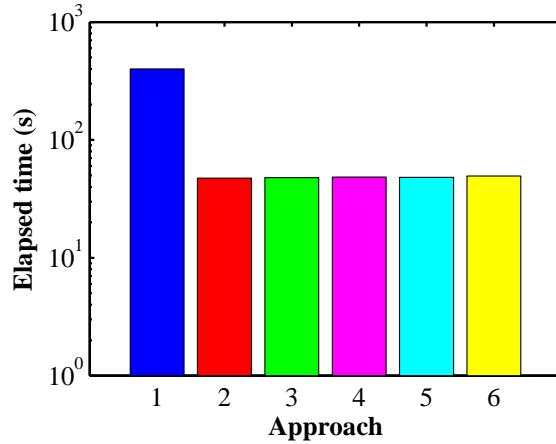
Figure 3.25: Elapsed time involved in the forced response analysis of a 3D beam-like structure subjected to uniformly distribu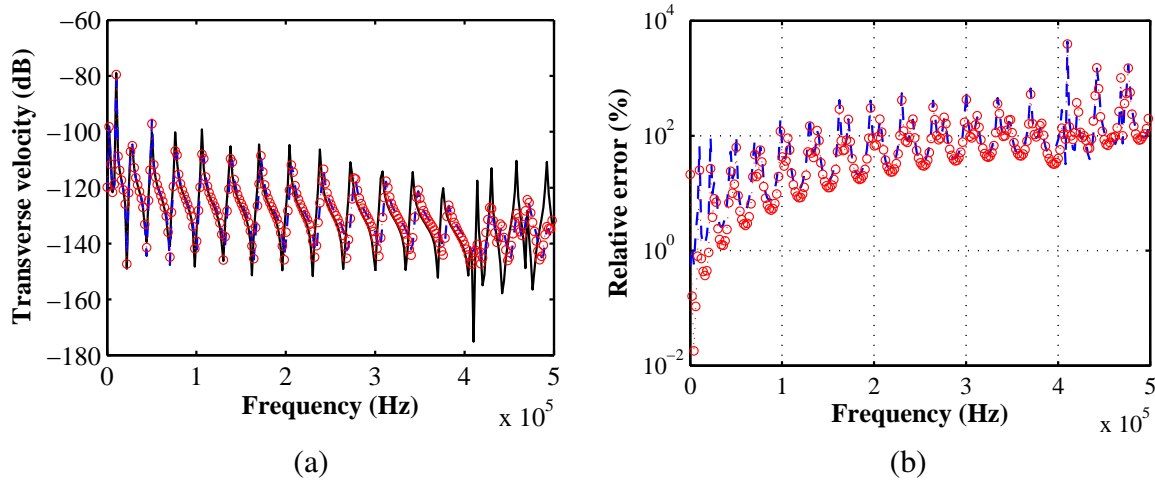ted transverse forces over the left surface boundary: **1** (blue) WFE-based DSM approach; **2** (red) WSFEM for Timoshenko's beam; **3** (green) RO WFE-based approach with ($\epsilon_Q = 10^{-6}, n_w = 2$); **4** (magenta) RO WFE-based approach with ($\epsilon_Q = 10^{-6}, n_w = 5$); **5** (cyan) RO WFE-based approach with ($\epsilon_Q = 10^{-6}, n_w = 10$); **6** (yellow) RO WFE-based approach with ($\epsilon_Q = 10^{-6}, n_w = 15$).

symmetry conditions are applied to the free edges standing along the $x$-axis — *i.e.*, normal displacement and tangential rotations are set to zero. The characteristics of the cylindrical shell and stiffeners (stringers and frames) are provided in Table 3.4. The full structure is composed of 30 identical substructures periodically arranged along the $x$-axis. Within the framework of the WFE method, only one substructure is modeled using conventional finite elements issued from ANSYS®. Indeed, quadrilateral Reissner-Mindlin shell finite elements, with four nodes and six DOFs per node — *i.e.*, translations in the $x$, $y$ and $z$ axes and rotations about the same axes —, the SHELL181 elements from ANSYS®, are used to model the substructure. Each substructure (Figure 3.26(b)) is of length $\Delta = 0.4$ m and it is discretized by means of 456 DOFs, with $n = 126$ DOFs over its left-/right boundary and 204 internal DOFs. As a result, the corresponding FE model (Figure 3.26(a)) of the global periodic structure contains 10,026 DOFs.

The forced responses of the global structure under either axial or transverse loads are analyzed over a frequency band $\beta_f = [0\text{---}215]$ Hz, which involves discrete frequencies equally spaced steps of $0.2083$ Hz.

Within the WFE framework, and by considering the symmetry boundary conditions, 120 right-going and 120 left-going wave modes are obtained through the WFE eigenvalue problem stated in Equation (2.49). Thus, regarding the WFE-based superelement approaches which makes

Table 3.4: Characteristics of the stiffened cylindrical shell.

| Parameter | cylindrical shell | frames | stringers |
|---|---|---|---|
| Thickness ($t$) | 0.001 m | 0.0012 m | 0.0012 m |
| Radius ($R$) | 2 m | – | – |
| Height ($h$) | – | 0.05 m | 0.05 m |
| Density ($\rho$) | 2700 kg/m$^3$ | | |
| Young's modulus ($E$) | 70 GPa | | |
| Poisson's ratio ($\nu$) | 0.3 | | |
| Loss factor ($\eta$) | 0.02 | | |
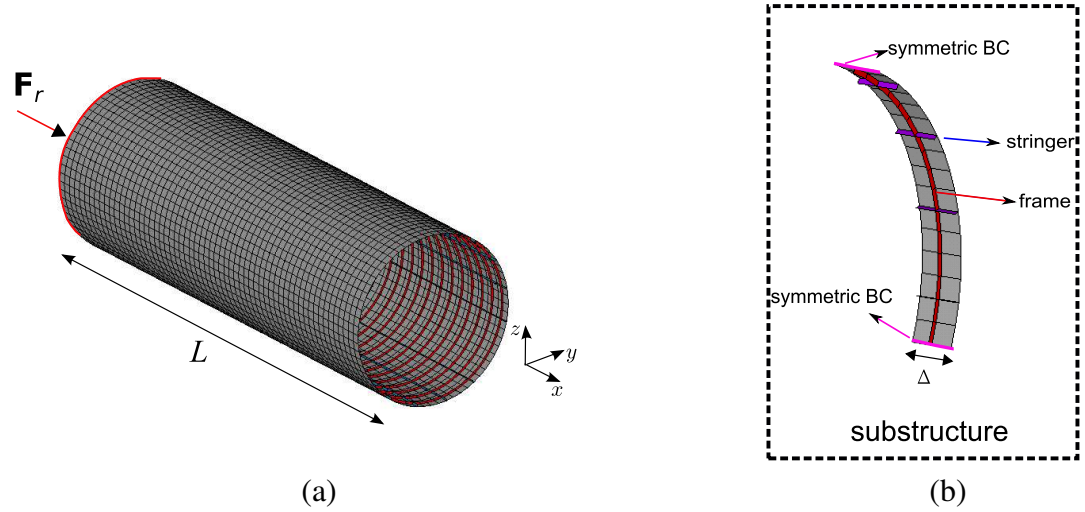


Figure 3.26: FE models of the 3D stiffened fuselage-like structure: (a) full periodic structure, (b) substructure.

use of the full wave basis, the dimension of the problem is $2n$, *i.e.*, 240, which corresponds to the number of boundary DOFs of the periodic structure. Besides, one may use the CB method to model the periodic structure. In this case, if all fixed-interface modes whose eigenfrequencies are below $2 \times \omega_{max}$ are considered — *i.e.*, the rule of thumb —, 484 fixed-interface modes are kept, which means that the size of the model is 964, which corresponds to the sum of static and fixed-interface modes. On the other hand, the dimension of the reference FE model is 9,480 after applying symmetry boundary conditions. The WFE-based solutions are compared with the results issued from the conventional FE method in terms of accuracy. The relative error of the WFE-based solutions, averaged over several sub-frequency bands of same width $\{\beta_f^i\}_i$, is expressed as

$$\epsilon_{\beta_f^i} = \frac{< \|\mathbf{q}_{\text{RMS}}\|_2 - \|\mathbf{q}_{\text{RMS}}^{\text{ref}}\|_2 >_{\beta_f^i}}{< \|\mathbf{q}_{\text{RMS}}^{\text{ref}}\|_2 >_{\beta_f^i}}, \tag{3.106}$$
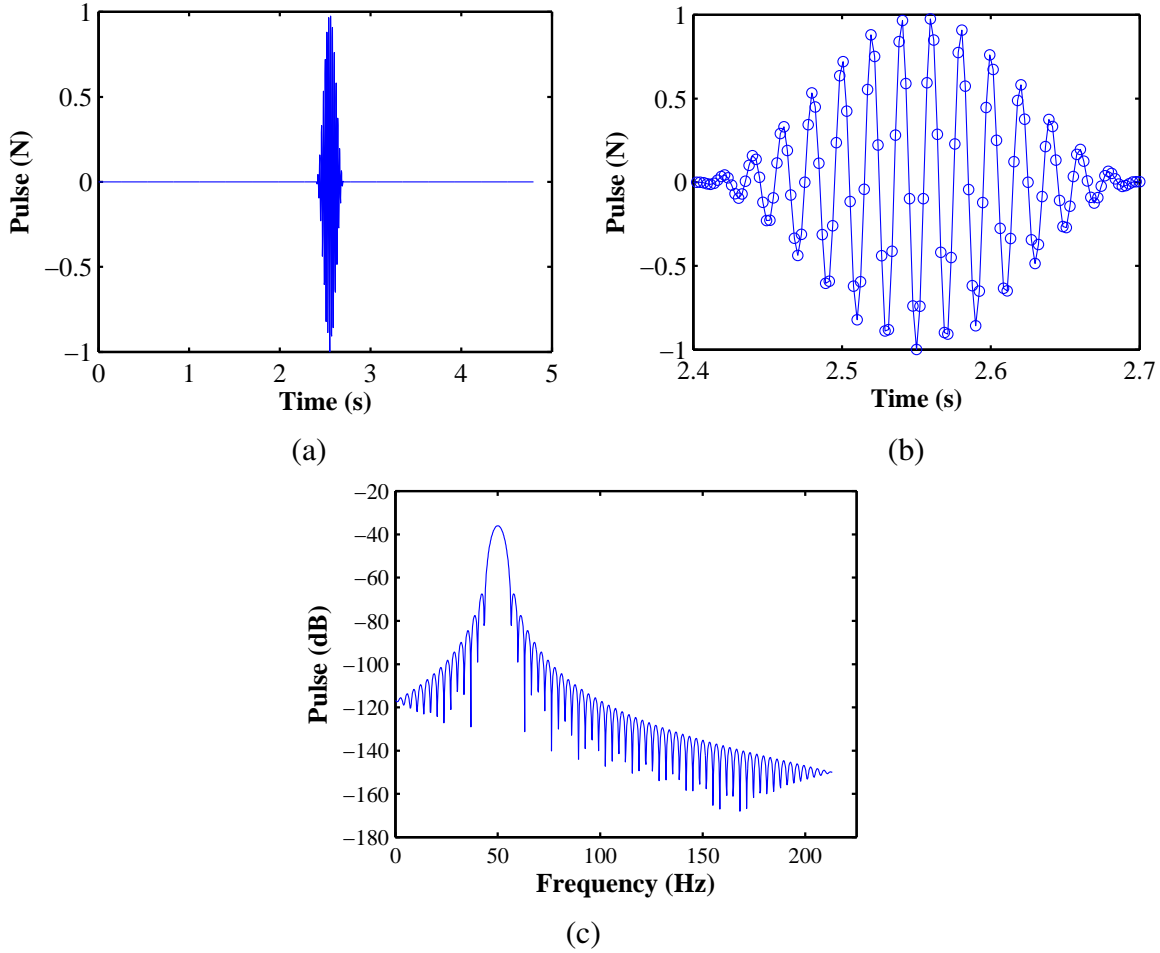
Figure 3.27: Excitation signal applied to the aircraft fuselage in the radial direction, at $x = 0$ m: (a) in the time domain; (b) in the time domain zoomed between $[2.4\,2.7]\,s$; (c) in the frequency domain.

where $\mathbf{q}_{\text{RMS}}$ denote the RMS value of the nodal total displacements over the left boundary of the structure, ref is used to denote the reference solution, while the notation $< . >_{\beta_i}$ denotes the quadratic mean over a sub-frequency band $\beta_f^i$. Here, twenty sub-frequency bands $\{\beta_f^i\}_i$ are considered which cover the whole frequency band $\beta_f$ (*i.e.*, $\beta_f = \cup_i \beta_f^i$). Regarding CPU time, the WFE-based solutions are compared with that expended by the CB method.

In the following, WFE-based solutions which makes use of the full wave mode basis — *i.e.*, DSM and RM approaches (Sections 3.2.2 and 3.2.3, respectively) — are compared to solutions issued from the DSM approach proposed by Duhamel *et al.* (2006) and the conventional FE method in Figures 3.28 and 3.29. There, the RMS value of the total velocity at either the left or the right boundary of the fuselage-like structure is analyzed over the frequency range $\beta_f$. The relative errors
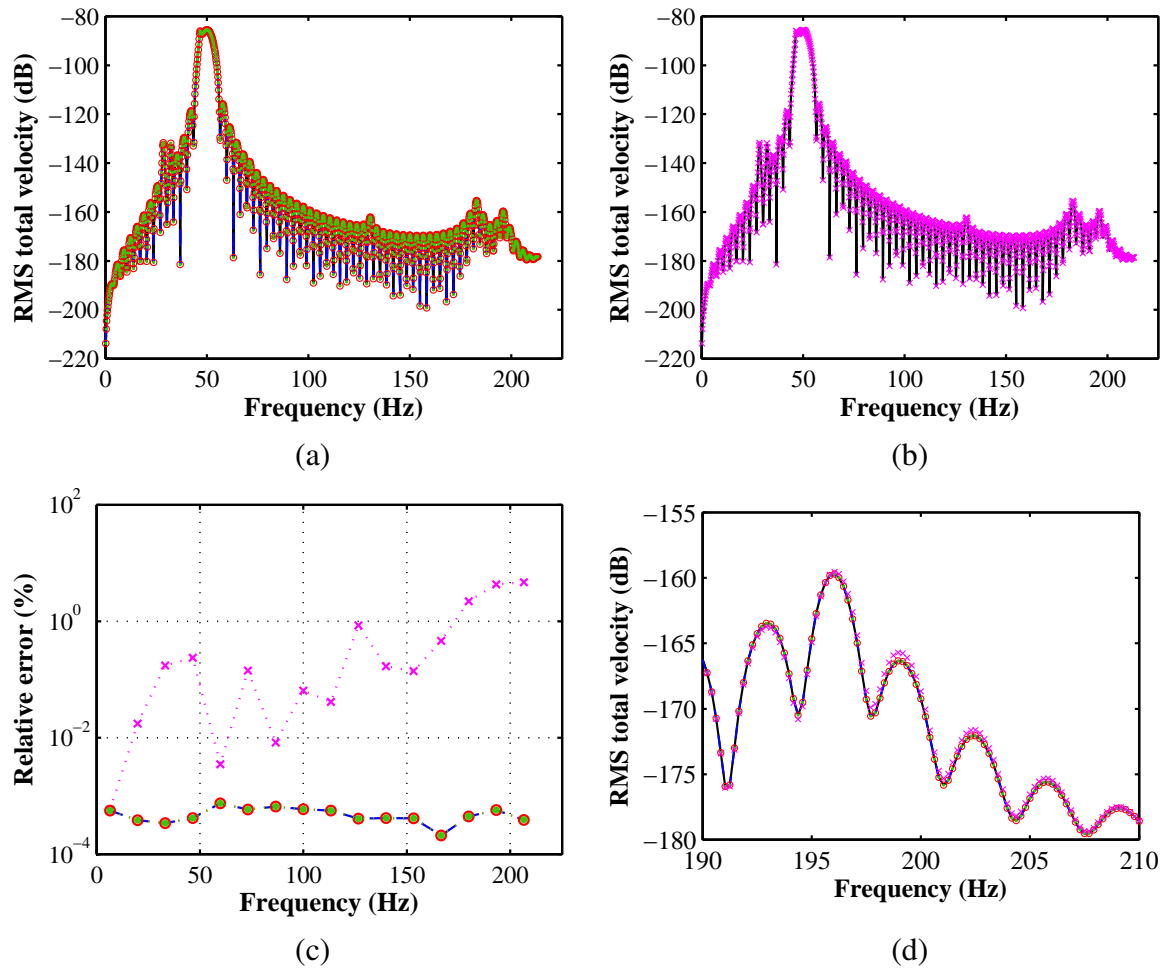
Figure 3.28: (a,b) RMS total velocity in the frequency domain at the left end ($x = 0$) of the free-free 3D fuselage-like structure subjected to radial forces over the cylindrical shell at $x = 0$, (c) relative error (Equation (3.106)), and (d) zoom over forced-response solutions within $[190 — 210]$ Hz: (——) FE solution; ( x ) CB method which makes use of $484$ fixed-interface modes; (- - -) WFE-based DSM; ( ○ ) WFE-based RM; ( ● ) WFE-based Duhamel's DSM.

of WFE-based solutions are displayed in Figure 3.28(c) for $x = 0$, and in Figure 3.29(c) for $x = 30\Delta$. As it can be seen, all approaches are completely in agreement and show extremely low error with respect to the conventional FE solution — *i.e.*, of order $10^{-3}\%$—, which validates the proposed DSM and RM approaches and confirms that WFE-based solutions which make use of the full wave mode basis can be considered as accurate as the conventional FE solution for equivalent mesh density.

Time-domain responses can also be computed using the Fourier transform in Matlab®. The
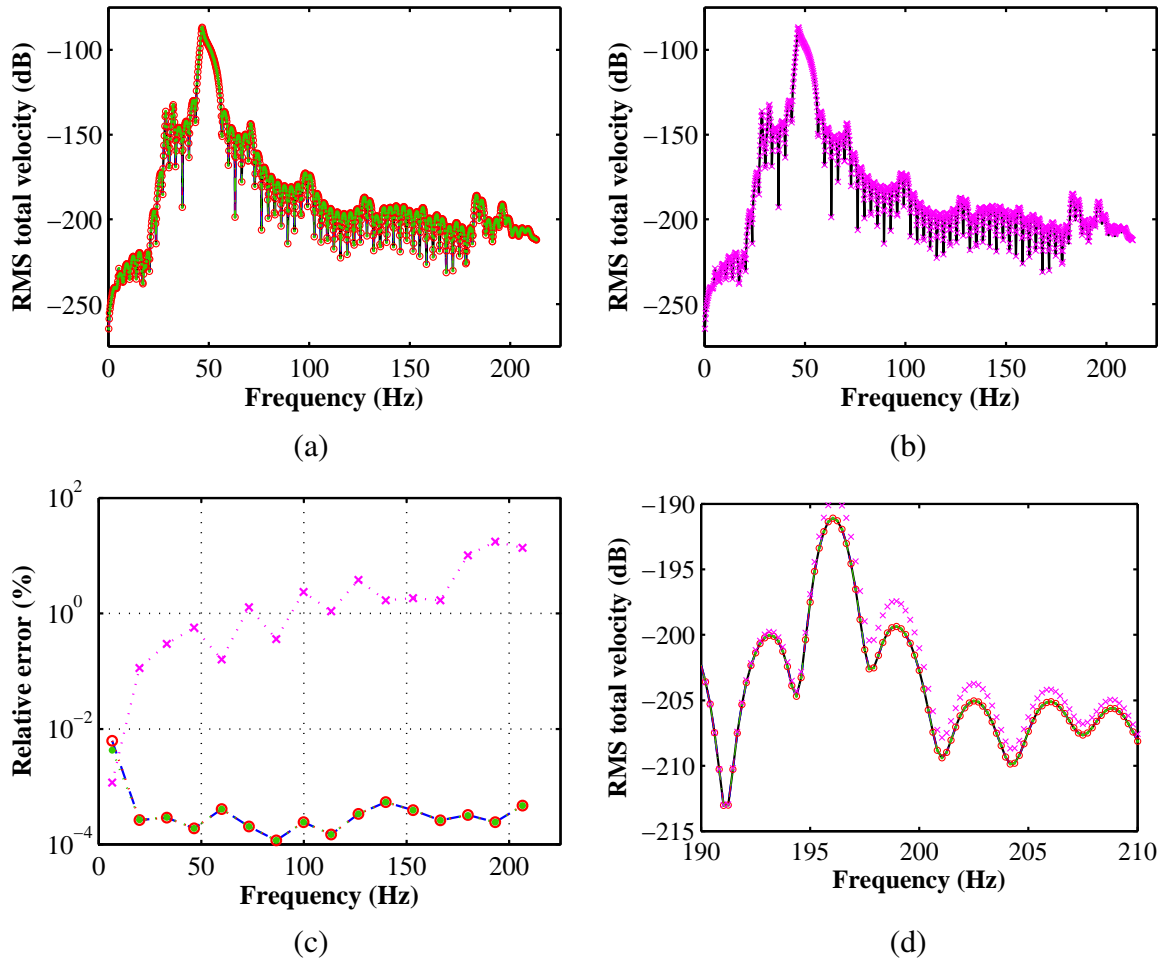
Figure 3.29: (a,b) RMS total velocity in the frequency domain at the right end ($x = 30\Delta$) of the free-free 3D fuselage-like structure subjected to radial forces over the cylindrical shell at $x = 0$, (c) relative error (Equation (3.106)), and (d) zoom over forced-response solutions within $[190 — 210]$ Hz: (——) FE solution; ( x ) CB method which makes use of $484$ fixed-interface modes; (- - -) WFE-based DSM; ( ○ ) WFE-based RM; ( ● ) WFE-based Duhamel's DSM.

responses in the time domain computed by means of the WFE-based approaches, conventional FE method or CB method are shown in Figure 3.30.

As discussed previously, the WFE-based DSM, RM and Duhamel's DSM approaches involve the inversion of sparse matrices (Equations (3.103), (3.104) and (3.105), respectively). In the case of the fuselage-like structure, the condition numbers of these matrices within the frequency range $\beta_f$ are shown in Figure 3.31. Here, one may notice that the condition numbers relative to the WFE-based DSM and RM approaches are relatively small (of order of $10^2$), while those relative to the
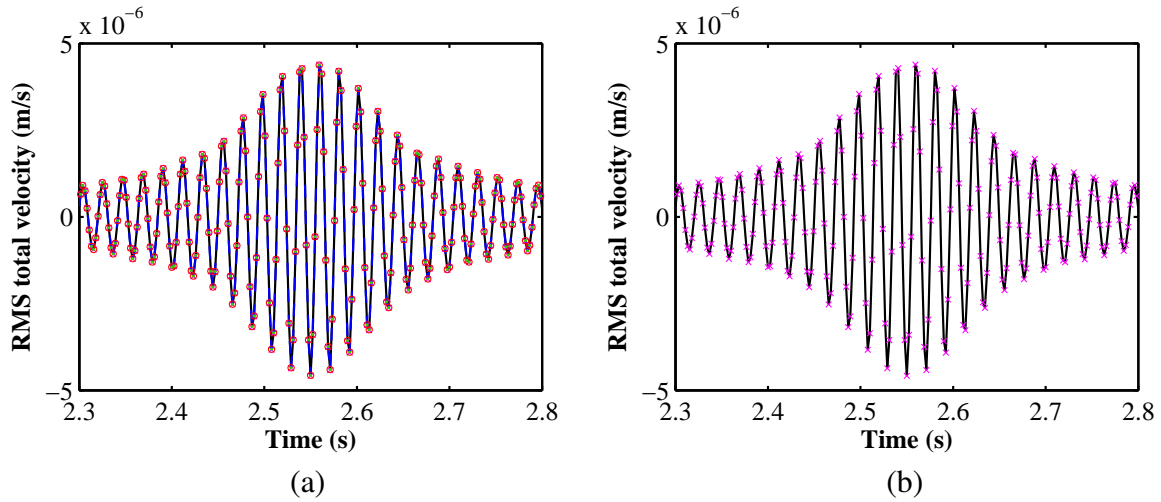
Figure 3.30: (a,b) RMS total velocity in the time domain at the right end ($x = 30\Delta$) of the free-free 3D fuselage-like structure subjected to radial forces over the cylindrical shell at $x = 0$: (——) FE solution; ( x ) CB method which makes use of $484$ fixed-interface modes; (- - -) WFE-based DSM; ( ○ ) WFE-based RM; ( ● ) WFE-based Duhamel's DSM.
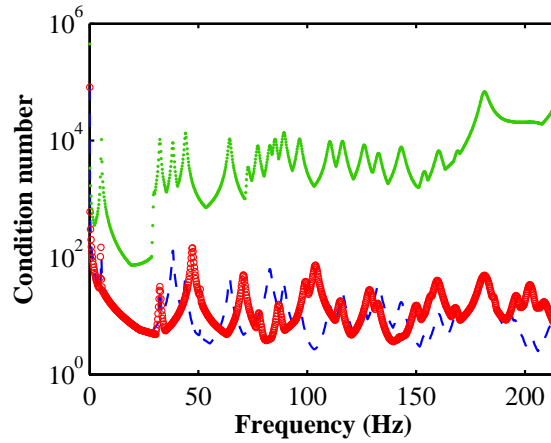


Figure 3.31: Condition number of the sparse matrix required to be inverted in order to build: (- - -) WFE-based DSM, ( ○ ) WFE-based RM and ( ● ) WFE-based Duhamel's DSM.

WFE-based Duhamel's DSM formulation are always greater and of order of $10^4$. Regarding elapsed time, as in the case of the beam-like structure, all the three WFE-based superelement approaches seems to be equivalent and more efficient than the conventional CB method (see Figure 3.32). An average reduction of $63\,\%$ in elapsed time is obtained by means of WFE-based superelement approaches which make use of the full wave basis. Table 3.5 summarizes the number of DOFs,

maximum errors and elapsed times involved in the forced response analysis of the fuselage-like structure.
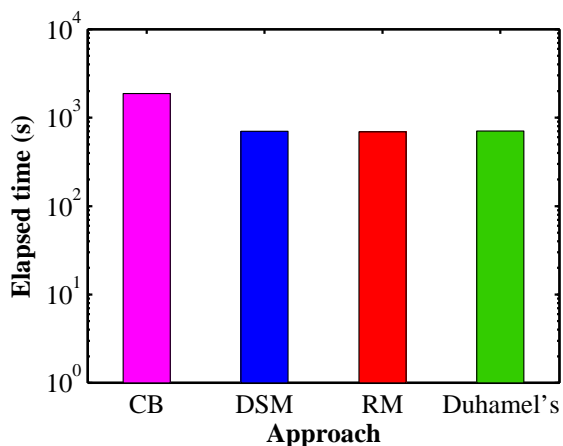


Figure 3.32: Elapsed times for the forced response computation of the fuselage-like structure subjected to uniformly distributed radial forces: (magenta color) CB method which makes use of $484$ fixed-interface modes, (blue color) WFE-based DSM, (red color) WFE-based RM and (green color) WFE-based Duhamel's DSM.

Table 3.5: Total number of DOFs, maximum errors, and elapsed times involved by the proposed approaches regarding the clamped-free beam-like structure subjected to a uniformly distributed transverse load.

| Approach | Total number of DOFs | Maximum error | Elapsed time | Reduction |
|---|---|---|---|---|
| FE | 10,026 | ref | — | — |
| CB | 964 | 17.5 % | 1,875 s | ref |
| DSM | 240 | 0.006 % | 702 s | 63 % |
| RM | 240 | 0.006 % | 694 s | 63 % |
| Duhamel's DSM | 240 | 706 % | 1,639 s | 62 % |

The reduced-order superelement model of the free-free fuselage-like structure is also investigated. To begin with, the effect of the threshold value ($\epsilon_Q$) is investigated in Figure 3.33. Notice that differently from the beam case, here the number of kept wave modes does not converge for a specific value as the threshold value decreases. From Figure 3.33(b), it is not so clear that there is a set of wave modes which has a strong influence on the structure response.

The forced response and the associated error for the 3D stiffened fuselage-like structure subjected to uniform radial forces over the cylindrical shell at $x = 0$ are shown in Figure 3.34 for
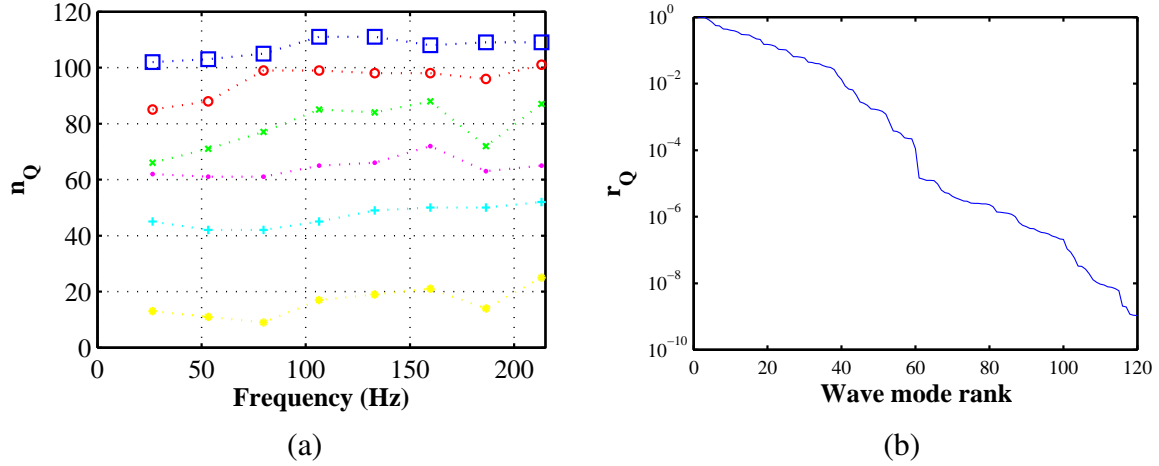
Figure 3.33: Free-free 3D fuselage-like structure subjected to uniform radial forces on the left boundary: (a) number of kept wave modes using the selection strategy proposed in Section 3.3.1 for ten sub-bands of frequencies within $\beta_f$ and six values for $\epsilon_Q$ , (b) at the maximum frequency, value of $\max(r_Q, r_Q^\star)$ for each wave mode. Threshold values: ($\cdot\square\cdot$) $10^{-6}$, ($\cdot\circ\cdot$) $10^{-5}$, ($\cdot\bullet\cdot$) $10^{-4}$, ($\cdot$x$\cdot$) $10^{-3}$, ($\cdot+\cdot$) $10^{-2}$ and ($\cdot*\cdot$) $10^{-1}$.

$\epsilon_Q = 10^{-6}$ at the maximum frequency within $\beta_f$. This yields the consideration of $87$ over $120$ wave modes, which were computed at the maximum frequency and used to build the reduced RM. Accurate responses are obtained, the errors being comparable to that obtained using WFE-based approaches which make use of the full wave basis. In terms of elapsed time, the ROM which makes use of $87$ wave modes yields a reduction of $48$ % compared to the WFE-based RM which makes use of the full wave basis, and $81\%$ with respect to the CB method. These features of the RO RM are highlighted in Table 3.6, which presents the number of DOFs, maximum errors and elapsed times involved in the CB method, WFE-based RM and WFE-based RO RM.

Table 3.6: Total number of DOFs, maximum errors, and elapsed times involved by the proposed approaches regarding the clamped-free beam-like structure subjected to a uniformly distributed transverse load.

| Approach | Total number of DOFs | Maximum error | Elapsed time | Reduction |
|---|---|---|---|---|
| FE | 10,026 | ref | — | — |
| CB | 964 | 17.5 % | 1,875 s | ref |
| RM | 240 | 0.006 % | 694 s | 63 % |
| RO RM | 174 | 0.005 % | 363 s | 81 % |
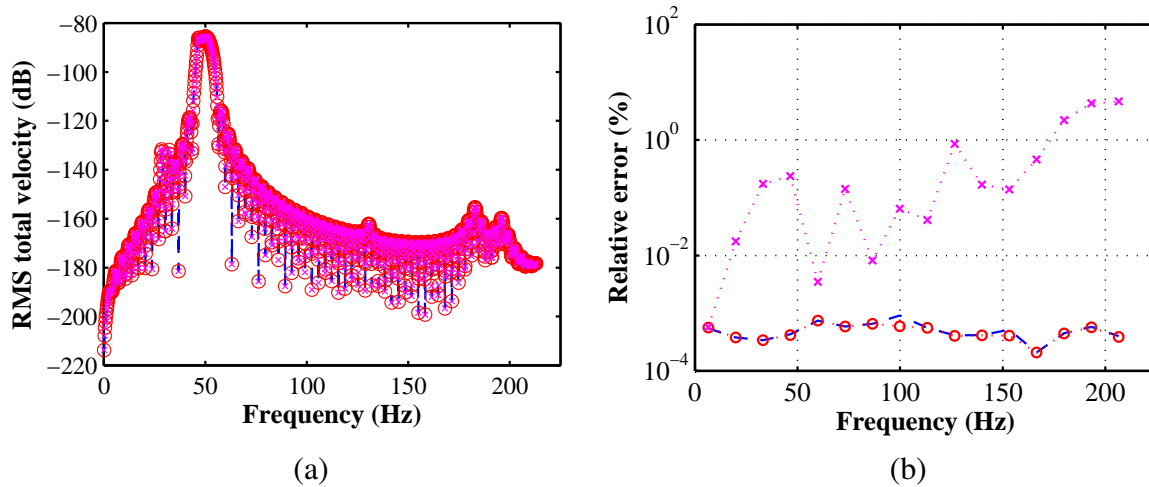
Figure 3.34: Free-free 3D fuselage-like structure subjected to uniformly distributed radial forces over the cylindrical shell at $x = 0$: (a) RMS total velocity in the frequency domain at the left boundary and (b) relative error (Equation (3.106)) in the frequency domain: ( x ) CB method which makes use of $484$ fixed-interface modes; ( o ) WFE-based RM; (- - -) WFE-based reduced-order RM which makes use of $87$ over $120$ wave modes.
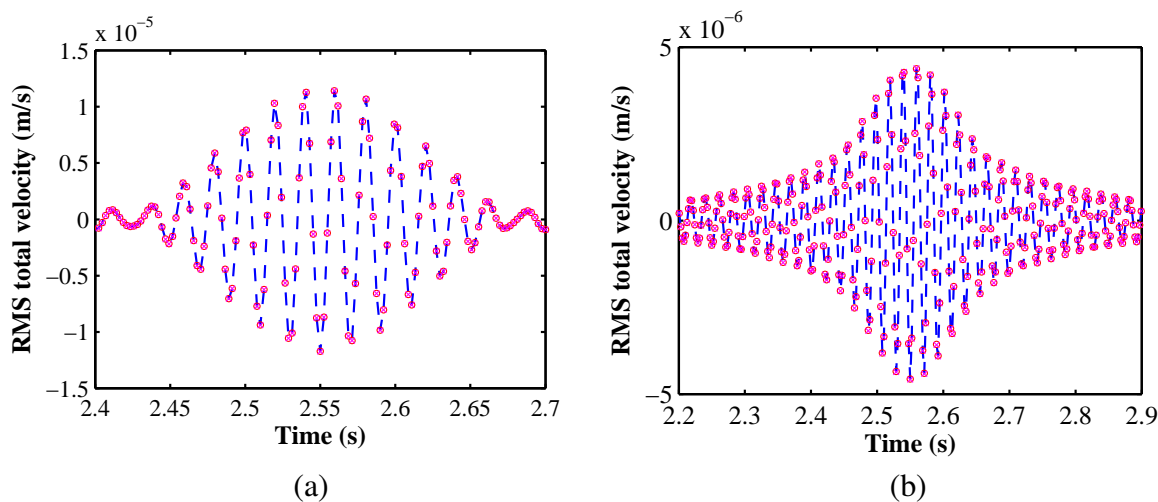


Figure 3.35: Free-free 3D fuselage-like structure subjected to uniformly distributed radial forces over the cylindrical shell at $x = 0$, RMS total velocity in the time domain (a) at the left boundary, and (b) at the right boundary: ( x ) CB method which makes use of $484$ fixed-interface modes; ( o ) WFE-based RM; (- - -) WFE-based reduced-order RM which makes use of $87$ over $120$ wave modes.

110
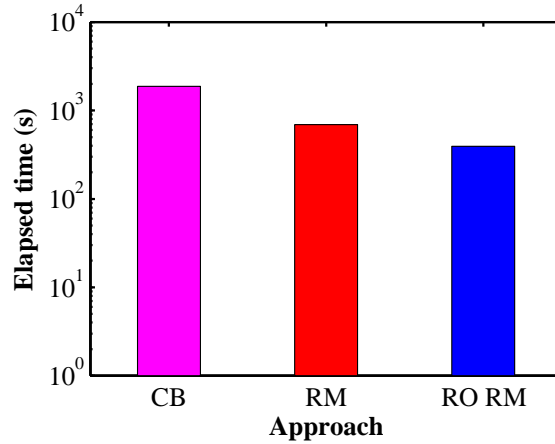
Figure 3.36: Elapsed times involved in the proposed approaches regarding the 3D fuselage-like structure subjected to uniformly distributed radial forces over the cylindrical shell at $x = 0$, for $\epsilon_Q = 10^{-6}$ compared to the CB method and WFE-based RM approach which makes use of the full wave basis: (magenta color) CB method that uses $484$ fixed-interface modes, (red color) WFE-based RM, (blue color) WFE-based reduced-order (RO) RM which considers $87$ over $120$ wave modes.

## 3.6 Conclusions

This chapter addressed the forced response analysis of periodic structures via WFE-based approaches. The main idea here was to construct superelement models of periodic structures from a wave description. At first, the full basis of wave modes computed by means of the WFE method were used to formulate dynamic stiffness and receptance matrices of a periodic structure. These matrices are of reduced size as they are expressed in terms of the degrees of freedom (DOFs) on the left and right boundaries of a periodic structure. Indeed, external loads and kinematic constraints are assumed confined on the left and right boundaries of the superelement model. A reduced-order WFE-based approach for the forced response analysis of a periodic structure was also proposed. It involves three main steps, which are: the selection of the most contributing wave modes, the formulation of a reduced WFE-based eigenvalue problem and the formulation of a receptance matrix for the reduced-order superelement model. Alternatively, a reduced-order semi-analytical model of a periodic structure can be built via WSFEM. This method was presented in general form and applied to the case of a Timoshenko beam in this chapter. The superelement models proposed here

were used to compute the forced responses of a 3D beam-like structure and a 3D fuselage-like structure. Thus, the case of a simple waveguide and a periodic structure involving heterogeneities (the stiffeners) were addressed. Frequency and time-domain solutions were presented. For both numerical test cases, it was shown that accurate solutions can be obtained via the proposed WFE-based approaches. They also showed to be faster than the conventional CB method. In addition, the improvement in performance when using reduced-order models was highlighted. Moreover, it was shown that the WFE method can used to build spectral superelement models of arbitrary order.

# 4 WFE-based superelements for forced response analysis of coupled systems via dynamic substructuring

## 4.1 Overview

In this chapter, the WFE method is used for assessing the harmonic response of coupled mechanical systems that involve one-dimensional periodic structures and coupling elastic junctions. The periodic structures under concern are composed of complex heterogeneous substructures like those encountered in real engineering applications. The issue may be viewed as circumventing the computational cost of the conventional FE method when large-sized numerical models are to be solved at many discrete frequencies, while keeping a high level of accuracy. The challenge especially concerns the development of efficient numerical approaches that outperform, in terms of accuracy and computational time savings, the usual substructuring techniques like the CB method (Craig and Bampton, 1968a). A strategy is proposed which uses the concept of numerical wave modes to express the DSM, or the RM, of each periodic structure. Also, the CB method is used to model each coupling junction by means of static modes and fixed-interfaces modes. An efficient WFE-based criterion is considered to select the junction modes that are of primary importance. The consideration of several periodic structures and coupling junctions is achieved through classic finite element assembly procedures, or domain decomposition techniques. Numerical experiments are carried out to highlight the relevance of the WFE-based DSM and RM approaches. The following test cases are considered: a 2D frame structure under plane stresses; a 3D aircraft fuselage-like structure involving stiffened cylindrical shells.

The contribution of this chapter is in assessing the potentiality of the proposed WFE-based substructuring technique for simulating non-academic coupled systems like those encountered in engineering applications, and which involve several truly periodic structures and arbitrarily-shaped elastic junctions. The developments presented in this chapter constitute part of the research paper by Silva *et al.* (2015b) submitted to the International Journal for Numerical Methods in Engineering (IJNME).

The rest of the chapter is organized as follows. In Section 4.2, the CB-based modeling of a coupling junction is investigated. In Section 4.3, the modeling of coupled systems is investigated by means of the so-called DSM and RM approaches. The DSM approach uses the concept of classic

FE assembly procedures for connecting subsystems to each other, while the RM approach involves domain decomposition techniques by means of Lagrange multipliers. In Section 4.4, numerical experiments are carried out regarding the following test cases: (i) a 2D frame structures under plane stresses that involves beam-like structures and curved junctions; (ii) a 3D aircraft fuselage-like structure involving stiffened cylindrical shells, holes and a conical head. The relevance of the WFE-based DSM and RM approaches, in terms of accuracy and computational time savings, is highlighted in comparison with the conventional FE and CB methods.

## 4.2 CB-based super-element modeling for non-periodic coupling junctions

The problem of predicting the dynamic behavior of several periodic structures coupled to elastic junctions is addressed. For the sake of clarity, two periodic structures (e.g., curved stiffened panels) — namely $(P_1)$ and $(P_2)$ — which are connected to an elastic junction $(P_3)$ (e.g., stiffened panel with a hole) are shown in Figure 4.1. Here, the vectors of wave amplitudes for the modes traveling along the periodic structures $(P_1)$ and $(P_2)$ towards the junction $(P_3)$ are denoted as $\mathbf{Q}_1$ and $\mathbf{Q}_2$, respectively, while those for the modes traveling outward from the junction are denoted as $\mathbf{Q}_1^\star$ and $\mathbf{Q}_2^\star$. A WFE-based super-element modeling of periodic structures has been proposed in Section 3.2. In the present section, the FE method combined with the Craig-Bampton (CB) method (Craig and Bampton, 1968a) is used to model the coupling junctions. In this framework, a coupling junction is modeled by means of static modes and fixed-interface modes. The key idea behind the proposed approach is to select among all the fixed-interface modes those which actually contribute to the system forced response. As just a few modes are involved, the proposed procedure yields significant computational savings, which improves the performance of the CB method for MF analysis. Within the WFE framework, a norm-wise selection criterion of contributing fixed-interface modes has been developed by Mencik (Mencik, 2011). The procedure is briefly recalled hereafter.

Consider the general problem of a coupling junction $(P_c)$ which is coupled to an arbitrary number $R_p$ of periodic structures over boundary interfaces $\left\{\Gamma_p^{(c)}\right\}_{p=1,\cdots,R_p}$ and which is meshed by means of internal and boundary DOFs. Here, the internal DOFs are free from external excitation sources, while the boundary DOFs are those contained on the boundary interfaces $\left\{\Gamma_p^{(c)}\right\}_{p=1,\cdots,R_p}$. The dynamic equilibrium equation of the junction, which links the vectors of displacements/rota-
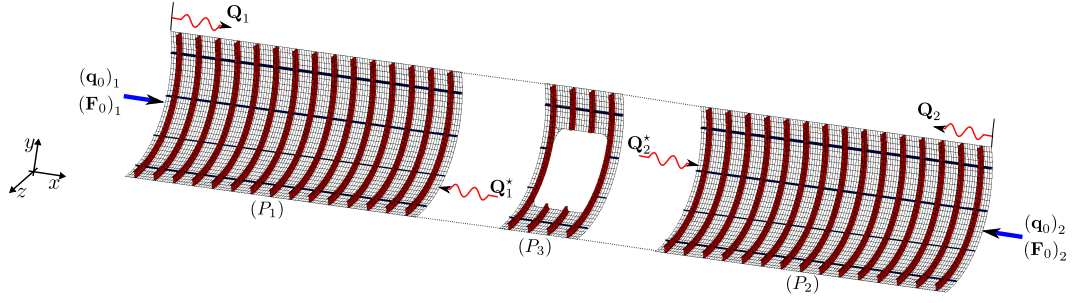
Figure 4.1: Illustration of two periodic structures $(P_1)$ and $(P_2)$ connected to a coupling junction $(P_3)$.

tions $\mathbf{q}^{(c)}$ and forces/moments $\mathbf{F}^{(c)}$ on the boundary DOFs, is expressed as

$$\mathbf{D}^{(c)}\mathbf{q}^{(c)} = \mathbf{F}^{(c)}, \tag{4.1}$$

where $\mathbf{D}^{(c)}$ is the dynamic stiffness matrix of the junction condensed at the boundary DOFs. Within the CB framework (see Annexe A), the matrix $\mathbf{D}^{(c)}$ is expressed in terms of static modes and fixed-interface modes, as follows (Craig and Bampton, 1968a):

$$\mathbf{D}^{(c)} \approx \bar{\mathbf{D}}^{(c)}, \tag{4.2}$$

where

$$\bar{\mathbf{D}}^{(c)} = \mathbf{D}_{\mathtt{st-st}} - \bar{\mathbf{D}}_{\mathtt{el-st}}^T \bar{\mathbf{D}}_{\mathtt{el-el}}^{-1} \bar{\mathbf{D}}_{\mathtt{el-st}}, \tag{4.3}$$

$$\mathbf{D}_{\mathtt{st-st}} = -\omega^2(\mathbf{X}_{\mathtt{st}}^T \mathbf{M}_{\mathtt{II}}^{(c)} \mathbf{X}_{\mathtt{st}} + \mathbf{M}_{\mathtt{BI}}^{(c)} \mathbf{X}_{\mathtt{st}} + \mathbf{X}_{\mathtt{st}}^T \mathbf{M}_{\mathtt{IB}}^{(c)} + \mathbf{M}_{\mathtt{BB}}^{(c)}) + (1+\mathtt{i}\eta^{(c)})(\mathbf{K}_{\mathtt{BI}}^{(c)} \mathbf{X}_{\mathtt{st}} + \mathbf{K}_{\mathtt{BB}}^{(c)}), \tag{4.4}$$

$$\bar{\mathbf{D}}_{\mathtt{el-st}} = -\omega^2 \bar{\mathbf{X}}_{\mathtt{el}}^T (\mathbf{M}_{\mathtt{II}}^{(c)} \mathbf{X}_{\mathtt{st}} + \mathbf{M}_{\mathtt{IB}}^{(c)}), \tag{4.5}$$

$$\bar{\mathbf{D}}_{\mathtt{el-el}} = \mathtt{diag}\left\{\bar{\gamma}_j(-\omega^2 + \bar{\omega}_j^2(1+\mathtt{i}\eta^{(c)}))\right\}_j. \tag{4.6}$$

In these equations, $\mathbf{K}^{(c)}$ and $\mathbf{M}^{(c)}$ are the stiffness and mass matrices of the coupling junction; the subscripts I and B relate the internal and boundary DOFs, respectively. Also, $\mathbf{X}_{\mathtt{st}}$ is the matrix of static modes, defined as $\mathbf{X}_{\mathtt{st}} = -\mathbf{K}_{\mathtt{II}}^{(c)-1}\mathbf{K}_{\mathtt{IB}}^{(c)}$, while $\bar{\mathbf{X}}_{\mathtt{el}}$ is the matrix of fixed-interface modes $\{(\bar{\mathbf{X}}_{\mathtt{el}})_j\}_j$, which are obtained by solving the following eigenproblem $\mathbf{K}_{\mathtt{II}}^{(c)}(\mathbf{X}_{\mathtt{el}})_j = \omega_j^2 \mathbf{M}_{\mathtt{II}}^{(c)}(\mathbf{X}_{\mathtt{el}})_j$ ($\{\bar{\omega}_j\}_j$ being the eigenpulsations that refer to the free vibrations of the undamped junction whose boundary interface DOFs are fixed). The bar sign indicates that a reduced number of fixed-interface modes are retained to formulate the matrix $\mathbf{D}^{(c)}$. Finally, $\eta^{(c)}$ is the loss factor of the junction, while $\{\bar{\gamma}_j\}_j$ denote the modal masses ($\bar{\gamma}_j = (\bar{\mathbf{X}}_{\mathtt{el}})_j^T \mathbf{M}_{\mathtt{II}}^{(c)}(\bar{\mathbf{X}}_{\mathtt{el}})_j \ \forall j$).

The procedure to select the contributing fixed-interface modes $\{(\bar{\mathbf{X}}_{\texttt{el}})_j\}_j$ is based on a perturbation analysis of a matrix $\mathbb{C}$ which relates the reflection/transmission coefficients of wave modes traveling along the periodic structures towards the junction. In case where the FE meshes of the periodic structures are compatible with that of the junction over the coupling interfaces, the matrix $\mathbb{C}$ is defined as (Mencik, 2011)

$$\mathbb{C} = -[\bar{\mathbf{D}}^{(c)}\boldsymbol{\Psi}_{\texttt{q}}^{\star} + \boldsymbol{\Psi}_{\texttt{F}}^{\star}]^{-1}[\bar{\mathbf{D}}^{(c)}\boldsymbol{\Psi}_{\texttt{q}} + \boldsymbol{\Psi}_{\texttt{F}}], \tag{4.7}$$

where

$$\boldsymbol{\Psi}_{\texttt{q}} = \begin{bmatrix} \mathcal{N}_1^{(c)}(\boldsymbol{\Phi}_{\texttt{q}})_1 & \cdots & \mathbf{0} \\ \vdots & \ddots & \vdots \\ \mathbf{0} & \cdots & \mathcal{N}_R^{(c)}(\boldsymbol{\Phi}_{\texttt{q}})_R \end{bmatrix} \quad , \quad \boldsymbol{\Psi}_{\texttt{q}}^{\star} = \begin{bmatrix} \mathcal{N}_1^{(c)}(\boldsymbol{\Phi}_{\texttt{q}}^{\star})_1 & \cdots & \mathbf{0} \\ \vdots & \ddots & \vdots \\ \mathbf{0} & \cdots & \mathcal{N}_R^{(c)}(\boldsymbol{\Phi}_{\texttt{q}}^{\star})_R \end{bmatrix}, \tag{4.8}$$

$$\boldsymbol{\Psi}_{\texttt{F}} = \begin{bmatrix} \mathcal{N}_1^{(c)}(\boldsymbol{\Phi}_{\texttt{F}})_1 & \cdots & \mathbf{0} \\ \vdots & \ddots & \vdots \\ \mathbf{0} & \cdots & \mathcal{N}_R^{(c)}(\boldsymbol{\Phi}_{\texttt{F}})_R \end{bmatrix} \quad , \quad \boldsymbol{\Psi}_{\texttt{F}}^{\star} = \begin{bmatrix} \mathcal{N}_1^{(c)}(\boldsymbol{\Phi}_{\texttt{F}}^{\star})_1 & \cdots & \mathbf{0} \\ \vdots & \ddots & \vdots \\ \mathbf{0} & \cdots & \mathcal{N}_R^{(c)}(\boldsymbol{\Phi}_{\texttt{F}}^{\star})_R \end{bmatrix}. \tag{4.9}$$

Here, the superscript $\star$ relates the wave modes that travel outward from the junction; also, $\mathcal{N}_p^{(c)}$ denotes a direction cosine matrix which links the coordinate system of the junction $(P_c)$ to that of a given periodic structure $(P_p)$ with $p = 1, \cdots, R_p$. In other words, $\mathcal{N}_p^{(c)}$ plays the role of expressing the vectors of displacements/rotations $\mathbf{q}^{(p)}\big|_{\Gamma_p^{(c)}}$ and forces/moments $\mathbf{F}^{(p)}\big|_{\Gamma_p^{(c)}}$ of each periodic structure $(P_p)$, on the coupling interface $\Gamma_p^{(c)}$, in the coordinate system of the coupling junction. This means that the coupling conditions between the junction and the periodic structure are expressed as follows: $\mathbf{q}^{(c)}\big|_{\Gamma_p^{(c)}} = \mathcal{N}_p^{(c)}\mathbf{q}^{(p)}\big|_{\Gamma_p^{(c)}}$ and $\mathbf{F}^{(c)}\big|_{\Gamma_p^{(c)}} = -\mathcal{N}_p^{(c)}\mathbf{F}^{(p)}\big|_{\Gamma_p^{(c)}}$.

The selection of the fixed-interface modes is carried out by assessing how much the matrix $\mathbb{C}$ is perturbed when a given mode $(\mathbf{X}_{\texttt{el}})_j$ is not taken into account in the reduced basis $\{(\bar{\mathbf{X}}_{\texttt{el}})_j\}_j$. Clearly speaking, consider the condensed dynamic stiffness matrix $\mathbf{D}^{(c)}$ of the junction that results from the consideration of all the fixed-interface modes. Omitting one mode $(\mathbf{X}_{\texttt{el}})_j$ yields the perturbed matrix $\bar{\mathbf{D}}^{(c)} = \mathbf{D}^{(c)} + \Delta_j\mathbf{D}^{(c)}$, $\Delta_j\mathbf{D}^{(c)}$ being expressed as (Equations (4.3-4.6)):

$$\Delta_j\mathbf{D}^{(c)} = \frac{\omega^4}{\bar{\gamma}_j(-\omega^2 + \bar{\omega}_j^2(1 + \mathtt{i}\eta^c))}\left(\mathbf{B}^T(\bar{\mathbf{X}}_{\texttt{el}})_j\right)\left(\mathbf{B}^T(\bar{\mathbf{X}}_{\texttt{el}})_j\right)^T, \tag{4.10}$$

where $\mathbf{B} = \mathbf{M}_{\texttt{II}}^{(c)}\mathbf{X}_{\texttt{st}} + \mathbf{M}_{\texttt{IB}}^{(c)}$. Considering $\mathbf{D}^{(c)} + \Delta_j\mathbf{D}^{(c)}$, instead of $\mathbf{D}^{(c)}$, yields the perturbed

matrix $\mathbb{C} + \Delta_j \mathbb{C}$. Hence, the proposed selection procedure consists in retaining the fixed-interface modes which satisfy the following criterion,

$$\frac{\|\Delta_j \mathbb{C}\|_F}{\|\mathbb{C}\|_F} \geq \epsilon \qquad \forall j, \tag{4.11}$$

where $\epsilon$ is a given small tolerance threshold, while $\|.\|_F$ denotes the Frobenius norm. In other words, the selection procedure consists in rejecting the fixed-interface modes for which the relative error $\|\Delta_j \mathbb{C}\|_F / \|\mathbb{C}\|_F$ is below $\epsilon$, meaning that they weakly contribute to the dynamic behavior of the periodic structures that are connected to the junction.

Note that the computation of the relative error $\|\Delta_j \mathbb{C}\|_F / \|\mathbb{C}\|_F$, for each mode $(\mathbf{X}_{\mathtt{el}})_j$, should be performed once, *i.e.*, at the maximum discrete frequency involved in the frequency band of interest. This is understood since a maximum number of wave modes are likely to contribute to the dynamic behavior of periodic structures at the maximum frequency, meaning that reaches $\|\Delta_j \mathbb{C}\|_F / \|\mathbb{C}\|_F$ its maximum value.

## 4.3 Coupled system modeling

The WFE-based numerical model of a fully coupled system, which involves several periodic structures and coupling junctions, is presented. Two well-known procedures are recalled hereafter, which use, respectively, the dynamic stiffness matrices and receptance matrices of subsystems. For the sake of simplicity, it is assumed throughout this section that the FE meshes of the subsystems — *i.e.*, periodic structures and junctions — are compatible at the coupling interfaces.

### 4.3.1 Dynamic stiffness matrix (DSM) method

Consider a coupled system that involves $N_p$ periodic structures and $N_c$ coupling junctions. Also, denote as $\mathcal{O}_p$ and $\mathcal{O}_c$ ($\mathcal{O}_p \cap \mathcal{O}_c = \emptyset$) the sets of integers used to number the periodic structures and the coupling junctions, respectively. Within the DSM framework, the global dynamic stiffness matrix of the coupled system — namely $\mathbf{D}^{\mathtt{gl}}$ — is constructed from the dynamic stiffness matrices

of the periodic structures and coupling junctions (see Sections 3.2.2 and 4.2). The construction of $\mathbf{D}^{\mathrm{gl}}$ follows from a classic assembly procedure, *i.e.*,

$$\mathbf{D}^{\mathrm{gl}} = \sum_{p \in \mathcal{O}_p} \mathcal{L}^{(p)T} \hat{\mathbf{D}}^{(p)} \mathcal{L}^{(p)} + \sum_{c \in \mathcal{O}_c} \mathcal{L}^{(c)T} \hat{\mathbf{D}}^{(c)} \mathcal{L}^{(c)}, \tag{4.12}$$

where $\mathcal{L}^{(p)}$ and $\mathcal{L}^{(c)}$ are mesh incidence matrices; also, $\hat{\mathbf{D}}^{(p)}$ and $\hat{\mathbf{D}}^{(c)}$ are defined as

$$\hat{\mathbf{D}}^{(p)} = \mathcal{N}^{(p)T} \mathbf{D}^{(p)} \mathcal{N}^{(p)} \quad , \quad \hat{\mathbf{D}}^{(c)} = \mathcal{N}^{(c)T} \mathbf{D}^{(c)} \mathcal{N}^{(c)}, \tag{4.13}$$

where $\mathcal{N}^{(p)}$ and $\mathcal{N}^{(c)}$ are direction cosine matrices which link the local coordinate frames of the periodic structures and coupling junctions, respectively, to the global coordinate frame of the coupled system.

The dynamic equilibrium equation of a coupled system, free from kinematic constraints — *i.e.*, prescribed displacements/rotations —, is expressed as $\mathbf{D}^{\mathrm{gl}} \mathbf{q}^{\mathrm{gl}} = \mathbf{F}^{\mathrm{gl}}$, where $\mathbf{q}^{\mathrm{gl}}$ and $\mathbf{F}^{\mathrm{gl}}$ are vectors of nodal displacements/rotations and forces/moments, respectively. More generally, the consideration of kinematic constraints yields the following dynamic equilibrium equation:

$$\mathbf{D}_{\mathrm{II}}^{\mathrm{gl}} \mathbf{q}_{\mathrm{I}}^{\mathrm{gl}} = \mathbf{F}_{\mathrm{I}}^{\mathrm{gl}} - \mathbf{D}_{\mathrm{IB}}^{\mathrm{gl}} \mathbf{q}_{\mathrm{B}}^{\mathrm{gl}}, \tag{4.14}$$

where $\mathbf{q}_{\mathrm{B}}^{\mathrm{gl}}$ denotes a vector of prescribed displacements/rotations. Here, the subscript B (resp. I) relates the DOFs subject to (resp. free from) kinematic constraints. The vector of nodal displacements/rotations of the coupled system is finally assessed by solving Equation (4.14), *i.e.*,

$$\mathbf{q}_{\mathrm{I}}^{\mathrm{gl}} = (\mathbf{D}_{\mathrm{II}}^{\mathrm{gl}})^{-1} \left( \mathbf{F}_{\mathrm{I}}^{\mathrm{gl}} - \mathbf{D}_{\mathrm{IB}}^{\mathrm{gl}} \mathbf{q}_{\mathrm{B}}^{\mathrm{gl}} \right). \tag{4.15}$$

### 4.3.2 Receptance matrix (RM) method

An alternative strategy is investigated to determine the vector of nodal displacements/rotations of the coupled system. It uses the concept of domain decomposition techniques in which

receptance matrices of subsystems are involved. In fact, the receptance matrix $\mathbf{R}^{(p)}$ of a periodic structure ($P_p$) can be easily computed from Equation (3.29), without the need of explicitly inverting a dynamic stiffness matrix. This means computational time savings compared to the DSM method, *i.e.*, when the inverse of a global matrix $\mathbf{D}_{\mathtt{II}}^{\mathtt{gl}}$ (Equation (4.15)) is estimated. This interesting feature has motivated the development of the present RM method. The latter is detailed as follows.

Recall that the FE meshes of the subsystems are compatible at the coupling interfaces. By considering the conventional domain decomposition method with Lagrange multipliers, the local dynamic equilibrium equations, for the periodic structures and coupling junctions, can be expressed in the following way:

$$\hat{\mathbf{D}}^{(p)}\hat{\mathbf{q}}^{(p)} = \hat{\mathbf{F}}^{(p)} - \mathcal{B}^{(p)T}\boldsymbol{\lambda}_{\mathtt{LM}} \quad , \quad \hat{\mathbf{D}}^{(c)}\hat{\mathbf{q}}^{(c)} = \hat{\mathbf{F}}^{(c)} - \mathcal{B}^{(c)T}\boldsymbol{\lambda}_{\mathtt{LM}}, \tag{4.16}$$

where $\hat{\mathbf{q}}$ and $\hat{\mathbf{F}}$ relate, respectively, vectors of nodal displacements/rotations and forces/moments in the global reference frame of the coupled system; also, $\mathcal{B}^{(p)}$ and $\mathcal{B}^{(c)}$ are Boolean matrices, while $\boldsymbol{\lambda}_{\mathtt{LM}}$ is to be understood as a vector of Lagrange multipliers. Notice that the length of the vector $\boldsymbol{\lambda}_{\mathtt{LM}}$ is equal to the total number of interface DOFs — *i.e.*, those involved in the coupling between the subsystems — and boundary DOFs where prescribed displacements/rotations are applied.

The consideration of receptance matrices yields

$$\hat{\mathbf{q}}^{(p)} = \hat{\mathbf{R}}^{(p)}\left(\hat{\mathbf{F}}^{(p)} - \mathcal{B}^{(p)T}\boldsymbol{\lambda}_{\mathtt{LM}}\right) \quad , \quad \hat{\mathbf{q}}^{(c)} = \hat{\mathbf{R}}^{(c)}\left(\hat{\mathbf{F}}^{(c)} - \mathcal{B}^{(c)T}\boldsymbol{\lambda}_{\mathtt{LM}}\right). \tag{4.17}$$

Here, $\hat{\mathbf{R}}^{(p)} = \mathcal{N}^{(p)T}\mathbf{R}^{(p)}\mathcal{N}^{(p)}$ where $\mathbf{R}^{(p)}$ is the receptance matrix of a periodic structure ($P_p$) in its local coordinate frame ( Equation (3.29)), while $\mathcal{N}^{(p)}$ is a direction cosine matrix defined after Equation (4.13). Also, the receptance matrix of a coupling junction ($P_c$) is to be expressed as $\hat{\mathbf{R}}^{(c)} = (\hat{\mathbf{D}}^{(c)})^{-1}$, $\hat{\mathbf{D}}^{(c)}$ being the dynamic stiffness matrix of the junction in the global reference frame (Equation (4.13)).

The consideration of kinematic constraints — which relate the coupling conditions between subsystems as well as the boundary conditions where prescribed displacements/rotations apply — leads to

$$\sum_{p\in\mathcal{O}_p} \mathcal{B}^{(p)}\hat{\mathbf{q}}^{(p)} + \sum_{c\in\mathcal{O}_c} \mathcal{B}^{(c)}\hat{\mathbf{q}}^{(c)} = \mathbf{q}_0^{\mathtt{gl}}, \tag{4.18}$$

where $\mathbf{q}_0^{\mathtt{gl}}$ is a vector of prescribed displacements/rotations, which may be partitioned as $\mathbf{q}_0^{\mathtt{gl}} =$

$[\mathbf{0}^T (\mathbf{q}_{\text{B}}^{\text{gl}})^T]^T$, where $\mathbf{q}_{\text{B}}^{\text{gl}}$ has been defined previously, see Equation (4.14). The determination of the vector of Lagrange multipliers $\boldsymbol{\lambda}$ in Equation (4.16) follows from Equation (4.18) as (Klerk *et al.*, 2006):

$$\boldsymbol{\lambda}_{\text{LM}} = \left(\mathcal{B}\mathbf{R}^{\text{gl}}\mathcal{B}^T\right)^{-1} \left(\mathcal{B}\mathbf{R}^{\text{gl}}\mathbf{F}^{\text{gl}} - \mathbf{q}_0^{\text{gl}}\right), \tag{4.19}$$

where $\mathcal{B} = [\mathcal{B}^{(1)}\mathcal{B}^{(2)} \cdots \mathcal{B}^{(N_p+N_c)}]$, and

$$\mathbf{R}^{\text{gl}} = \begin{bmatrix} \hat{\mathbf{R}}^{(1)} & \mathbf{0} & \cdots & \mathbf{0} \\ \mathbf{0} & \hat{\mathbf{R}}^{(2)} & \cdots & \mathbf{0} \\ \vdots & \vdots & \ddots & \vdots \\ \mathbf{0} & \mathbf{0} & \cdots & \hat{\mathbf{R}}^{(N_p+N_c)} \end{bmatrix} , \quad \mathbf{F}^{\text{gl}} = \begin{bmatrix} \hat{\mathbf{F}}^{(1)} \\ \hat{\mathbf{F}}^{(2)} \\ \vdots \\ \hat{\mathbf{F}}^{(N_p+N_c)} \end{bmatrix} . \tag{4.20}$$

The determination of the vector of nodal displacements/rotations of the coupled system finally results from Equation (4.17).

It is worth pointing out that the computation of the vector of Lagrange multipliers $\boldsymbol{\lambda}_{\text{LM}}$ involves inverting a matrix $(\mathcal{B}\mathbf{R}^{\text{gl}}\mathcal{B}^T)$ whose size relates the number of kinematic constraints only. This means that the size of $(\mathcal{B}\mathbf{R}^{\text{gl}}\mathcal{B}^T)$ can be small compared to the global dynamic stiffness matrix $\mathbf{D}_{\text{II}}^{\text{gl}}$ appearing in Equation (4.15), provided that the number of kinematic constraints is small compared to the total number of coupling interface DOFs and boundary DOFs of the whole system. In this case, the RM method appears to be interesting for improving the computational speed of the proposed WFE approach. Notice, however, that the matrix $(\mathcal{B}\mathbf{R}^{\text{gl}}\mathcal{B}^T)$ is expected to be dense as opposed to $\mathbf{D}_{\text{II}}^{\text{gl}}$, which contains several zero block components. In other words, the RM method can be considered efficient only when the size of $(\mathcal{B}\mathbf{R}^{\text{gl}}\mathcal{B}^T)$ is significantly small compared to $\mathbf{D}_{\text{II}}^{\text{gl}}$. This feature will be highlighted in Section 4.4.2.

## 4.4   Numerical results

The WFE-based DSM and RM methods are applied to compute the frequency forced response of two elastic systems involving periodic structures and elastic junctions. Recall that, within the present framework, the periodic structures are modeled using the WFE method (Section 3.2), while the coupling junctions are modeled using the CB method (Section 4.2). Here, a reduced set of fixed-interface modes, which are selected by means of the WFE-based strategy proposed in Section 4.2,

is used to model the junctions.

The following test cases are considered: (1) a 2D frame structure under plane stresses (Figure 4.3); (2) a 3D aircraft fuselage-like structure involving stiffened cylindrical shells (Figure 4.8). The first test case is rather simple, while the second one includes complexities of real engineering applications.

For each test case, the frequency response functions (FRFs) provided by the WFE-based DSM and RM approaches are compared with a reference FE solution issued from the ANSYS® software, which uses a sparse direct solver. Also, the DSM and RM approaches are compared with the conventional CB method, *i.e.*, when each subsystem (periodic structure, junction) is modeled in terms of static modes and fixed-interface modes. For the sake of clarity, the numerical tasks and platform environments involved when simulating the DSM and RM approaches are shown in Figure 4.2. Regarding the WFE and CB modelings, ANSYS® is used as a means to assess the mass and stiffness matrices of substructures and subsystems. Post-treatment of those matrices is achieved using MATLAB® with a view to computing the forced response of the coupled system. All the numerical simulations are performed in double precision using a 64-bit CPU equipped with an Intel® Xeon® E5-2609 2.40 GHz processor and 32GB of RAM memory. It is worth emphasizing that the MATLAB® environment is used as a means to assess the performances of the DSM and RM approaches in terms of computational time savings, when compared to the conventional CB method.

### 4.4.1   2D frame structure

**Problem description**

This section investigates the harmonic response of a 2D frame structure undergoing plane stresses. The structure can be partitioned into three straight beam-like structures $(P_1)$, $(P_2)$ and $(P_3)$, and two quarters of torus (junctions $(P_4)$ and $(P_5)$), as shown in Figure 4.3. Here, the beam-like structures are considered periodic, it being understood that their meshes are periodic (as outlined in Chapter 2). The whole structure is clamped over its left bottom edge while being subject to harmonic nodal loads $(F_x = 100\ N, F_y = 50\ N)$ over the whole right bottom edge. The periodic structures and junctions exhibit the following characteristics: Young's modulus $E = 2.1 \times 10^{11}$ Pa,
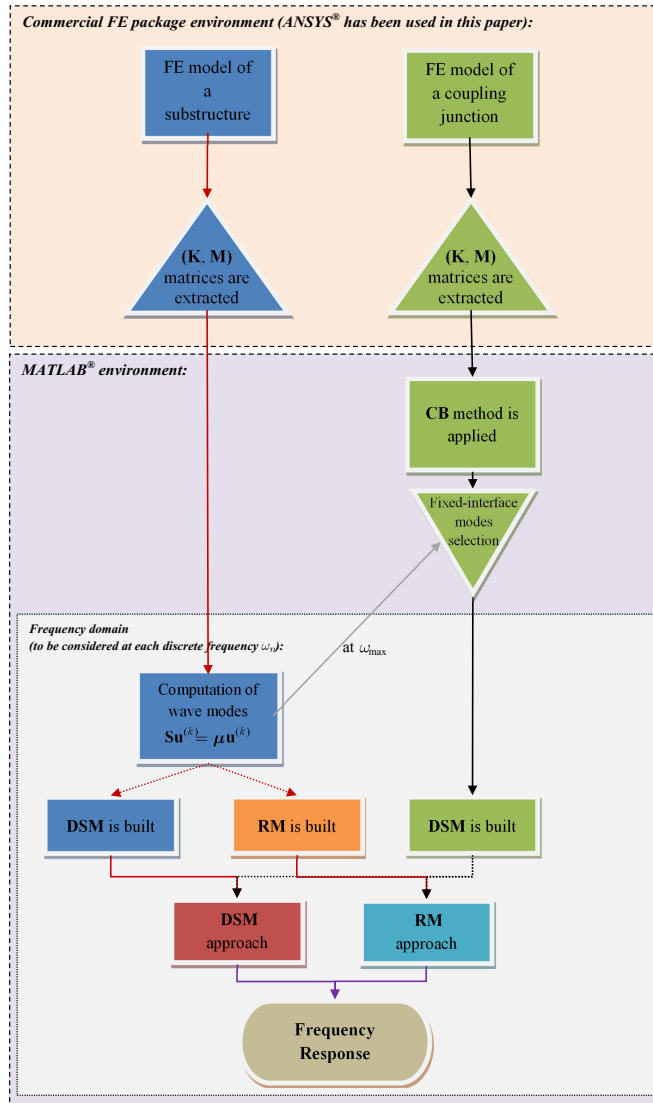
Figure 4.2: Numerical steps involved in the DSM and RM approaches.

density $\rho = 7850\,\text{kg.m}^{-3}$, Poisson's ratio $\nu = 0.3$, loss factor $\eta = 0.01$, thickness $0.001$ m and width $0.4$ m. The length of the periodic structures $(P_1)$ and $(P_3)$ is $2$ m, while that of the periodic structure $(P_2)$ is $1.5$ m. Besides, the coupling junctions $(P_4)$ and $(P_5)$ exhibit an internal and external radius of curvature of $0.2$ m and $0.4$ m, respectively.

Within the WFE framework, each periodic structure is modeled by means of identical substructures, as explained in Chapter 2. Here, the substructures used are similar (up to a rotation of $90^o$), with a length $\Delta = 0.01$ m (Figure 4.3). Thus, it turns out that the periodic structures $(P_1)$
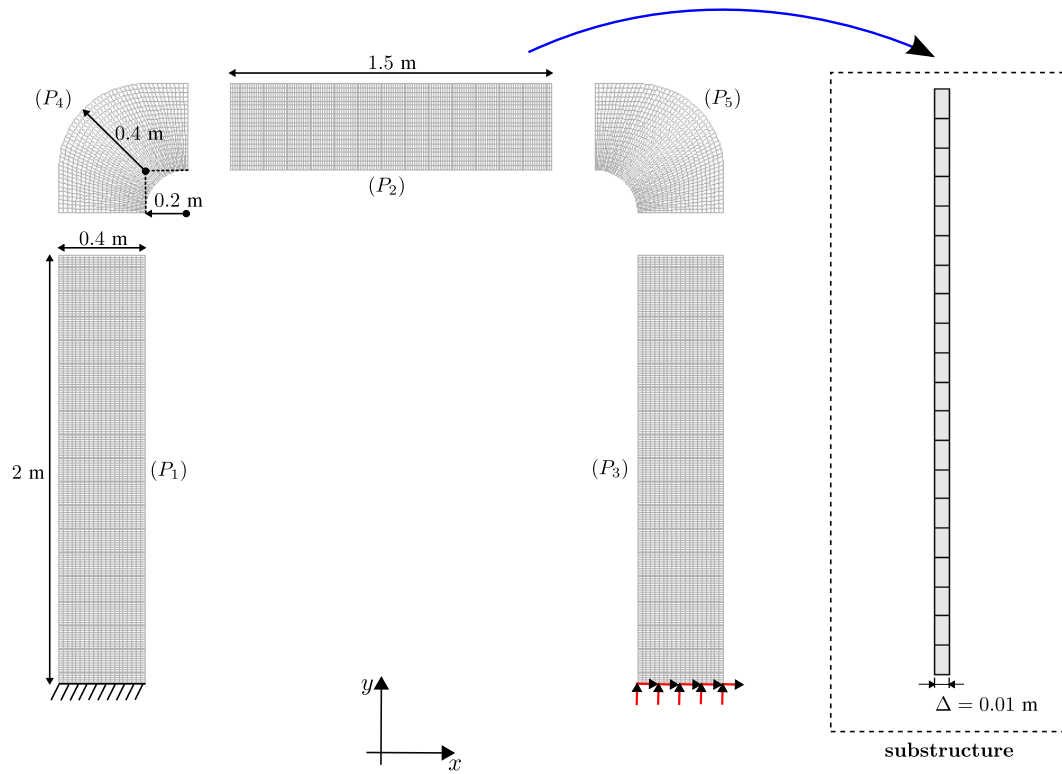
Figure 4.3: 2D frame structure composed of three periodic structures $(P_1)$, $(P_2)$ and $(P_3)$, and two coupling junctions $(P_4)$ and $(P_5)$; FE model of a substructure that is used to model the periodic structure $(P_2)$.

and $(P_3)$ are composed of $N_1 = N_3 = 200$ substructures, while the periodic structure $(P_2)$ is composed of $N_2 = 150$ substructures. Besides, 2D plane stress quadrilateral elements, with four nodes and two translational DOFs per node, are used to model the substructures as well as the coupling junctions (Figure 4.3). Each substructure is meshed by means of 20 finite elements over its width, which yields $n = 42$ DOFs over the left/right boundary and no internal DOFs. Also, each coupling junction is meshed by means of $2{,}226$ DOFs that incorporate $42$ DOFs over each coupling interface. As a result, the number of DOFs involved for modeling the whole coupled system is $27{,}468$. This mesh is expected to be fine enough to capture the local stress fields, which can be sharp in the vicinity of the corners, as well as the propagating wave modes along the periodic structures. Here, about $30$ elements, at least, are used to capture the wavelengths of the propagating wave modes at the highest frequency considered[1], which fully agrees with the classic rule of thumb of $8$ elements per wavelength.

---

[1]This can be proved by plotting the related dispersion curves which are not shown here for the sake of conciseness.

The harmonic response of the coupled system is analyzed over a frequency band $\beta_f = [110 - 10{,}000]$ Hz that involves discrete frequencies that are equally spaced with a step of 10 Hz. This frequency band is supposed to be wide enough so that the periodic structures and the junctions exhibit local resonances.

## Junction modeling

The modeling of each junction is carried out by considering the CB strategy proposed in Section 4.2. Recall that the standard strategy for selecting the fixed-interface modes of a junction is to retain those for which the eigenfrequencies are below a certain frequency limit, while rejecting the other modes. As a rule of thumb, this frequency limit is classically chosen as twice the maximum frequency of the frequency band of interest, *i.e.*, 20,000 Hz in the present case. This yields 51 fixed-interface modes to be retained (cf. Figure 4.4(a)). In contrast, the selection strategy proposed in Section 4.2 enables one to retain 43 fixed-interface modes only, which means subsequent computational time savings. This is done by considering a tolerance threshold $\epsilon = 1\%$ in Equation (4.11), when the ratio $\|\Delta_j\mathbb{C}\|_F / \|\mathbb{C}\|_F$ is calculated for each of the aforementioned 51 modes (see Figure 4.4(b)). This result confirms that the contribution of a junction mode is not necessarily linked to its rank.

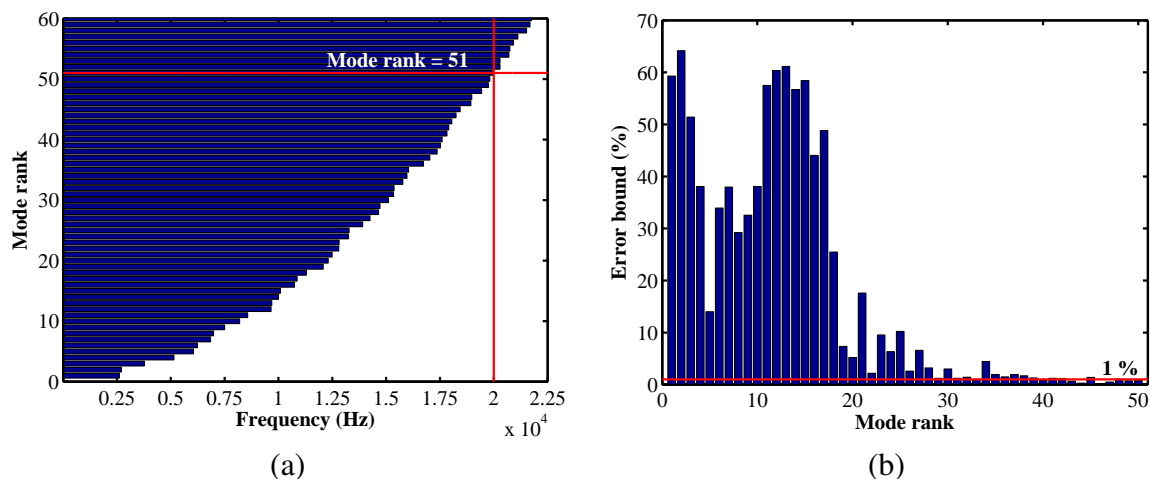

Figure 4.4: Strategies used to select the fixed-interface modes of the coupling junctions $(P_4)$ and $(P_5)$ occurring in the 2D frame structure: (a) classic strategy consisting in retaining the modes whose eigenfrequencies are below twice the maximum frequency of the frequency band of interest (this yields $51$ modes); (b) WFE-based strategy proposed in Section 4.2 (this yields $43$ modes).

**Forced response computation**

The FRF of the 2D frame structure is assessed by means of the WFE-based DSM and RM approaches depicted in Section 4.3. In this framework, each periodic structure is modeled using the WFE method (Section 3.2), while the coupling junctions are modeled using the CB method (Section 4.2). In the present case, the number of right/left-going wave modes involved for modeling each periodic structure is $n = 42$. Here, the magnitude of the velocity ($y$-direction) of the periodic structure $(P_3)$ is analyzed at a corner node on the right excited edge. The WFE solutions are compared with the results issued from the conventional FE method in Figure 4.5(a). Also, the relative error of the WFE solutions, averaged over several sub-frequency bands $\{\beta_f^i\}_i$ of same width, is displayed in Figure 4.5(b). Such an average procedure is used here as a means to clearly highlight the frequency zone over which the relative error is high. Also, it acts like a filter to smoothen the effects of slight shifts between the resonance frequencies of the WFE and FE solutions, which generate high errors locally although they are of minor importance. The relative error is expressed as

$$\frac{< \|\mathbf{q}_{\texttt{meas}}^{\texttt{WFE}}\|_2 - \|\mathbf{q}_{\texttt{meas}}^{\texttt{FE}}\|_2 >_{\beta_f^i}}{< \|\mathbf{q}_{\texttt{meas}}^{\texttt{FE}}\|_2 >_{\beta_f^i}}, \tag{4.21}$$

where $\mathbf{q}_{\texttt{meas}}$ denotes the vector of nodal displacements at the measurement point, while the notation $< \, . \, >_{\beta_i}$ denotes the quadratic mean over a sub-frequency band $\beta_f^i$. Here, ten sub-frequency bands $\{\beta_f^i\}_i$ are considered which cover the whole frequency band $\beta_f$ (*i.e.*, $\beta_f = \cup_i \beta_f^i$). As it can be seen, the WFE results completely match the reference FE solution over the whole frequency band where the relative error (Equation (4.21)) never exceeds 5%. This fully validates the proposed approaches.

Besides, the WFE approaches are compared with the conventional CB method that consists in modeling each subsystem (periodic structure, junction) in terms of static modes and fixed-interface modes. For the purpose of the conventional CB method, each junction is modeled by means of 51 fixed-interface modes, as suggested by the rule of thumb consisting in selecting the modes whose eigenfrequencies are below twice the maximum frequency of the frequency band of interest. Within the CB method, two procedures are investigated to model the periodic structures, *i.e.*: (1) by considering a large number of fixed-interface modes whose eigenfrequencies are below four times the maximum frequency of the frequency band of interest — this yields 531 fixed-interface modes for the periodic structures $(P_1)$ and $(P_3)$, and 396 fixed-interface modes for the periodic structure $(P_2)$; (2) by considering a small number of fixed-interface modes which is equal to that of the right/left-going wave modes of each periodic structure — this yields 42 fixed-interface modes only.
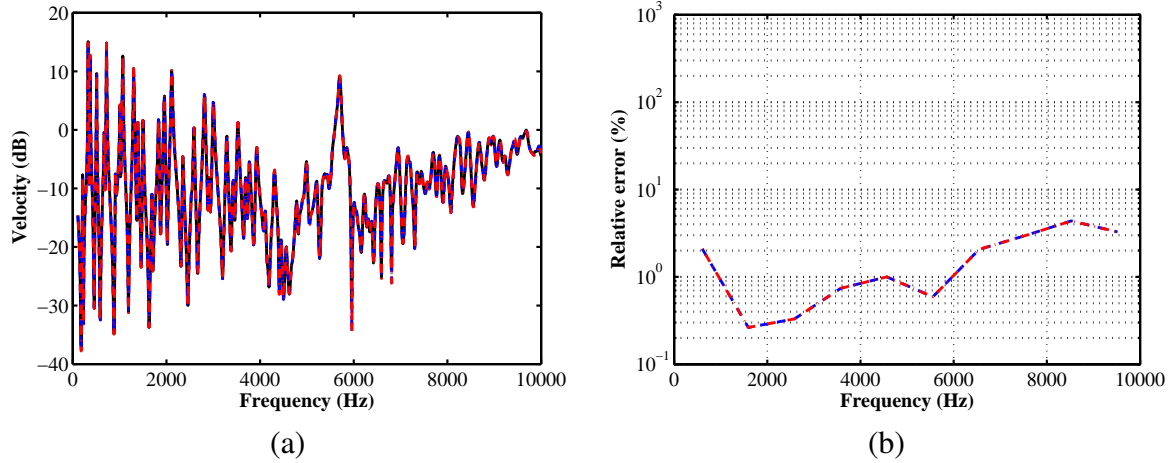
Figure 4.5: FRF of the 2D frame structure (a) and relative error, Eq. (4.21) (b): FE solution (——);
WFE-based DSM approach (- - -); WFE-based RM approach (- - -).

The related FRFs are displayed in Figure 4.6(a), along with the following relative error (Figure 4.6(b)):

$$\frac{< \|\mathbf{q}_{\text{meas}}^{\text{CB}}\|_2 - \|\mathbf{q}_{\text{meas}}^{\text{FE}}\|_2 >_{\beta_f^i}}{< \|\mathbf{q}_{\text{meas}}^{\text{FE}}\|_2 >_{\beta_f^i}}, \tag{4.22}$$

As it can be seen, the relative error involved in the first CB modeling remains confined below $5\%$ in the same way as the WFE-based approaches. In contrast, the second CB modeling which uses $42$ fixed-interface modes for each periodic structure yields erroneous results, as shown in Figure 4.6(a). In this case, the basis of fixed-interface modes and static modes used to model each periodic structure has been chosen so that its dimension is equal to that of the wave mode basis used by the DSM and RM approaches. From this point of view, the WFE-based DSM and RM approaches are much more accurate than the CB method. For the sake of clarity, the maximum values of the relative errors — *i.e.*, when averaged over all the sub-frequency bands $\{\beta_f^i\}_i$ — involved in the WFE and CB solutions are compared as shown in Figure 4.7(a).

Regarding the elapsed/running times, it takes $183$ s and $190$ s to compute the forced response of the coupled system with the WFE-based DSM and RM approaches, respectively, against $838$ s with the conventional CB method that uses $531$ and $396$ fixed-interface modes for the periodic structures. It is worth recalling that those elapsed times are obtained using MATLAB® regarding both the WFE and CB techniques. This yields a computational saving of $78\%$ in benefit of the DSM and RM approaches, which clearly highlights the relevance of the proposed approaches. It should be emphasized that the WFE-based DSM and RM methods give almost the same elapsed
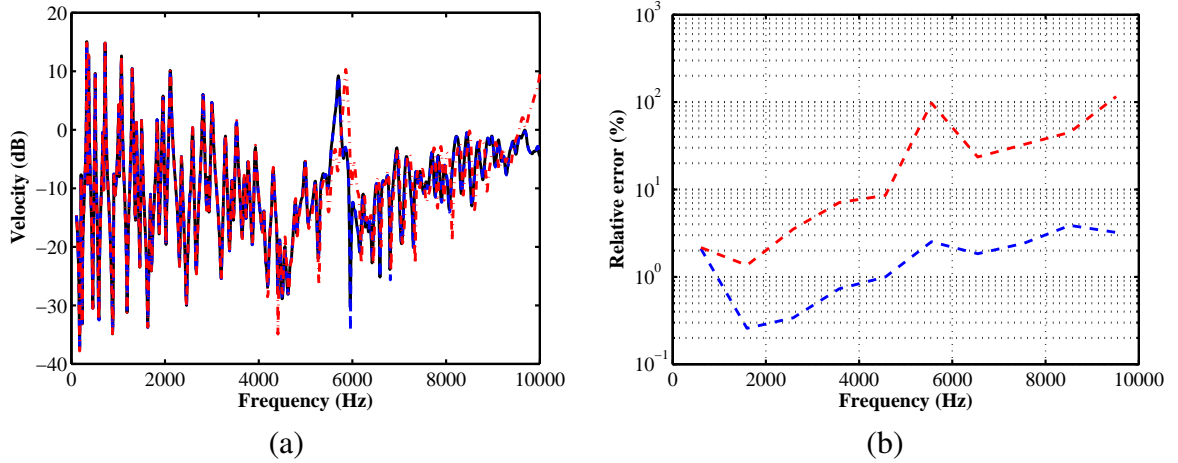
Figure 4.6: FRF of the 2D frame structure (a) and relative error, Eq. (4.22) (b): FE solution (——);
CB method that uses $531$ and $396$ fixed-interface modes to model the periodic structures (- - -); CB
method that uses $42$ fixed-interface modes to model the periodic structures (- - -).

time, which might be explained because the matrices $\mathbf{D}^{gl}{}_{\mathrm{II}}$ and $(\mathcal{B}\mathbf{R}^{gl}\mathcal{B}^T)$ which are inverted in
Equations 4.15 and 4.19 have the same size. This is due to the fact that, in the present case, the
number of boundary DOFs where prescribed forces are applied is equal to that where prescribed
displacements are considered.

For the sake of clarity, the elapsed time involved when computing the full FE model with
MATLAB® has been also assessed. For this purpose, a matrix system is to be solved which requires
the inversion of a $27{,}468 \times 27{,}468$ sparse dynamic stiffness matrix at several frequency steps. This
gives $21{,}612$ s, which appears to be $26$ times larger compared to the first CB modeling and means
$99\%$ time saving in benefit of the WFE method.

Finally, note that the conventional CB method that uses $42$ fixed-interface modes for the
periodic structures yields a elapsed time of $138$ s, which appears small compared to the WFE ap-
proaches. However, as outlined previously, such a method appears inefficient to accurately capture
the FRF of the system. For the sake of conciseness and clarity, the elapsed times involved in the
WFE and CB approaches are shown in Figure 4.7(b) and Table 4.1. Also, the total number of
physical and generalized DOFs managed by each approach is listed in Table 4.1. Regarding the
FE method, this number corresponds to the total number of DOFs involved in the full FE model;
regarding the conventional CB method, it corresponds to the sum of the numbers of static modes
and fixed-interface modes among all the structural components (periodic structures and junctions);
regarding the WFE approaches, it corresponds to the sum of the number of boundary DOFs of

the periodic structures with the number of static modes and fixed-interface modes of the junctions. This provides a coarse estimate of the size of the matrix equations which are to be managed by each approach. As it can be seen, the total number of DOFs involved in the WFE-based DSM and RM approaches constitutes a better compromise between accuracy and performance than it is the case with the CB method.



(a)  (b)
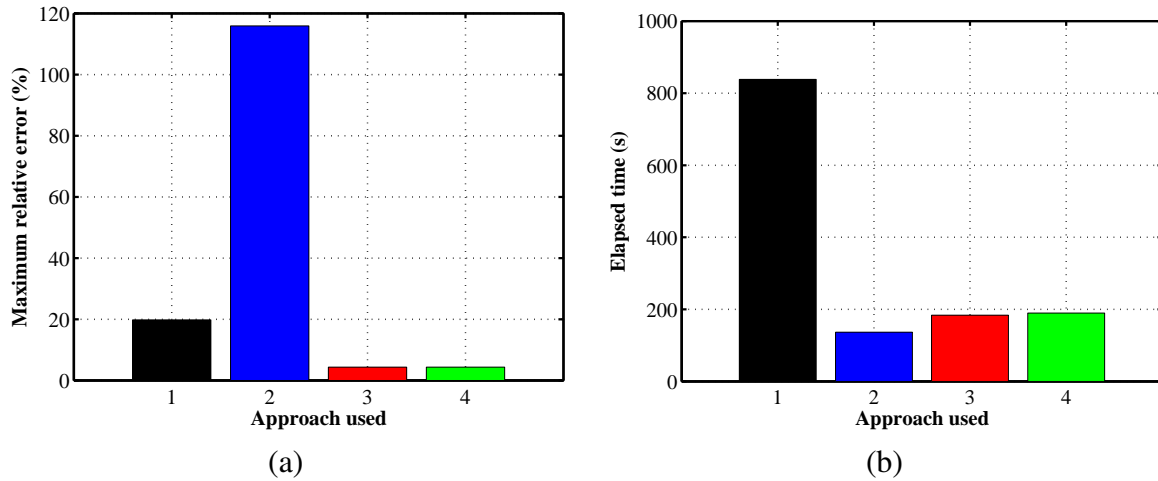
Figure 4.7: Maximum relative errors (a), and elapsed times (b) involved regarding the 2D frame structure: (black) CB method that uses $531$ and $396$ fixed-interface modes to model the periodic structures; (blue) CB method that uses $42$ fixed-interface modes to model the periodic structures; (red) WFE-based DSM approach; (green) WFE-based RM approach.

Table 4.1: Total number of DOFs and elapsed times involved by the proposed approaches regarding the 2D frame structure.

| Approach | Total number of DOFs | Elapsed time (s) | Reduction (%) |
|---|---|---|---|
| FE | 27,468 | 21,612 | — |
| CB (531 and 396 modes) | 1,595 | 838 | — |
| CB (42 modes) | 648 | 137 | 84 |
| DSM | 506 | 184 | 78 |
| RM | 506 | 190 | 77 |

### 4.4.2 Aircraft fuselage-like structure

### Problem description

This section investigates the harmonic response of an aircraft fuselage-like structure. The structure under concern consists of a conical head (coupling junction $(P_3)$), a long cylindrical shell (periodic structure $(P_1)$), a short cylindrical shell with holes (coupling junction $(P_4)$) that may correspond to aircraft doors, and a short cylindrical shell (periodic structure $(P_2)$) (Figure 4.8). The cylindrical shells incorporate axial and circumferential flat stiffeners (*i.e.*, stringers and frames, respectively) so as to include true periodicities. The coupled system is subject on its right end to two vertical forces acting in opposite directions, as shown in Figure 4.8.

The periodic structures and junctions share the same material characteristics, *i.e.*: Young's modulus $E = 7 \times 10^{10}$ Pa, density $\rho = 2700$ kg.m$^{-3}$, Poisson's ratio $\nu = 0.3$ and loss factor $\eta = 0.01$. The cylindrical shells exhibit a diameter of $4$ m and a thickness of $0.001$ m. The circumferential and axial stiffeners have a height of $0.035$ m, and respective thicknesses of $0.005$ m and $0.002$ m. Those stiffeners are periodically distributed over the cylinders (*i.e.*, periodic structures $(P_1)$ and $(P_2)$, and coupling junction $(P_4)$), two consecutive circumferential (resp. axial) stiffeners being spaced with a length of $0.4$ m (resp. an angle of $11.25°$). Besides, the conical head $(P_3)$ has a parabolic curvature and it does not have stiffeners.

Within the WFE framework, the periodic structures $(P_1)$ and $(P_2)$ are modeled by means of $N_1 = 30$ and $N_2 = 10$ identical substructures, respectively, as shown in Figure 4.8. The substructures and coupling junctions are meshed by means of quadrilateral Reissner-Mindlin shell elements with six DOFs per node, *i.e.*, translations in the $x$, $y$ and $z$ directions and rotations about the same axes. Here, the total number of DOFs used to discretize the whole coupled system is $32,586$. Each substructure is meshed by means of $n = 288$ DOFs over its left/right boundary, and $384$ internal DOFs. Also, the coupling junctions $(P_3)$ and $(P_4)$ are meshed by means of $3,174$ and $2,724$ DOFs, respectively. Finall,y note that the coupling interface between the components $(P_1)$ and $(P_3)$ involves $192$ DOFs — this results from the fact that the conical head $(P_3)$ does not have stiffeners — while the coupling interfaces between the components $(P_1)$ and $(P_4)$, and between the components $(P_2)$ and $(P_4)$, involve $288$ DOFs, respectively.
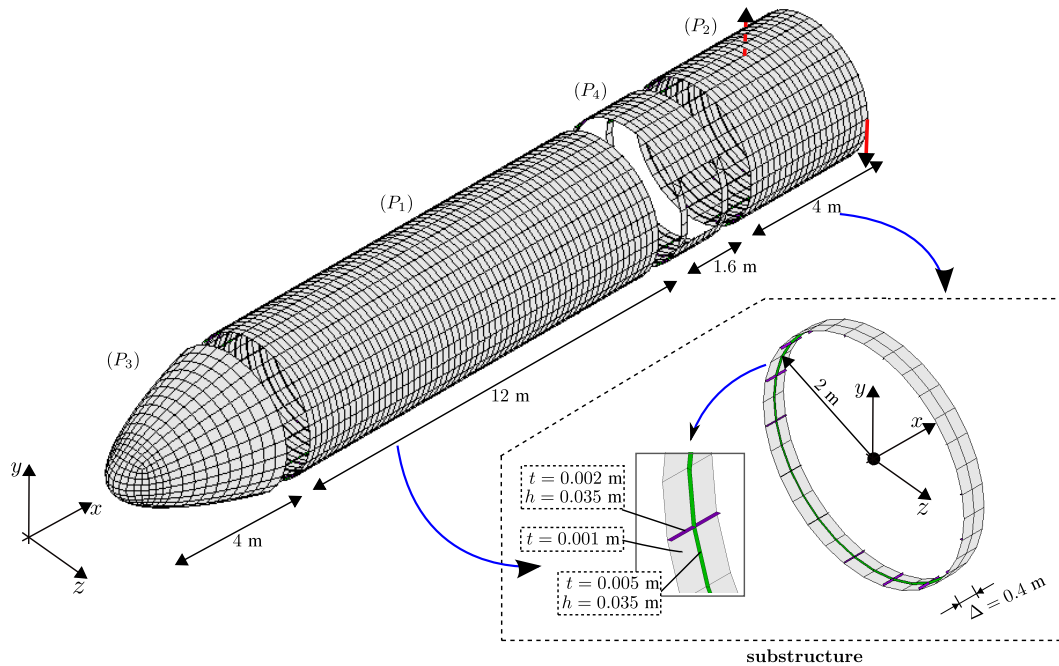
Figure 4.8: 3D aircraft fuselage-like structure composed of two periodic structures $(P_1)$ and $(P_2)$, and two coupling junctions $(P_3)$ and $(P_4)$; FE model of a substructure (cylindrical shell with longitudinal and circumferential stiffeners) that is used to model the periodic structures.

The harmonic response of the coupled system is analyzed over a frequency band $\beta_f = [20 - 200]$ Hz that involves discrete frequencies that are equally spaced with a step of $0.2$ Hz.

## Junction modeling

The CB strategy proposed in Section 4.2 is used to model the coupling junctions $(P_3)$ and $(P_4)$. Again, a tolerance threshold $\epsilon = 1\%$ is considered to carry out the selection of the fixed-interface modes being involved by means of Equation (4.11). Recall that the classic selection strategy consists in retaining the fixed-interface modes for which the eigenfrequencies are smaller than a certain frequency limit, which, in the present case, is chosen as four times the maximum frequency of the frequency band of interest (*i.e.*, $800$ Hz). The choice of this frequency limit is justified by the fact that the coupled system under concern is rather complex — i.e, its geometry is locally heterogeneous, due to stiffeners and holes —, meaning that high order modes are likely to contribute

130

to its dynamic behavior, even at low frequency. This classic selection strategy yields, respectively, 350 and 114 fixed-interface modes for the coupling junctions $(P_3)$ and $(P_4)$, as shown in Figures 4.9(a) and 4.10(a). On the other hand, the WFE-based CB strategy proposed in Section 4.2 enables 107 and 58 fixed-interface modes to be retained among those aforementioned modes, as shown in Figures 4.9(b) and 4.10(b). Notice that high order junction modes are expected to contribute to the system forced response, hence giving credit to the choice of the extended frequency limit (as discussed previously). To summarize, it appears that the proposed selection strategy yields a large decrease in the number of fixed-interface modes to be retained, which means subsequent computational time savings.



(a)                                              (b)

Figure 4.9: Strategies used to select the fixed-interface modes of the coupling junction $(P_3)$ occurring in the fuselage-like structure: (a) classic strategy consisting in retaining the modes whose eigenfrequencies are below four times the maximum frequency of the frequency band of interest (this yields 350 modes); (b) WFE-based strategy proposed in Section 4.2 (this yields 107 modes).

### Forced response computation

The FRF of the aircraft fuselage-like structure is assessed by means of the WFE-based DSM and RM approaches depicted in Section 4.3. Recall that the periodic structures $(P_1)$ and $(P_2)$ (*i.e.*, the stiffened cylindrical shells) are modeled by means of the WFE method (Chapter 3), while the coupling junctions $(P_3)$ and $(P_4)$ (conical head and cylindrical part with doors) are modeled by means of static modes and fixed-interface modes (Section 4.2). Here, the number of right/left-going wave modes involved for modeling each periodic structure — *i.e.*, which relates the number of DOFs used to discretize the cross-section — is $n = 288$, which appears to be large compared to
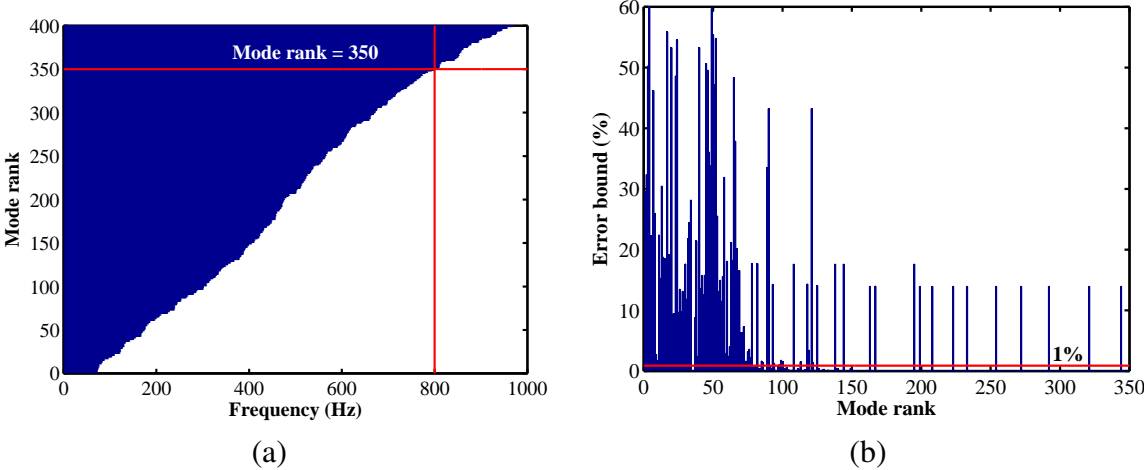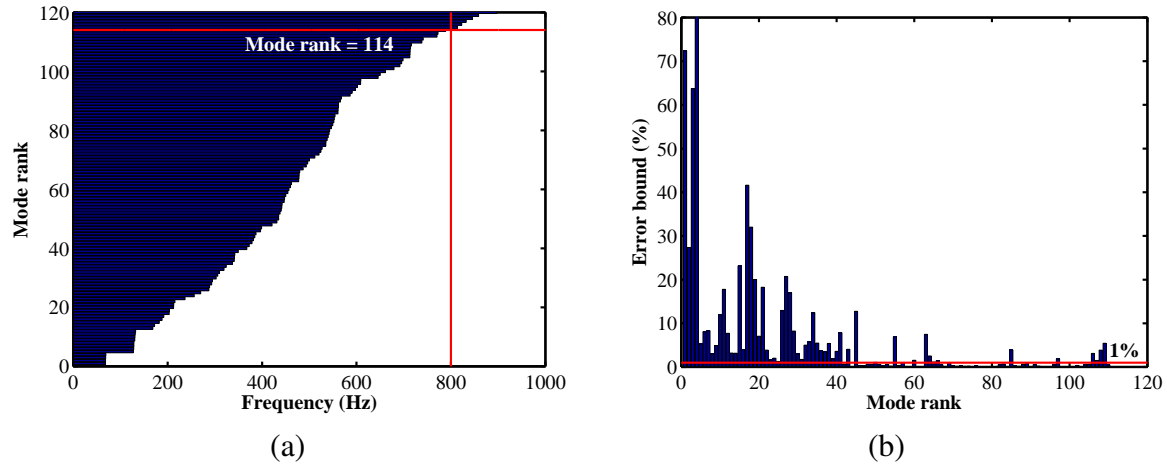
Figure 4.10: Strategies used to select the fixed-interface modes of the coupling junction $(P_4)$ occurring in the fuselage-like structure: (a) classic strategy consisting in retaining the modes whose eigenfrequencies are below four times the maximum frequency of the frequency band of interest (this yields $114$ modes); (b) WFE-based strategy proposed in Section 4.2 (this yields $58$ modes).

the previous test case. The magnitude of the velocity in the vertical $y$-direction, at an excited node, is analyzed over the frequency $\beta_f = [20-200]$ Hz (Figure 4.11(a)). Also, the relative error of the WFE solutions is displayed in Figure 4.11(b). The relative error is expressed by Equation (4.21) when $\mathbf{q}_{\text{meas}}$ denotes the vector of displacements/rotations at the excitation point. As it can be seen, the WFE solutions perfectly agree with the FE results. The relative error of the WFE solutions appears smaller than $6\%$ over the whole frequency band, which fully validates the proposed approaches.
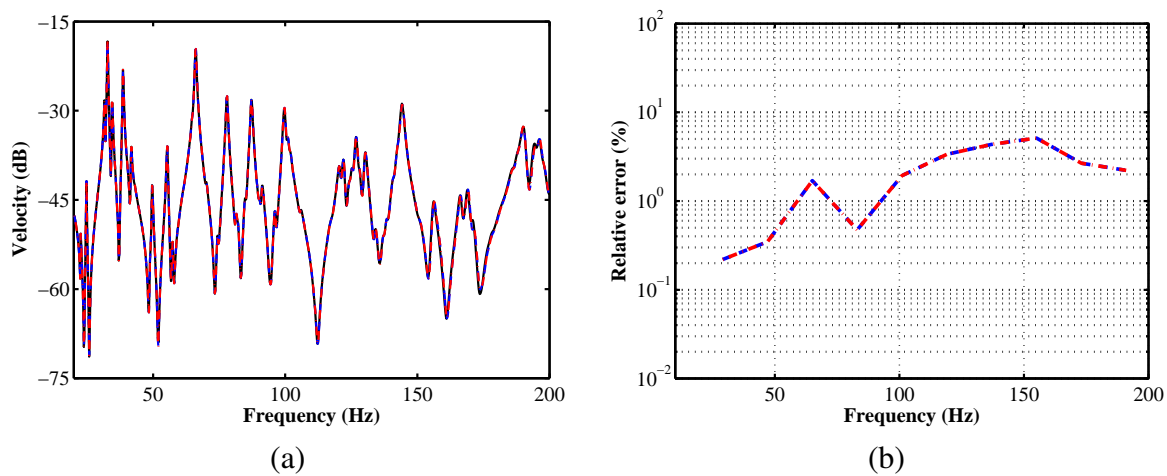


Figure 4.11: FRF of the fuselage-like structure (a) and relative error, Eq. (4.21) (b): FE solution (——); WFE-based DSM approach (- - -); WFE-based RM approach (- - -).

132

Again, the WFE-based approaches are compared with the conventional CB method when each subsystem (periodic structure, coupling junction) is modeled by means of static modes and fixed-interface modes. Here, the coupling junctions $(P_3)$ and $(P_4)$ are modeled by means of $350$ and $114$ fixed-interface modes, respectively, as explained earlier. Also, two procedures are investigated to model the periodic structures $(P_1)$ and $(P_2)$, *i.e.*: (1) when the fixed-interface modes are selected by means of the rule of thumb that consists in retaining those for which the eigenfrequencies are smaller than four times the maximum frequency of the frequency band of interest — this yields $1,133$ fixed-interface modes for the periodic structure $(P_1)$ and $350$ fixed-interface modes for the periodic structure $(P_2)$; (2) when the number of fixed-interface modes is equal to that of the right/left-going wave modes of each periodic structure — this yields $288$ fixed-interface modes for each periodic structure. The related FRFs are displayed in Figure 4.12(a), along with the relative error, Equation (4.22) (Figure 4.12(b)). In addition, the elapsed times and total numbers of physical and generalized DOFs involved in performing the WFE-based approaches and CB methods are listed in Table 4.2. As it can be seen, the WFE-based DSM and RM approaches outperform both CB procedures in terms of computational times. Also, they appear to be more accurate compared to the CB procedure (2), *i.e.*, when the dimension of the basis of static modes and fixed-interface modes is equivalent to that of the basis of wave modes. The solution provided by the CB procedure (2) exhibits a relative error that reaches $29\%$, while the related elapsed time appears almost $50\%$ greater than those involved by the WFE-based approaches. In other words, the CB method requires a mode basis of large dimension to reach the convergence of its solution. Regarding the CB procedure (1), the relative error is very small, but the related elapsed time appears tremendous, *i.e.*, almost $300\%$ greater than those required by the WFE-based approaches. A comparison between the maximum relative errors and the elapsed times involved in the WFE and CB methods is proposed in Figure 4.13. Again, it is clear that the WFE-based DSM and RM approaches constitute the best compromise between accuracy and performance.

To summarize, the WFE-based DSM and RM approaches constitute two efficient numerical tools for assessing the dynamic behavior of coupled systems that involve complex periodic structures. Also note that, in the present case, the elapsed time involved in the RM method is smaller than that of the DSM method. This interesting feature has been underlined in Section 4.3.2 and results from the fact that the size of the matrix $(\mathcal{B}\mathbf{R}^{gl}\mathcal{B}^T)$ in Equation (4.19) — *i.e.*, $768 \times 768$ in the present case — is significantly small compared to that of the matrix $\mathbf{D}_{\mathrm{II}}^{gl}$ in Equation (4.15), which is $1,152 \times 1,152$. This highlights the capability of the proposed RM approach for treating complex coupled systems with many DOFs.

(a)          (b)
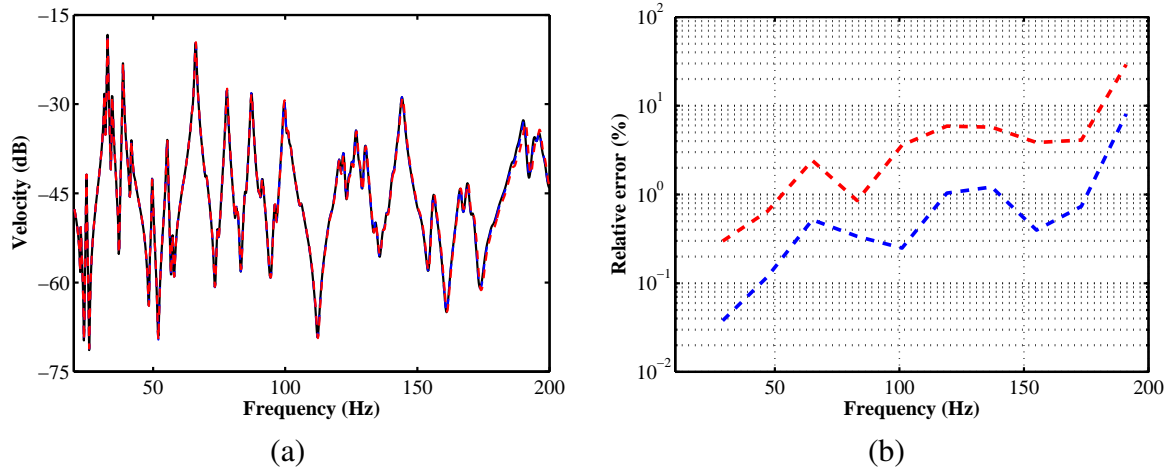
Figure 4.12: FRF of the fuselage-like structure (a) and relative error, Equation (4.22) (b): FE solution (——); CB method that uses $1,133$ and $350$ fixed-interface modes to model the periodic structures (- - -); CB method that uses $288$ fixed-interface modes to model the periodic structures (- - -).



(a)          (b)
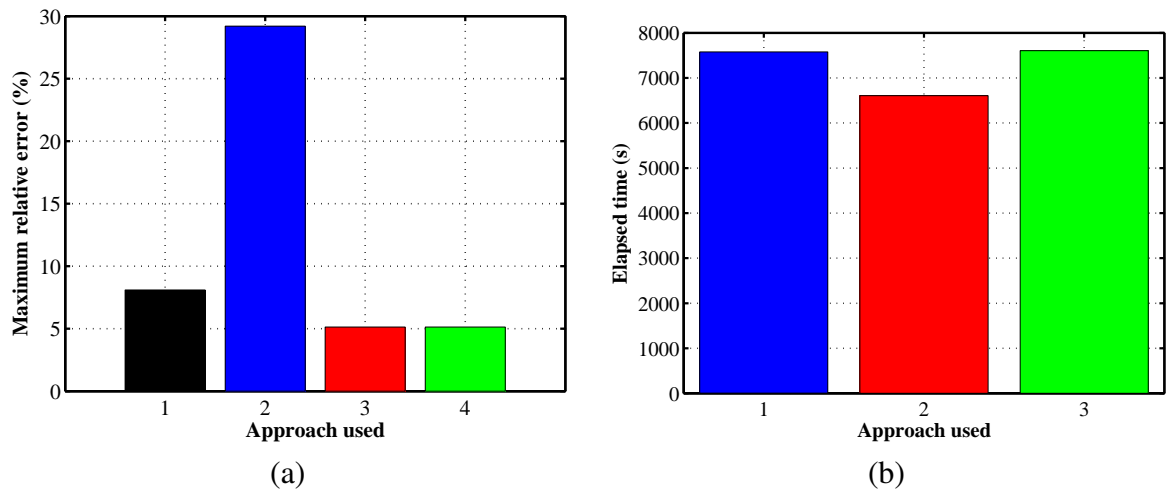
Figure 4.13: Maximum relative errors (a), and elapsed times (b) involved regarding the fuselage-like structure: (black) CB method that uses $1,133$ and $350$ fixed-interface modes to model the periodic structures; (blue) CB method that uses $288$ fixed-interface modes to model the periodic structures; (red) WFE-based DSM approach; (green) WFE-based RM approach.

As a last advantage of the WFE-based approaches, the spatial distribution of the displacement/rotation fields of periodic structures can be assessed without difficulty at a very small computational cost. This is done by considering the vectors of nodal displacements/rotations on the interfaces, between subsystems, and making use of the wave expansion in Equation (3.5). Then,

134

Table 4.2: Total number of DOFs and elapsed times involved by the proposed approaches regarding the aircraft fuselage-like structure.

| Approach | Total number of DOFs | Elapsed time (s) | Reduction (%) |
|---|---|---|---|
| FE | 32,586 | — | — |
| CB (1,133 and 350 modes) | 3,867 | 30,532 | – |
| CB (288 modes) | 2,960 | 11,404 | 63 |
| DSM | 2,085 | 7,577 | 75 |
| RM | 2,085 | 6,608 | 78 |

the vector of nodal displacements/rotations, on any substructure boundary $k$, is expressed as

$$\mathbf{q}^{(k)} = \begin{bmatrix} \mathbf{\Phi}_{\mathsf{q}}\boldsymbol{\mu}^{k-1} & \mathbf{\Phi}_{\mathsf{q}}^{\star}\boldsymbol{\mu}^{N-k+1} \end{bmatrix} \begin{bmatrix} \mathbf{I} & \mathbf{\Phi}_{\mathsf{q}}^{-1}\mathbf{\Phi}_{\mathsf{q}}^{\star}\boldsymbol{\mu}^{N} \\ \mathbf{\Phi}_{\mathsf{q}}^{\star-1}\mathbf{\Phi}_{\mathsf{q}}\boldsymbol{\mu}^{N} & \mathbf{I} \end{bmatrix}^{-1} \begin{bmatrix} \mathbf{\Phi}_{\mathsf{q}}^{-1} & \mathbf{0} \\ \mathbf{0} & \mathbf{\Phi}_{\mathsf{q}}^{\star-1} \end{bmatrix} \begin{bmatrix} \mathbf{q}_{\mathrm{L}}^{(1)} \\ \mathbf{q}_{\mathrm{R}}^{(\mathrm{N})} \end{bmatrix}. \qquad (4.23)$$

For instance, the displacement field ($y$-direction) of the periodic structures $(P_1)$ and $(P_2)$, at 123 Hz, is displayed in Figure 4.14. The WFE and FE solutions are shown in Figure 4.14. As shown, the WFE-based approaches seem to be highly accurate for predicting the spatial dynamics of the coupled system.
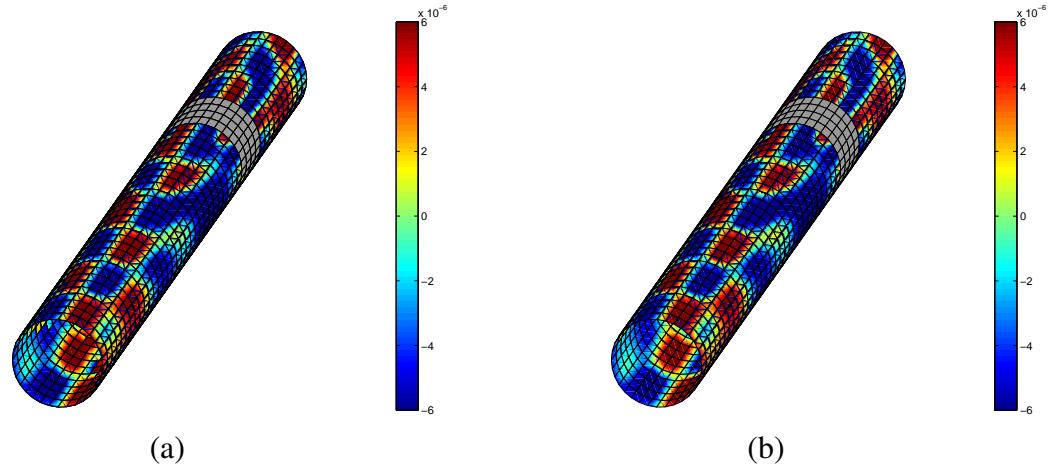


(a)            (b)

Figure 4.14: Displacement field (real part, $y$-direction) of the periodic structures $(P_1)$ and $(P_2)$ occurring in the fuselage-like structure, at 123 Hz: (a) FE solution; (b) WFE-based solution.

**Additional comparisons**

Other simulations are carried out to highlight the efficiency of the proposed approaches further. For this purpose, the approach proposed by Duhamel *et al.* (2006) is considered which provides an alternative WFE-based expression of the dynamic stiffness matrices of periodic structures. Although it has never been applied to the study of coupled systems like those depicted in the current work, the Duhamel's approach may be considered here, which provides almost the same time reduction as the proposed DSM approach. The interesting feature of the DSM and RM approaches lies in the consideration of well-conditioned matrices which can be inverted without difficulties in Equations (3.18) and (3.29), as explained in Sections 3.2.2 and 3.2.3. In comparison, the expression of the dynamic stiffness matrix proposed by Duhamel *et al.* (2006) involves the inverse of a matrix (see Equation (3.105)) whose condition number can be much higher, which may be the source of computational issues. This is highlighted by plotting the condition numbers of those matrices (*i.e.*, for the Duhamel's, DSM and RM approaches) over the frequency domain, regarding for instance the periodic structure (P2) (see Figure 4.15(a)). As it can be seen, the Duhamel's approach yields a condition number which is about $10^2$ times higher than those in the DSM and RM approaches, as expected. For the sake of clarity, the elapsed times involved in those three approaches are displayed in Figure 4.15(b), where it is seen that the proposed RM approach gives the best reduction.



(a)                                        (b)
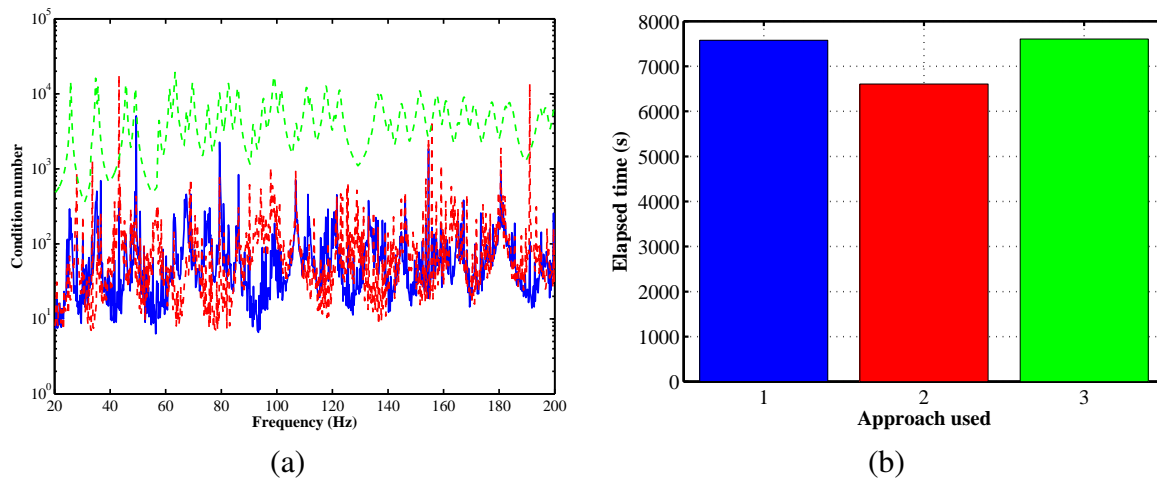
Figure 4.15: Condition numbers of the matrices involved in the WFE-based modelings (a), and related elapsed times (b): (blue) DSM approach; (red) RM approach; (green) Duhamel's approach.

## 4.5  Conclusions

Two WFE-based approaches have been proposed for modeling complex periodic structures. The consideration of sophisticated systems involving several periodic structures and arbitrary coupling junctions follows from classic FE assembly procedures or domain decomposition techniques, which make the proposed approaches quite simple of use. The CB method has been applied for modeling the coupling junctions in terms of static modes and fixed-interface modes. A WFE-based strategy was considered for efficiently selecting the fixed-interface modes being retained. This is done by assessing how much they contribute to the system forced response. Such a strategy enables the number of junction modes to be considerably reduced compared to the classic CB strategy that consists in retaining those for which the eigenfrequencies are below a certain frequency limit. The proposed WFE based DSM and RM approaches were applied to describe the harmonic response of a simple structure (2D frame) and a complex system (3D aircraft fuselage-like structure) that involves truly periodic structures. In both cases, the WFE-based approaches proved to be highly accurate in comparison with the conventional FE method. Also, they yielded large computational savings in comparison with the conventional CB method that makes use of fixed-interface modes for modeling the periodic structures and coupling junctions.

# 5 On the use of the WFE method for passive vibration control of periodic structures

## 5.1 Overview

In this chapter, a strategy for passive vibration control of periodic structures is proposed which involves adding a periodic array of simple resonant devices for creating band gaps. It is shown that such band gaps can be generated at low frequencies as opposed to the well known Bragg scattering effects when the wavelengths have to meet the length of the elementary cell of a periodic structure. For computational purposes, the WFE method is employed, which provides a straightforward and fast numerical means for identifying band gaps through the analysis of dispersion curves. Also, the WFE method constitutes an efficient and fast numerical means for analyzing the impact of band gaps in the attenuation of the frequency response functions of periodic structures. In order to highlight the relevance of the proposed approach, numerical experiments are carried out on a 1D academic rod and on a 3D aircraft fuselage-like structure.

The contribution of this chapter is threefold. First, the effect of attaching a vibration absorber or an array of periodic local resonators to a structure is investigated by means of a simple rod model. Second, the feasibility of using periodic arrays of locally resonant devices for band gaps generation and passive vibration control of periodic structures is shown. Moreover, the potential of the use of a WFE-based approach in the design of periodic structures exhibiting band gaps at targeted frequency bands is concerned. The developments presented in this chapter constitute part of the research paper by Silva *et al.* (2015a) to be published in a Special Issue in Advances in Aircraft and Spacecraft Sciences.

The chapter is organized as follows. In Section 5.2, a comprehensive numerical analysis is carried out regarding a 1D homogeneous rod which is connected to periodic arrays of harmonic oscillators or to a single vibration absorber. Additional experiments are brought in Section 5.3 regarding a 3D fuselage-like structure equipped with a periodic array of locally resonant devices. Finally, conclusions are drawn in Section 5.4.

## 5.2  Comparing local and global attenuation effects

Vibration absorbers are mass-spring or mass-spring-damper systems which are widely used in the field of vibration control engineering. Since the early development of the theory of dynamic vibration absorbers (Ormondroyd and Den Hartog, 2008), they have been applied in a wide range of applications. In many situations, a single vibration absorber punctually attached to one structure is considered so as to avoid the vibrations induced by some vibrational modes. The use of periodic arrays of these locally resonant devices, along structures, is very recent (Thompson, 2008). It has been first investigated by Kashina and Tyutekin (1990) who proposed the use of a set of undamped resonators to reduce the longitudinal and flexural motions in beams and plates. This idea has received new attention with the publication of the work of Liu *et al.* (2000), in which emphasis is placed on exploring the impact of using periodic arrays of resonant devices on wave propagation in artificial periodic composites known as phononic crystals. In such systems, band gaps can be optimized by tuning the resonator's natural frequency on the control procedure targeted one.



(a)                                  (b)                                  (c)
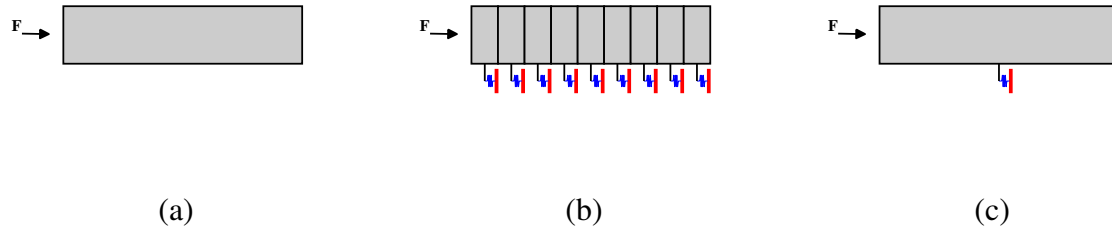
Figure 5.1: 1D homogeneous rod: (a) without resonant devices; (b) with a periodic array of resonant devices; (c) with a single vibration absorber.

In this section, the decrease of the vibration levels produced by adding a periodic array of resonant devices to a periodic structure is analyzed by means of the WFE method. The efficiency in using such devices is highlighted through comparisons with the vibration levels produced by a single vibration absorber. While a single vibration absorber produces local vibration attenuation, a periodic array of small absorbers yields global vibration control. These phenomena are illustrated for a simple 1D homogeneous rod structure as shown in Figure 5.1, whose material and geometric properties are listed in Table 5.1. The left and right ends of the rod are, respectively, excited by a unitary axial harmonic force and free. Here, the structure is either connected to a periodic array of nine spring-mass systems (Figure 5.1(b)), or connected to one single spring-mass system (Figure 5.1(c)). The dispersion curves and the FRFs of the free and the coupled structure are computed

140

using the WFE method (see Chapter 2). Within this framework, the substructure being considered represents either a single rod cell (see Figure 5.1(a)), or a rod cell with a spring-mass resonant system (see Figure 5.1(b)).Notice that each substructure is modeled by means of the spectral element method (SEM) which provides an exact analytical expression of the dynamic stiffness matrix $\mathbf{D}$ (Equation (3.18)) (Doyle, 1997; Xiao *et al.*, 2012). Within the analytical framework, the displacement field of a rod cell is described in a standard way by means of two longitudinal waves, *i.e.*, two propagating ones traveling in opposite directions along a one-dimensional system. The consideration of mass-spring-damper systems is simply achieved through basic kinematic compatibility and force equilibrium equation.

Table 5.1: Characteristics of the 1D homogeneous rod.

| Parameter | Value |
|---|---|
| Density ($\rho$) | 1200 kg/m$^3$ |
| Young's modulus ($E$) | 3 GPa |
| Poisson's ratio ($\nu$) | 0.3 |
| Structural damping ($\eta$) | 0.01 |
| Cross-section area ($A$) | $100 \times 10^{-6}$ m$^2$ |
| Total length ($L$) | 4.5 m |

Band gaps formed by Bragg scattering mechanisms occur in periodic structures when the wavelength $\lambda$ of a traveling wave is equal to twice the substructure length $\Delta$ (Sigalas *et al.*, 2005). The corresponding frequency $f_{\texttt{ref}}$, which is the frequency-edge of the first Bragg scattering band gap, in the case of longitudinal wave propagation is given by

$$f_{\texttt{ref}} = \frac{1}{2\Delta}\sqrt{\frac{E}{\rho}}. \tag{5.1}$$

To begin with, a periodic array of resonant devices (Figure 5.1(b)) is considered so that their resonance frequency is $0.5 f_{\texttt{ref}} = 790.6$ Hz. Two test cases are considered which involve a periodic array whose total mass represents, respectively, $44\%$ and $14\%$ of that of the rod with the periodic array. The related dispersion curves of the longitudinal wave traveling in the coupled rod are displayed in Figure 5.2, along with the dispersion curve that concerns the uncoupled rod. Here the non-dimensional wavenumber $\beta\Delta$ is analyzed as a function of the non-dimensional frequency $f/f_{\texttt{ref}}$, where $f = \omega/2\pi$. As it can be seen in Figure 5.2(a), the longitudinal wave in the rod without resonant devices is always propagative, as expected. Notice that the imaginary part of $\beta\Delta$, although small, is not equal to zero due to damping effects. Regarding the resonant devices, three

141

band gaps (*i.e.*, attenuation zones) occur in Figures 5.2(b) and (c): one is around $0.5 f_{\text{ref}}$ while others are around $f_{\text{ref}}$ and $2 f_{\text{ref}}$. It is seen that the first band gap occurs at the resonance frequency of the spring-mass system, which is a characteristic of band gaps formed by local resonance mechanism. On the other hand, other band gaps occur at multiples of the reference frequency and have constant phase angle, which characterize them as band gaps of Bragg-type.

To highlight further those band gaps, the 2D maps of the frequency response functions (FRFs) of the rod are shown in Figure 5.3. In these figures, the FRFs are plotted as functions of the position along the length of the rod. Regarding Figure 5.3(a), the resonance frequencies of the rod are clearly identified by red lines. Attenuation zones occur in Figures 5.3(b) and (c) in accordance with the band gaps in Figures 5.2(b) and (c), which extend along the structure length except at $x = 0$ m, *i.e.*, in the vicinity of the excitation. The interesting feature when using a periodic array of resonant devices is that it generates band gaps with global attenuation of the vibration levels (*i.e.*, in frequency and space) along the structure. By comparing resonant devices of different masses to each other, one may notice that higher mass fractions produce higher levels of attenuation and larger attenuation zones (see Figures 5.3(b) and (c)).

Consider now the 2D maps of the FRFs of the rod with one single vibration absorber. The results are shown in Figure 5.4 for different mass fractions ($8\%$, $44\%$ and $14\%$) and positions of the vibration absorber ($x = L/2$ and $x = \Delta/2$). Those results are issued from a conventional analytical approach that consists in modeling each rod component (before and after the resonator) by means of a spectral element (Doyle, 1997) — *i.e.*, by modeling its dynamic stiffness matrix by means of two longitudinal waves propagating in right and left directions, respectively — and modeling the resonator by means of a spring-mass system. As it can be seen, band gaps formed by Bragg scattering mechanisms — *i.e.*, for $f/f_{\text{ref}} = 1$ and $f/f_{\text{ref}} = 2$ — are not observed in any case, as opposed to the periodic array of resonant devices even though in case when the added masses involved are the same. Also, the attenuation zone remains restricted to a short frequency bandwidth around $f/f_{\text{ref}} = 0.5$. Notice that the attenuation zone is local, *i.e.*, concentrated at anti-resonance points. Moreover, it depends on the locations of the vibration absorber and excitation point along the structure. In contrast, due to their global attenuation effect, periodic arrays of resonant devices have the potentiality to be used for excitations located at arbitrary location, *i.e.*, which are not necessarily known. This feature is clearly highlighted in Figure 5.5 in which the spatial variations in the reduction of the vibration levels produced, respectively, by the vibration absorber and a periodic array of resonant devices of same masses, are plotted at the target resonance frequency $f = 0.5 f_{\text{ref}}$.
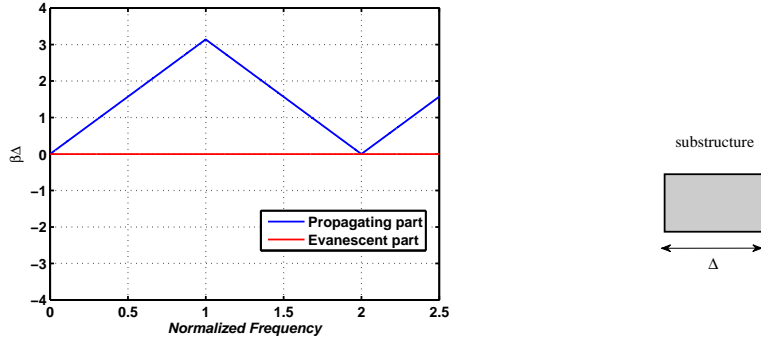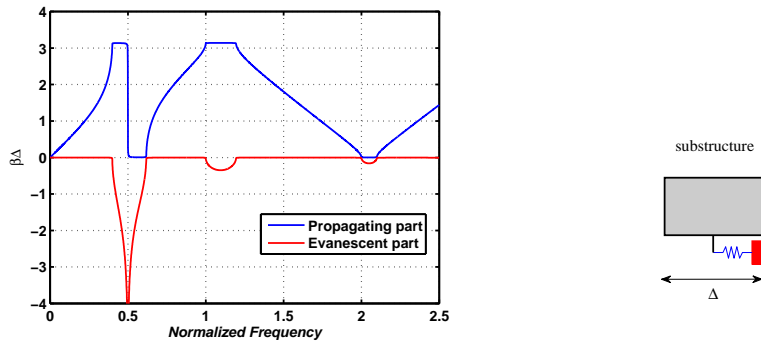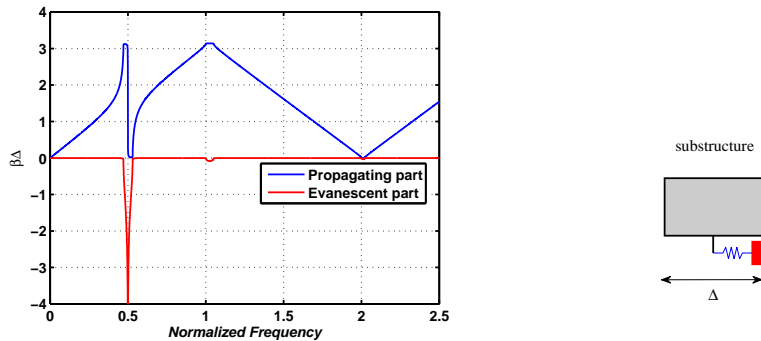
Figure 5.2: Dispersion curves of the longitudinal wave in the homogeneous rod: (a) without resonant devices; (b) with a periodic array of resonant devices composed of $9$ resonators with a mass ratio of $44\%$; (c) with a periodic array of resonant devices composed of $9$ resonators with a mass ratio of $14\%$. (blue color) real part of $\beta\Delta$; (red color) imaginary part of $\beta\Delta$.
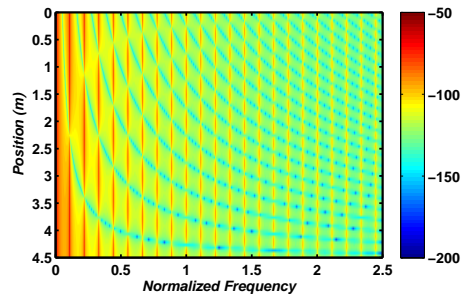
(a)
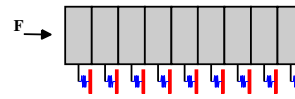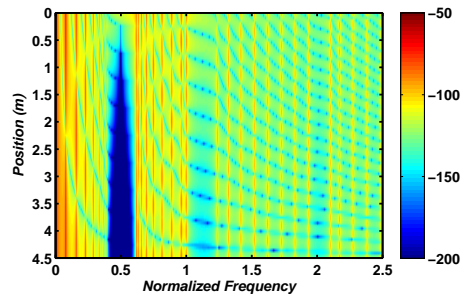


(b)
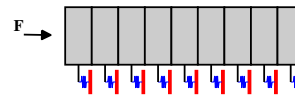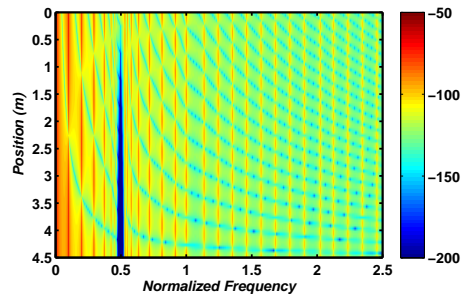


(c)

Figure 5.3: 2D maps of the FRF (in dB) of the homogeneous rod: (a) without resonant devices; (b) with a periodic array of resonant devices composed of $9$ resonators with a mass ratio of $44\%$; (c) with a periodic array of resonant devices composed of $9$ resonators with a mass ratio of $14\%$.
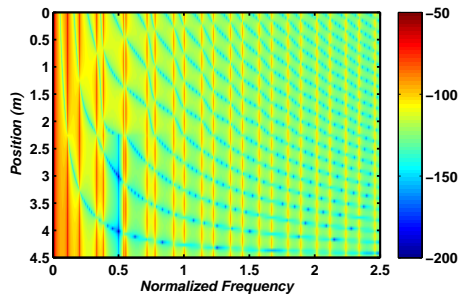
(a)
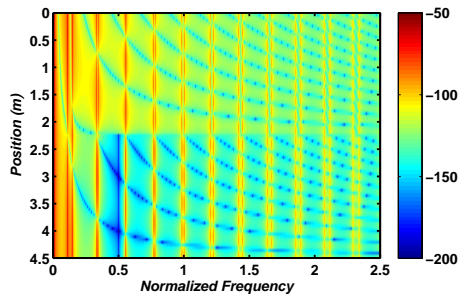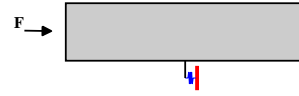


(b)
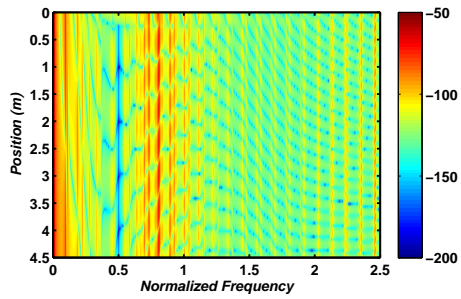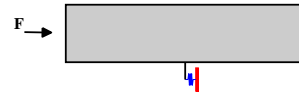


(c)

Figure 5.4: 2D maps of the FRF (in dB) of the homogeneous rod with one vibration absorber: (a) mass fraction of $8\%$, location at $x = L/2$; (b) mass fraction of $44\%$, location at $x = L/2$; (c) mass fraction of $14\%$, location at $x = \Delta/2$.
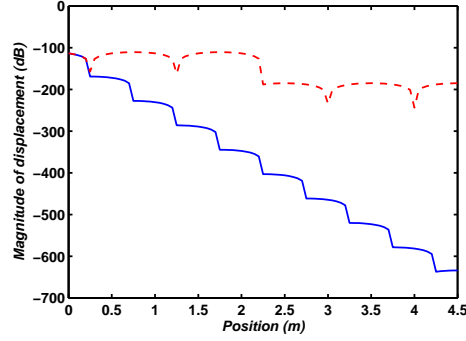
Figure 5.5: Spatial variations in the reduction of the vibration levels at $f = 0.5 f_{\mathrm{ref}} = 790.6$ Hz: (—) periodic array of resonant devices with $9$ resonators and mass fraction of $44\%$, (- - -) vibration absorber located at $x = \Delta/2$ and with a mass fraction of $44\%$.

## 5.3 Tuning local resonators for vibration attenuation in a 3D aircraft fuselage-like structure

### 5.3.1 Problem description

In this section, one aims at showing that important reduction of the vibration levels of complex periodic structures can be achieved through the use of a lightweight periodic array of resonant devices whose parameters are adequately tuned. The periodic structure that is considered here represents a coarse approximation of a 3D aircraft fuselage-like structure, consisting in a cylindrical thin shell with axial stiffeners (stringers) and circumferential stiffeners (frames). Those stiffeners are periodically distributed over the cylinder, two consecutive circumferential (resp. axial) stiffeners being spaced of $0.4$ m (resp. of $11.25°$). The material and geometric characteristics of the stiffened cylindrical shell are listed in Table 5.2.

Within the framework of the WFE method (Chapter 2), a substructure is considered as shown in Figure 5.6(b), which consists in a quarter of the stiffened cylindrical shell with a length $\Delta = 0.4$. Symmetry boundary conditions are considered so as to model the structure along the whole circumference. Regarding the substructure, both cylinder and stiffeners are meshed by means of quadrilateral Reissner-Mindlin shell elements with six DOFs per node, *i.e.*, translations in the $x$, $y$ and $z$ directions and rotations about the same axes. Here, the total number of DOFs used to discretize the substructure is $1,578$, with $246$ DOFs over the left/right boundary and $1086$ internal DOFs. The

146

Table 5.2: Characteristics of the stiffened cylindrical shell.

| Parameter | cylindrical shell | frames | stringers |
|---|---|---|---|
| Thickness ($t$) | 0.001 m | 0.0012 m | 0.005 m |
| Radius ($R$) | 2 m | – | – |
| Height ($h$) | – | 0.10 m | 0.05 m |
| Density ($\rho$) | 2700 kg/m$^3$ | | |
| Young's modulus ($E$) | 70 GPa | | |
| Poisson's ratio ($\nu$) | 0.3 | | |
| Loss factor ($\eta$) | 0.01 | | |

whole periodic structure is modeled by means of $N = 40$ identical substructures connected along the $x$-direction (see Figure 5.6(c)). It is excited by unitary harmonic radial and axial forces and moments which are applied on the left end at $\theta = 45^o$, and it is free from excitations on its right end.
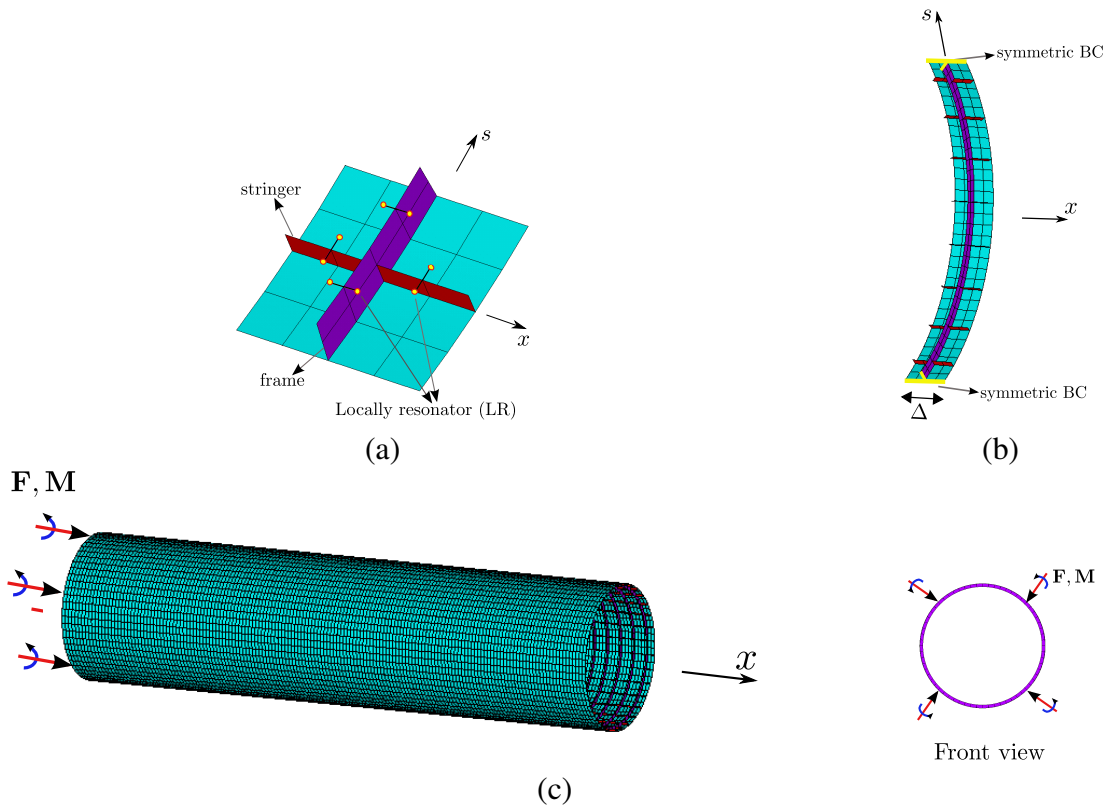


Figure 5.6: FE model of the 3D aircraft fuselage-like structure: (a) unit cell; (b) substructure; (c) whole structure.

Periodic arrays of resonant devices are considered so as to attenuate the vibration levels

147

throughout the whole structure. The motivation behind the present study is to design lightweight resonant devices which may be effectively attached to a real aircraft fuselage. In the present study, each resonant device is modeled as a beam with a concentrated mass, without rotary inertia, on one end and whose other end is connected to the stringers and frames of the periodic structure, as shown in Figure 5.6(a). Here, the first flexural resonances of the resonators, which are attached to the frames and stringers, are assigned to be 197 Hz — which corresponds to a resonance frequency of the whole periodic structure — and 275 Hz, respectively. The characteristics of the resonators are listed in Table 5.3. Notice that the added mass induced by the periodic array of these resonant devices represents about 12.5% of the total mass to the original periodic structure, *i.e.*, it remains small. Within the WFE framework, a new substructure is thus being considered which takes into account the FE modeling of the resonant beams. This yields 3,114 DOFs for modeling the substructure, with 246 DOFs over the left/right boundary and 2,622 internal DOFs. By considering the symmetry boundary conditions, this makes $n = 240$ right-going and left-going wave modes which are to be computed by means of the WFE method.

Table 5.3: Characteristics of resonant devices.

| Parameter | mounted on frames | mounted on stringers |
|---|---|---|
| Beam cross-section area ($A_{rl}$) | 5.4359 mm$^2$ | 7.5878 mm$^2$ |
| Beam length ($L_{rl}$) | 0.03 m | |
| Beam density ($\rho_{rl}$) | 1400 kg/m$^3$ | |
| Beam Young's modulus ($E_{rl}$) | 70 GPa | |
| Beam Poisson's ratio ($\nu_{rl}$) | 0.3 | |
| Beam loss factor ($\eta_{rl}$) | 0.01 | |
| Concentrated mass ($m_{rl}$) | 0.0125 kg | |

## 5.3.2 Numerical analysis and discussion

The dispersion curves of the periodic structure are assessed by means of the WFE method as shown in Figure 5.7. Regarding Figure 5.7(a) (without resonant devices), it should be noticed that one particular wave mode which propagates along the 3D aircraft fuselage-like structure becomes evanescent between 230 Hz and 240 Hz, which characterizes a band gap phenomenon. This might be explained by the fact that the circumferential stiffeners (frames) exhibit some flexural vibration modes in this frequency band. Regarding Figure 5.7(b) (with resonant devices), it is seen that the added periodic array of resonant devices yields large evanescent parts around the target frequencies 197 Hz and 275 Hz, which means that the propagation of waves is strongly attenuated.

Also, the 2D maps of the FRFs of the periodic structure are shown in Figure 5.8. Here, the RMS levels of the radial, tangential and axial displacements (over each cross-section between two consecutive substructures) are displayed as functions of the frequency and position along the structure. As it can be seen, the consideration of the periodic array of resonant devices induces a large decrease of the vibration levels around the target frequency 197 Hz, as expected. Vibration decrease is also observed around the other target frequency 275 Hz, even though it does not correspond to a resonance frequency of the periodic structure. The attenuation between the FRFs of the controlled and uncontrolled structure are plotted in Figure 5.8 in dB. Such a decrease in the vibration levels appears to be widely spread over the length of the structure, even near the excited cross-section. This phenomenon is clearly highlighted in Figures 5.9-5.10, which show the spatial distributions of the structure displacements at 197 Hz and 275 Hz. This provides a clear evidence that the magnitude of the whole displacement field of the structure can be strongly decreased.



(a)                                        (b)
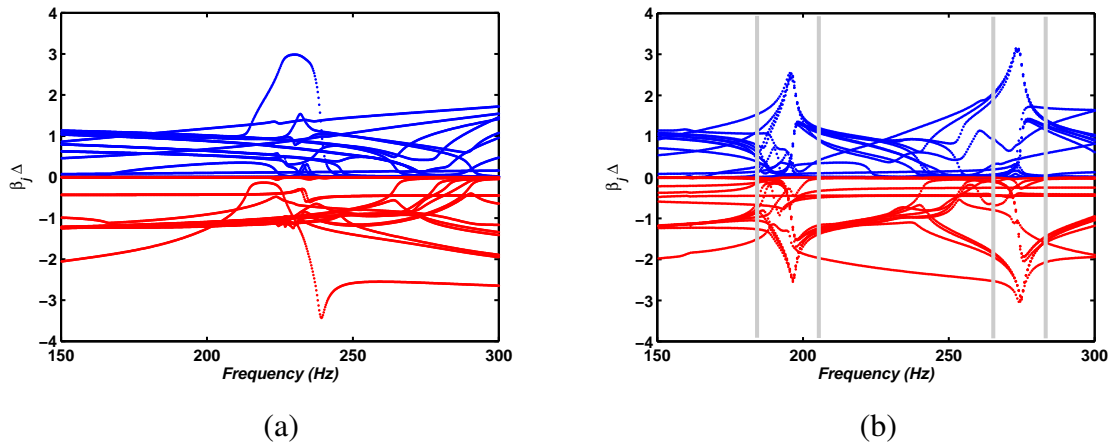
Figure 5.7: Dispersion curves of the waves traveling along the 3D aircraft fuselage-like structures: (a) without resonant devices; (b) with the periodic array of resonant devices. (blue color) real part of $\beta_j \Delta$; (red color) imaginary part of $\beta_j \Delta$.

It is worth pointing out that the proposed WFE approach makes use of a full wave mode bases to model the aircraft fuselage-like structures, *i.e.*, they do not invoke either basis truncation processes or the reduction of the number of interface DOFs. In other words, the WFE method provides, in theory, the same level of accuracy as the FE method for modeling periodic structures. Besides, the WFE method improves the computational efficiency as the FE model of just a single substructure needs to be modeled. Further evidence of the efficiency of the WFE method is shown by comparing the problem size involved in the conventional FE method and in the WFE method. Considering the present case, the corresponding FE model of the structure with resonant devices would have involved 114,966 DOFs, compared to 3,144 DOFs with the WFE method.
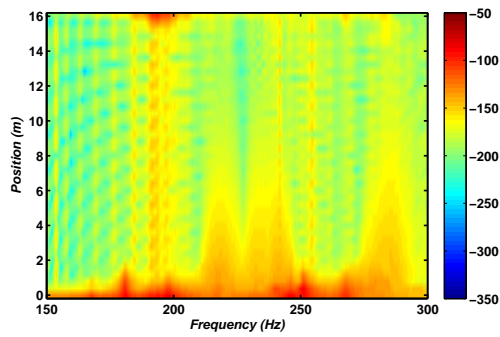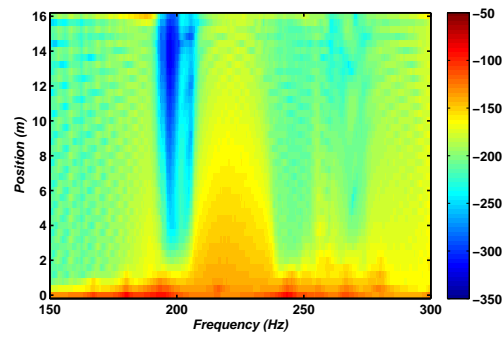
(a)  (b)
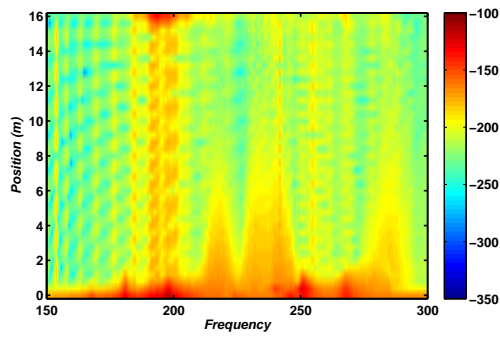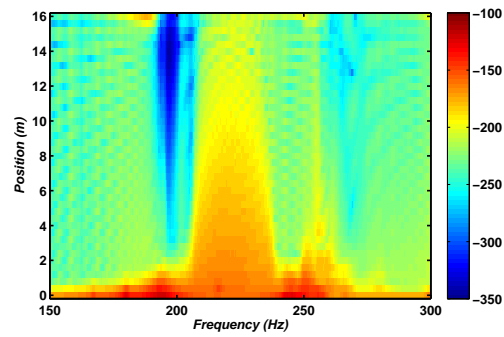
(c)  (d)
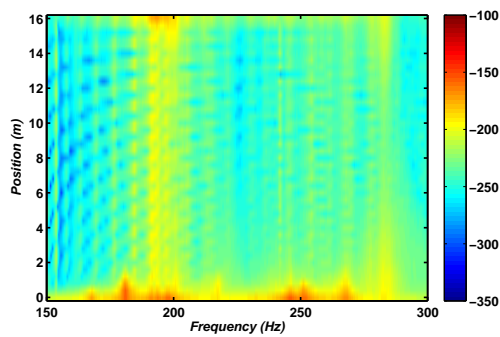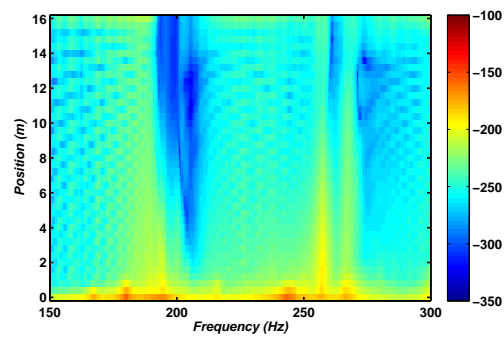
(e)  (f)

Figure 5.8: RMS levels of the radial (a,b), tangential (c,d) and axial (e,f) displacements of the structure without devices (left) and with resonant devices (right).
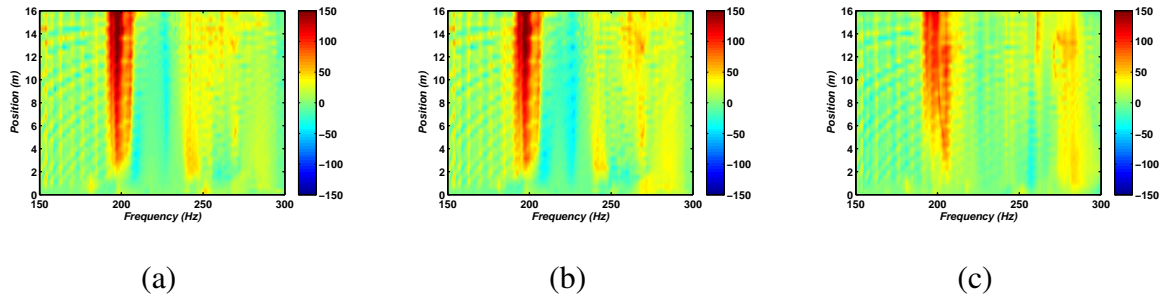
Figure 5.9: Attenuation between the FRFs of the controlled and uncontrolled structure (in dB): (a) radial displacements; (b) tangential displacements; (c) axial displacements.
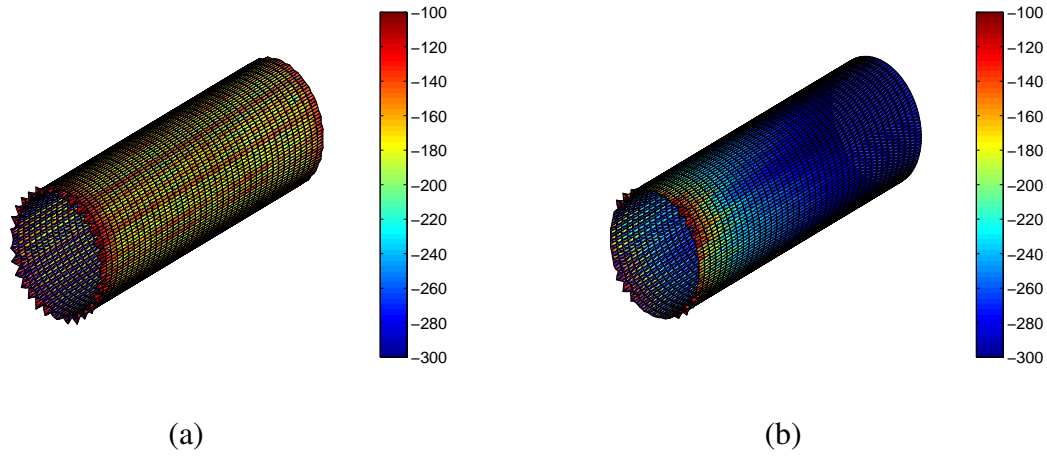


Figure 5.10: Spatial distribution of the total displacement of the periodic structure (in dB), at 197 Hz: (a) without resonant devices; (b) with resonant devices.
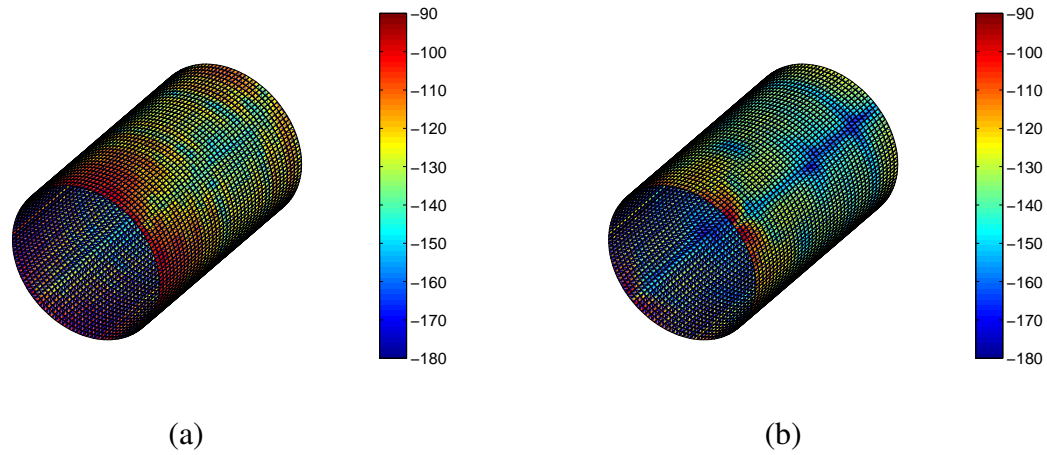


Figure 5.11: Spatial distribution of the axial displacement of the periodic structure (in dB), at 275 Hz: (a) without resonant devices; (b) with resonant devices.

151

## 5.4 Conclusions

In this chapter, a passive vibration control of periodic structures has been analyzed which involves considering periodic arrays of simple resonant devices. The WFE method has been used for this purpose which constitutes a fast and efficient means for assessing the dispersion curves and FRFs of periodic structures. It was been shown that the consideration of lightweight periodic arrays of resonant devices yields large and global decreases of the vibration levels, even at low frequencies. Such resonant devices have proved to be relevant for treating large-sized complex 3D structures such as aircraft fuselages.

# 6    General conclusions

Wave-based approaches have been used for a long time in the dynamic analysis of structures. However, the widespread use of finite element techniques has promoted the dominance of modal-based approaches. Although of simple use, these approaches may require excessive computational resources (time and memory) for the analysis of large complex structures, specially as the frequency rises. In this thesis, it was shown that it is possible to combine the benefits of wave-based and element-based approaches, and develop efficient wave-based superelement models for the forced response analysis of periodic structures and coupled systems.

The numerical approaches proposed here are based on the WFE method. Within the framework of this thesis, this method was used to provide a numerical wave description for the periodic structures under consideration. A summary of the main formulations for the WFE-based eigenvalue problem was presented. For the case of a 3D solid waveguide, it was shown that the eigenvalue problem that involves symmetric matrices provides the best compromise between accuracy and computational time.

From the numerical wave basis provided by the WFE method, original dynamic stiffness and receptance matrices (DSM and RM) of periodic structures were formulated. The interesting feature here is that, within the WFE framework, the receptance matrix is expressed without need of explicitly inverting the DSM. These WFE-based matrices have been shown to provide very accurate solutions for the forced response analysis of 3D beam-like and fuselage-like structures. They have also been shown to provide faster computations than the conventional CB method. In one of the cases studied in Chapter 3, more than $90\%$ of the computational time was saved. Indeed, the advantages of the proposed DSM and RM approaches are better highlighted when sufficiently high frequency effects are analyzed.

With the aim of further improving the performance of WFE-based approaches, a strategy for building reduced-order WFE-based superelement models was proposed. It is assumed that the problem boundary conditions are known a priori. Hence, the strategy allows the selection of the most contributing wave modes to the structure response and uses them to formulate reduced WFE-based eigenproblem and receptance matrix. The originality here lies in proposing a complete procedure for computing accurate free and forced responses of periodic structures in terms of a reduced set of wave modes. The results obtained with this strategy have shown to be as accurate as the WFE-based

approach which makes use of the full basis of wave modes, and provide greater computational time savings. In addition, it was shown that the number of kept wave modes increases as the excitation load becomes more spatially concentrated. It was shown that in the limit, *i.e.*, when a punctual force is applied, the full basis of wave modes must be kept.

The development of a reduced-order WFE-based approach was also motivated by the possibility of building numerical spectral elements. At first, this issue was addressed within the framework of the WSFEM (Arruda and Nascimento, 2008). This method is presented in general form, and, then, used to formulate the spectral element of a Timoshenko beam. The use of the numerical spectral element of a Timoshenko beam to model a 3D solid waveguide shows a very good agreement with solutions provided by the analytical SEM and the WFE-based DSM approach that makes use of the full basis of wave modes at low frequencies. Also, compared to the latter, it also provides a great reduction in computational time. Moreover, by adding a second criterion for the selection of wave modes, it is possible to use the reduced-order WFE-based strategy to build spectral elements of arbitrary order. In other words, the frequency limit of the numerical spectral model increases with the number of kept wave modes.

The forced response analysis of coupled systems involving periodic structures and arbitrarily-shaped coupling elastic junctions has also been addressed in this thesis. It was shown that superelement models of periodic structures and coupling elastic junctions can be assembled through a classic finite element assembly procedure — *i.e.*, the dynamic stiffness method — or a domain decomposition technique — for instance, the receptance method, which involves the use of Lagrange multipliers. The CB method enhanced with a WFE-based criterion to select the most contributing fixed-interface modes has been used to express the dynamic stiffness matrix of coupling elastic junctions. The two WFE-based approaches proposed in this thesis (DSM and RM) were applied to compute the forced responses of a 2D frame structure and a 3D aircraft fuselage-like structure. The latter is a complex coupled system involving periodic structures with heterogeneities. In both cases, the DSM and RM approaches showed to be accurate compared to conventional FE solutions, and more efficient than the classic CB method, as they yielded considerable computational time savings. The potential of the WFE-based RM approach for modeling large coupled systems was also highlighted.

The WFE-based approaches have also been used in the investigation of an interesting physical phenomenon in periodic structures, *i.e.*, the existence of frequency bands in which waves cannot propagate: the band gaps. Here, the use of the WFE method was motivated by: (i) the possibility

of predicting band gaps through free wave propagation analysis — *i.e.*, by means of the dispersion curves —, and (ii) the possibility of computing forced responses of finite periodic structures. The potential of the attachment of lightweight periodic arrays of resonant devices to large-sized complex 3D structures such as an aircraft fuselage-like structure has been shown.

## 6.1 Future work

In the following, topics which appear as future prospects for continuation of the research developed in this thesis are listed.

- Perform a broad study on the approximation level of wavenumbers and wave mode shapes computed by means of the WFE method as a function of the discretization of the substructure into finite elements. The issue of considering internal nodes within a substructure modeled with solid finite elements has been addressed in this thesis. However, the effect of the consideration of an increasing number of internal elements and the impact on the performance of the approach have not yet been addressed.

- Improve the performance of the numerical approaches proposed in this thesis by making use of parallel programming, sparse representation, and code optimization.

- Extend the WFE-based approaches proposed in this thesis to describe vibroacoustic periodic systems, *i.e.*, structures in interaction with internal and external acoustic fields. During this thesis, the formulation of WFE-based superelement models of periodic structures with internal fluid has been investigated, but it has not been included in the thesis because it is still under development.

- Extend the WFE-based approach to multiphysics problems with periodic symmetry, for instance, to study the acoustic-optic coupling in phoxonic structures — *i.e.*, periodic structures that can simultaneously control the propagation of phonons and photons—, or the thermo-mechanical coupling in nanostructures.

- Formulate WFE-based DSM and RM superelement models for structures with two and three-dimensional periodicities. In this thesis, only the case of structures which are periodic along one direction has been addressed.

- Investigate the formulation of the WFE method for quasiperiodic structures. Within the framework of the WFE method, Duhamel (2012) studied for the first time the propagation of waves in waveguides whose section sizes increase proportionally to the distance from an origin. However, he addressed only the case of acoustic radiation in the exterior domain of convex bodies. To the author's knowledge, the case of a finite quasiperiodic structure has not yet been addressed.

- Compare the reduced-order models built by means of the WFE-based strategy proposed in this thesis with spectral elements derived from higher-order analytical theories. Here, it has been shown that numerical spectral elements of arbitrary-order can be built and their forced-responses were compared to the response of a Timoshenko beam model. However, it would be interesting to investigate the convergence rate of the reduced-order models proposed in this thesis with respect to analytical solutions and alternative numerical strategies such as Carrera unified formulation (Carrera, 2003).

- Propose strategies to couple reduced-order superelement models of periodic structures described in terms of generalized coordinates with models of coupling junctions modeled by means of SEM, FEM or BEM,

- Investigate the use of WFE-based DSM and RM approaches in optimization and uncertainty quantification analyses. In these cases, either the best configuration among a set of available possibilities or confidence levels of the system response are sought. As they are computationally intensive analyses, they require efficient resolution methods, such as the WFE-based approaches proposed in this thesis. This is because the WFE-based model size is considerably reduced with respect to the whole structure model, which allows the simulation of more complex structures or dynamics at a lower computational cost.

  - One of the potential applications is the the use of WFE-based approaches in topological optimization to design structures with optimal band gaps at specific frequencies, and the desired vibration reduction.

  - The consideration of uncertainties in modeling parameters within the framework of the WFE method is an open research field, as in this case the periodic assumption breaks down.

- The use of WFE-based approaches for describing the dynamics of structures made of complex materials which do not follow the theory of linear elasticity as, for instance, nanostruc-

tures modeled using non-local elasticity theories, periodic materials with nonlinear constitutive laws. In this thesis, only linear elastic materials have been considered.

- Investigate the use of the WFE-based approaches proposed in this thesis for structural damage identification. This is motivated by the possibility of building reduced-order numerical spectral elements and getting accurate frequency response functions from them. In this case, only those wave modes which interact with the damage can be used to construct the WFE-based superelement model.

## 6.2  List of publications

- Articles in indexed Journals

    ○ P. B. Silva, J.-M. Mencik and J. R. F. Arruda, "On the use of the wave finite element method for passive vibration control of periodic structures", Special Issue in Advances in Aircraft and Spacecraft Sciences (in press).

    ○ P. B. Silva, J.-M. Mencik and J. R. F. Arruda, "Wave finite element based super-elements for forced response analysis of coupled systems via dynamic substructuring", International Journal of Numerical Methods in Engineering (under review).

    ○ D. Beli, P. B. Silva and J. R. F. Arruda, "Vibration Analysis of Flexible Rotating Rings Using a Spectral Element Formulation", Journal of Vibration and Acoustics 137, p. 041003-1 - 041003-11, 2015.

    ○ P. B. Silva, A. L. Goldstein and J. R. F. Arruda, "Building spectral element dynamic matrices using finite element models of waveguide slices and elastodynamic equations", Shock and Vibration 20(3), p. 439-458, 2013.

- Book Chapters

    ○ P. B. Silva, D. Beli and J. R. F. Arruda, "Spectral Finite Element Approach for Structural Dynamics", In: Michael Beer, Ioannis A. Kougioumtzoglou, Edoardo Patelli, Ivan SiuKui Au. (Org.). Encyclopedia of Earthquake Engineering. 1 ed. Springer Berlin Heidelberg, v.1, p. 1-25, 2014.

    ○ J. R. F. Arruda and P. B. Silva, "Wave-Based Structural Modeling", In: Stephen A. Hambric, Shung Sung, Donald J. Nefske, (Org.). Engineering Vibroacoustic Analysis:

Methods and Applications, John Wiley & Sons (in press), 2015.

- Full Papers and Abstracts in Conference Proceedings

  ○ P. B. Silva, J.-M. Mencik and J. R. F. Arruda, "On the use of the wave finite element method for passive vibration control of periodic structures", Proceedings of Noise and Vibration - Emerging Technologies (NOVEM), April 13th-15th, Dubrovnik, Croatia, 2015.

  ○ P. B. Silva, J.-M. Mencik and J. R. F. Arruda, "On the forced harmonic response of coupled systems via a WFE-based super-element approach", Proceedings of the International Conference on Noise and Vibration Engineering (ISMA), September 15th-17th, Leuven, Belgium, 2014.

  ○ P. B. Silva, D. Beli and J. R. F. Arruda, "Using a hybrid approach to model curved beams with non-symmetric cross sections", Proceedings of Seventh M.I.T. Conference on Computational Fluid and Solid Mechanics, June 12th-14th, Cambridge, USA, 2013.

  ○ J. R. F. Arruda and P. B. Silva, "On the renewed interest for the wave propagation approach to structural dynamics", Proceedings of the International Conference on Structural Engineering Dynamics, June 17th-19th, Sesimbra, Portugal, 2013.

  ○ P. B. Silva and J. R. F. Arruda, "Wave spectral finite element analysis of two-dimensional waveguides", Proceedings of the Eleventh Conference in the Computational Structures Technology series (CST), September 4th-7th, Dubrovnik, Croatia, 2012.

  ○ P. B. Silva and J. R. F. Arruda, "Forced response of structural waveguides using the wave spectral finite element method", Proceedings of the Conference Innovations in Wave Modelling (Innowave), September 3rd-7th, Nottingham, UK, 2012.

  ○ P. B. Silva and J. R. F. Arruda, "A direct method to build the spectral dynamic stiffness matrix of waveguides from finite element models", Proceedings of Noise and Vibration: Emerging Methods (NOVEM), April 1st-4th, Sorrento, Italy, 2012.

  ○ A. L. Goldstein, P. B. Silva and J. R. F. Arruda, "The wave spectral finite element method applied to the design of periodic waveguide", Proceedings of the 18th International Congress on Sound & Vibration (ICSV), July 10th-14th, Rio de Janeiro, Brazil, 2011.

○ P. B. Silva, A. L. Goldstein and J. R. F. Arruda, "Study of Elastic Band-Gaps in Finite Periodic Structure Using Finite Element Models", Proceedings of the XIV International Symposium on Dynamic Problems of Mechanics (DINAME), March 13th-18th , São Sebastião, Brazil, 2011.

○ A. L. Goldstein, J. R. F. Arruda and P. B. Silva, "Building Spectral Element Dynamic Matrices Using Finite Element Models of Waveguide Slices", Proceedings of the International Conference on Noise and Vibration Engineering (ISMA), September 20th-22th, Leuven, Belgium, 2010.

# REFERENCES

AALAMI, B. Waves in prismatic guides of arbitrary cross section. **Journal of Applied Mechanics**, v. 40, n. 4, 1067–1072, 1973.

ABRAHAMSON, A.L. Flexural wave mechanics - an analytical approach to the vibration of periodic structures forced by convected pressure fields. **Journal of Sound and Vibration**, v. 28, n. 2, 247–258, 1973.

ALLEMANG, R.J. Modal assurance criterion - twenty years of use and abuse. **Sound and Vibration**, v. 37, 14–23, 2003.

ARPACI, A.; BOZDAG, S.E. and SUNBULOGLU, E. Triply coupled vibrations of thin-walled open cross-section beams including rotary inertia effects. **Journal of Sound and Vibration**, pp. 889–900, 2003.

ARRUDA, J.R.F.; AHMIDA, K.M.; ICHCHOU, M.N. and MENCIK, J.M. Investigating the relations between the wave finite element and spectral element methods using simple waveguides. In **Proceedings of the 19th International Congress of Mechanical Engineering (COBEM)**, p. 10. Brasília, Brazil, November 5-9 2007.

ARRUDA, J.R.F. and NASCIMENTO, R.F. Building spectral elements from finite element models of waveguide slices. In B. Topping and M. Papadrakakis, editors, **Proceedings of the Ninth International Conference on Computational Structures Technology (CST)**, 41. Civil-Comp Press, Stirlingshire, Scotland, 2008.

ARRUDA, J.R.F. and SILVA, P.B. **Engineering Vibroacoustic Analysis: Methods and Applications**, chapter Wave-Based Structural Modeling. John Wiley & Sons, UK (in press), 2015.

BANACHIEWICZ, T. Zur berechnung der determinanten, wie auch der inversen, und zur darauf basierten auflosung der systeme linearer gleichungen. **Acta Astronomica, Serie C**, v. 3, 41–67, 1937.

BARDELL, N.S. and MEAD, D.J. Free vibration of an orthogonally stiffened cylindrical shell, part i: discrete line simple supports. **Journal of Sound and Vibration**, v. 134, 29–54, 1989a.

BARDELL, N.S. and MEAD, D.J. Free vibration of an orthogonally stiffened cylindrical shell, part ii: Discrete general stiffeners. **Journal of Sound and Vibration**, v. 134, 55–72, 1989b.

BELI, D.; SILVA, P.B. and ARRUDA, J.R.F. Vibration analysis of flexible rotating rings using a spectral element formulation. **Journal of Vibration and Acoustics**, v. 137, 041003–1 – 041003–11, 2015.

BENMEDDOUR, F.; TREYSSÈDE, F. and LAGUERRE, L. Numerical modeling of guided wave interaction with non-axisymmetric cracks in elastic cylinders. **International Journal of Solids and Structures**, v. 48, n. 5, 764 – 774, 2011.

BENNETT, M.S. and ACCORSI, M.L. Free wave propagation in periodically ring stiffened cylindrical shells. **Journal of Sound and Vibration**, v. 171, n. 1, 49–66, 1994.

BETTESS, P. Infinite elements. **International Journal of Numerical Methods in Engineering**, v. 11, 53–64, 1977.

BETTESS, P. and ZIENKIEWCZ, O.C. Diffraction and refraction of surface waves using finite and infinite elements. **International Journal of Numerical Methods in Engineering**, v. 11, 1271–1290, 1977.

BIRGERSSON, F.; FINNVEDEN, S. and NILSSON, C.M. A spectral super element for modelling of plate vibration. part 1: general theory. **Journal of Sound and Vibration**, v. 287, n. 1-2, 297–314, 2005.

BLOCH, F. Über die quantenmechanik der elektronen in kristallgittern. **Zeitschrift für Physik**, v. 52, 555–600, 1928.

BOUCHOUCHA, F.; AKROUT, M.; FAKHFAKH, T.; ICHCHOU, M.N. and HADDAR, M. Damage detection in cylindrical pipe through diffusion matrix in wave finite element method. **Advances in Structural Engineering**, v. 15, 435, 2012.

BRILLOUIN, L. **Wave Propagation in Periodic Structures: Electric Filters and Crystal Lattices**. McGraw-Hill, 1946.

BUSCH, K.; VON FREYMANN, G.; LINDEN, S.; MINGALEEV, S.F.; TKESHELASHVILIA, L. and WEGENER, M. Periodic nanostructures for photonics. **Physics Reports**, v. 444, 101–202, 2007.

CARRERA, E. Theories and finite elements for multilayered and shells: a unified compact formulation with numerical assessment and benchmarking. **Archives of Computational Methods in Engineering**, v. 10, 216 – 296, 2003.

CHRONOPOULOS, D.; TROCLET, B.; BAREILLE, O. and ICHCHOU, M.N. Wave finite elements for low and mid-frequency description of coupled structures with damage. **Composite Structures**, v. 96, 111–120, 2013.

CRAIG, R.R. and BAMPTON, M.C.C. Coupling of substructures for dynamic analyses. **American Institute of Aeronautics and Astronautics Journal**, v. 6, n. 7, 1313–1319, 1968a.

CRAIG, R.R. and BAMPTON, M.C.C. Coupling of substructures for dynamic analyses. **American Institute of Aeronautics and Astronautics Journal**, v. 6, n. 7, 1313–1319, 1968b.

CRAIG, R.R. and CHANG, C.J. On the use of attachement modes in substructure coupling for dynamics analysis. In **Proceedings of 18$^{st}$ Structures, Structural Dynamics and Material Conference**, pp. 89–99. San Diego, USA, March 21-23 1977.

CREMER, L. and LEILICH, H.O. Zur theorie der biegekettenleiter. **Archiv der Elektrischen Ubertragung**, v. 7, n. 261, 1953.

DESMET, W.; PLUYMERS, B. and ATAK, O., editors. **"MID-FREQUENCY" - CAE Methodologies for Mid-Frequency Analysis in Vibration and Acoustics**. Katholieke Universiteit Leuven - Faculty of Engineering, 2012.

DESMET, W. and VANDEPITTE, D. Mid-frequency vibroacoustic modelling: challenges and potential solutions. In **Proceedings of the International Conference on Noise and Vibration Engineering (ISMA)**. Leuven, Belgium, September 2002.

DEYMIER, P.A., editor. **Acoustic Metamaterials and Phononic Crystals**. Springer-Verlag, Berlin, 2013.

DONG, S.B. and NELSON, R.B. On natural vibrations and waves in laminated orthotropic plates. **Journal of Applied Mechanics**, v. 39, 739–745, 1972.

DOYLE, J.F. **Wave Propagation in Structures: an FFT-based spectral analysis methodology**. Springer-Verlag, New York, 1st ed., 1989.

DOYLE, J.F. **Wave Propagation in Structures**. Springer-Verlag, New York, 2nd ed., 1997.

DROZ, C.; LAINÉ, J.P.; ICHCHOU, M.N. and INQUIETÉ, G. A reduced formulation for the free-wave propagation analysis in composite structures. **Composite Structures**, v. 113, 134–144, 2014.

DUHAMEL, D. Study of waveguides with sections of proportional sizes: application to wave radiation. In **Proceedings of the Eleventh International Conference on Computational Structures Technology (CST)**. Dubrovnik, Croatia, September 2012.

DUHAMEL, D.; MACE, B.R. and BRENNAN, M.J. Finite element analysis of the vibrations of waveguides and periodic structures. **Journal of Sound and Vibration**, v. 294, n. 1-2, 205–220,

2006.

ECONOMOU, E.N. and SIGALAS, M.M. Classical wave propagation in periodic structures: Cermet versus network topology. **Physical Review B**, v. 48, n. 18, 13434–13438, 1993.

FARHAT, C.; HARARI, I. and FRANCA, L.P. The discontinuous enrichment method. **Computer Methods in Applied Mechanics and Engineering**, v. 190, n. 48, 6455–6479, 2001.

FASSBENDER, H. **Symplectic Methods for the Symplectic Eigenproblem**, chapter 3: The Butterfly Form for Symplectic Matrices and Matrix Pencils. Springer US, 2002.

FINNVEDEN, S. Spectral finite element analysis of the vibration of straight fluid-filled pipes with flanges. **Journal of Sound and Vibration**, v. 199, n. 1, 125 – 154, 1997.

FLOQUET, G. Sur les équations différentielles linéaires à coefficients périodiques. In **Annales de l'École Normale Supérieure**, v. 12, pp. 47–88. 1883.

GAVRIĆ, L. Finite element computation of dispersion properties of thin-walled waveguides. **Journal of Sound and Vibration**, v. 173, n. 1, 113 – 124, 1994.

GAVRIĆ, L. Computation of propagative waves in free rail using a finite element technique. **Journal of Sound and Vibration**, v. 185, n. 3, 531 – 543, 1995.

GAZELET, J.; DUPONT, S.; KASTELIK, J.C.; ROLLAND, Q. and DJAFARI-ROUHANI, B. A tutorial survey on waves propagating in periodic media: Electronic, photonic and phononic crystals. perception of the bloch theorem in both real and fourier domains. **Wave Motion**, v. 50, 619–654, 2013.

GENECHTEN, B.V.; VANDEPITTE, D. and DESMET, W. On the coupling of wave based models with modally reduced finite element models for 3d interior acoustic analysis. In **Proceedings of Proceedings of the International Conference on Noise and Vibration Engineering (ISMA)**, pp. 1631–1651. Leuven, September 15-17 2008.

GOFFAUX, C.; SÀNCHEZ-DEHESA, J.; YEYATI, A.L.; LAMBIN, P.; KHELIF, A.; VASSEUR, J.O. and DJAFARI-ROUHANI, B. Evidence of fano-like interference phenomena in locally resonant materials. **Physical Review Letters**, v. 88, n. 22, 225502, 2002.

GOLDSTEIN, A.L.; ARRUDA, J.R.F.; SILVA, P.B. and NASCIMENTO, R. Building spectral element dynamic matrices using finite element models of waveguide slices. In **Proceedings of the International Conference on Noise and Vibration Engineering (ISMA)**, v. 24, pp. 1–13. Leuven, Belgium, September 2010.

GOLDSTEIN, A.L.; SILVA, P.B. and ARRUDA, J.R.F. The wave spectral finite element method applied to the design of periodic waveguides. In **Proceedings of 18th International Congress on Sound and Vibration (ICSV)**. Rio de Janeiro, Brazil, July 2011.

GOLUB, G.H. and LOAN, C.F.V. **Matrix Computations**. The John Hopkins University Press, Baltimore, 3$^{rd}$ ed., 1998.

GRAFF, K.F. **Wave motion in elastic solids**. Oxford University Press, 1975, Dover Publications, New York, 1975.

GRY, L. and GONTIER, C. Dynamic modelling of railway track: a periodic model based on a generalized beam formulation. **Journal of Sound and Vibration**, v. 199, 531–558, 1997.

HECKL, M.A. Investigations on the vibrations of grillages and other simple beam structures. **The Journal of the Acoustical Society of America**, v. 36, n. 7, 1335–1343, 1964.

HOGBEN, L. **Handbook of Linear Algebra**, chapter 63: Structured Eigenvalue Problems - Structure-Preserving Algorithms, Structured Error Analysis. CRC Press, FL, 2$^{nd}$ ed., 2013.

ICHCHOU, M.N.; MENCIK, J.M. and ZHOU, W.J. Wave finite elements for low and mid-frequency description of coupled structures with damage. **Computer Methods in Applied Mechanics and Engineering**, v. 198, 1311–1326, 2009.

JERRY, A.J. The shannon sampling theorem – it various extensions and applications: A tutorial review. In **Proceedings of the IEEE**, v. 65, pp. 1565–1596. November 1977.

JOHN, S. Strong localization of photons in certain disordered dielectric superlattices. **Physical Review Letters**, v. 58, n. 23, 2486–2489, 1987.

KAPLAN, M. F. **Implementation of automated multilevel substructuring for frequency response analysis of structures**. 2001. PhD Thesis. The University of Texas at Austin.

KASHINA, V.I. and TYUTEKIN, V.V. Waveguide vibration reduction of longitudinal and flexural modes by means of a multielement structure of resonators. **Soviet Physics Acoustics**, v. 36, 383–385, 1990.

KIM, N.I. and KIM, M.Y. Spatial free vibration of shear deformable circular curved beams with non-symmetric thin-walled sections. **Journal of Sound and Vibration**, pp. 245–271, 2004.

KLERK, D.; RIXEN, D.J. and DE JONG, J. The frequency based substructuring (fbs) method reformulated according to the dual domain decomposition method. In **Proceedings of IMAC-XXIV: Conference & Exposition on Structural Dynamics**, 136, p. 14. St. Louis, 2006.

KLERK, D.; RIXEN, D.J. and VOORMEEREN, S.N. General framework for dynamic substructuring: history, review and classification of techniques. **American Institute of Aeronautics and Astronautics Journal**, v. 46, n. 5, 1169–1181, 2008.

KOLOUSEK, V. Anwendung des gesetzes der virtuellen verschiebungen und des reziprozitatssatzes in der stabwerksdynamic. **Ingenieur Archiv**, v. 12, 363–370, 1941.

KUSHWAHA, M.S.; HALEVI, P.; DOBRZYNSKI, L. and DJAFARI-ROUHANI, B. Acoustic band structure of periodic elastic composites. **Physical Review Letters**, v. 71, n. 13, 2022–2025, 1993.

KUSHWAHA, M.S.; HALEVI, P.; MARTINEZ, G.; DOBRZYNSKI, L. and DJAFARI-

ROUHANI, B. Theory of acoustic band structure of periodic elastic composites. **Physical Review B**, v. 49, n. 4, 2313–2322, 1994.

LACHAT, J.C. and WATSON, J.O. Effective numerical treatment of boundary integral equations. **International Journal of Numerical Methods in Engineering**, v. 10, 991–1005, 1976.

LADEVÈZE, P. and RIOU, H. Calculation of medium-frequency vibrations over a wide frequency range. **Computer Methods in Applied Mechanics and Engineering**, v. 194, n. 27-29, 3167–3191, 2005.

LANGLEY, R.S. A wave intensity technique for the analysis of high frequency vibrations. **Journal of Sound and Vibration**, v. 159, n. 3, 483–502, 1992.

LANGLEY, R.S. On the modal density and power flow characteristics of periodic structures. **Journal of Sound and Vibration**, v. 172, 491–511, 1994.

LANGLEY, R.S. and BREMNER, P. A hybrid method for the vibration analysis of complex structural-acoustic systems. **Journal of the Acoustical Society of America**, v. 105, n. 3, 1657–1671, 1999.

LEE, S.; VLAHOPOULOS, N. and WAAS, A.M. Analysis of wave propagation in a thin composite cylinder with periodic axial and ring stiffeners using periodic structure theory. **Journal of Sound and Vibration**, v. 329, n. 16, 3304–3318, 2010.

LEE, U. **Spectral Element Method in Structural Dynamics**. John Wiley & Sons, Singapore, 2009.

LEUNG, A.Y.T. **Dynamic Stiffness and Substructures**. Springer-Verlag, London, 1993.

LIN, Y.K. and MCDANIEL, T.J. Dynamics of beam-type periodic structures. **Journal of Manufacturing Science and Engineering**, v. 91, 1133–1141, 1969.

LIU, Z.; ZHANG, X.; MAO, Y.; ZHU, Y.Y.; YANG, Z.; CHAN, C.T. and SHENG, P. Locally resonant sonic materials. **Science**, v. 289, n. 5485, 1734–1736, 2000.

LOVEDAY, P. Simulation of piezoelectric excitation of guided waves using waveguide finite elements. **Ultrasonics, Ferroelectrics and Frequency Control, IEEE Transactions on**, v. 55, n. 9, 2038–2045, 2008.

LYON, R.H. **Statistical energy analysis of dynamical systems : theory and applications**. MIT Press, Cambridge, Massachussetts, 1975.

MACE, B.R.; DUHAMEL, D.; BRENNAN, M.J. and HINKE, L. Finite element prediction of wave motion in structural waveguides. **The Journal of the Acoustical Society of America**, v. 117, n. May, 2835–2843, 2005.

MACE, B.R. and MANCONI, E. Modelling wave propagation in two-dimensional structures using finite element analysis. **Journal of Sound and Vibration**, v. 318, 884–902, 2008.

MACNEAL, R.H. A hybrid method of component mode synthesis. **Computers & Structures**, v. 1, n. 4, 581–601, 1971.

MAIDANIK, G. Extension and reformulation of sea with use of room acoustics concepts. **Journal of Sound and Vibration**, v. 78, n. 3, 417–423, 1981.

MANCONI, E.; MACE, B.R. and GAZIERA, R. Wave finite element analysis of fluid-filled pipes. In **Proceedings of Noise and Vibration: Emerging Methods (NOVEM)**, 82, p. 12. Oxford, April 5-8 2009.

MARBURG, S. Discretization requirements: How many elements per wavelength are necessary? In S. Marburg and B. Nolte, editors, **Computational Acoustics of Noise Propagation in Fluids - Finite and Boundary Element Methods**, pp. 309–332. Springer Berlin Heidelberg, 2008.

MARZANI, A. Time-transient response for ultrasonic guided waves propagating in damped cylin-

ders. **International Journal of Solids and Structures**, v. 45, n. 25-26, 6347 – 6368, 2008.

MAXIT, L. and GUYADER, J.L. Estimation of sea coupling loss factors using a dual formulation and fem modal information, part i: Theory. **Journal of Sound and Vibration**, v. 239, n. 5, 907–930, 2001a.

MAXIT, L. and GUYADER, J.L. Estimation of sea coupling loss factors using a dual formulation and fem modal information, part ii: Numerical applications. **Journal of Sound and Vibration**, v. 239, n. 5, 931–948, 2001b.

MAZUCH, T. Wave dispersion in anisotropic shells and rods by the finite element method. **Journal of Sound and Vibration**, v. 198, 429–438, 1996.

MEAD, D. Free wave propagation in periodically supported, infinite beams. **Journal of Sound and Vibration**, v. 11, n. January 1969, 181–197, 1970.

MEAD, D. A general theory of harmonic wave propagation in linear periodic systems with multiple coupling. **Journal of Sound and Vibration**, v. 27, 235–260, 1973.

MEAD, D.J. Wave propagation in continuous periodic structures: research contributions from southampton, 1964-1995. **Journal of Sound and Vibration**, v. 190, n. 3, 495–524, 1996.

MEAD, D.J. The forced vibration of one-dimensional multi-coupled periodic structures: an application to finite element analysis. **Journal of Sound and Vibration**, v. 319, n. 1–2, 282–304, 2009.

MEAD, D.J. and BARDELL, N.S. Free vibration of a thin cylindrical shell with discrete axial stiffeners. **Journal of Sound and Vibration**, v. 111, 229–250, 1986.

MEAD, D.J. and BARDELL, N.S. Free vibration of a thin cylindrical shell with periodic circumferential stiffeners. **Journal of Sound and Vibration**, v. 115, 499–520, 1987.

MEAD, D.J.; ZHU, D.C. and BARDELL, N.S. Free vibration of an orthogonally stiffened flat plate. **Journal of Sound and Vibration**, v. 127, 19–48, 1988.

MENCIK, J.M. On the low-and mid-frequency forced response of elastic structures using wave finite elements with one-dimensional propagation. **Computers & Structures**, v. 88, n. 11-12, 674–689, 2010.

MENCIK, J.M. Model reduction and perturbation analysis of wave finite element formulations for computing the forced response of coupled elastic systems involving junctions with uncertain eigenfrequencies. **Computer Methods in Applied Mechanical Engineering**, v. 200, 3051–3065, 2011.

MENCIK, J.M. A wave finite element based formulation for computing the forced response of structures involving rectangular flat shells. **International Journal of Numerical Methods in Engineering**, v. 95, n. 2, 91–120, 2013.

MENCIK, J.M. New advances in the forced response computation of periodic structures using the wave finite element (wfe) method. **Computational Mechanics**, v. 54, n. 3, 789—-801, 2014.

MENCIK, J.M. and DUHAMEL, D. A wave-based model reduction technique for the description of the dynamic behavior of periodic structures involving arbitrary-shaped substructures and large-sized finite element models. **Finite Elements in Analysis and Design**, v. 101, n. 1, 1—-14, 2015.

MENCIK, J.M. and ICHCHOU, M. A substructuring technique for finite element wave propagation in multi-layered systems. **Computer Methods in Applied Mechanics and Engineering**, v. 197, n. 6-8, 505–523, 2008.

MENCIK, J.M. and ICHCHOU, M.N. Multi-mode propagation and diffusion in structures through finite elements. **European Journal of Mechanics, A/Solids**, v. 24, 877–898, 2005.

METROPOLIS, N. and ULAM, S. The monte carlo method. **Journal of the American Statistical Association**, v. 44, n. 247, 335–341, 1949.

MITRA, M. and GOPALAKRISHNAN, S. Extraction of wave characteristics from wavelet-based spectral finite element formulation. **Mechanical Systems and Signal Processing**, v. 20, n. 8, 2046 – 2079, 2006.

MIYASHITA, T. Sonic crystals and sonic wave-guides. **Measurement Science and Technology**, v. 16, R47–R63, 2005.

NARAYANAN, G.V. and BESKOS, D.E. Use of dynamic influence coefficients in forced vibration problems with the aid of fast fourier transform. **Computers & Structures**, v. 9, n. 2, 145–150, 1978.

NASCIMENTO, R. F. **Propagação de ondas utilizando modelos de elementos finitos em guias de onda estruturais**. 2009. PhD Thesis. Universidade Estadual de Campinas, Faculdade de Engenharia Mecânica.

NEFSKE, D.J. and SUNG, S.H. Power flow finite element analysis of dynamic systems: Basic theory and application to beams. **Journal of Vibration, Acoustics, Stress, and Reliability in Design**, v. 111, n. 1, 94–100, 1989.

NELSON, R.B.; DONG, S.B. and KALRA, R.D. Vibrations and waves in laminated orthotropic circular cylinders. **Journal of Sound and Vibration**, v. 18, 429–444, 1971.

NEWTON, I. **"Principia" Book II**. , 1687.

NILSSON, C.-M. **Waveguide finite elements for thin-walled structures**. 2002. PhD Thesis. Institutionen för farkostteknik.

OHAYON, R. and SOIZE, C. **Structural Acoustics and Vibration: Mechanical Models, variational Formulations and Discretization**. Academic Press, San Diego, 1998.

ORMONDROYD, J. and DEN HARTOG, J.P. The theory of the dynamic vibration absorber. **Transactions of the American Society of Mechanical Engineers**, v. 50, A9–A22, 2008.

ORRIS, R. and PETYT, M. A finite element study of harmonic wave propagation in periodic structures. **Journal of Sound and Vibration**, v. 33, 223–236, 1974.

PETYT, M. **Finite Element Vibration Analysis**. Cambridge University Press, New York, 2$^{nd}$ ed., 2010.

PUNTANEN, S. and STYAN, G.P.H. **The Schur Complement and Its Applications**, v. 4 of *Numerical Methods and Algorithms*, chapter Historical Introduction: Issai Schur and the Early Development of the Schur Complement. Springer US, 2005.

RAFEZY, B. and HOWSON, W.P. Exact dynamic stiffness matrix of a three-dimensional shear beam with doubly asymmetric cross-section. **Journal of Sound and Vibration**, pp. 938–951, 2006.

RAYLEIGH, L. On the maintenance of vibrations by forces of double frequency, and on the propagation of waves through a medium endowed with a periodic structure. **Philosophical Magazine Series 5**, v. 24, n. 147, 145–159, 1887.

RENNO, J.M. and MACE, B.R. On the forced response of waveguides using the wave and finite element method. **Journal of Sound and Vibration**, v. 329, 5474–5488, 2010.

RENNO, J.M. and MACE, B.R. Calculating the forced response of two-dimensional homogeneous media using the wave and finite element method. **Journal of Sound and Vibration**, v. 330, 5913–5927, 2011.

RENNO, J.M. and MACE, B.R. Calculation of reflection and transmission coefficients of joints using a hybrid finite element / wave and finite element approach. **Journal of Sound and Vibration**, pp. 1–16, 2012.

RENNO, J.M. and MACE, B.R. Calculating the forced response of cylinders and cylindrical shells using the wave and finite element method. **Journal of Sound and Vibration**, v. 333, 5340–5355, 2014.

RIXEN, D. A dual craig-bampton method for dynamic substructuring. **Journal of Computational Mathematics**, v. 168, n. 1-2, 383–391, 2004.

RIXEN, D.J. Dual craig-bampton with enrichment to avoid spurious modes. In **Proceedings of the IMAC-XXVII**, p. 14. Orlando, USA, February 9-12 2009.

RUBIN, S. Improved component-mode representation for structural dynamic analaysis. **American Institute of Aeronautics and Astronautics Journal**, v. 13, n. 8, 995–1006, 1975.

SEN-GUPTA, G. Natural frequencies of periodic skin-stringer structures using a wave approach. **Journal of Sound and Vibration**, v. 16, 567–580, 1971.

SHORTER, P. and LANGLEY, L. On the reciprocity relation between direct field radiation and diffuse reverberant loading. **Journal of the Acoustical Society of America**, v. 117, 85–95, 2004.

SHORTER, P. and LANGLEY, L. Vibro-acoustic analysis of complex systems. **Journal of Sound and Vibration**, v. 288, n. 3, 669–699, 2005.

SIGALAS, M.; KUSHWAHA, M.S.; ECONOMOU, E.N.; KAFESAKI, M.; PSAROBAS, I.E. and STEURER, W. Classical vibrational modes in phononic lattices: theory and experiment. **Zeitschrift für Kristallographie**, v. 220, 765–809, 2005.

SIGALAS, M.M. and ECONOMOU, E.N. Elastic and acoustic wave band structure. **Journal of Sound and Vibration**, v. 158, n. 2, 377–382, 1992.

SIGMUND, O. and JENSEN, J. Systematic design of phononic band–gap materials and structures by topology optimization. **Philosophical Transactions of the Royal Society A**, v. 361, 1001–1019, 2003.

SIGNORELLI, J. and VON FLOTOW, A. Wave propagation, power flow, and resonance in a truss beam. **Journal of Sound and Vibration**, v. 126, 127–144, 1988.

SILVA, P.B. and ARRUDA, J.R.F. Wave spectral finite element analysis of two-dimensional waveguides. In **Proceedings of the Eleventh International Conference on Computational Structures Technology (CST)**. Dubrovnik, Croatia, September 2012.

SILVA, P.B.; BELI, D. and ARRUDA, J.R.F. Using a hybrid approach to model curved beams with non-symmetric cross sections. In **Proceedings of the Seventh MIT Conference on Computational Fluid and Solid Mechanics**. Cambridge, MA, June 2013a.

SILVA, P.B.; BELI, D. and ARRUDA, J.R.F. **Encyclopedia of Earthquake Engineering**, chapter Spectral Finite Element Approach for Structural Dynamics. Springer, Berlin Heidelberg, 2014a.

SILVA, P.B.; GOLDSTEIN, A.L. and ARRUDA, J.R.F. Building spectral element dynamic matrices using finite element models of waveguide slices and elastodynamic equations. **Shock and Vibration**, v. 20, 439–458, 2013b.

SILVA, P.B.; MENCIK, J.M. and ARRUDA, J.R.F. On the forced harmonic response of coupled systems via a wfe-based super-element approach. In **Proceedings of the International Conference on Noise and Vibration Engineering (ISMA)**. Leuven, Belgium, September 2014b.

SILVA, P.B.; MENCIK, J.M. and ARRUDA, J.R.F. On the use of the wave finite element method for passive vibration control of periodic structures. **Advances in Aircraft and Spacecraft Sciences**, v. 00, –, 2015a. In press.

SILVA, P.B.; MENCIK, J.M. and ARRUDA, J.R.F. Wave finite element-based superelements for forced response analysis of coupled systems via dynamic substructuring. **International Journal for Numerical Methods in Engineering**, v. 00, 2–55, 2015b. Under review.

SOIZE, C. A model and numerical method in the medium frequency range for vibroacoustic predictions using theory of structural fuzzy. **Journal of the Acoustical Society of America**, v. 94, n. 2, 849–866, 1993.

SOROKIN, S.V. and ERSHOVA, O.A. Plane wave propagation and frequency band gaps in periodic

plates and cylindrical shells with and without heavy fluid loading. **New Journal of Physics**, v. 278, n. 3, 501–526, 2004.

THOMAS, D.L. Standing waves in rotationally periodic structures. **Journal of Sound and Vibration**, v. 37, n. 2, 288 – 290, 1974.

THOMPSON, D.J. Wheel-rail noise generation, part 3: Rail vibration. **Journal of Sound and Vibration**, v. 161, 421–446, 1993.

THOMPSON, D.J. A continuous damped vibration absorber to reduce broad-band wave propagation in beams. **Journal of Sound and Vibration**, v. 311, 824–842, 2008.

VANMAELE, C.; VANDEPITTE, D. and DESMET, W. An efficient wave based prediction technique for plate bending vibrations. **Computer Methods in Applied Mechanics and Engineering**, v. 196, n. 33-34, 3178–3189, 2007.

VOLOVOI, V.; HODGES, D.; BERDICHEVSKY, V. and SUTYRIN, V. Dynamic dispersion curves for non-homogenous anisotropic beams with cross-section of arbitrary geometry. **Journal of Sound and Vibration**, v. 215, 1101–1120, 1998.

WAKI, Y.; MACE, B.R. and BRENNAN, M.J. Free and forced vibrations of a tyre using a wave/finite element approach. **Journal of Sound and Vibration**, v. 323, n. 3-5, 737–756, 2009a.

WAKI, Y.; MACE, B.R. and BRENNAN, M.J. Numerical issues concerning the wave and finite element method for free and forced vibrations of waveguides. **Journal of Sound and Vibration**, v. 327, n. 1-2, 92–108, 2009b.

WANG, Z.; ZHANG, P. and ZHANG, Y. Locally resonant band ga´s in flexural vibrations of a timoshenko beam with periodically attached multioscillators. **Mathematical Problems in Engineering**, v. 2013, 146975, 2013.

WATKINS, D.S. On hamiltonian and symplectic lanczos processes. **Linear Algebra and its**

**Applications**, v. 385, 23–45, 2004.

WATKINS, D.S. **The Matrix Eigenvalue Problem: GR and Krylov subspace methods**, chapter 9: Krylov Subspace Methods. The Society for Industrial and Applied Mathematics (SIAM), Philadelphia, 2007.

XIAO, Y.; MACE, B.R.; WEN, J. and WEN, X. Formation and coupling of band gaps in a locally resonant elastic system comprising a string with attached resonators. **Physics Letters A**, v. 375, 1485–1491, 2011.

XIAO, Y.; WEN, J. and WEN, X. Longitudinal wave band gaps in metamaterial-based elastic rods containing multi-degree-of-freedom resonators. **New Journal of Physics**, v. 14, 033042, 2012.

XIAO, Y.; WEN, J.; YU, D. and WEN, X. Flexural wave propagation in beams with periodically attached vibration absorbers: Band-gap behavior and band formation mechanisms. **Journal of Sound and Vibration**, v. 332, 867–893, 2013.

YABLONOVITCH, E. Inhibited spontaneous emission in solid-state physics and electronics. **Physical Review Letters**, v. 58, n. 20, 2059–2062, 1987.

YAO, W.; ZHONG, W. and LIM, C.W. **Symplectic Elasticity**. World Scientific, Singapore, 2009.

ZHONG, W. and WILLIAMS, F. On the direct solution of wave propagation for repetitive structures. **Journal of Sound and Vibration**, v. 181, 485–501, 1995.

ZHOU, W.J. and ICHCHOU, M.N. Wave propagation in mechanical waveguide with curved members using wave finite element solution. **Computer Methods in Applied Mechanics and Engineering**, v. 199, 2099–2109, 2010.

ZHOU, W.J.; ICHCHOU, M.N. and BAREILLE, O. Finite element techniques for calculations of wave modes in one-dimensional structural waveguides. **Structural Control and Health Monitoring**, v. 18, 737–751, 2011.

# ANNEXE A – Craig-Bampton method

The Craig-Bampton method is shortly recalled hereafter. More details can be found in (Craig and Bampton, 1968b). In this framework, a structure $(S_s)$ is modeled by means of static and fixed-interface modes.
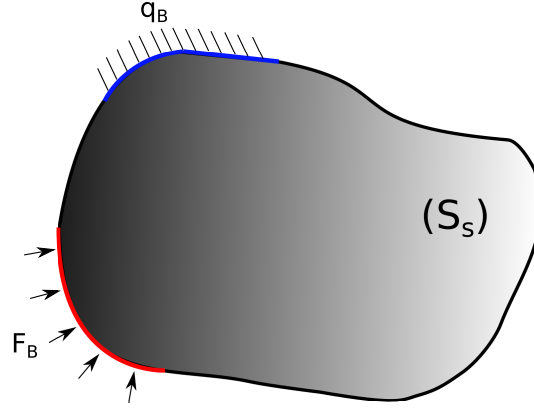


Figure A.1: Illustration of a general structure modeled by means of the Craig-Bampton method: (—) boundary interface subjected to external excitation, (—) boundary interface subjected to kinematic constraints, (—) coupling interface.

Consider a general structure which is meshed with conventional finite elements. The DOFs may be classified into internal or boundary DOFs. Here, the boundary DOFs relate the coupling interfaces, the DOFs subjected to external excitation, and those subjected to kinematic constraints. The equilibrium equations of the structure are expressed as

$$\mathbf{D}^{(s)}\mathbf{q}^{(s)} = \mathbf{F}^{(s)}, \tag{A.1}$$

where $\mathbf{D}^{(s)} = -\omega^2\mathbf{M}^{(s)} + (1 + \mathrm{i}\eta^{(s)})\mathbf{K}^{(s)}$ is the dynamic stiffness matrix of the structure, with $\mathbf{K}^{(s)}$ and $\mathbf{M}^{(s)}$ being the stiffness and mass matrices of the structure, and $\eta^{(s)}$, the loss factor of the structure, while $\mathbf{q}^{(s)}$ and $\mathbf{F}^{(s)}$ are, respectively, the vectors of displacements/rotations and forces/moments, which are of the form

$$\mathbf{q}^{(s)} = \begin{bmatrix} \mathbf{q}_{\mathtt{B}}^{(s)} \\ \mathbf{q}_{\mathtt{I}}^{(s)} \end{bmatrix}, \qquad \mathbf{F}^{(s)} = \begin{bmatrix} \mathbf{F}_{\mathtt{B}}^{(s)} \\ \mathbf{F}_{\mathtt{I}}^{(s)} \end{bmatrix}, \tag{A.2}$$

where the subscripts I and B relate the internal and boundary DOFs, respectively.

Within the framework of the CB method, the total displacement vector is written as a sum of a static part ($\mathbf{q}_{\text{st}}^{(s)}$) and a dynamic part ($\mathbf{q}_{\text{d}}^{(s)}$). The static part follows from Guyan reduction, which allows one to write

$$\mathbf{q}_{\text{st}}^{(s)} = \begin{bmatrix} \mathbf{I} \\ \mathbf{X}_{\text{st}} \end{bmatrix} \mathbf{q}_{\text{B}}^{(s)}, \tag{A.3}$$

where $\mathbf{X}_{\text{st}}$ is the matrix of static modes, defined as $\mathbf{X}_{\text{st}} = - \left( \mathbf{K}_{\text{II}}^{(s)} \right)^{-1} \mathbf{K}_{\text{IB}}^{(s)}$. The dynamic part of the displacement vector consists in writing the internal displacement DOFs as a linear combination of a reduced set of constraint or fixed-interface normal modes, as follows

$$\mathbf{q}_{\text{d}}^{(s)} = \begin{bmatrix} \mathbf{0} \\ \bar{\mathbf{X}}_{\text{el}} \end{bmatrix} \bar{\chi} \tag{A.4}$$

which are obtained by solving the eigenvalue problem $\mathbf{K}_{\text{II}}^{(s)} (\mathbf{X}_{\text{el}})_j = \omega_j^2 \mathbf{M}_{\text{II}}^{(s)} (\mathbf{X}_{\text{el}})_j$, where $\{\omega_j\}_j$ is the set of eigenpulsations. As only a subset of the fixed-interface modes is considered, — in general, those modes with eigenpulsations $\omega_j$ in the frequency band $[0, m_{CB} \times \omega_{max}]$, where $\omega_{max}$ is the maximum angular frequency within the frequency range of interest and $m_{CB}$ is a factor which depends on the problem under study (usually $m_{CB} = 2$, as a rule of thumb) — it provides approximate solutions which are expected to be sufficiently accurate. Using Equations (A.3) and (A.4), the total displacement vector is expressed as

$$\mathbf{q}^{(s)} = \mathbf{q}_{\text{st}}^{(s)} + \mathbf{q}_{\text{d}}^{(s)} = \bar{\mathbf{T}}\bar{\mathbf{p}}, \tag{A.5}$$

where

$$\bar{\mathbf{T}} = \begin{bmatrix} \mathbf{I} & \mathbf{0} \\ \mathbf{X}_{\text{st}} & \bar{\mathbf{X}}_{\text{el}} \end{bmatrix} \tag{A.6}$$

is the transformation matrix and

$$\bar{\mathbf{p}} = \begin{bmatrix} \mathbf{q}_{\text{B}}^{(s)} \\ \bar{\chi} \end{bmatrix} \tag{A.7}$$

is the vector of component generalized coordinates, which consists in boundary DOFs ($\mathbf{q}_{\text{B}}^{(s)}$) and a selected set of generalized DOFs ($\bar{\chi}$). Using the expression in Equation (A.5) into Equation (A.1) and left multiplying the resultant system of equations by $\mathbf{T}^T$, it yields

$$\begin{bmatrix} \mathbf{D}_{\text{st-st}}^{(s)} & \bar{\mathbf{D}}_{\text{el-st}}^{(s)T} \\ \bar{\mathbf{D}}_{\text{el-st}}^{(s)} & \bar{\mathbf{D}}_{\text{el-el}}^{(s)} \end{bmatrix} \begin{bmatrix} \mathbf{q}_{\text{B}}^{(s)} \\ \bar{\chi} \end{bmatrix} = \begin{bmatrix} \mathbf{F}_{\text{B}}^{(s)} + \mathbf{X}_{\text{st}}^T \mathbf{F}_{\text{I}}^{(s)} \\ \bar{\mathbf{X}}_{\text{el}}^T \mathbf{F}_{\text{I}}^{(s)} \end{bmatrix}, \tag{A.8}$$

where

$$\mathbf{D}^{(s)}_{\mathtt{st-st}} = -\omega^2(\mathbf{X}^T_{\mathtt{st}}\mathbf{M}^{(s)}_{\mathtt{II}}\mathbf{X}_{st} + \mathbf{M}^{(s)}_{\mathtt{BI}}\mathbf{X}_{st} + \mathbf{X}^T_{st}\mathbf{M}^{(s)}_{\mathtt{IB}} + \mathbf{M}^{(s)}_{\mathtt{BB}}) + (1+\mathtt{i}\eta^{(s)})(\mathbf{K}^{(s)}_{\mathtt{BI}}\mathbf{X}_{\mathtt{st}} + \mathbf{K}^{(s)}_{\mathtt{BB}}),$$
(A.9a)

$$\bar{\mathbf{D}}^{(s)}_{\mathtt{el-st}} = -\omega^2\bar{\mathbf{X}}^T_{\mathtt{el}}(\mathbf{M}^{(s)}_{\mathtt{II}}\mathbf{X}_{\mathtt{st}} + \mathbf{M}^{(s)}_{\mathtt{IB}}),$$
(A.9b)

$$\bar{\mathbf{D}}^{(s)}_{\mathtt{el-el}} = \mathtt{diag}\left\{\bar{\gamma}_j(-\omega^2 + \bar{\omega}_j^2(1+\mathtt{i}\eta^{(s)}))\right\}_j.$$
(A.9c)

In these equations, $\{\bar{\gamma}_j\}_j$ denote the modal masses ($\bar{\gamma}_j = (\bar{\mathbf{X}}_{\mathtt{el}})^T_j\mathbf{M}^{(s)}_{\mathtt{II}}(\bar{\mathbf{X}}_{\mathtt{el}})_j \ \forall j$).

Alternatively, the equilibrium equations in Equation (A.8) can be written in terms of the boundary DOFs only, as follows

$$\bar{\mathbf{D}}^{(s)}\mathbf{q}^{(s)}_{\mathtt{B}} = \mathbf{F}^{(s)}_{\mathtt{B}} - \bar{\mathbf{D}}^{(s)T}_{\mathtt{el-st}}\bar{\mathbf{D}}^{(s)-1}_{\mathtt{el-el}}\bar{\mathbf{X}}^T_{\mathtt{el}}\mathbf{F}^{(s)}_{\mathtt{I}},$$
(A.10)

where

$$\bar{\mathbf{D}}^{(s)} = \mathbf{D}^{(s)}_{\mathtt{st-st}} - \bar{\mathbf{D}}^{(s)T}_{\mathtt{el-st}}\bar{\mathbf{D}}^{(s)-1}_{\mathtt{el-el}}\bar{\mathbf{D}}^{(s)}_{\mathtt{el-st}}.$$
(A.11)

# APPENDIX A – Implemented codes

## A.1 Codes for FE data extraction

### A.1.1 ANSYS® code

```
filename = solid2
filename_K = solid2_K
filename_M = solid2_M
filename_MAPP = solid2_MAPP

h = 0.003
w = 0.004
d = 0.004/36

Nh = 6 !* Nb of elements along y/z-axes
Nd = 1 !* Nb of elements along x-axis

rho = 7800
Young = 210e9
Poisson = 0.3

/FILNAME,filename

/PREP7

!* Element type
et,1,45

!* Material properties
mp,ex,1,Young
mp,nuxy,1,Poisson
mp,dens,1,rho

!* Geometric properties
block,0,d,0,h,0,w

!* Building substructure model
LSEL,S,LENGTH,,h
LSEL,A,LENGTH,,w
CM,LINE1,LINE
LESIZE,LINE1,,,Nh
LSEL,ALL
CMDELE,LINE1

LSEL,S,LENGTH,,d
```

```
CM,LINE2,LINE
LESIZE,LINE2,,,Nd
LSEL,ALL
CMDELE,LINE2

!* Mesh
VMESH,ALL

NUMMRG,ALL
NUMCMP,ALL

FINISH

!****************************************************************!
!* Solution
/SOLU
ANTYPE,MODAL
MODOPT,LANB,20,1,10000,
WRFULL,1

SOLVE

FINISH
!****************************************************************!
!* Getting matrices
/AUX2
FILE,solid2,FULL
HBMAT,filename_K,,,ASCII,STIFF,NO,NO
HBMAT,filename_M,,,ASCII,MASS,NO,NO
HBMAT,filename_MAPP,,,ASCII,MASS,NO,YES

NLIST,ALL,,,COORD,NODE
!****************************************************************!
```

## A.1.2  MATLAB® codes

1. Code: Ansys2mat-HBMAT-SYM.m

```
% Ansys2mat_KMC ---> Converts Ansys output file of stiffness and mass
% matrices to MAT-file of Matlab
%
% - For symmetric problems: one physics (structural or acoustic)
$\%$
%Using HB_to_MAT converter
%
% This program converts ANSYS matrices to matlab
% 1 - First, it asks for the mapping file (obtained with the command HBMAT
% in ANSYS while extracting stiffness or mass matrices)
```

184

```
% 2 - Second,
%
% COMMANDS IN ANSYS:
% AFTER MODAL ANALYSIS SOLUTION
% \AUX2
% NLIST,NODE1,NODE2,NINC,LCOORD (blank or COORD (just XYZ coord)),SORT1
%(sorting process),SORT2,SORT3,KINTERNAL
% SAVE MANUALLY THE OPENED CHART
%
% FILE,FILENAME(RESULTS),EXT(FULL),
% HBMAT,FILENAME(FOR MATRIX FILE),EXT(DEFAULT .MATRIX),,ASCII,MATRIX TYPE
% (STIFF, MASS, or DAMP),RIGHT HAND SIDE(YES** or NO),MAPPING FILE (YES or
% NO)
%
%
% MAPPING FILE: presents matrix order (LINE NB, NODE NB, DOF)
% SYMMETRIC MATRICES: Just lower triangular part is extracted
% UNSYMMETRIC MATRICES: Full TRANSPOSED matrices are extracted
%
% EXAMPLE (MOST COMMON):
% NLIST,ALL,,,COORD,NODE
% FILE,TEST,FULL,
% HBMAT,M_TEST,,,ASCII,MASS,NO,YES
% HBMAT,K_TEST,,,ASCII,STIFF,NO,NO
%
%%%%%%%%%%%%%%%%%%%%%%%%%%%%%%%%%%%%%%%%%%%%%%%%%%%%%%%%%%%%%%%%%%%%%%%%%%%%

clear all
close all
fclose all
clc

% addpath('C:\Users\Priscilla_2\Documents\MATLAB\HBtoMATLAB\');

Data=1:64;Data=(Data'*Data)/64;
headt=['DMC/FEM/UNICAMP'];
message=strvcat(' Ansys2Mat_KMC ',...
    'using HB_to_MAT converter',...
    'revised by Priscilla B. Silva');
msgbox(message,headt,'custom',Data,hsv(64),'Modal')
clear Data

[FileInput,pathname]=uigetfile('*.*', 'Input FileName for MAPPING file[HB-file]');
if FileInput==0
    clc;
    flag1=0;
    return;
else
    flag=1;
end
dir_name=[pathname FileInput];
[fid]=fopen(dir_name,'r');
```

185

```
frewind(fid);
close

prompt={'Output-Data FileName for nodal coordinates[MAT-file]: '};
titlm='Enter required data';
lineNo=1;
def={'Ansys3D_data'};
FileOut=inputdlg(prompt,titlm,lineNo,def);
FileOut=FileOut{1};
if isempty(FileOut);
    break;
    return;
end
clear prompt def titlm lineNo
close

while feof(fid)==0;
    job=fgetl(fid);
    data=textscan(fid,'%f %f %s');
    mapDOF = [data{1,1} data{1,2}];
end
fclose(fid);

nbDOF = size(mapDOF,1);
L_inc = zeros(nbDOF);
true_nodes = unique(mapDOF(:,2));
nbnode = length(true_nodes);

dof_pos = 0;
for i1 = 1:nbnode
    ind1=find(mapDOF(:,2)==true_nodes(i1));
    nbdof = length(ind1);
    L_inc(ind1,dof_pos+(1:nbdof)) = eye(nbdof);
    dof_pos = dof_pos+nbdof;
end

[FileInput,pathname]=uigetfile('*.*', 'Input nodal coordinate data file');
if FileInput==0
    clc;
    flag1=0;
    return;
else
    flag=1;
end
dir_name=[pathname FileInput];
[fid]=fopen(dir_name,'r');
frewind(fid);
close

datai = [];
while feof(fid)==0;
    job=fgetl(fid);
```

```matlab
    if strcmp(job,'   NODE       X              Y              Z') ...
       || strcmp(job,'NODE       X              Y              Z')
        data=fscanf(fid,'%f');
        datai = [datai; data];
    end
end
fclose(fid);
cord_xyz=(reshape(datai,4,length(datai)/4))';

prompt={'Input FileName for mass matrix[HB-file]:'};
titlm='Enter required data';
lineNo=1;
filename=inputdlg(prompt,titlm,lineNo);
filename=filename{1};
% M_ini = hb_to_msm(filename);
newfile=newHBMAT(filename);
M_ini = readHBMAT(newfile);

prompt={'Input FileName for stiffness matrix[HB-file]:'};
titlm='Enter required data';
lineNo=1;
filename=inputdlg(prompt,titlm,lineNo);
filename=filename{1};
% K_ini = hb_to_msm(filename);
newfile=newHBMAT(filename);
K_ini = readHBMAT(newfile);

lowK = tril(K_ini,-1);
K1 = lowK+lowK.'+diag(diag(K_ini));
K2 = (K1+K1.')/2;

lowM = tril(M_ini,-1);
M1 = lowM+lowM.'+diag(diag(M_ini));
M2 = (M1+M1.')/2;

K=(L_inc.'*K2*L_inc);
M=(L_inc.'*M2*L_inc);


eval(['save ' FileOut ' cord_xyz K M nbnode nbdof']);
close all
clc
```

## 2. Code: ListDOF-solid.m

```matlab
clear all
close all
fclose all
clc
```

187

```matlab
%%  FE Model (Solid model)
data_file = 'Ansys3D_solid2_data';
print_file = 'id_solid5_data.mat';

%  Extracting matrices from FE model
% file containing K,M,C & other data of slice modeled in ANSYS
load(data_file);

% Obtaining Global Kg,Mg,Cg (Different from K,M,C if there are constrained DOFs)
xcord=cord_xyz(:,2);
ycord=cord_xyz(:,3);
zcord=cord_xyz(:,4);
minx = min(xcord);
maxx = max(xcord);
miny = min(ycord);
maxy = max(ycord);
minz = min(zcord);
maxz = max(zcord);

Ls  = maxx - minx; % Slice Length
DOF_node = nbdof;

Cg=zeros(nbnode*DOF_node);
Kg = K;
Mg = M;

% This is because periodic structure has been built in the negative part of
% x-axis
IL=intersect(find(xcord>minx-1e-5),find(xcord<minx+1e-5)); % junction - index of nodes at Left
IR=intersect(find(xcord>maxx-1e-5),find(xcord<maxx+1e-5)); % junction - index of nodes at Right

% Left Nodes
NCord1=unique(ycord(IL)); % No. of different values of x-coordinate
NCord2=unique(zcord(IL)); % No. of different values of y-coordinate
NodesIn1=length(NCord1);  % No. of divisions in x-coordinate
NodesIn2=length(NCord2);  % No. of divisions in y-coordinate
I13L=[];
for i1=1:NodesIn1;
    I11=find(ycord(IL)==NCord1(i1));
    [lixo,I12]=sort(zcord(IL(I11)));
    I13L=[I13L ; IL(I11(I12))];
  end
L_nodes=I13L;
cordL = cord_xyz(L_nodes,1:4);


% Right Nodes
NCord1=unique(ycord(IR)); % No. of different values of y-coordinate
NCord2=unique(zcord(IR)); % No. of different values of z-coordinate
NodesIn1=length(NCord1);  % No. of divisions in y-coordinate
NodesIn2=length(NCord2);  % No. of divisions in z-coordinate
```

```
I13R=[];
for i2=1:NodesIn1;
    I11=find(ycord(IR)==NCord1(i2));
    [lixo,I12]=sort(zcord(IR(I11)));
    I13R=[I13R ; IR(I11(I12))];
end
R_nodes=I13R;
cordR = cord_xyz(R_nodes,1:4);

L_DOFs=[]; % DOFs at LEFT (x=0)
R_DOFs=[]; % DOFs at RIGHT (x=L)

%   LEFT DOFs
for i1=1:length(L_nodes);
    Node=L_nodes(i1);
    L_DOFs=[L_DOFs  (Node-1)*DOF_node+(1:DOF_node)];
end

%   RIGHT DOFs
for i2=1:length(R_nodes);
    Node=R_nodes(i2);
    R_DOFs=[R_DOFs  (Node-1)*DOF_node+(1:DOF_node)];
end

%   INTERNAL DOFs
I_nodes=(setxor(cord_xyz(:,1),[L_nodes' R_nodes']))'; % INTERNAL node numbers
I_DOFs=[]; % internal DOFs (not left & not right)
for i=1:length(I_nodes);
    Node=I_nodes(i);
    I_DOFs=[I_DOFs  (Node-1)*DOF_node+(1:DOF_node)];
end
cordI = cord_xyz(I_nodes,1:4);
cord = [cordL; cordR; cordI];
dofL=length(L_DOFs);

% save data
save(print_file,'dofL','Mg','Kg','L_DOFs','R_DOFs','I_DOFs','cord');
```

# APPENDIX B  –  Reduced-order WFE method: alternative scheme

The reduced order procedure can be either applied to the dynamic equilibrium system of equations (Equation (2.1)) or directly to the state space formulation (Equation (2.8)). In the former case, the displacement/rotation components of the selected right-going wave mode shapes are used to express a transformation matrix $\tilde{\mathbf{T}}$, as follows

$$\tilde{\mathbf{T}} = \operatorname{orth}\left[\Re\left(\mathbf{\Phi}_{\mathbf{q}k}(\omega_i^{\mathtt{ref}})\right) \quad \Im\left(\mathbf{\Phi}_{\mathbf{q}k}(\omega_i^{\mathtt{ref}})\right)\right]. \tag{B.1}$$

It is used to write the vector of displacements/rotations, i.e. the physical DOFs, at the left end (or at the right end) of a substructure in terms of a condensed vector of generalized DOFs of size $n_k \times 1$, as follows

$$\mathbf{q}_{\mathrm{L}}^{(k)} = \tilde{\mathbf{T}}\tilde{\mathbf{q}}_{\mathrm{L}}^{(k)}, \quad \mathbf{q}_{\mathrm{R}}^{(k)} = \tilde{\mathbf{T}}\tilde{\mathbf{q}}_{\mathrm{R}}^{(k)}, \tag{B.2}$$

which, in matrix form, yields

$$\mathbf{q}^{(k)} = \tilde{\mathbf{T}}_{\mathrm{R}}\tilde{\mathbf{q}}^{(k)}, \tag{B.3}$$

where

$$\tilde{\mathbf{T}}_{\mathrm{R}} = \begin{bmatrix} \tilde{\mathbf{T}} & \mathbf{0} \\ \mathbf{0} & \tilde{\mathbf{T}} \end{bmatrix}, \tag{B.4}$$

and

$$\tilde{\mathbf{q}}^{(k)} = \begin{bmatrix} \tilde{\mathbf{q}}_{\mathrm{L}}^{(k)} \\ \tilde{\mathbf{q}}_{\mathrm{R}}^{(k)} \end{bmatrix}. \tag{B.5}$$

Due to the orthogonalization step in Equation (3.33), $\tilde{\mathbf{T}}_{\mathrm{L}} = \tilde{\mathbf{T}}_{\mathrm{R}}^T$. Then, $\tilde{\mathbf{T}}_{\mathrm{L}}$ and $\tilde{\mathbf{T}}_{\mathrm{R}}$ can be used as in Equation (3.42) to reduce the dynamic equilibrium equations for a substructure (Equation (2.3)), which yields

$$\tilde{\mathbf{D}}^{*(k)}(\omega)\tilde{\mathbf{q}}^{(k)}(\omega) = \tilde{\mathbf{F}}^{(k)}(\omega), \tag{B.6}$$

where

$$\tilde{\mathbf{D}}^{*(k)}(\omega) = \tilde{\mathbf{T}}_{\mathrm{R}}^T \mathbf{D}^{*(k)}(\omega)\tilde{\mathbf{T}}_{\mathrm{R}} \tag{B.7}$$

and

$$\tilde{\mathbf{F}}^{(k)}(\omega) = \begin{bmatrix} \tilde{\mathbf{F}}_{\mathrm{L}}^{(k)} \\ \tilde{\mathbf{F}}_{\mathrm{R}}^{(k)} \end{bmatrix} = \tilde{\mathbf{T}}_{\mathrm{R}}^T \mathbf{F}^{(k)}(\omega). \tag{B.8}$$

The generalized variables can be expanded in wave components by making use of Bloch's theorem, as stated in Section 2.2.3. This yields a reduced eigenvalue problem to be solved, which, in general form, can be expressed as

$$\tilde{\mathbf{S}}\tilde{\boldsymbol{\varphi}}_j = \tilde{\mu}_j\tilde{\boldsymbol{\varphi}}_j. \tag{B.9}$$

The eigenvectors of the reduced eigenproblem are related to the ones defined in terms of the physical DOFs, as follows

$$\tilde{\boldsymbol{\Phi}}_j(\omega) = \tilde{\mathbf{T}}_{\mathrm{R}}\tilde{\boldsymbol{\varphi}}_j. \tag{B.10}$$

From Equations (2.22), (B.3), and (B.8), the following relations between pairs of reduced left- and right-going waves shapes must be satisfied as the substructure is symmetric with respect to a plane perpendicular to the $x$-axis

$$\tilde{\boldsymbol{\varphi}}_{\mathrm{q}}^{\star}(\omega) = \tilde{\mathbf{T}}^T\mathcal{R}\tilde{\mathbf{T}}\tilde{\boldsymbol{\varphi}}_{\mathrm{q}}(\omega), \quad \tilde{\boldsymbol{\varphi}}_{\mathrm{F}}^{\star}(\omega) = -\tilde{\mathbf{T}}^T\mathcal{R}\tilde{\mathbf{T}}\tilde{\boldsymbol{\varphi}}_{\mathrm{F}}(\omega). \tag{B.11}$$